FRICTION STIR SPOT WELDING OF SANDWICH SHEETS MADE OF AA5052-H32 SKIN AND HDPE CORE

A Thesis Submitted in Partial Fulfilment of the Requirements

for the Degree of

DOCTOR OF PHILOSOPHY

by

PRITAM KUMAR RANA

(Roll No. 146103017)

Department of Mechanical Engineering

Indian Institute of Technology Guwahati

Guwahati – 781039

INDIA

January 2021

Department of Mechanical Engineering

Indian Institute of Technology Guwahati

Guwahati-781039 INDIA

CERTIFICATE

It is certified that the work contained in the thesis entitled "**FRICTION STIR SPOT WELDING OF SANDWICH SHEETS MADE OF AA5052-H32 SKIN AND HDPE CORE"** submitted by **Mr. PRITAM KUMAR RANA** to the Indian Institute of Technology Guwahati for the award of the degree of Doctor of Philosophy has been carried out under my supervision in the Department of Mechanical Engineering, Indian Institute of Technology Guwahati. This work has not been submitted elsewhere for the award of any other degree or diploma.

(Prof. R. Ganesh Narayanan)

Professor

Department of Mechanical Engineering

Indian Institute of Technology Guwahati

Guwahati-781039

INDIA

Dedicated to

My Family

ACKNOWLEDGMENT

At foremost, I express my deepest gratitude to my supervisor, Prof. R. Ganesh Narayanan, for his invaluable guidance and immense support throughout my Ph.D. work. His innovative ideas and advice in doing systematic and constructive research with a focused mind are remarkable. His approach, combined with professional ethics, providing full freedom in doing research, focusing on smart work, and the presence of mind, will remain a source of inspiration for the rest of my life.

I am thankful to my Doctoral Committee members, Prof. U.S. Dixit, Prof. S. Pal, and Prof. Arbind Kr. Singh, for their insightful comments and valuable suggestions during the progress of my research work.

I want to express my sincere thanks to Prof. S. K. Dwivedy, Department Head of Mechanical Engineering, for his support.

Special thanks to Prof. K. S. R. Krishna Murthy, Department of Mechanical Engineering, IIT Guwahati, for his support and providing full privilege to utilize the Universal Testing Machine in the Strength of Material Laboratory.

I thank Prof. Satish Vasu Kailas, Department of Mechanical Engineering, IISc. Bangalore, for providing full excess to SIAM lab to conduct a part of my experiments.

I thank IIT Guwahati and the department of Mechanical Engineering administration for providing all facilities. I thank Mr. N. K Das, Asst. Workshop Superintendent very much for providing appropriate solutions to any kind of experimental difficulty at the right time. I thank Mr. Pranjol Paul, the Technical Officer, for resolving the functioning of the IR camera used in my research work. I thank very much Technical Superintendents of various labs, Mr. Mrinal Sarma, Mr. Dilip Chetri, Mr. D Khaklary, Mr. M. Medhi, Mr. U. Gohain, Mr. Sanjib Sarma, Mr. S. Ahmed, Mr. J. Basumatary, Mr. C. Banikya, and Mr. Nip Bora for supporting me to conduct my experiments smoothly. I am very much thankful to Lab Technicians, Mr. G. Nath, Mr. G.Baro, Mr. Dulumoni Das, Mr. Gokul Das, Mr. Santush Gogoi, Mr. Gautam Gogoi, and Mr. Ratan Medhi for their prompt action required.

I thank Dr. Satheeshkumar V and Dr. Arvind K. Agrawal for their constant support and

help in all the ways.

The company of my beloved friends and their support at IIT Guwahati made my five years of stay enjoyable. Notably, Mr. Sujit Das, Mr. Sujoy Tikader, Mr. Saptarshi Dutta, and Mr. Pranay K. Sarkar. Each of them deserves special thanks for their invaluable support during my studies and immense help in all critical situations.

I am very much grateful to my beloved lab mates, Dr. T. P. Saju, Mr. S. K. Barik, Mr. N. Bharadwaj, Mr. Sukanta Das, Mr. Priyabrata Nath, and Mr. R. Saxena, for their invaluable support and joyful life.

Special gratitude to my brother in law, Mr. Ashish Kumar, for steady help in all the ways and dealing with my family instead of me moreover.

Finally, I am very much happy to thank my loving wife, Mrs. Pinki Kumari, who supported me a lot and made me stay at IIT Guwahati comfortably.

Pritam Kumar Rana

ABSTRACT

In automotive industries, total weight reduction has become a prime concern for manufacturers to reduce fuel consumption and meet environmental legislation. It is observed that a wide variety of materials is developed for different components in automobiles to improve their overall performance. In this context, the use of lightweight aluminum components has extensively increased for automotive body panels. Of course, not all the materials can be joined using existing joining techniques because of intermetallic compounds' formation, oxide formation. Hence, a large number of advanced joining technologies are also invented to join similar or dissimilar materials. In the past few decades, sandwich materials have drawn particular interest from automobile manufacturers because of their excellent weight-saving characteristics, good flexural rigidity, excellent formability, and considerable damping resistance. These sandwich sheets are usually made up of aluminum skin and a polymer core. Despite so many advantages, sandwich sheets' implementation is still limited due to difficulties in joining by conventional joining technologies during assembly. Apart from joining problems, the delamination of sandwich sheets is also observed during various forming processes. Earlier attempts show that joining a sandwich sheet using fusion welding is not good because of excessive damage to the polymeric core material. Although CO_2 laser welding techniques are already developed to join two sandwich sheets together in butt weld configuration, in most cases single-point joining process is required for assembly purposes where two overlapping sheets are joined in the lap-joint structure. However, many single-point joining techniques are already being used in auto industries, such as resistance spot welding, laser spot welding, etc. However, resistance spot welding cannot be applied to polymer cored sandwich material since the polymer is an electrical insulator, and laser spot welding may vaporize the core material by keyhole formation.

Nevertheless, these methods are inefficient when applied to aluminum sandwich sheets since aluminum itself is not suitable for both resistance spot welding and laser welding. The joining techniques using welding could be replaced by adopting mechanical joining like riveting and other similar techniques, but it enhances the extra weight and cost. Similarly, another attempt was made to join sandwich sheets by self-pierce riveting (SPR), but here some substrate defects are also generated due to the soft polymeric core's inability to

support the rivet tail during setting. Furthermore, the weight addition can be eliminated by applying the clinching process to join sandwich sheets, but it is again restricted to secondary joints where no high strength is required.

A newly developed joining technique using friction stir spot welding (FSSW), which is a process variant of friction stir welding, is successfully applied for joining aluminum sheets and polymer sheets. It is found that many defects like substrate formation, weight addition, and high cost of joining can be eliminated by using this non-traditional method of joining process. It is believed that the delamination of sandwich sheets during forming can also be avoided. Therefore, the friction stir spot welding (FSSW) process can be adopted to join sandwich sheets also.

The thesis's main objectives are to analyze the influence of FSSW on the joining and forming performance of sandwich sheets and to predict the joining and forming performance of sandwich sheets for efficient process design. In the experimental investigations, the FSSW of sandwich sheets is investigated by changing process parameters. Furthermore, the quality of sandwich sheets is analyzed by changing the quality of the core layer. Finally, an optimum window for successful FSSW of sandwich sheets is derived. The comparative assessment of bimetallic and sandwich sheets are also analyzed. Both joining and forming performances of FSSW of sandwich sheets are monitored. In joining, the micro-and macro-structure and joint quality indexes are monitored. Forming performance includes mechanical tests like lap shear tensile test, cross tension test, and peel tests to quantify the joint strength and strain at failure. Forming behavior is analyzed by the uniaxial tensile test of the joints. Furthermore, the FE simulation is performed to predict failure mode and to understand material flow in the sandwich sheet.

Further, the joint behavior of friction stir spot welded sandwich sheets is assessed by changing the quality of the epoxy core layer. The core property is altered by changing the hardener to resin (h/r) ratio within a suitable range. In the numerical simulation, cohesive zone modeling has been incorporated in Abaqus to monitor the hook formation and interface delamination, which is not performed until now in literature. Cohesive zone modeling helped in the accurate prediction of delamination, and without it, the hook geometry and plastic energy dissipation predictions are approximated. It has been suggested to incorporate the cohesive zone model during FE simulations to have a realistic prediction of sandwich performance.

ABBREVIATIONS

BM	Bimetallic sheets
CZ	Cohesive zone
CZM	Cohesive zone modeling
FE	Finite element
FSW	Friction stir welding
FSSW	Friction stir spot welding
HAZ	Heat affected zone
HDPE	High density polyethylene
H/R	Hardener/resin ratio
IR	Infrared
LS	Lower sheet
PD	Plunge depth
SW	Sandwich sheets
SZ	Stir zone
TH	Thermocouple
TMAZ	Thermomechanically affected zone
TZ	Transition zone
US	Upper sheet
Wt.%	Weight %

NOMENCLATURE

σ	True stress in MPa
ε	True strain
K	Material strength coefficient in MPa
n	Strain hardening exponent
r	Plastic strain ratio
r_0, r_{45}, r_{90}	Plastic strain ratio in 0º, 45º, and 90º to the rolling direction of the sheets

CONTENTS

LIST OF FIGURES

LIST OF TABLES

Chapter 1

Introduction, Literature review, Significance, and Objective of the work

1.1 Introduction

The requirement for lightweight vehicles has dramatically increased in recent years because of economic demand and strict environmental policies. Although lightweight materials have shown promising effects in vehicle weight reduction with some additional cost, further weight reduction is possible by implementing cost-effective sandwich sheets. The light sandwich sheets are mainly used to fabricate the interior panels of the automobiles. Apart from lightweight, a sandwich sheet has many advantages: better formability, high flexural rigidity, and good damping properties. These sandwich sheets often need to be assembled with the automobile's chassis, where joints are made at many spots. Due to the different skin and core material properties, the joining of the sandwich sheet is problematic.

So far, Friction Stir Spot Welding (FSSW) has proven its acceptance in joining a wide variety of materials. Besides, it is also capable of joining materials having extreme property differences. Knowing the suitability of FSSW in the joining of aluminum and polymer, the process is applied to the polymer core aluminum sandwich sheet. Moreover, critical experimental investigation on FSSW of the sandwich is not available in the existing literature. The polymer core's presence makes the FSSW of sandwich sheets interesting compared to bimetallic lap joints. There is no attempt to understand the effect of rotational speed, plunge depth, tool profile, etc., on the joint formation and mechanical performance after FSSW of sandwich sheets.

The present work's main objective is to analyze the influence of FSSW on the joining and forming performance of sandwich sheets and to predict the joining and forming performance of sandwich sheets for efficient process design. In FSSW, the process parameters have varied within a suitable range, and the joint morphology and joint mechanical performance are studied through systematic and comprehensive experiments. This analysis finally revealed the acceptable range of each process parameters for joining sandwich sheets with acceptable mechanical performance.

In Chapter 1, the literature review, the significance of the work, objectives of the work, and tasks involved are presented. The experimental investigations on the influence of rotational speed on FSSW of sandwich and bimetallic sheet are presented in Chapter 2. The effect of plunge depth is investigated in Chapter 3. The significance of plunge speed and its effect is demonstrated in Chapter 4. The influence of changing dwell time during FSSW is explored in Chapter 5. The delamination phenomenon in the sandwich sheet is explained, and the effect of changing core properties is demonstrated using experiments and numerical techniques in Chapter 6.

1.2 Literature review

In this section, the foundation of joining techniques, classification, advantages, and disadvantages are discussed. Furthermore, the effect of process parameters of Friction Stir Welding (FSW) and Friction Stir Spot Welding (FSSW) on the joint performance is explored via a detailed literature survey. Following this, the sandwich sheet is introduced, its applications, advantages, and disadvantages are discussed. The influence of parameters affecting the quality or performance of the sandwich sheet is also highlighted.

1.2.1 Introduction to joining

Joining is the process of putting or bringing separate parts or components together to produce a continuous or single unit. The ability to join similar or dissimilar materials has been core to the manufacture of products, erection of structures, and the creation of useful tools (Messler, 2004) from the very beginning. With the development of new and advanced materials, parallelly, many joining processes have also developed. Joining technology is advancing very rapidly and is crucial to future global competitiveness. After developing a wide variety of joining processes, researchers have started classifying all the processes into various categories such as mechanical joining, adhesive bonding, welding, and hybrid processes according to some commonness. Although every process has its significance, welding becomes the most popular joining technology in the industries due to its inherent advantages.

The history of welding is ancient. Sumerians have done the first welding in the early 4000 BC. At that time, they used it to weld gold to gold. It then took a very long time until the next major step in the field of welding technology is achieved. In 2700 BC, the Egyptians constructed copper lines by fire welding. The tubes are then sealed as water pipes for the urban water supply. Fire welding is also used for making jewelry. In the following centuries, many important discoveries are made in the field of welding technology. The big breakthrough, however, came only from

1880–87. During this period, the Russian Nikolai Nikolaijewitsch Bernados developed what today is known as the arc welding process (Vural, 2014). After this, a wide range of welding technologies is discovered.

Some of the recent developments in the welding industry include friction stir welding and friction stir spot welding, where the materials are being joined by plastic deformation or, in other words, by forming.

1.2.2 Classification of joining technologies

Joining can be classified based on the fundamental forces involved in it. Joining is made possible by the following three - and only three - fundamental forces: (1) mechanical forces, (2) chemical forces, and (3) physical forces, which have their origin in electromagnetic forces (Messler, 2004). Based on these three forces, the joining process can be broadly classified into three types, namely mechanical joining, welding, and adhesive bonding. The welding is further classified into a liquid state, solid-state, and solid-liquid state welding based on the state transformation occurring during the process. There are numerous types of solid-state welding processes in practice, such as ultrasonic welding, diffusion welding, forge welding, roll welding, explosive welding, and friction welding. Friction welding has got three variants, namely Friction Stir Welding (FSW), Friction Stir Spot Welding (FSSW), and Friction Stir Processing (FSP).

1.2.3 Friction Stir Welding (FSW)

Friction stir welding is a solid-state welding process. It consists of a non-consumable rotating tool with a specially designed pin and shoulder is first inserted into the adjoining edges of the sheets to be welded with a proper tilt angle and then moved all along the joint (Mishra and Ma, 2005). This method lies in the direct conversion of mechanical energy to thermal energy to form the weld without the application of heat from any external source.

1.2.3.1 Background

Friction welding is being used to join materials in a solid-state mode for many years before inventing FSW. The process consists of compressing two metal pieces against each other and moving relative to each other. The heat generated by friction causes the material to be plasticized in the joint region. The joining mechanism involved is applying pressure to the softened material to make a strong metallurgical joint. Though it is a simple process, it has some constraints in the dimensional point of view of the specimen, and it has limited application.

Researchers from The Welding Institute (TWI) in the United Kingdom (UK) have spent many years for various R&D and industrial activities on friction welding. During their work, W. Thomas has proposed an idea of joining two materials using a rotational tool with a pin of a harder material than the work-piece. It is found that the rotating tool could plasticize the work-piece material and by the traversing of the tool, an effective material transportation mechanism provides plasticized material to join the work-pieces together. Hence, friction stir welding is invented (Thomas et al., 1994).

1.2.3.2 Terminologies

For the proper understanding of FSW, specific terminologies associated with the process are required to understand. Threadgill (2007) has tried to give exact definitions of each and every term, which are being frequently used to describe the FSW process. The material which has to be welded is known as the work-piece. Sometimes it is also referred to as part/ sample/welded plate/ specimen. The rotating component of the friction stir welding system, which is designed to generate heat by friction with the work-piece, is known as the tool or FSW tool. The part of the tool which remains below the surface of the work-piece is termed the probe. It is also known as "pin," particularly for cylindrical shape. The part of the tool which rests directly on or slightly embedded in the surface of the work-piece during the process is termed as the shoulder. In the case of a tilted tool, the portion of the shoulder which experiences more penetration into the work-piece is termed as the heel. The maximum penetration of the shoulder into the work-piece is termed as heel plunge depth. The angle made by the tool rotation axis with vertical is termed as tilt angle or travel angle. The rate of tool travel along the interface of the work-pieces is termed as traversing speed/ traversing rate/ welding speed/ travel speed. The angular velocity of the tool is known as the rotational speed/ rotation rate. The force applied parallel to the axis of rotation of the tool is termed as downforce. Force applied parallel to the welding direction is termed as traversing force. The component of sideways force generated at the right angles to the direction of travel is referred to as the side force. The side of the weld, where the local direction of the tool rotation and the traversing direction is the same, is referred to as the advancing side. The side of the weld where the local direction of the tool rotation is opposite of the traversing direction is referred to as the retreating side.

1.2.3.3 Working principle

FSW produces welds using a non-consumable rotating tool with a probe at its one end that softens the material due to friction produced between the tool and the work-piece contact area.

The complete process can be divided into four stages, namely clamping work-pieces, tool plunging, tool traversing, and tool removal. In the first stage, the work-pieces have to be clamped rigidly and aligned correctly according to the type of joint to be made. It should be restricted in all directions in order to withstand several forces develop within the process and to achieve perfect and defect-free welds. In the tool plunging stage, the rotating tool slowly penetrates into the work plates, which are rigidly clamped in a tool fixture. The plunging of tools has a significant effect in FSW, such as preheating the entire work-piece. Frictional heat generated between the tool probe and the work-piece transfers from the plunging zone to the entire work-piece. After the tool plunged into the work-piece, there should some dwell time to bring the metal pieces to a plastic state so that the tool traverses easily and makes a good joint. In the tool traversing stage, there is a dwell time for which the tool is kept in contact at the same depth in order to bring the work-pieces into a plasticized state. Then the tool traversed along the welding line. Here an important point to be addressed, i.e., material flow. While tool traversing, the material from advancing or the front side will be carried to the retreating or backside of the tool. The last one is the tool removal. The tool has to be removed or un-plunged from the work-pieces in a vertical direction. This process leaves a keyhole on the work-piece.

1.2.3.4 FSW welded zones

Like many fusion welding processes, various welded zone formed in friction stir welding also. However, the characteristic features of these zones are very much different from that of fusion welding. Aluminum is used in the present analysis. Although it is very difficult to distinguish the nugget zone from the rest, after seeing the microstructure of the cross-section of the welded sample near the weld, different zones can be revealed. It is observed that grains of aluminum at the weld is dynamically recrystallized due to a high degree of plastic deformation (Threadgill, 2007).

The cross-section of the joint can be divided into four distinct regions as Base Material or Parent Material (BM), Heat Affected Zone (HAZ), Thermo Mechanically Affected Zone (TMAZ), and Stir Zone (SZ). In the BM zone, the material does not deform, and although it may have experienced a thermal cycle from the weld, it is not affected by the heat in terms of microstructure or mechanical properties. The HAZ lies closer to the weld center, where the material has experienced a thermal cycle and so has modified the microstructure and/or the mechanical properties. However, there is no plastic deformation occurring in this area. In TMAZ, the material is plastically deformed by the friction stir welding tool, and the heat from the process also exerts some influence on the material. In the case of aluminum, it is possible to get significant plastic

strain without recrystallization in this region, and there is generally a distinct boundary between the recrystallized zone and the deformed zones of the TMAZ. The recrystallized area in the TMAZ in aluminum alloys is traditionally called the nugget.

1.2.3.5 Process parameters and their influence

The FSW involves many parameters, and precise control of these parameters influences the weld quality. Some welding parameters have constraints with the equipment or machine, and others with the material to be welded. To consider the feasibility of such parameters for the smooth running of the mechanism for each step of welding is very much essential while implementing the process.

The optimization of welding parameters is necessary to obtain good quality joint. In this context, Bozkurt (2012) has conducted an experiment to optimize friction stir welding process parameters to achieve maximum tensile strength in high-density polyethylene sheets (HDPE). By doing the analysis of variance (ANOVA), it is concluded that the tool rotation rate is the most significant parameter, and the tilt angle is found to be the least contribution welding parameter. In this regard, the primary welding parameters are considered as tool welding speed, rotational speed, tool plunge depth, tool plunging force, and tool shoulder diameter

Lee et al. (2003) have studied the effect of tool welding speed on FSW of AZ91D magnesium sheets, and the longitudinal and transverse tensile strength is checked. The longitudinal tensile strength and hardness value of friction stir welded AZ91D magnesium alloy is improved at a higher welding speed due to the smaller grain size. The smaller grain size is attributed to lower heat input per unit weld at a higher welding speed. However, transverse tensile strength is unaffected by welding speed.

Zhang et al. (2015) have conducted an experiment to observe the effect of welding parameters on microstructure and mechanical properties of friction stir welded joints of a super high strength Al–Zn–Mg–Cu aluminum alloy. They also observed smaller grain sizes at higher welding speed due to a lower degree of recrystallization due to less deformation temperature, deformation rate, and deformation degree. Further, they have measured microhardness at the mid thickness of the transverse cross-section and found that the average microhardness value in the nugget zone is increased at higher welding speed, which can be attributed to the smaller grain size.

Cavaliere et al. (2009) have also reported a similar finding in the case of dissimilar AA6082–

AA2024 joints produced by friction stir welding. An increment in vertical force with an increase in welding speed is also observed for all joints.

Lee et al. (2003) have further tried to investigate the effect of welding speed on the weld strength of friction stir welded A356 aluminum alloy, and they found that the longitudinal tensile shear strength is improved at increased welding speed. The improvement in joint strength is attributed to the breaking up of plate-like Si particles in base metal into slightly finer particles. However, they have also noted that at very high welding speed, the strength reduced due to larger Si particle size because of insufficient stirring.

Xu et al. (2013) have found better strength and ductility for friction stir welded AA2219-T62 Al alloy at higher traverse speed due to grain refinement as a result of the reduction in heat input per unit length. However, opposite behavior is also observed in an experiment conducted by Sakthivel et al. (2009), where they have observed a decrease in ultimate tensile strength of friction stir welded commercial-grade aluminum at higher welding speed because of the generation of insufficient heat input.

Cavaliere et al. (2008) have reported a similar finding for both static and dynamic response of AA6082 joints produced by friction stir welding. It is observed that there exists a critical welding speed at which the joint tensile strength, as well as the endurance limit during fatigue testing, are superior.

Apart from experimental observations, the modeling and simulations have also been done to predict the influence of various input parameters on some intermediate and output parameters, which affects the final weld quality. Chen and Kovacevic (2003) have predicted the influence of welding speed on the residual stress developed across the cross-section of friction stir welding of 6061 Al alloy sheets. The heat transfer model is developed using Fourier's equation to predict temperature distribution across the cross-section, which is further implemented through finite element modeling in ANSYS. It is inferred from simulation results that a higher traverse speed induces a high longitudinal stress zone and narrower lateral stress zone.

Ulysse (2002) has proposed a three-dimensional finite element model to predict the effect of welding speed on the forces acting on the tool. The temperature distribution and forces are calculated by numerical modeling, which showed a decrease in temperature with increasing welding speed. Further experiments are also conducted, which confirmed the numerical results. In addition, after doing parametric studies, it is predicted that with increasing welding speed, the

axial and shear force acting on the tool also increased. The results are very much crucial in designing tools.

Rajamanickam et al. (2009) have predicted the effect of welding speed on the thermal history and mechanical properties of friction stir welding of aluminum alloy AA2014 through finite element simulation using ANSYS. It is reported that with increasing welding speed, ultimate tensile strength also increased. Moreover, from the statistical analysis of tensile test data done using ANOVA, it is observed that the welding speed has the greatest influence on the tensile properties of the joint.

Kundu et al. (2013) have investigated the effect of process parameters on the microstructure and tensile strength of friction stir welded joints between interstitial free steel and commercially pure aluminum. Increasing rotational speed results in high-temperature generation due to more friction and an intense degree of deformation. An increase in temperature promotes the formation of intermetallic compounds, particularly for dissimilar metal joints. The presence of intermetallic is confirmed by SEM images and increased hardness in the stir zone. Intermetallic compounds reduce the weld strength due to their brittle nature. Further, they have also observed grain growth in the stir zone due to high-temperature generation at higher rotational speed, an increase in grain size also responsible for weak strength.

Xu et al. (2013) have also concluded poor strength and ductility for friction stir welded AA2219-T62 Al alloy at a higher rotational speed. It is observed that the second-phase particles piled up together at a higher rotational speed, which caused micro-stress concentration resulted in early failure during tensile testing.

The influence of temperature in friction stir welding is already known; hence controlling the temperature by changing different process parameters must be appropriately designed. Cui et al. (2007) have made an attempt to investigate the influence of temperature on the microstructure of high carbon steel under friction stir welding by changing tool rotation rate. A dramatic change in the joint microstructure is observed. At higher rotational speed, the peak temperature crossed the critical temperature, and the cooling rate exceeded the lower critical cooling rate resulted in martensite formation led to an increase in hardness. On the other hand, welding performed below the critical temperature led to the formation of refined microstructure resulted in improved joint strength.

Kalaiselvan and Murugan (2013) have investigated the influence of rotational speed on

transverse tensile strength of friction stir welded AA6061−B4C composite, where they found that the UTS value is increased with an increase in rotational speed reaches a peak value and then decreases. It is believed that with increasing rotational speed, heat addition is more, which causes better stirring resulting in grain refinement. This results in increasing joint performance with increasing tool rotational speed. However, if the rotational speed is increased beyond a critical value, an excessive release of stirred material on the top surfaces results in the formation of microvoids into the stirred zone, ultimately reducing the joint strength. Also, the coarsening of grains occurred at more than the desired temperature, which is also responsible for the reduction in strength.

Hirata et al. (2007) have also observed similar findings in the case of friction stir welding of 5083 aluminum alloy. It is seen that increasing rotational speed resulted in coarser grain size in the weld zone due to increased net heat input per unit length, which gave poor strength. Again bulge test results revealed poor formability at a higher rotational speed.

It is clear from the above reviews that tool travel speed and rotational speed have the opposite effect on the tensile strength of the joint made by friction stir welding since the heat input per unit length reduces with increasing travel speed and increases with increasing rotational speed. But the too high or too low value of any of these two parameters is again a problem in achieving sound weld. So there must be an optimum combination of these two parameters for good weld strength. Simoncini & Forcellese (2012) have experimented and found that strength and ductility of the welded joint initially increases then decreases after a critical value of the ratio of rotational speed to travel speed.

Apart from process parameters, there are some other factors affecting the weld like material position, tool axis offset, tool pin profile, shoulder profile, shoulder diameter, penetration depth, surface roughness, etc. These are the factors that are not convenient or sometimes not possible to alter during the process; instead, it is set before the process started.

It is reported that there is a slightly higher temperature on the advancing side of the joint (Yuan et al., 2012). Therefore, it is reasonable to believe that for joining dissimilar material using friction stir welding, the position of the material across the joint is important. Guo et al. (2014) have concluded that slightly higher transverse tensile strengths of joints are obtained with softer aluminum alloy on the advancing side since it is easy for the harder alloy to penetrate the softer nugget since the dominant material in the weld zone mainly came from the harder retreating side.

Park et al. (2010) have also made a similar conclusion.

It is observed that in the case of friction stir welding of dissimilar materials like aluminum to steel, the rotating pin is required to maintain some offset from the faying surface towards the softer aluminum side to prevent quicker wearing of the tool pin. One more objective of the rotating pin is to remove the oxide layer from the steel's faying surface by continuous rubbing. But at zero offsets of the pin, poor oxide removal resulted in insufficient mixing and, finally, less joint strength. However, a very high tool offset resulted in the excessive scattering of Fe fragments into the Al matrix, creating some voids, which again decreased the joint strength (Watanabe et al., 2006).

Furthermore, for friction stir welding of dissimilar materials using a tapered cylindrical tool, tool offset greatly influence weld strength. As the tool axis shifts towards steel, a portion of the tool penetrating steel, and the depth of penetration increases, so more volume is stirred, giving better joint strength. But too much offset towards steel caused excessive wearing of tool pin and generation of enormous heat resulted in intermetallics formation, hence reduced strength (Ramachandran et al., 2015).

Elangovan and Balasubramanian (2008) have investigated the effect of tool pin profile on the formation of friction stir processing zone in AA2219 aluminum alloy. They have used five tools, namely straight cylindrical, taper cylindrical, threaded cylindrical, square, and triangular, each having different pin profiles. Out of these five, the tool with a square pin has given the finest microstructure due to the highest no. of pulsating effect. The highest microhardness value is achieved for a straight cylindrical tool suggesting good quality weld. Tensile tests also revealed that the joint produced using a straight cylindrical tool had given superior strength. Trimble et al. (2015) have also characterized the shape of the tool pin for increased speed during friction stir welding of AA2024-T3. They have used three different tools, each having different pin profiles, namely cylindrical, tri-flute, and square. They found that among all three types of pin profile, the tri-flute pin profile resulted in the best tensile strength along with the maximum micro-hardness value in the nugget zone. They concluded this is due to increased plastic deformation, and stirring of the work-piece produces finer grains within the nugget zone since the value of volume displacement ratio (dynamic volume/static volume) for the tri-flute tool is maximum.

Rajakumar et al. (2013) have also examined the influence of various tool pin profiles on the joint strength of friction stir spot welded AZ61A magnesium alloy sheets. It is observed that the straight cylindrical tool pin profile is unable to move material from the upper part to the lower part

of the joint due to the smooth pin periphery led to less frictional heat generation and resulted in relatively coarse grains in the nugget region compared to the other tool pin profiles. On the other hand, the tool with threaded pin gave improved joint strength due to the most refined grain at the weld nugget formed by intense material flow.

It is documented that shoulder profile also influence welding properties along with pin profile. Scialpi et al. (2007) have tried to investigate the influence of shoulder geometry on microstructure and mechanical properties of friction stir welded 6082 aluminum alloy. They have used three different tools having different shoulder profiles, namely fillet + scroll tool (T_{FS}), fillet + cavity tool (T_{FC}), and fillet tool (T_F). The tool with fillet and cavity have the least contact surface area, generating maximum heat flux resulted in more severe plastic deformation and degree of dynamic recrystallization, in turn, exhibited maximum hardness in the stirred zone. They have further concluded that a tool with fillet and scroll results in best UTS value due to scroll shoulder very little amount of flash generation results in more compaction of material in stir zone (SZ).

It is also reported that the diameter of the tool shoulder plays a vital role in friction stir welding. As the shoulder diameter increases, the contact area between the tool and work-piece increases gives more frictional heat generation. An increase in the heat generation during the process resulting in grain growth (Commin et al., 2009).

For the joining of dissimilar materials using FSW, apart from so many existing welding parameters, tool plunge depth becomes an important factor, which needed to be optimized. An increase or decrease in plunge depth affects the process temperature, which needs to be controlled because the low temperature of the weld prevents the formation of a strong bond between aluminum and steel while higher heat generation develops a wide IMCs region in the weld zone (Dehghani et al., 2013).

Dawood et al. (2015) have investigated the influence of the surface roughness on the microstructures and mechanical properties of 6061 aluminum alloy using friction stir welding. Detailed experimental results suggested that decreasing surface roughness produced very fine nano-sized grains in the weld due to reduced heat flux. The formation of nano-grains improved the tensile strength and hardness of the joint.

The FSW joint performance of aluminum alloy 7020-T6 is studied at varying axial loads. It is observed that the joint strength is poor at a lower axial load. The lower axial load results in inadequate pressure and temperature generation, which leads to insufficient coalescence of

transferred material, resulting in defect formation. The defects are evident in the joint produced at lower axial loads (Kumar and Kailas, 2008).

There are other research works in which the effect of process parameters is studied on various joint features like grain size, hardness, and mechanical performance of the joint. Some of the important works are summarised in Table 1.1.

Table 1.1: Summary of FSW parameters and their influence on output parameters.

FSW Parameter	Change	Effect	Reference
Tool welding speed	Increased	Longitudinal tensile strength improved, hardness values at weld increased.	Lee et al. (2003)
		The average micro-hardness value in the nugget zone increased	Zhang et al. (2015)
		longitudinal tensile strength improved	Lee et al. (2003)
		Strength and ductility improved.	Xu et al. (2013)
		Tensile strength reduced	Sakthivel et al. (2009)
		Tensile strength first increased then decreased.	Kalaiselvan and Murugan (2013)
		Tensile strength increased, Formability improved	Hirata et al. (2007)
Tool rotational speed	Increased	Hardness in stir zone increased, Tensile strength reduced, Grain size increased	Kundu et al. (2013)
		Tensile strength decreased	Xu et al. (2013)
		Tensile strength first increased then decreased.	Kalaiselvan and Murugan (2013)
		Tensile strength decreased, Formability reduced	Hirata et al. (2007)
Rotational speed/welding speed ratio	Increased	Tensile strength and ductility first increased than decreased.	Simoncini and Forcellese (2012)
Tool offset from the faying surface	Increased	Tensile strength first increased then decreased.	Watanabe et al. (2006)
		Tensile strength first increased then decreased.	Ramachandran et al. (2015)
Shoulder diameter	Increases	Grain size increases	Commin et al. (2009)
Surface roughness	Decreased	Grain size reduced, Hardness improved, Tensile strength increased	Hasan et al. (2015)

1.2.3.6 Advantages

The most significant benefit of friction stir welding is the ability to join dissimilar materials. Besides that, there are many advantages, such as an environment-friendly process, a non-consumable tool, suitable for welding in all positions. Surface preparation is not required, very little distortion of the samples, no filler material is required, the process is cost-effective, dissimilar metals can be welded, automation is possible.

1.2.3.7 Limitations

Besides many advantages of FSW, there are some limitations too, such as welding speeds are moderately slower, work-pieces must be rigidly clamped, backing bar required, keyhole at the end of each weld.

1.2.3.8 Applications

FSW is widely used in shipbuilding and marine, aerospace, railway, land transportation, construction, and electrical industries.

1.2.4 Friction stir spot welding (FSSW)

Friction stir spot welding is a solid-state joining process where a specially designed rotating tool is plunged into overlapping sheets at a single point and is retracted from the joint after the process completion (Gerlich et al., 2005). The tool of the FSSW is comprised of a shoulder and a pin, both having various types of surface profiles. However, many researchers have successfully developed a pin-less tool for this operation where the objective of the pin is fulfilled by introducing some special surface pattern or design on the face of the shoulder. P pin-less tool configuration has many advantages to a pinned tool, like better surface appearance and absence of any keyhole (Chen et al., 2013); (Li et al., 2014).

1.2.4.1 Background

During assembly of sheet metal parts in automobiles, it is required a huge number of single point joints or spot joints. Laser spot welding, resistance spot welding, and riveting have been widely used for that. But none of these joining methods is defect free. Porosity is observed in laser spot welding, while resistance spot welding imparts more distortion and riveting ads extra cost of drilling and increased weight. Therefore friction stir spot welding (FSSW) has been developed as a new single point joining technique joining aluminum sheet metals (Yang et al., 2014). FSSW has been considered as a good alternative for existing spot welding technologies (Mortimer, 2005). There are many advantages of FSSW over existing spot joining techniques, such as reasonably quick process, non-requirement of additional material, cost-effectiveness, and ability to join a wide range of lightweight materials.

1.2.4.2 Terminology

Most of the terms in friction stir spot welding are common with friction stir welding described in the earlier section since FSSW is a process variant of FSW. However, some new terminologies are included here because of special weld geometry formation due to the absence of transverse movement of the tool, such as effective top sheet thickness, hook height, hook width, and stir zone width. The effective top sheet thickness is the distance between the shoulder indentation surface and the position at which the partial metallurgical bond of the hook begins. The hook height is the distance between the interface of the two sheets and the point at which the partial metallurgical bond of the hook begins. The hook width is the distance between the keyhole's vertical face and the point at which the partial metallurgical bond of the hook begins. The stir zone width is the distance between the edge of the keyhole and the widest region of the stir zone.

1.2.4.3 Working Principle

The process is completed in three stages, namely plunging, stirring, and retracting. The rotating pin slowly goes into the overlapping sheets up to a predetermined depth in the plunging state. In the stirring stage, the rotating pin generates heat and plasticizes the material. In this step, the tool rotates for a predetermined time, which mixes the materials from both the sheets properly and makes the metallurgical bond between the two sheets. The retracting stage is the final step where the rotating tool is retracted from the sheets leaving a keyhole (Merzoug et al., 2010).

1.2.4.4 FSSW welded zones

The characteristic features of the welded zone in friction stir spot welding are symmetrical about the tool's geometrical axis, unlike friction stir welding since there is no transverse movement of the tool in FSSW. During FSSW of overlapping sheets, as the tool penetration into the sheets increases, the lower sheet material moves upward. Simultaneously, the upward movement of lower sheet material is repelled outward from the center due to the stirring of material by tool pin rotation. The tool shoulder restricts the material to come out from the stir zone, so the materials trying to move upward continuously is pushed back into the stir zone, and the proper mixing takes place. Due to this change in the path of motion of lower sheet material, a curved profile develops, which is referred to as the hook (Badarinarayan et al., 2009).

1.2.4.5 Process Parameters and their influence

The joint quality and performance of friction stir welded sheet are affected by the process parameters as well as the tool geometry. Major process parameters are plunge depth, dwell time, rotation rate, and plunge speed, while pin profile and shoulder profile are two important tool

geometry that affects the joint property.

FSSW has been successfully applied to study the influence of tool geometry in the joining of similar materials AA 2024-T3 to AA 2024-T3. The tool geometry considerably affects the joint characteristics (Paidar et al., 2015). In another attempt, FSSW is used to join dissimilar materials like low carbon steel and Al-Mg alloy to investigate the effect of tool plunge depth. Formation of the intermetallic layer is observed during the process, and it is found that a good joint can be produced at a specified welding parameter (Lee et al., 2009). Further, the FSSW is also applied to join polymeric materials like HDPE to HDPE, where dwell time has emerged as the most influencing process parameter (Bilici et al., 2011). FSSW of polypropylene sheet is done by Arici and Mert (2008). They found that dwell time and plunge depth are the two main process parameters that affected the joint behavior. Bilici and Yükler (2012) have applied FSSW on polyethylene. The tool geometry significantly affects the joint strength. Oliveira et al. (2010) have investigated the feasibility of FSSW of poly (methyl methacrylate) PMMA and found that it is possible to obtain considerable weld strength by parameter optimization.

AA6111 and polyphenylene sulfide are joined by FSW, and the effect of process parameters like translational speed and distance to backing on the joint performance, joining mechanism, and failure modes are investigated (Ratanathavorn and Melander, 2015). Khodabakhshi et al. (2014) have joined AA5059 and High-Density Polyethylene (HDPE) by FSW. The results suggest that two mechanisms achieve bonding between aluminum and polymer. One is the formation of micro- and macro- constraints, which create mechanical interlocking between the layers. Another is interfacial chemical adhesion between the aluminum and consolidated polymeric layers. FSW between polycarbonate and AA7075 is done by Moshwan et al. The effect of process parameters on temperature evaluation, mechanical, and the microstructural property is investigated (Moshwan et al., 2015). Friction spot joining of AA6181-T4 with Carbon fiber-reinforced poly (phenylene sulfide) composite laminate is done by Esteves et al. An important tool slippage phenomenon to decrease in viscosity of plasticized metal at high temperature has been presented (Esteves et al., 2015). FSSW of adhesive bonded blanks is also done. Chowdhury et al. have attempted FSSW of AZ31B-H24 Mg and AA5754-O Al alloy sheets bonded with Terokal 5089 adhesive. The joint performance of samples with adhesive is better than that of without adhesive during the lap shear test and fatigue test (Chowdhury et al., 2013). The friction stirring process can join materials with extreme property differences, making it possible to develop an aluminum-polymer composite system by FSSW. A similar technique is used by Lacki and Derlatka, where a composite beam

made up of aluminum and titanium is fabricated by refill friction stir spot welding (RFSSW) (Lacki and Derlatka, 2017).

Friction Stir Spot Welding (FSSW) is utilized for joining Al sheets meant for autobody applications. Mazda Motor Corporation reports the first application in its RX-8 sports car (Mazda , 2003). FSSW applies to similar and dissimilar materials (Baskoro et al., 2020); (Ferreira et al., 2020). FSSW is also used for welding polymers. For instance, FSSW of acrylonitrile butadiene styrene sheet is performed by Yan et al. (2019), and it is concluded that lap shear strength of the joint is reduced at higher tool rotational speed and lower plunge speed. Pabandi et al. performed refill FSSW of aluminum/polymer composite structures, where the joint strength is improved at higher tool rotational speed (Salonitis et al., 2013).

Rao et al. (2015) have investigated the influence of plunge depth on the lap-shear failure load of friction stir spot welded joint of aluminum alloy 6022-T4 and magnesium alloy AM60B sheets. Increasing plunge depth raises the temperature rapidly due to an increase in load, and it is well known that welding of dissimilar materials at high temperature frequently produce hard and brittle intermetallic compounds. The presence of the intermetallics in the parent material may improve or reduce the material's strength depending upon its distribution inside the base metal. However, in this particular case, the SEM micrographs showed a typical interlocking of aluminum and magnesium sheet between intermetallic compounds. Further, it is also seen that the weld width increased at higher plunge depth. Hence, it is inferred that with an increase in tool shoulder plunge depth, the failure load during lap shear tensile is also increased.

Tutar et al. (2014) have observed that increasing plunge depth enhances heat input and material mixing, which results in the broader stir zone, TMAZ, and HAZ. The increased welded zones gave higher lap shear tensile strength. However, increased heat input also promoted grain growth in weld nugget resulted in reduced hardness.

Two sheets of aluminum AA 5182-O are joined using friction stir spot welding at constant rotational speed and by varying pin plunge depth and shoulder plunge depth independently. Experimental results showed that there is no significant effect of pin plunge depth variation on the tensile shear strength, but varying shoulder plunge depth has a considerable influence on tensile shear strength. It is observed that with increasing shoulder plunge depth, the joint strength initially improved due to the flattening of the interface tip. This reduces the chance of crack initiation during tensile shear testing. However, a too high value of shoulder plunge depth further reduced the

strength because of excessive localized thinning of the top sheets promotes severe stress concentration (Bozzi et al., 2010).

Baek et al. (2010) have also observed the effect of changing tool penetration depth on the strength of the joint. Overlapping galvanized steel sheets are bonded together using friction stir spot welding over a varying range of tool penetration depth at a constant tool rotation rate. It is seen that as the penetration depth increased, the gap at the joint region decreased; thereby, the width of the weld increased. It is concluded that the tensile shear fracture load increases with increasing tool penetration depth due to the fact of increased bond width.

Friction stir spot welding is not limited to join only metallic materials. Some researchers have already joined polymer to polymer and metal to polymer successfully. In this context, Yusof et al. (2012) have joined aluminum alloy (A5052) to polyethylene terephthalate (PET) using FSSW. FSSW is applied at two different plunge depths with varying plunge speed. A slightly different kind of bonding mechanism is observed here. It is seen that some bubbles are forming at the center of the joint area due to high heat generation. The size of bubbles is larger and densely distributed at higher plunge depth. After conducting the tensile shear test on the welded samples, it is concluded that with an increase in tool plunge depth, the tensile shear strength is improved. It is believed that larger bubbles gave enough interfacial force, which caused the polymer to stick to the metal tightly.

Mitlin et al. (2006) have studied the effect of tool penetration depth on the lap shear strength in friction stir spot welded 6111 aluminum sheets. It is observed that the lap shear, tensile strength increased with increasing tool penetration due to an increase in the width of the partially metallurgical bond area under the tool shoulder. However, at excessive tool penetration, the generation of hole reduced the joint strength. A similar observation is made by Arici and Mert (2008), where friction stir spot welding is applied for polypropylene. It is observed that increasing tool penetration increases the temperature, which enhances the plastic deformation resulting in a sound joint.

Rao et al. (2015) have investigated the influence of tool rotation rate on mechanical property of friction stir spot welded AM60B with AA6022-T4. The lap shear tensile test suggested that with the increase in tool rotation rate, weld strength decreased. It is reported that a high tool rotation rate generates high frictional heat, causes a reduction in the viscosity of the material right under the tool shoulder and material adjacent to the pin in the keyhole region, which results in the

slippage between the tool and material rather than stirring. The material flow in a much-localized region results in reduced weld bond width. This decreased weld bond width results in poor joint strength.

It is reported by Bozzi et al. (2010) that higher rotational speed results in more intense stirring, which increases the size of the stir zone, but residual stress also developed due to high heat generation. The higher width of the stir zone strengthens the joint, while residual stress has a negative impact on the joint strength. Tensile shear test results also revealed that with an increase in rotation speed, the failure load initially increases, but after attaining a peak value, it further decreased.

Arul et al. (2008) examined the failure modes of friction stir spot welded 6111-T4 aluminum alloy sheets at different rotation speeds. Shear mode of fracture and mixed mode of fracture are predicted as the two modes of fracture in this case. It is observed that the mode of fracture is controlled by hook geometry, which depends on many factors, including rotational speed. Lap shear, the tensile test revealed that the failure load first increased then decreased with increasing rotation speed.

The variation in tool rotation speed affects the amount of heat generated due to friction. More frictional heat is generated at a higher rotation rate, which results in a larger bonded region. Hence improved strength is obtained at higher rotational speed (Pathak et al., 2013).

Bilici and Yükler (2012) have applied FSSW to join polyethylene sheets to investigate the influence of tool geometry and process parameters on the mechanical properties of the weld. Lap shear tensile test of the welded sample revealed that failure load increased initially with rotational speed due to larger bonded area developed by high frictional heat while further increase in rotation rate reduced the strength due to excessive residual stress on the top sheet.

The effective weld width greatly influences the weld strength, as reported by many. The effective weld width increases with an increase in tool rotation speed. It is also observed that greater this value leads to better joint strength. 6061-T4 aluminum alloy sheets are joined by friction stir spot welding (FSSW) for different duration time at a varying rotation speed. It is observed that the lap shear, the tensile strength of the welded sample increased with increasing rotational speed under any given duration time (Shen et al., 2013).

Yin et al. (2010c) have discussed the formation of the hook and its influence on the mechanical

properties of friction stir spot welded magnesium alloy AZ31 sheets. It is observed that the stir zone and bonded widths increased at higher dwell time. So it can be directly inferred that the lap shear tensile strength should increase. However, it is also observed that the angle of curvature of the hook region increases with increasing dwell time due to a more upward flow of material from the bottom sheet. A higher angle of curvature leads to lesser strength. Because of these two counteracting factors, the lap shear tensile strength revealed that the failure load initially increased, but later it is decreased with an increase in dwell time.

Bilici and Yükler (2012) have examined the behavior of high-density polyethylene sheets under the application of friction stir spot welding. It is observed that the heat input due to friction increased as the dwell time increased, which leads to larger weld width resulting in increased joint strength. The variation in temperature with dwell time showed that the temperature initially rises linearly with dwell time but becomes constant at a higher duration of dwell time. It is believed that the heat input and heat loss are almost balanced at a higher range of dwell time. Lap shear tensile test conducted on the welded samples also revealed similar characteristics by showing an initial rise in failure load, which saturated at higher values of dwell time.

Choi et al. (2011) have studied the formation of intermetallics and its influence on the mechanical properties of friction stir spot welded joints of 6K21 Al alloy and AZ31 Mg alloy sheets. It is seen that the lap shear tensile strength of the joint decreased at a higher duration time, which resulted from the thicker intermetallics formation at higher heat input.

Tran et al. (2009) have discussed the effects of processing time on strengths and failure modes of dissimilar spot friction welds between aluminum 5754-O and 7075-T6 sheets. Experimental results showed that the lap shear tensile strength increased after increasing processing time due to the increased size of the weld.

Lin et al. (2012) have reported that failure behavior is governed mainly by bond width in friction stir spot welding. The effect of various process parameters on the strength of friction stir spot welded Mg alloy AZ61 has been studied. Better strength is observed at higher dwell time due to the extended bonding area. However, at a very high dwell time, FSSW strength decreased due to grain coarsening.

Dashatan et al. (2013) have conducted an experiment to join two polymer sheets using friction stir spot welding. The influence of various process parameters is observed. Significant improvement on the lap shear tensile test is noted at a higher dwell period due to a larger nugget

formed by more heat generation.

Song et al. (2014) have closely observed the effect of hook feature on the failure mode under lap shear tensile testing of friction stir spot welded aluminum A6061-T6 sheets. It is seen that with an increase in plunging speed, the effective weld width decreased, and effective sheet thickness increased. The mode of fracture depends upon these two parameters. At lower effective weld width, joined sheets failed in shear fracture while tensile/shear mixed fracture is observed at lower effective sheet thickness. Further lap shear tensile tests conducted on the welded sheets showed initial improvement on the fracture load, followed by a slight reduction in failure load due to change in the mode of fracture.

Apart from various process parameters, the geometrical features on the tool such as pin profile and shoulder profile also influence the performance of sheet metal bonded by friction stir spot welding.

Lin et al. (2008) have investigated the failure modes of spot friction welds in lap-shear specimens of aluminum 6111-T4 sheets. Two types of tools are used; tool with a flat shoulder and tool with a concave shoulder. Experimental results revealed that lap shear tensile strength of the joint produced by a tool with the concave shoulder is higher than that for the flat shoulder. Optical micrographs of the cross-section showed a small weld size and thickness of the upper sheet near the weld resulted in reduced strength for the flat shoulder tool.

Yin et al. (2010) have observed the influence of changing pin profile on the lap shear tensile strength of friction stir spot welded dissimilar magnesium alloy (AZ31 and AZ91D) sheets. Three types of tools having different features of the pin have been used; threaded tool, three-flat/0.7 mm/threaded tool, and three-flat/non-threaded tool. A large number of samples are prepared at different rotation speeds for each type of tool. Lap shear tensile test results revealed that the entire threaded tools gave better joint strength than the non-threaded tool, and three-flat/0.7 mm/threaded tool gave maximum strength among all the threaded tools.

Bilici and Yükler (2012) have examined the lap shear tensile strength of high-density polyethylene joined by friction stir spot welding using six tools, each having different pin profiles. The pin profiles used in the particular experiment are straight cylindrical (SC), tapered cylindrical (TC), threaded cylindrical (TH), square (SQ), triangular (TR), and hexagonal (HG). Experimental results showed that the tool with a tapered cylindrical pin profile gave the best strength.

Pathak et al. (2013) have used two different tools with a circular pin and tapered pin to apply friction stir spot welding on aluminum-5754 sheets. It is observed that weld made by circular pin gave higher lap shear tensile strength because of less hook height and increased weld width formed due to higher heat input.

Hirasawa et al. (2010) have predicted the effect of tool geometry on plastic flow during friction stir spot welding using the particle method. In the particle method, the work-piece material is assumed to be composed of several particles, and the movements of these particles are computed through elastic-plastic deformation equations. The movement of the particles is used to calculate temperature change, which is further used to calculate the change in the yield strength. A significant influence of tool geometry is observed in material mixing. It is predicted that a triangular pin with a concave shoulder results in a joint with high strength.

It has also been observed that the tool with a threaded pin gives higher strength in comparison with a non-threaded tool, specifically at lower tool rotational speed. It is found that the presence of the thread on the tool pin promotes material flow resulting in a larger stir zone (Ikuta et al., 2012).

The FSSW joint strength is evaluated at varying process parameters by many researchers. The important findings are summarized in Table 1.2.

1.2.4.6 Advantages

FSSW process has several advantages, such as a very fast process, extremely low energy consumption, the ability to join a wide range of materials. In contrast with existing joining processes, the FSSW results in better performance under dynamic loading (Uematsu and Tokaji, 2009), lesser distortion, fewer environmental hazards, and no consumable parts are used.

Table 1.2: Summary of FSSW parameters and their influence on output parameters.

FSSW Parameter	Change	Effect	Reference
Plunge depth	Increase	Weld strength increases	Rao et al. (2015)
		Weld strength increases	Baek et al. (2010)
		Weld strength increases	Yusof et al. (2012)
		Weld strength first increases then decreases	Bozzi et al. (2010)
		Weld strength first increases then decreases	Mitlin et al. (2006)
		Weld strength increases and hardness decreases	Tutar et al. (2014)
Rotational speed	Increases	Weld strength first increases then decreases	Bozzi et al. (2010)
		Weld strength decreases	Rao et al. (2015)
		Weld strength first increases then decreases	Arul et al. (2008)

		Weld strength increases	Pathak et al. (2013)
		Weld strength first increases then decreases	Bilici and Yukler (2012)
		Weld strength increases	Shen et al. (2013)
		Weld strength first increases then decreases	Bilici and Yukler (2012)
Dwell Time	Increases	Weld strength first increases then decreases slightly	Yin et al. (2010c)
		Weld strength first increases then remains unaffected	Bilici and Yukler (2012)
		Weld strength decreases	Choi et al. (2011)
		Weld strength increases	Tran et al. (2009)
		Lap shear tensile strength improved	Dashatan et al. (2013)
Plunge speed	Increases	Weld strength increases	Song et al. (2014)

1.2.4.7 Disadvantages

Usually, all the FSSW joints consist of a characteristic keyhole unless the tool is pinless. The presence of a keyhole reduces joint strength significantly. Nguyen et al. (2011) have predicted the variation of material properties in the welding zone of friction stir spot welded AA6061-T6 sheets. It is seen that the hardness, yield strength, and UTS values are least in the heat-affected zone nearest to the thermo-mechanically affected zone. Results obtained by finite element modeling of the welded specimens under different loadings such as shear-tension, peel-tension, and cross-tension revealed that the mode of failure is button pullout in every case.

Several modifications have been made in conventional friction stir spot welding, such as refill FSSW, pinless FSSW, and swing FSSW to remove keyhole from the joint, and it is continually developing (Yang et al., 2014).

1.2.4.8 Applications

The FSSW process is widely used in the manufacture of automobile hoods and assembling door panels in automobiles.

1.2.5 Introduction to sandwich sheet

A sandwich can be defined as a composite which constitutes of two faces, or skins, separated by and linked to a core that is less stiff and less dense (Gibson and Ashby, 1997). The thickness of the core material is usually higher than the faces. Kim & Yu (1997) have reported that to achieve structural integrity across the panel thickness, adhesives are used at the interfaces.

1.2.5.1 Background of sandwich sheet

In the past decades, the application of lightweight materials and lightweight structures has

drawn significant attention due to the gradual requirement of fuel savings and structural weight reduction in industries (Liu and Xue, 2013). Researchers started describing the behavior of sandwich structure theoretically after World War Two (Akour and Maaitah, 2010). It is reported that the aluminum/plastic/aluminum sandwich sheets have generated considerable interest in the transportation sector as potential light-weight materials for the body panels because of their high specific strength, impact resistance, sound-deadening properties, and damping resistance (Kim et al., 2009). Honeycomb has been used widely for aircraft construction for a wide range of temperature exposures, including those made of aluminum alloys, stainless steel, and glass fiber reinforced phenolic and polyimide (Kim and Yu, 1997). In addition to weight saving, it also reduces the requirement for the number of additional processes. Despite great advantages, there are many limitations, also like joining sandwich sheets, mainly limited to mechanical fastening or adhesive bonding (Salonitis et al., 2013).

1.2.5.2 Fabrication

Sandwich sheets can be prepared by many techniques such as roll bonding, warm roll bonding, and hot pressing. But the selection of the appropriate fabrication process is very important since the significant difference in sandwich behavior is observed as the fabrication method changed (Carradò et al., 2011). Some of the processes are described below.

(a) Roll bonding: Shin et al. (1999) have applied roll bonding to fabricate Al/PP/Al sandwich sheets where pre-rolled polypropylene sheet is used as core material. In between the core and skin layers, a sheet type ethylene-vinyl acetone (EVA) adhesives is used to get good bond strength. In the roll bonding process, the skin and core layers are stacked in overlapped conditions and passed through a rolling mill. The application of mechanical pressure integrates all layers together at the exit of the rolling mill.

(b) Warm roll bonding: Mousa and Kim (2015) have prepared AL1100/PU/AL1100 by warm roll bonding. The process slightly differs from the roll bonding process. No adhesive is used for the process, and bonding between each component is achieved by making modifying the faying surfaces and preheating. The aluminum strips and polyurethane (PU) sheets are cut into the same length and width. After cutting, all the surfaces are properly cleaned by using ethyl alcohol. Sandpaper is used to make the inner surface of the metallic sheets slightly rougher. The bonding is performed immediately after sanding. The preheating of aluminum samples were done. Then, each sample is assembled by inserting the PU sheet between the two aluminum strips and preheated for some additional time. The preheated overlapped sheets are then passed through the

rolling mill to make the sandwich.

1.2.5.3 Process parameters and their influence

The mechanical properties and formability of sandwich sheets are determined by a number of factors, including the composition and characteristics of the individual constituents, the forming methods, loading and environmental conditions, and the geometry of the final products as well as the way how they are combined together (Kim and Yu, 1997). Further, it is reported that the forming properties of layered sandwich plates are dependent on the geometry of the tools as well as the dimensions of the samples (Sokolova et al., 2012).

Parsa et al. (2010) have evaluated the limiting draw ratio of polypropylene core sandwich sheet and found that increasing core layer thickness leads to poor formability. Liu et al. have used polyethylene core to fabricate sandwich sheets, and better formability is achieved as compared to the monolithic sheet (Liu et al., 2013).

Weiss et al. (2007) investigated the influence of temperature on the forming behavior of A1/PP/Al sandwich sheet through shear and tensile tests, four points bend, and channel tests. It is concluded that the core material properties influence the forming behavior of the metal/polymer laminates in some, but not all, forming processes.

It is reported that the load-carrying capacity of the sandwich panel can be increased by increasing core stiffness since yielding started in the face of the sheet before the core material, and hence more load is transferred from core material to the sheet metal (Akour and Maaitah, 2010).

The tensile properties of aluminum/polypropylene/aluminum (Al/PP/Al) sandwich sheets are examined at room and elevated temperatures. It is observed that the sandwich sheet with hard skin and low-volume fraction of the polypropylene core have better tensile strength than the sandwich sheet with soft skin and a high-volume fraction of the polypropylene core. Also, at elevated temperatures, the sandwich sheet with hard skin showed a much smaller work hardening rate than that with soft skin at elevated temperatures. It is inferred that the influence of temperature on the tensile strength of the sandwich sheet with a high-volume fraction of polypropylene core is more significant than that with a low-volume fraction of polypropylene core (Shin et al., 1999).

Sokolova et al. (2012) have investigated the effect of core material thickness on deep drawability of 316L/PP–PE/316L sandwich sheet. It is observed that as the thickness of the polymeric core layer increases, drawing depth decreases initially because of high resistance to

deformation due to the overall increased thickness of the sandwich. But after crossing critical thickness, the drawing depth further improved because of the slight insertion of harder skin material into a relatively much softer core, thereby decreasing the stresses in the critical zones of the metal skin.

Parsa et al. (2009) predicted the influence of core material fraction on the limiting draw ratio (LDR) in Al/PP/Al sandwich sheet materials. It is concluded that with an increase in polymer core thickness, the LDR decreases.

Harhash et al. (2014) have also confirmed that the core thickness has a remarkable effect on mechanical properties. They have used low carbon austenitic stainless steel 316L for skin and a commercial polypropylene–polyethylene (PP–PE) copolymer foil as a core sheet material. After conducting tensile tests on the prepared sandwich sample, it is concluded that the yield strength (YS) and the ultimate tensile strength (UTS), as well as Young's modulus (E), decrease with increasing the thickness of the core.

Liu and Xue (2013) have conducted hemispherical punch tests to investigate the formability of AA5052/polyethylene/AA5052 sandwich sheets. It is concluded that increasing polyethylene core thickness improves the formability of sandwich sheets. They have further examined the influence of lubrication on AA5052/polyethylene/AA5052 sandwich sheets. Two lubrication conditions are applied to the punch–stretch tests to examine the influence of lubrication. The friction coefficient decreases in the order of dry, polytetrafluoroethene film. It is seen that the maximum dome height of the sandwich sheet and the maximum punch load increased with improving the lubricant condition.

Liu et al. (2012) have concluded that the interface condition between skin sheets and core materials also influences the forming behavior of sandwich sheets significantly. They predicted that with an increase in the interfacial adhesion strength, the formability and the FLD of AA5052/polyethylene/AA5052 sandwich sheet has improved.

Weiss et al. (2004) have investigated the effect of core thickness on the wall spring-back for steel/polymer/steel (SPS) laminates during draw bending. It is concluded that the spring-back reduced as the polymeric core thickness increases. Experiments are further carried out to examine the influence of core material strength on the wall spring-back. Polyvinyl chloride (PVC) and Polypropylene (PU) are used for the particular case. Experimental results showed that the PU cored laminates have a lesser wall spring-back than PVC cored SPS laminates. It is believed that

more volume fraction of SPS laminates has undergone plastic deformation due to the lower yield strength of PU.

An attempt is made to predict the failure of sandwich panels during hydro-forming using finite element simulation. It is seen that de-lamination could occur (Wang and Yang, 2013). Sokolova et al. (2012) have predicted that failure location in 316L/PP–PE/316L sandwich sheet during deep drawing. It is concluded that the failure occurred in all samples in the outer metallic sheet in the transition region between the head and edges of the cup. It is concluded, that these regions are the ones with the highest stresses in the material.

The effect of process variables on the properties of the sandwich sheet investigated by many researchers is summarised in Table 1.3.

Table 1.3: Summary of process variables in sandwich sheets and their influence on output parameters.

Process variables	Change	Effect	Reference
Stiffness of core material	Increases	The load-carrying capacity of the sandwich increases	Akour and Maaitah (2010)
Hardness of skin material	Increases	The load-carrying capacity of the sandwich increases	Shin et al. (1999)
Thickness of core material	Increases	Deep drawability decreases initially then increase slightly	Sokolova et al. (2012)
		LDR decreases	Parsa et al. (2009)
		Yield strength and UTS decreases	Harhash et al. (2014)
		Formability of sandwich sheets increases	Liu et al. (2013)
		Springback of sandwich sheet reduces	Weiss et al. (2004)
Lubricant condition	Improved	Maximum dome height increased, Maximum punch load increased	Liu et al. (2013)
Interfacial adhesion strength	Increased	FLD of sandwich sheet improved	Liu et al. (2012)

1.2.5.4 Advantages

The sandwich sheet poses many advantages such as exceptionally high stiffness to weight ratio, greater bending rigidity, increased mechanical damping, increased acoustical damping, reduced thermal conductivity, and reduced electrical conductivity. The sandwich sheet application resulted in many advantages such as excellent weight reduction, reduced noise, improved dent resistance, and better appearance of the surface—these benefits achieved with existing manufacturing

processes with minor modifications. Apart from significant weight reduction, sandwich sheets also provide many advantages such as better formability (Kim et al., 2003) and reduced noise and vibration (Rao, 2003).

1.2.5.5 Disadvantages

Difficult to join, damage detection is very difficult in the service life, the application is limited to secondary structures, and repair during service is difficult and ineffective are some of the disadvantages associated with the sandwich sheets.

1.2.5.6 Applications

It is widely used in automotive body panels and military and commercial aircraft (Rao, 2003). Some of the notable examples are the bonnet of Volkswagen Lupo, top floor panels in the new Audi A2, and outer panels of Alleweder Velomobile (Burchitz et al., 2005). Palkowski and Carradò (2014) have found the use of HYLITE in Audi A2, which is a polypropylene core aluminum sandwich. The application of HYLITE resulted in many advantages such as excellent weight reduction, reduced noise, improved dent resistance, and better appearance of the surface. The application of lightweight polymer core sandwich sheets in automobile industries has increased in the last few decades due to their lightweight characteristics (Burchitz et al., 2005). These sandwich sheets are mainly used to fabricate the automobiles' doors, fenders, and interior panels (Chao et al., 1994). The sandwich sheet's specific application is first seen in automobiles in Audi A2, where an aluminum/polypropylene/aluminum sandwich system is fully used to fabricate the foot space floor panels (Carradò et al., 2011).

1.2.6 Joining of sandwich sheet

Due to the diverse properties of skin and core material, the joining of the sandwich sheet is difficult. Most of the permanent joining techniques used for metals come under fusion welding. The same technique cannot be directly employed to join metals to polymers because of the poor solubility of metal in the polymer (Filho and Santos, 2009).

A few attempts are made to assemble or join sandwich sheets with other materials and other sandwich materials. The joining of the sandwich sheet by laser welding is analyzed by Salonitis et al. (2010) using finite element modeling. It is found that at the core layer, the temperature reached above the evaporation temperature of the polymer resulting creation of voids between two metallic skins. This further reduces the acoustic and damping properties of the material ending with limited

applicability.

Pickin et al. (2007) attempted to join polymer core sandwich sheets by self-pierce riveting (SPR). Despite successful joining, non-uniform deformation of metallic skin, tail buckling, and cavity formation are some of the drawbacks in SPR, which creates a poor joint. Apart from joining sandwich sheets, considerable research activities are focused on joining metal to polymer also. Katayama and Kawahito (2008) have developed a laser direct joining process of metal and plastic lap plates. But the process involves too many parameters and is not environment friendly. Balle et al. (2007) have applied ultrasonic spot welding to join aluminum to CFRP. However, the process is only applicable to the joining of small parts. Friction riveting is another technique successfully applied by Amancio (2007) to join aluminum with polyetherimide. Filho and Santos (2009) have reported that mechanical fastening, riveting, and adhesive bonding are other joining metal methods to the polymer. However, the requirement of additional consumable materials and surface preparation of parts are the drawbacks of these processes.

Salonitis et al. (2010) have done a finite element analysis of laser welding of sandwich sheets. Evaporation of polymer takes place due to overheating. This resulted in the formation of voids leading to loss of damping property. Gower et al. (2006) investigated spot welding of the metal-polymer sandwich by pulsed laser welding. In order to prevent excessive thermal degradation of the polymer, a high cooling rate is required. Nevertheless, proper control on cooling is difficult due to the high power of the pulsed laser.

The research details related to the sandwich sheet's joining techniques are limited only to the literature discussed above. Welding of aluminum-polymer sandwich is rather more difficult than other metal-polymer composites because aluminum itself is not suitable for fusion welding (Barnes and Pashby, 2000). Moreover, the rapid formation of the oxide layer, high thermal and electrical conductivity of aluminum alloys makes it unsuitable for resistance spot welding (Hao et al., 1996). Thus, the presence of polymer and aluminum creates challenges in finding suitable joining technique.

Ultrasonic Spot Welding (USW) is successfully applied by Balle et al. (2007) to join Al99.5 with carbon fiber reinforced polymer. However, the process is limited to join small parts only. Joining the AA6082-T6 sheet with a polycarbonate sheet is also attempted by the clinching process (Lambiase, 2015). Friction-based Injection Clinching Joining (F-ICJ) technique is applied to join polyetherimide to AA6082. The successful joint is formed; however, preparation of holes on the

metallic surface and stud on the polymer sheet would impart additional cost and complexity in the process (Abibe et al., 2016). Other joining methods for polymer-sandwich hybrid structure involves adhesive bonding and mechanical fastening. Though adhesive bonding offers the advantage of the continuous joint, the requirement of extensive surface preparation and curing time makes it a time-consuming and costly process. Further, hazardous elements present in the adhesive creates health and environmental issues (Barnes and Pashby, 2000). Mechanical fasteners can also be used for joining thick core sandwich panels (Matteis and Landolfo, 1999). However, pre-drilled holes for mechanical fastening create stress concentration around the hole. Furthermore, consumable fasteners impart additional weight to the structures.

Tanco et al. (2015) joined the polymer core steel sandwich sheet by RSW, where a separate shunt tool is used to create an electrical connection between the metallic skins. Moreover, Al alloys pose inherent problems while using RSW (Hao et al., 1996). Furthermore, the fusion welding of metal to polymer is troublesome because of the poor solubility of polymer into metal. The direct joining of stainless steel to polyethylene terephthalate (PET) by laser is also attempted (Katayama and Kawahito, 2008), but there are several parameters to control to obtain a successful joint.

Ozlati et al. (2019) used additive manufacturing-based joining techniques to join AA5083 and polypropylene sheets by filling a prefabricated hole with molten polymer, resulting in mechanical interlocking. However, the preparation of a predrilled hole before the joining makes it expensive and time-consuming. Mechanical fastening is another possibility to join sandwich sheets, which is also time-consuming and weight adding, making it unsuitable (Matteis and Landolfo, 1999). Hence, the selection of joining techniques for the sandwich sheet depends on its quality and whether it can be done in a single-stage or not.

FSSW of sandwich sheet

In comparison to FSSW of the bimetallic sheet, the FSSW of the sandwich has become more interesting due to the presence of a polymeric material in between two metallic sheets. The mechanical behavior of polymer core sandwich sheet during FSSW is not investigated critically in the existing literature, though sufficient study has been done in FSSW of metal to metal and polymer to polymer systems.

Since the ongoing activities reflect the application of FSSW of polymer sheets, it is proposed as a good alternative for spot joining of polymer core sandwich sheets in the present work.

Moreover, critical experimental investigation on FSSW of the sandwich sheet is not available in the existing literature. The polymer core's presence makes the FSSW of sandwich sheets interesting compared to bimetallic lap joints. There is no attempt made to understand the effect of rotational speed, plunge depth, tool profile, etc., on the joint formation and mechanical performance after FSSW of sandwich sheets.

So far, FSSW has proven its acceptance in the joining of a wide variety of materials. Besides, it is also capable of joining materials having extreme property differences. Knowing the suitability of FSSW in the joining of aluminum and polymer, the process is applied to the HDPE core aluminum sandwich sheet. The FSSW involves the plunging of a rotating tool along the rotating axis into sheets in lap configuration and retracting back. In contrast with existing joining processes, the FSSW results in better performance under dynamic loading (Uematsu and Tokaji, 2009), lesser distortion, fewer environmental hazards, and no consumable parts are used.

FSSW and sandwich sheets are already used in automobile industries, but the FSSW of polymer core sandwich panel is not yet comprehensively investigated. Particularly, the metal flow pattern in the presence of polymer core during FSSW is unknown.

1.2.7 FE modeling of FSSW of sandwich sheet

During the FSSW of the polymer core sandwich sheet, the welding process differs with core and interface conditions, which eventually decides the sandwich sheet's post welding behavior. In order to understand the evolution of such effects, the real-time changes during the process need to be observed. Finite Element Analysis (FEA) facilitates understanding the joining process during FSSW. Bagheri et al. (2020) conducted FEA to investigate the effect of work-piece vibration during FSSW of AA5053 alloy. The visualization of material flow and strain distribution in the joint highlights the role of vibration in measuring the strain attained by the joint. Therefore, grain refinement occurs in the stir zone resulting in improved joint performance. Awang and Mucino (2010) identified the energy generation in FSSW of Al6061-T6 by FEA and reported that most of the energy generated comes from frictional work between tool and work-piece. Hirasawa et al. (2010) analyzed the material flow during FSSW by FEA and observed that material beneath tool shoulder flows downward, whereas it is upward at the shoulder periphery resulting in hook formation. Fanelli et al. (2012) developed a FE model to predict the mechanical behavior of the FSSW at changing joint property. Jedrasiak and Shercliff conducted FEA for small strain for quick prediction of heat generation in FSSW, thereby reducing computational cost (Jedrasiak and Shercliff, 2019). The FE tool is also helpful for analyzing delamination and other features of

sandwich sheets. Park et al. integrated Cohesive Zone Modeling (CZM) and FE code to understand the delamination behavior of the sandwich sheet in bending. The initial stiffness and critical energy release rate of the cohesive layer are observed to govern the delamination (Park et al., 2020). Salih and Hussein observed a positive correlation between core stiffness and load-carrying capacity of sandwich sheets using FEA (Akour and Maaitah, 2010). Parsa et al. (2009) studied the effect of changing the skin thickness of the sandwich sheet on its formability by numerical simulations.

1.3 Significance of work

In automotive industries, total weight reduction has become a prime concern for manufacturers to reduce fuel consumption and meet environmental legislation. It is observed that a wide variety of materials is developed for different components in automobiles to improve their overall performance. In this context, the use of lightweight aluminum components is extensively increased for automotive body panels. Of course, not all the materials can be joined using existing joining techniques because of intermetallic compounds and oxide formation. Hence, a large number of advanced joining technologies are also invented to join similar or dissimilar materials. In the past few decades, sandwich materials have drawn special interest from automobile manufacturers because of their great weight saving characteristics, good flexural rigidity, excellent formability, and considerable damping resistance. These sandwich sheets are usually made up of aluminum skin and a polymer core. Despite so many advantages, the implementation of sandwich sheets is still limited due to difficulties in joining by conventional joining technologies during assembly. Apart from joining difficulties, the de-lamination of sandwich sheets is also observed during various forming processes. Earlier attempts show that joining a sandwich sheet using fusion welding is not good because of excessive damage to the polymeric core material. Although CO_2 laser welding techniques are already developed to join two sandwich sheets together in butt weld configuration, in most cases single-point joining process is required for assembly purpose where two overlapping sheets are joined in lap joint configuration. However, many single-point joining techniques are already being used in auto industries, such as resistance spot welding, laser spot welding etc. However, resistance spot welding cannot be applied to polymer cored sandwich material since the polymer is an electrical insulator, and laser spot welding may vaporize the core material by keyhole formation. Nevertheless, these methods are inefficient when applied to aluminum sandwich sheets since aluminum itself is not suitable for both resistance spot welding as well as laser welding. The joining techniques using welding could be replaced by adopting mechanical joining like riveting and other similar techniques, but it enhances the extra weight and cost onto it. Similarly, another attempt was made to join sandwich sheets by self-pierce riveting

(SPR), but here some substrate defects are also generated due to the inability of the soft polymeric core to support the rivet tail during setting. Furthermore, the weight addition can be eliminated by applying the clinching process to join sandwich sheets, but it is again restricted to secondary joints where no high strength is required.

A newly developed joining technique using friction stir spot welding (FSSW), which is a process variant of friction stir welding, is successfully applied for joining aluminum sheets as well as polymer sheets. It is found that many defects like substrate formation, weight addition, and high cost of joining can be eliminated by using this non-traditional method of joining process. It is believed that the de-lamination of sandwich sheets during forming can also be avoided. Therefore, the friction stir spot welding (FSSW) process can also be adopted to join sandwich sheets.

1.4 Objectives of the thesis

The main objective of the present thesis is two-fold – (i) To analyze the influence of FSSW on the joining and forming performance of sandwich sheets, and (ii) To predict the joining and forming performance of sandwich sheets for efficient process design.

The important sub-tasks to achieve the objectives are

1. Understanding the FSSW of sandwich sheets at changing process parameters.
2. Understanding the FSSW of sandwich sheets at changing the quality of sandwich sheets.
3. Deriving optimum window for successful FSSW of sandwich sheets.
4. Comparative analysis of bimetal FSSW and sandwich FSSW.

Both joining and forming the performance of FSSW of sandwich sheets will be monitored. In joining, the micro-and macro-structure and joint quality indexes will be monitored. Forming performance will include mechanical tests like lap shear tensile test, cross tension test, peel tests etc., for quantifying the joint strength and strain at failure. Forming behavior will be analyzed by the uniaxial tensile test of the joints. Finite element simulations are performed in ABAQUS/Explicit (ver. 6.17) FE code to evaluate the mechanical behavior, material flow, and delamination of sandwich sheets.

1.5 Organization of Thesis

The thesis consists of seven chapters, which are organized as follows:

- The first chapter has provided an introduction and literature review of the FSSW process, sandwich sheet, FSSW of the sandwich sheet, significance, and objectives of the present work.

- Chapter 2 investigates the influence of rotational speed on the FSSW of the sandwich sheet.
- Chapter 3 presents the effect of plunge depth on FSSW of sandwich sheet
- In Chapter 4, the effect of varying plunge speed on FSSW of the sandwich sheet is presented.
- Chapter 5 demonstrates the influence of dwell time on the mechanical behavior of the FSSWed sandwich sheets.
- Chapter 6 presents the experimental evaluation and numerical simulation of FSSW of the sandwich sheet at changing the hardener/resin ratio of the core layer.
- Conclusions from the thesis work are presented in Chapter 7, followed by the scope for future work and references.

Chapter 2

Effect of rotational speed on friction stir spot welding of AA5052-H32/HDPE/AA5052-H32 sandwich sheets

2.1 Methodology

In this section, the FSSW trials, sample preparation, mechanical testing, joint characterization, and temperature measurement procedures are described.

2.1.1 FSSW and sample preparation

The present investigation is done on a pair of 2 mm thick AA5052-H32 rolled sheets as skin materials and 1 mm thick HDPE as the core layer. The present thickness geometry is not intentionally selected. Since the FSSW is never used before on sandwich sheets, the preliminary facts need to be established first. These facts would help in further research in FSSW of actual sandwich components. Therefore, the material variant is of more concern rather than the geometry of a sandwich sheet. Essentially the sandwich panels should be composed of metallic skin and a polymeric core. The materials in the present work are selected as per the availability. The metallic layers are not bonded to the polymer core before joining to avoid the effect of the adhesive on the joint performance. Amongaluminum alloys, the 5000 series received special attention due to its excellent corrosion resistance, better formability, and good weldability (Takeo, 2008). In Honda NSX, AA5052-O alloys are used in the inner portion of the hood, door, and trunk due to less spring-back and good surface finish (Muraoka and Miyaoka, 1993). AA5052 is non-heat-treatable. Therefore, it is strengthened by cold working at the expense of ductility. The AA5052-H32 has a good balance between strength and ductility, which is suitable for fabricating the inner panels of automobiles. It is a quarter hardened and stabilized magnesium-rich aluminum alloy. The mechanical properties of AA5052-H32 and HDPE obtained from tensile tests are listed in Table 2.1. For AA5052-H32, the ASTM B557M-15 standard is used for evaluating tensile properties and ASTM E517-00 is used for evaluating the plastic strain ratio. ASTM D 638 – 14 is used to prepare tensile specimens of HDPE. Three numbers of specimens are tested in each case to check the repeatability. All the tests are done on a 200 kN Universal Testing Machine operated by hydraulic loading (Model: UTE 20, Make: FIE). The cross-head speed is kept at 1 mm/min. and

all the tests are carried out at room temperature. The typical tensile behavior of AA5052-H32 and HDPE is shown in Fig. 2.1. The HDPE sheet has not failed, and the test is manually terminated when the load-extension curve becomes asymptotic. The energy dispersive X-ray analysis is done to obtain the chemical composition of constituting elements in AA5052-H32 (Fig. 2.2). The nominal composition of each component (in weight %) is given in Table 2.2. The chemical composition fits in the range mentioned for AA5052 in ASM Handbook Volume (ASM International, 1990).

Table 2.1 Mechanical properties of AA5052-H32 and HDPE sheets

Material	Rolling direction	Yield strength (MPa)	Ultimate tensile strength (MPa)	Uniform elongation (%)	Total elongation (%)	Strain hardening coefficient	Strength coefficient (MPa)	Plastic strain ratio
AA5052-H32	0°	155±1	215±1	7±1	9±1	0.16	356±3	0.62
	45°	147±2	206±2	9±1	12±2	0.15	327±4	0.68
	90°	148±1	209±1	8±1	13±0	0.16	333±1	0.85
HDPE*	-	-	29±0.5	17.4±2.4	-	-	-	-

*Not failed

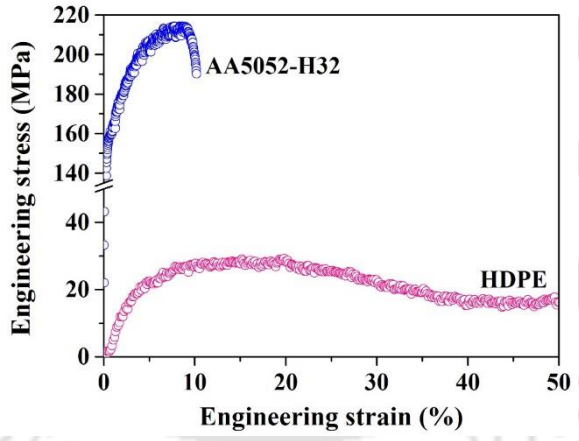

Fig. 2.1 Tensile behavior of AA5052-H32 and HDPE sheets

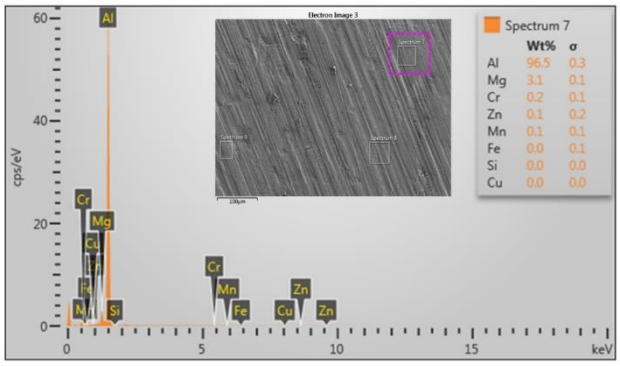

Fig. 2.2 EDX spectra of as received AA5052-H32

Table 2.2 Chemical composition of AA5052-H32 in weight %

Mg	Cr	Zn	Mn	Fe	Si	Cu	Al
3.2	0.23	0.12	0.08	0.20	0.05	0.03	Bal.

The sandwich structure is prepared by keeping AA5052-H32 as the outer skin and HDPE as the core layer. A tool made of H13 tool steel with a flat shoulder and straight cylindrical pin is selected to make entire FSSW joints in this study. The tool shoulder diameter, pin diameter, and pin height are 10 mm, 4 mm, and 3 mm, respectively. This particular tool has been selected because of the simplicity. Other tools with different shoulder and pin profiles can also be selected.

The FSSW is conducted on a three-axis FSW machine designed and developed by ETA Technologies, Bangalore, and the Indian Institute of Science, Bangalore. The FSSW of sandwich sheets is performed at six different tool rotational speeds, keeping all other process parameters fixed. In the case of bimetallic sheets, only the extreme levels of rotational speeds are considered for comparison. The selection of six rotational speeds is made based on several trials starting from 200 rpm up to 1000 rpm, at an interval of 200 rpm. No joining took place at 1000 rpm for the sandwich system. Hence the lower limit is fixed at 1000 rpm and the higher limit at 2000 rpm. However, even at 600 rpm and 800 rpm, joining is successful for the bimetallic system. But, to keep consistency in the analysis, all the rotational speeds are selected from 1000 rpm. Similarly, during tool plunge depth selection, joining did not take place for a sandwich system below 3.2 mm plunge depth. An increment of 0.2 mm is selected, and the upper limit is fixed at 3.8 mm since the thickness of the bimetallic system is 4 mm. The plunge speed and dwell time are selected cautiously based on existing literature on bimetallic FSSW. The final process window of welding parameters for the present work is shown in Table 2.3.

Table 2.3 FSSW process parameters followed in the present study

System	Tool rotational speed (rpm)	Tool plunge depth (mm)	Plunge speed (mm/min)	Dwell time (sec.)
Sandwich sheets	1000	3.6	8	15
	1200			
	1400			
	1600			
	1800			
	2000			
Bimetallic sheets	1200	3.6	8	15
	1800			

Five different types of samples are fabricated for sandwich sheets and bimetallic sheets to

perform FSSW. These include lap shear test samples, peel test samples, cross-tension test samples, uniaxial tension test samples, and microstructural characterization samples. The samples for the lap shear test, peel test, and cross-tension test are prepared according to AWS B4.0:2007 standard, while the last two are of non-standard type (Fig. 2.3).

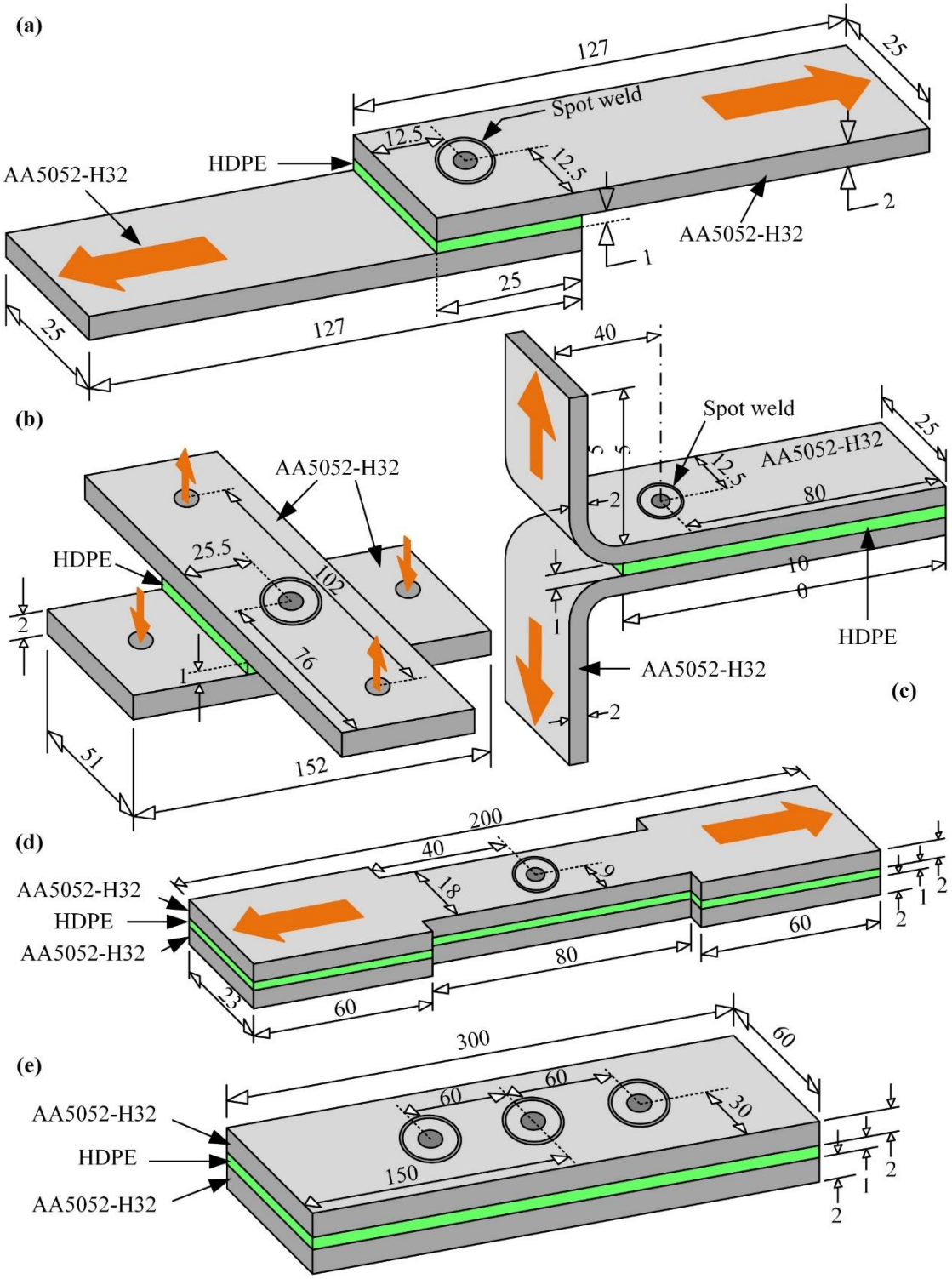

ALL DIMENSIONS ARE IN MM (NOT TO SCALE)

Fig. 2.3 Schematic drawing of specimens used for FSSW for (a) lap shear test, (b) cross-

tension test, (c) peel test, (d) uni-axial tension test, and (e) microstructural examination.

Before fabricating the FSSW joints, the polymer and AA5052-H32 sheets are properly cleaned to remove dirt and grease. Three sheets are put together, keeping polymer sheets in between at the appropriate position and clamped over the bed of the FSW machine. Here, it should be noted that the core layer is not bonded with metallic skin with the adhesive, and this is done to avoid any influence of adhesive on the joint behavior. After clamping, all the predefined set of parameters are entered through the computer screen and run the machine to fabricate the joint. Three samples are prepared at each set of process parameters for all five types of test specimens to check the repeatability.

2.1.2 FSSW joint characterization

The lap shear tests, cross tension tests, and peel tests are conducted on a 200 kN universal testing machine operated by hydraulic loading (Model: UTE 20, Make: FIE), while a 250 kN servo-hydraulic type universal testing machine (Model: UT-04-0250, Make: BISS) is used to carry out uniaxial tension test. All the tests are done at 1 mm/min cross-head speed and at room temperature. It is difficult to evaluate the actual load-bearing area in the lap shear test, cross tension test, and peel test. Therefore, the mechanical performance of the joint is evaluated by the peak load and extension obtained from tests. However, it is possible to estimate the load-bearing area in the uni-axial tensile test because the load is applied perpendicular to the joint cross-section. A typical value of the joint cross-sectional area is estimated by contour mapping. The estimated cross-sectional area is used to calculate the strength of the joint, which is compared with the strength of the base metal.

Macrostructural observations of welded samples are done at the joint cross-section. Perfectly polished surfaces are chemically etched with a solution containing 2 mL HF, 3 mL HCl, 5 mL HNO_3, and 10 mL H_2O at ambient temperature for 60-90 s. A Carl Zeiss make optical microscope is used to observe several macro features formed on the joint. The macro-structure is obtained by combining many photographs taken at 50× magnification.

Further stir zone microstructures of the sandwich and bimetallic sheet FSSW are also investigated for 1200 rpm and 1800 rpm. The microstructures are obtained by etching with the same chemical solution for 20-22 s. The average grain sizes are measured by the linear intercept method. The Vickers microhardness is measured on the joint cross-section across the joint width at two different levels of thicknesses (at the mid-thickness of the upper sheet and lower sheet) for both sandwich and bimetallic systems. The measurement is done on only one side of the keyhole,

assuming the weld symmetry. A load of 500 gf is applied for 10 s for the hardness measurements. The hardness measuring position is schematically shown in Fig. 2.4.

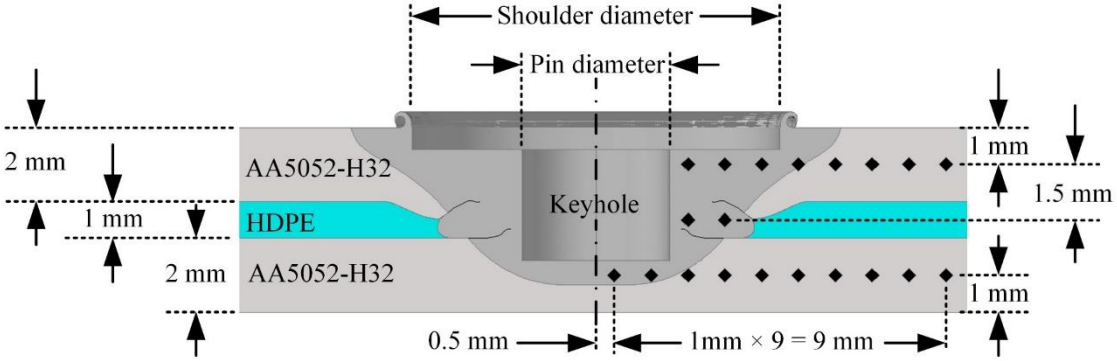

Fig. 2.4 Schematic view of micro-hardness measuring positions in the joint cross-section (not to scale)

2.1.3 Temperature measurement

In order to study the effect of the polymer during the FSSW of the sandwich sheet, it is important to obtain temperature distribution in the joint cross-section. Since it is difficult to attach the thermocouple inside the sandwich structure very close to the joint, the FSSW is done at the edge of the sandwich sheets. It is expected that the temperature developed in actual FSSW would be higher than FSSW at the edge. K type thermocouples are used to measure the temperature. The thermocouples are attached at the edge of the sheets by making holes of 1 mm diameter through the thickness of the sheets. Three thermocouples are attached to the upper sheet and three on the lower sheet. The gap between two adjacent thermocouples is kept 2 mm. The physical appearance of the FSSW at the edge of a sandwich sheet at different stages is shown in **Fig.** 2.5. It should be noted that during stirring, a large amount of material continuously comes out of the joint. The expelled material is a mixture of melted polymer and plasticized aluminum.

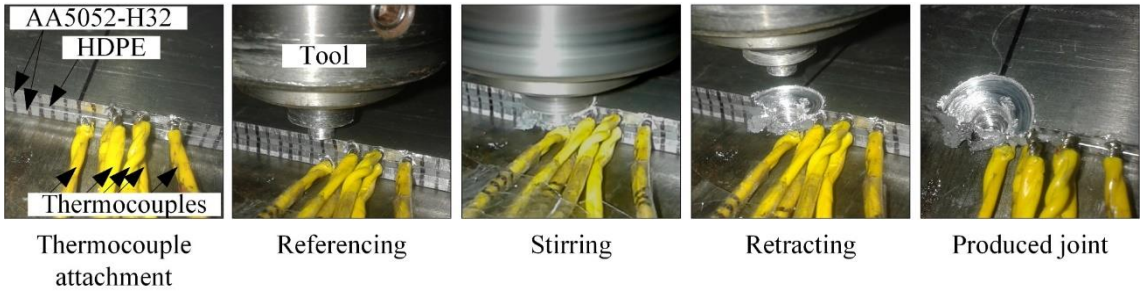

Fig. 2.5 Physical appearance of the FSSW at the edge of the sandwich sheet at different stages

An infrared (IR) camera is also used to measure temperature with the aim of proposing an

alternative method of temperature measurement. A comparative assessment is done between temperature measured by thermocouple and IR camera. Two extreme levels of each parameter are selected for comparison, assuming different heat input. The rotational speed, plunge depth, plunge speed, and dwell time are set at 1100 rpm, 3.2 mm, 4 mm/min. and 5 s respectively for lower level and 1500 rpm, 3.8 mm, 10 mm/min. and 20 s for a higher level. The observation is made on the upper sheet of the sandwich system. The IR camera is placed perpendicular to the tool axis at the nearest possible distance, as shown in Fig. 2.6a. The IR camera captures the infrared images in live mode from the beginning of the process to the moment when the joint comes to the ambient temperature. In order to measure temperature distribution across the joint, an accurate value of material emissivity should be known. The index converts the infrared image pattern into the amount of radiated energy from the object. The emissivity value for aluminum is taken as 0.35 (Raikoty et al., 2005). For HDPE, it is considered as 0.95 (Genna et al., 2017). The temperature at any location across the joint is continuously varying during the process; hence, the peak temperature attained at every point is taken for analysis. To obtain the peak temperature distribution across the joint, 3 numbers of virtual thermocouples are placed across the upper and lower sheets' mid-thickness, as shown in Fig. 2.6b. The locations of temperature measurement in the IR camera and with thermocouple are the same.

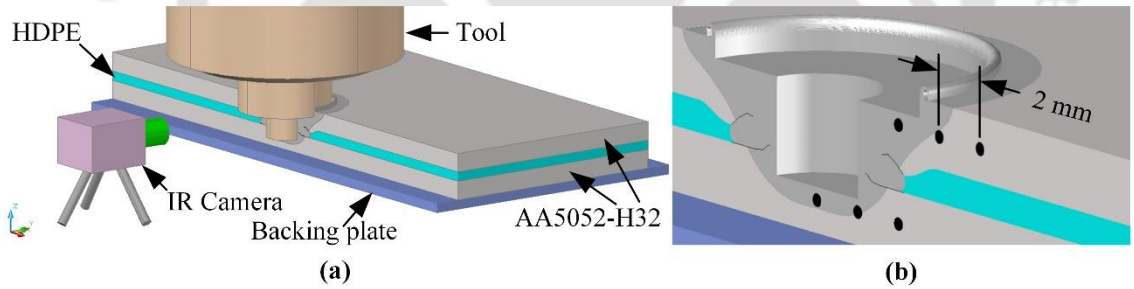

Fig. 2.6 Schematic representation of (a) IR camera position and (b) virtual thermocouples position at the sample edge (not to scale)

2.2 Results and discussion

2.2.1 Hook formation

The macrostructural examination of joint cross-section reveals two distinct features during FSSW of bimetallic and sandwich sheets, as shown in Fig. 2.7. Two hooks form in the case of the sandwich sheet, as compared to only one hook fully developed in the bimetallic sheet. Though the formation of two hooks gets initiated in the bimetallic case, the propagation of the upper hook is fully arrested. The formation of one hook is confirmed in the existing literature for bimetallic sheets. Since aluminum alloys are prone to oxide formation, the presence of an oxide layer at the

two sheets interface is obvious. The hook formation occurs due to the breaking up of oxide film present at the two sheet interface by the action of stirring. Since only one interface is present in the case of bimetallic sheets, the formation of a metallurgical bond between two sheets exhibits a single hook, as reported by Badarinarayan et al. (2009). FSSW of two dissimilar materials also exhibits only one hook (Rao et al., 2015). On the other hand, the presence of oxide film on two interfaces (one between the upper sheet and core and another between core and lower sheet) results in the formation of two hooks for sandwich sheets. Further, a part of the stirred material flows into the polymer core, which appear as an extruded zone for the sandwich sheet, as shown in Fig. 2.7b. The volume of expelled flash for the sandwich sheet is much lesser than the bimetallic sheet due to the fact that more metal can be accommodated in the soft polymeric region during plunging.

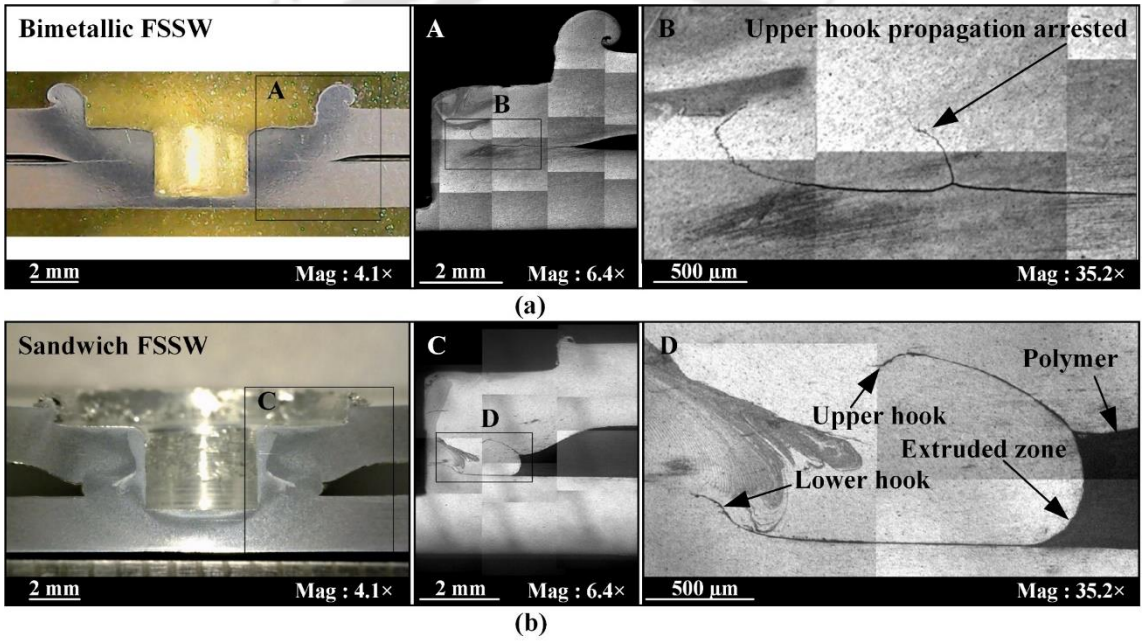

Fig. 2.7 Formation of the hook in (a) bimetallic and (b) sandwich sheets during FSSW

Fig. 2.8a shows the macroscopic view of joint morphology produced after FSSW of sandwich sheets. Five geometrical indexes are selected to observe the rotational speed effect. These are effective upper sheet thickness, upper bond width, upper hook height, lower bond width, and lower hook height. The effective upper sheet thickness is the shortest distance between the sheet surface on which the shoulder touches and the upper hook. This feature is significant when the failure occurs through the upper sheet. Badarinarayan et al. (2009) indicated that larger effective upper sheet thickness gives higher resistance to the loading. The upper bond width is the distance of the hook tip to the keyhole periphery. The upper hook height is the vertical distance of the hook tip from the hook initiation point. The lower bond width is the horizontal distance of the hook tip from

the keyhole periphery. The lower bond width is the vertical distance of the lower hook tip from the lower interface. It is reported by Yin et al. (2010) that a combination of larger effective upper sheet thickness, larger hook width, and smaller hook height can produce a joint with higher strength. However, the individual effect of upper and lower hook geometries is not available in the existing literature as there is not much work done on sandwich sheets.

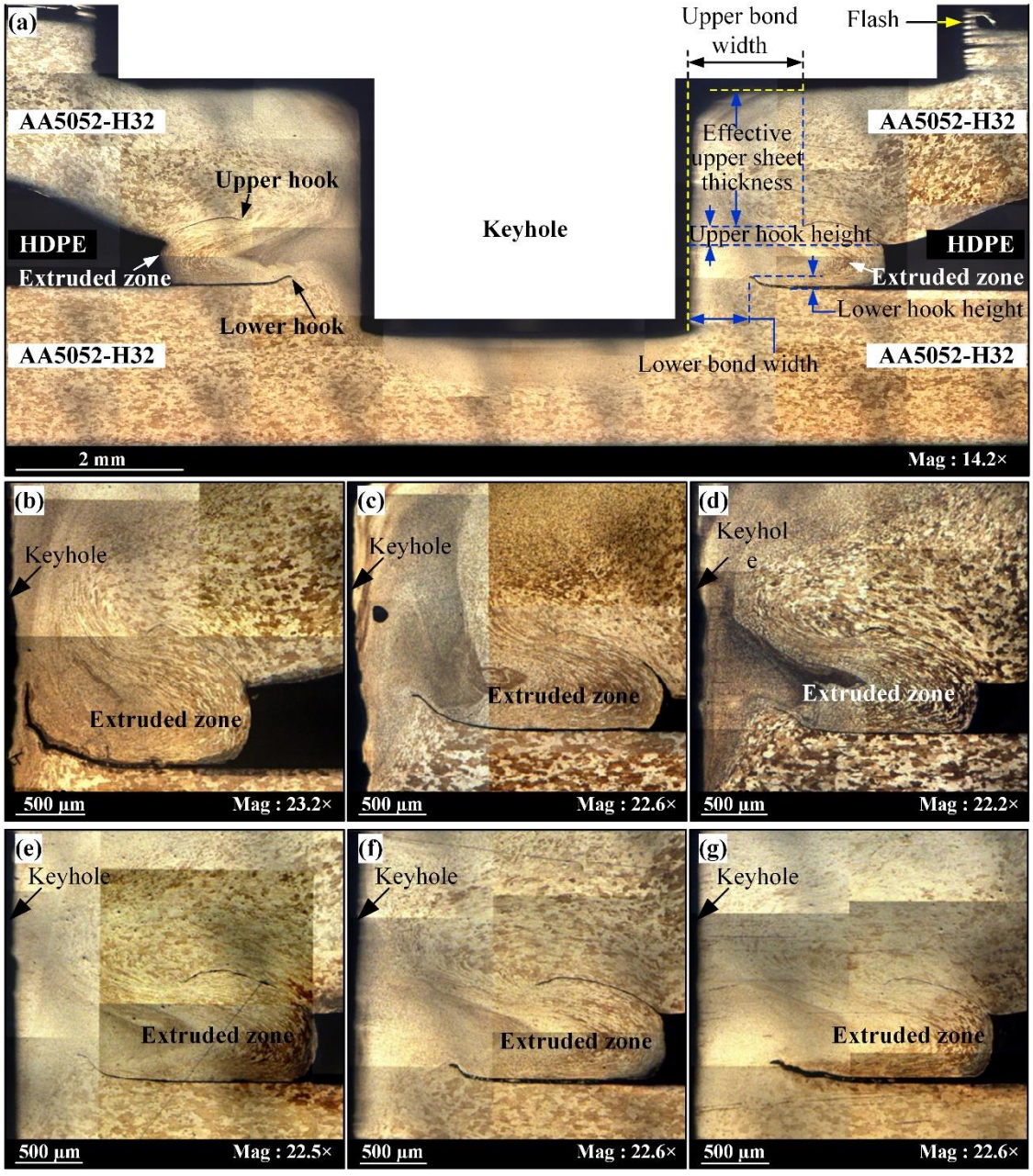

Fig. 2.8 (a) Optical macrograph of joint cross-section of sandwich sheet during FSSW and at hook formation region at (b) 1000 rpm, (c) 1200 rpm, (d) 1400 rpm, (e) 1600 rpm, (f) 1800 rpm, (g) 2000 rpm

The macrographs of the joint cross-section at the hook formation region for FSSW of the

sandwich sheet at six different rotational speeds are shown in Fig. 2.8 (b-g). The upper and lower hook tip shifts away from the keyhole periphery as the rotational speed increases. This is attributed to the larger bonded area of the joint at a higher rotational speed. Furthermore, the lower hook gets flattened as the rotational speed increases. The flattening of the lower hook occurs due to increased plasticized metal flow into the core region, which suppresses the vertical displacement of lower hook. The various weld geometries measured in the joint cross-section of sandwich sheets and bimetallic sheets are shown in Table 2.4.

The upper bond width is always larger than the lower bond width in all the cases suggesting a larger bond width near the upper hook than near the lower hook. It is investigated by Awang and Mucino (2010) that the major part of the total heat generation during FSSW comes from friction between tool and work-piece. The shoulder contact area is approximately 69 % more than the pin contact area in the present work. Therefore, more frictional heat is generated at the shoulder work-piece interface than at the pin work-piece interface resulting in larger bond width near the upper hook.

The influence of rotational speed on these features is also presented in Table 2.4. The upper and lower bond width increases with increasing rotational speed. At the same time, the upper and lower hook height decreases with an increase in rotational speed. The bond width increase indicates an increase in bonding width near the hook. Bozzi et al. (2010) observed that more frictional heat is generated at higher tool rotational speed due to extensive stirring, which helps in the formation of larger bonded width. The larger bonded region is associated with a larger bond width due to partial merging of the hook in the extruded zone.

Table 2.4 FSSW weld geometrical measurements of the joint morphologies.

System*	RPM	Upper bond width (µm)	Lower bond width (µm)	Upper hook height (µm)	Lower hook height (µm)	Effective top sheet thickness (µm)
	1000	934	159	306	682	1652
	1200	1201	507	527	175	1558
	1400	1236	614	400	222	1547
	1600	1301	705	308	109	1639
	1800	1343	612	290	165	1623
	2000	1412	615	229	141	1614
BM	1200	2119	1192	404	119	957
	1800	2010	1043	347	360	1065

* SW: Sandwich sheets; BM: Bimetallic sheets

The mechanism of change in hook dimensions by merging in the extruded zone is schematically illustrated in Fig. 2.9. By virtue of tool rotation, a part of the material near the tool surface gets heated and plasticized, and eventually, a boundary between plasticized metal and non–plasticized metal occurs. This boundary also separates the hook from the extruded zone. As the rotational speed increases, the amount of plastically deformed material increases, and the boundary displaces outward. With the outward movement of the boundary, a portion of the hook gets merged in the extruded zone, which results in bond width enlargement and hook height reduction. As shown in Fig. 2.9, it is clear that $w_1' > w_1$, $h_1' < h_1$, $w_2' > w_2$, and $h_2' < h_2$; where w_1, h_1, w_2, h_2, and w_1', h_1', w_2', h_2' are the values of upper bond width, upper hook height, lower bond width, lower hook height respectively when the boundary lies nearer and farther to the keyhole. Another important feature is the effective upper sheet thickness. However, it remains almost unchanged with the rotational speed with a mean variation of 3.7%.

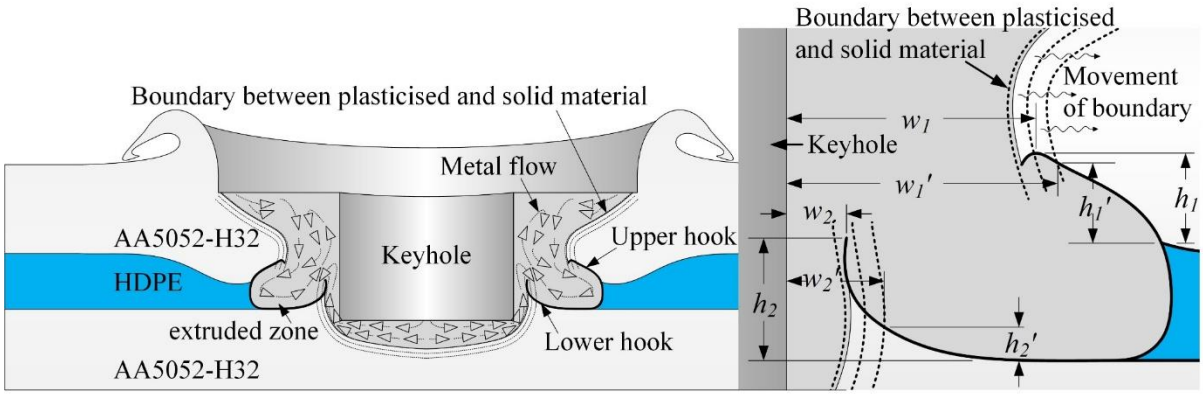

Fig. 2.9 Mechanism illustration of hook merging into the extruded zone

In comparison with the FSSW of sandwich sheets, bimetallic sheets show a larger bond width. In the case of sandwich sheets, the stirred material gets accommodated in the soft polymeric core more easily than spreading through the metallic skin. This results in the formation of an annular extruded zone and the closer existence of the boundary between plasticized and solid material. On the other hand, in the case of bimetallic sheets, since there is no polymer, most of the stirred material spread outward through the metallic skins only. Hence, the boundary between plasticized and solid material displaces away from the keyhole by a large distance, thereby merging a large portion of the hook into the stirred material. Furthermore, the lower hook height for bimetallic sheets is much lower than the sandwich sheets because of the seizure of the lower hook's upward movement due to the absence of a soft polymeric core.

The polymer surface's physical appearance near the joint at two extreme rotational speeds is

shown in Fig. 2.10. The degradation of the polymer at 1800 rpm is more because of higher heat generation.

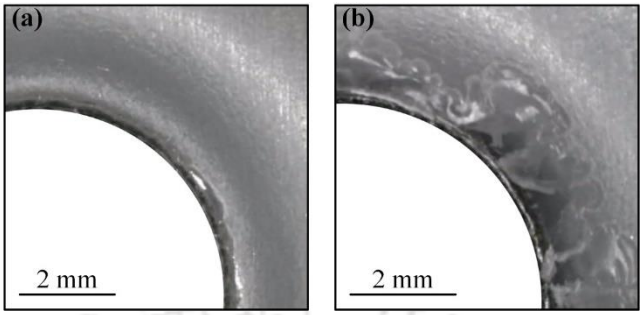

Fig. 2.10 Physical appearance of polymer surface at (a) 1200 rpm and (b) 1800 rpm

2.2.2 Temperature evaluation

The infrared image of the joint at the end of the process is shown in Fig. 2.11a. A higher temperature exists near the keyhole. The difference in the peak temperature recorded by the IR camera and thermocouple is shown in Fig. 2.11b for a particular case. The thermocouple shows a lesser temperature than the IR camera. This is because of reduction in friction force between tool and work-piece due to the presence of holes for fixing thermocouple. This could also be due to the selection of emissivity of aluminum. However, the repeatability of thermocouple data is better. Hence thermocouple measurements are selected for further analysis.

The peak temperature distribution around the joint is shown in Fig. 2.11c, and d. The peak temperature near the keyhole of the sandwich system is above 133°C for both the rotational speeds. The melting point of HDPE is 140°C reported in (Capiati and Porter, 1975). In actual FSSW, the temperature developed is higher than that in FSSW at the edge. Therefore, it is believed that the a portion of HDPE core gets melted during welding which is displaced away from the weld zone through the interfacial gap between skin and core sheet. Furthermore, there is burning odour during welding, which suggest that little amount of the polymer evaporated. The amalgamation of molten polymer with metal near the pin and shoulder would result in the slippage between the tool and the work-piece. This results in a reduction in frictional heat generation. Also, the friction between metal and polymer is much lesser than metal-metal, so the frictional heat generated would be lesser. Furthermore, heat energy contributed from deformation of polymer would be lesser than the metal. This could have possibly reduced the peak temperature in the upper and lower sheet of the sandwich system than in the bimetallic system, as shown in Fig. 2.11c, d. Moreover, the maximum temperature attained at any location is higher for higher rotational speed due to intense

stirring. This is true for both sandwich and bimetallic sheets.

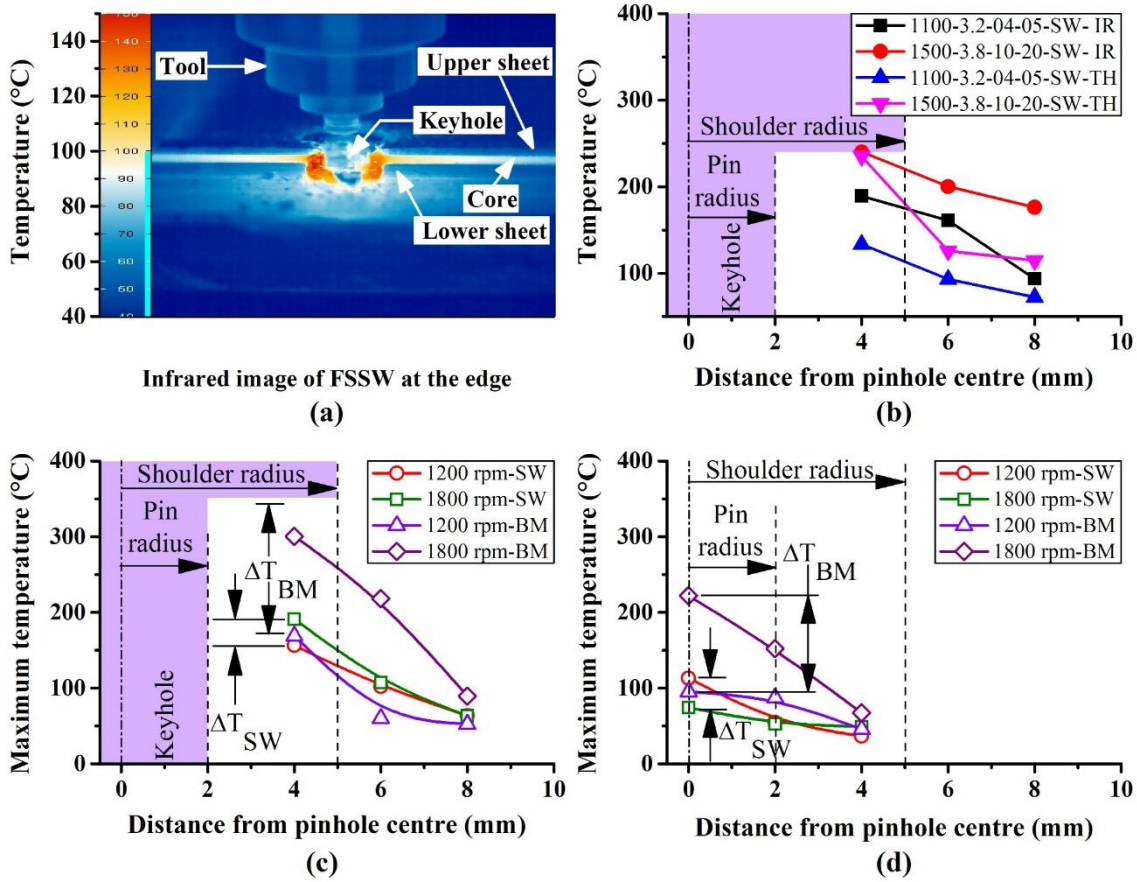

Fig. 2.11 (a) Infrared image of FSSW at edge; Peak temperature distribution at mid-thickness of (b) the upper sheet in SW, (c) the upper sheet in SW and BM, and (d) the lower sheet in SW and BM. Error variation in temperature = ± 13°C [SW: Sandwich sheets; BM: Bimetallic sheets; IR: Infrared; TH: Thermocouple]; the sequence in the legend in (c) is tool rotational speed-plunge depth-plunge speed-dwell time-type of sheet-method of measurement.

2.2.3 Grain size and hardness distribution

The stir zone microstructures of sandwich and bimetallic sheets FSSW at 1200 rpm and 1800 rpm are shown in Fig. 2.12a–f. The base metal microstructure is also presented. The grains in the stir zone are 4.2 µm, 14.6 µm for bimetallic sheets and 3.3 µm, 4.35 µm for sandwich sheets at 1200 rpm 1800 rpm, respectively. The grain size of the base metal is 22.5 µm. The fine grains in the stir zone are obtained due to dynamic recrystallization in all the FSSW cases. The stir zone of the sandwich sheet shows finer grains than bimetallic sheets at both rotational speeds due to the annihilation of grain growth at lower peak temperatures (Fig. 2.12f). The degree of heat input is very important, which decides the grain size in the stir zone. Zhang et al. (2011) have shown a coarser microstructure at higher rotational speeds for FSSW of 5052 aluminum alloy. Moreover,

in the sandwich and bimetallic sheets, slightly coarser grains are formed at 1800 rpm than at 1200 rpm due to higher peak temperature, as presented in Fig. 2.12b and d, respectively.

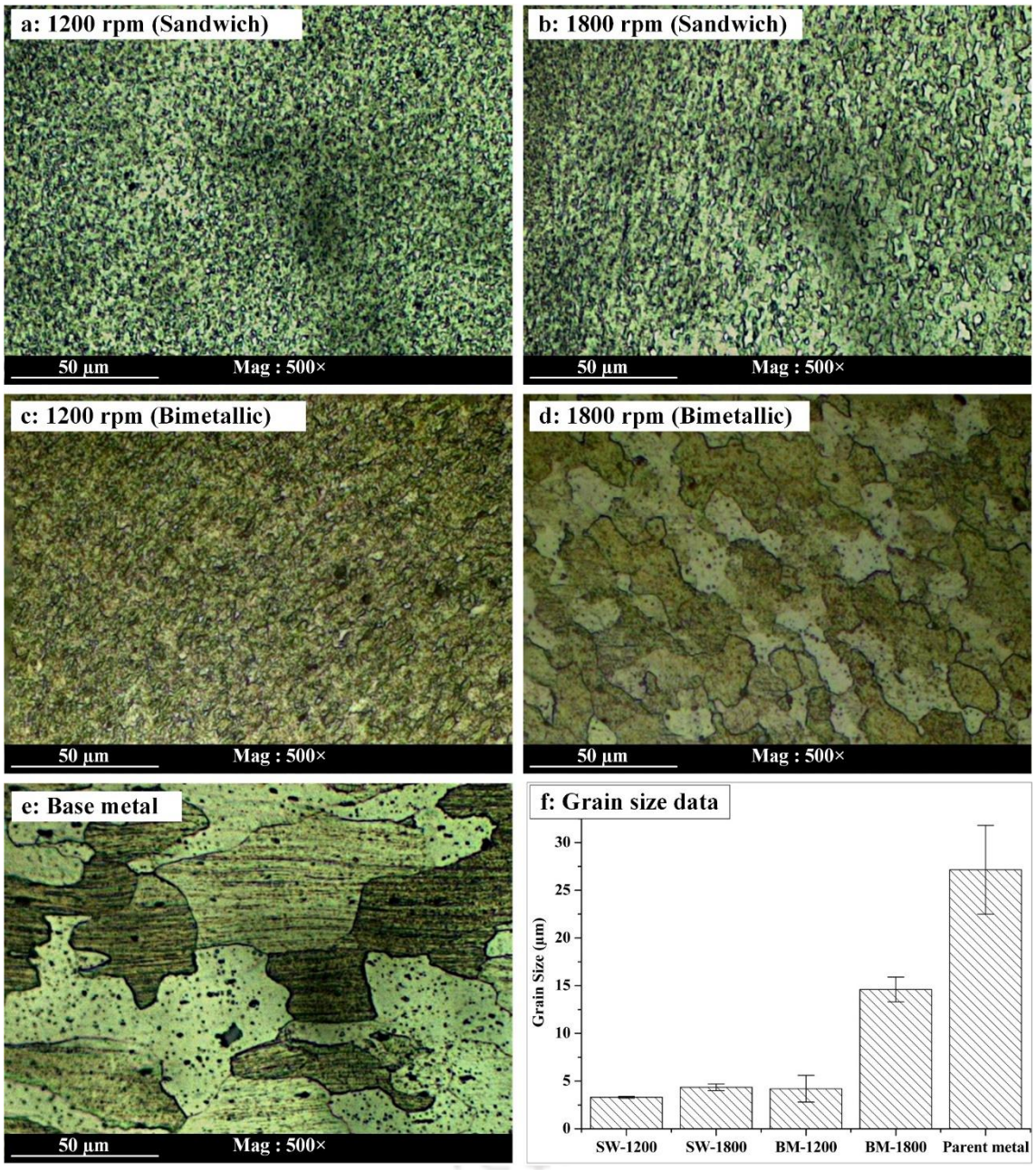

Fig. 2.12 Stir zone microstructure of (a) 1200 rpm-Sandwich, (b) 1800 rpm-Sandwich (c) 1200 rpm-Bimetallic, (d) 1800 rpm-Bimetallic, (e) base metal microstructure, and (f) grain size measurement [SW: Sandwich sheets; BM: Bimetallic sheets]

The hardness distribution on the joint cross-section at two different levels of thicknesses (at the mid-thickness of the upper sheet and lower sheet) for both the sandwich and the bimetallic systems is shown in Fig. 2.13a and b, respectively. The hardness near the keyhole is larger due to fine equiaxed grains in the stir zone (Fig. 2.12a–d). While moving away from the keyhole, there exists

a weak region in the upper and lower sheet of sandwich and bimetallic systems. This localized decrement in hardness is due to the softening as a result of the metallurgical recovery of the material. Kesharwani et al. (2014) have also reported that softening is caused by recovery due to thermal cycle in friction stir welding of AA5754-H22 and AA5052-H32. The hardness of as received AA5052-H32 is about 60-65 VHN. The hardness of HDPE is very low and difficult to measure in Vickers's Microhardness Tester. Literature reports a typical value of hardness of HDPE is about 5 VHN (Khodabakhshi et al., 2014).

For sandwich sheets, the softest region is about 0.5 mm inside the shoulder in upper sheet and 0.5 mm inside the pin in lower sheet as shown in Fig. 2.13a and Fig. 2.13b, respectively. On the other hand, the minimum hardness for bimetallic sheets is 0.5 mm outside the shoulder in upper sheet and 1.5 mm outside the pin in lower sheet.

So in the sandwich and bimetallic systems, the hardness variation is mainly controlled by the shoulder in the upper sheet and the pin in the lower sheet. The weakest region in the upper and lower sheets of the sandwich system lies closer to the keyhole than in the bimetallic system. This is attributed to another phenomenon of a large volume of stirred material getting accommodated in the soft polymeric core. This results in the presence of SZ much closer to the keyhole and hence the weaker location. Larger the material flow in the core, the shorter the SZ would be because of compensation of SZ expansion by the material flow into the core. However, the location of the weak zone is unaffected by the rotational speed.

Lower hardness at higher rotational speed is observed due to larger grain size for both sandwich and bimetallic sheets. However, in comparison to sandwich sheet, hardness of bimetallic sheet is higher, especially at 1200 rpm though the grain size is larger. The hardness of AA5XXX alloys is controlled by many other factors such as grain boundary strengthening, solid solution hardening, precipitation hardening, and dislocation density, where the most dominant one is the dislocation density, as reported by Huskins et al. (2010). With increasing dislocation density, the interaction between solute Mg atoms and dislocations increases, which raises the resistance to the movement of dislocation. Furthermore, Sato et al. (2001) analyzed that second-phase particles like Al3Fe, Mg2Si, and Al6Mn-type in Al5XXX alloy govern the dislocation movement and decides the hardness. These particles are present mostly inside the grains, which act as a strong barrier for dislocation movement. It is believed that in the bimetallic sheet, the stirring is more intense because of the absence of soft polymer. Intense stirring would result in fragmentation of second phase particles and increased density inside the grains leading to more resistance to dislocation

movement. This could be a possible reason for the higher hardness of bimetallic FSSW than sandwich FSSW at 1200 rpm, as shown in Fig. 2.13a and Fig. 2.13b. However, at 1800 rpm, excessive grain growth reduced the hardness of the bimetallic sheet despite intense stirring.

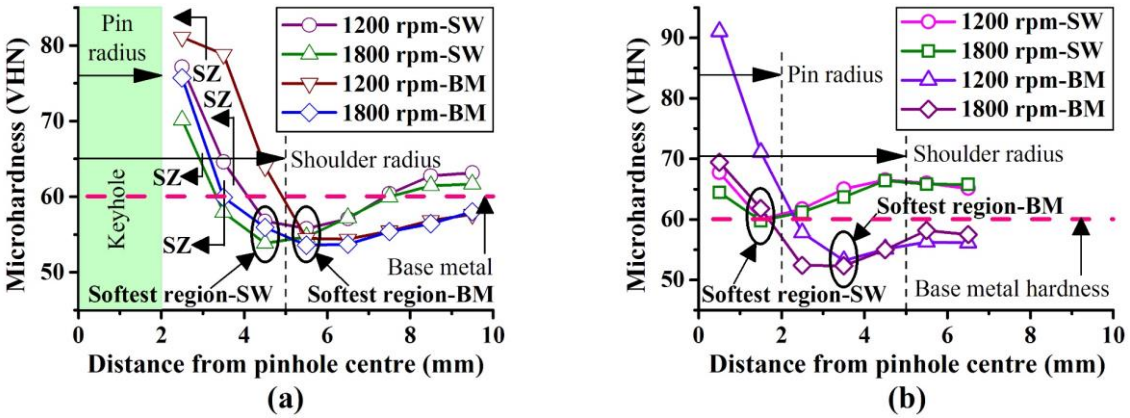

Fig. 2.13 Hardness distribution at (a) mid-thickness of the upper sheet, (b) mid-thickness of the bottom sheet. Error variation: ± 2 VHN [SW: Sandwich sheets; BM: Bimetallic sheets]

2.2.4 Mechanical performance and failure modes

Typical load-displacement behavior of welded sandwich and bimetallic sheet is shown in Fig. 2.14. In lap shear test, peak load and extension is larger for the bimetallic sheet than the sandwich sheet (Fig. 2.14a).

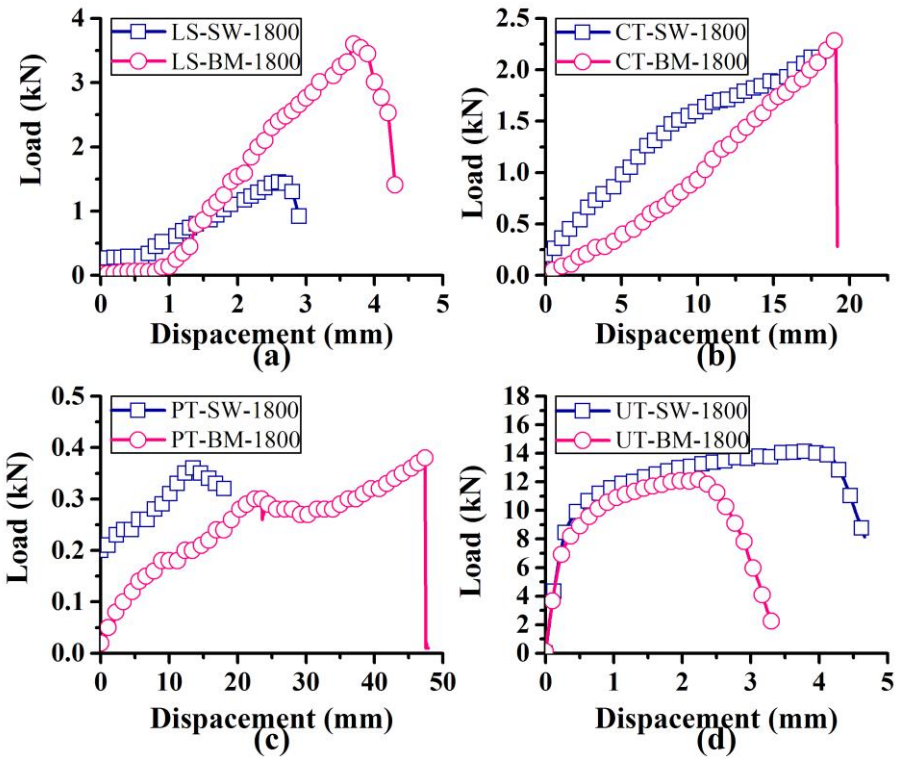

Fig. 2.14 Typical load-extension behavior of welded sandwich and bimetallic sheet: (a) lap shear test, (b) cross-tension test, (c) peel test, and (d) uniaxial tensile test

In the cross-tension test, the peak load for sandwich sheet is slightly lesser, but, the extension is almost the same as that of bimetallic sheet (Fig. 2.14b). In peel test, both the maximum load and extension at failure is lesser for the sandwich sheet in comparison to bimetallic sheet (Fig. 2.14c). It is seen that the load-displacement behavior of welded sandwich and bimetallic sheet are similar to that of a monolithic skin sheet. Moreover, the performance of the sandwich sheet is superior to the bimetallic sheet (Fig. 2.14d).

Fig. 2.15 shows the dependence of joint strength and extension at the failure of the sandwich and the bimetallic system with tool rotational speed. The lap shear test data shown in Fig. 2.15a suggest that for FSSW sandwich sheets, the joint strength slightly decreases (by about 10 %) up to 1800 rpm and then increases (by about 9 %) at 2000 rpm. The extension at failure is almost proportional to the maximum load at all the rotational speeds. This is related to ductility of the joint. Mitlin et al. (2006) also confirm that FSSW joints having high shear strength show good ductility and conversely, lesser ductility is found in poorly welded joints. For cross tension test a typical fixture is made. During testing, bending of upper and lower takes place. The cross – tension test results shown in Fig. 2.15b suggest that the strength and the extension at failure increase with rotational speed for sandwich sheets and the variation is almost uniform. At 2000 rpm, the failure load and extension is increased by 44 % and 56 %, respectively. However, the elongation recorded by the machine is not the exact extension in the joint, but is a combination of extension due to sheet bending and elongation in the joint. Only 1-2 mm extension at the end of the testing takes place in the joint and the remaining is due to bending of the sheets. The influence of rotational speed on the joint behavior is not found very significant in peel test and uniaxial tensile test as shown in Fig. 2.15c and d, respectively.

The bimetallic sheet shows superior strength in lap shear test, buts inferior strength in cross-tension, peel and uniaxial tensile test at higher rotational speed. The failure load at 1800 rpm increases by 8% in lap shear test, while it is decreased by 24% in cross-tension test and by 18% in peel test. On the other hand, the extension at failure increases by 13% in lap shear test, by 16% in cross-tension test, and decreased by 23% in peel test.

In comparison to sandwich sheets, the bimetallic sheets show superior strength and extension at failure, especially at lower rotational speeds, 1200 rpm. At 1200 rpm, the failure load for bimetallic sheet is 107%, 83% and 37% higher than sandwich sheet in lap shear, cross-tension, and peel test respectively. On the other hand, at 1800 rpm, the failure load for bimetallic sheet is 163%, 19%, and 8% higher than sandwich sheet in lap shear, cross-tension and peel test

respectively. So, it is inferred that higher rotational speed is favorable for sandwich sheet, but not for bimetallic sheet in this range. Similarly, the extension at failure for bimetallic sheet is more than the sandwich sheet in almost all cases. The reason for better joint strength of bimetallic sheet is superior hardness at weld zone, as presented in Fig. 2.13a and Fig. 2.13b. The harder joint needs larger failure load. Furthermore, the location of the softest region in bimetallic sheet lies farther than sandwich sheet, both in upper and lower sheets as shown in Fig. 2.13a and Fig. 2.13b. This suggests that a larger portion of the joint is stronger for bimetallic sheets than in sandwich sheets. This further contributes to the joint strength in the bimetallic sheet. Hence, it is inferred that presence of polymer in sandwich sheet has reduced the joint strength, but at higher tool rotational speeds, the joint performance approached near to that of bimetallic sheet.

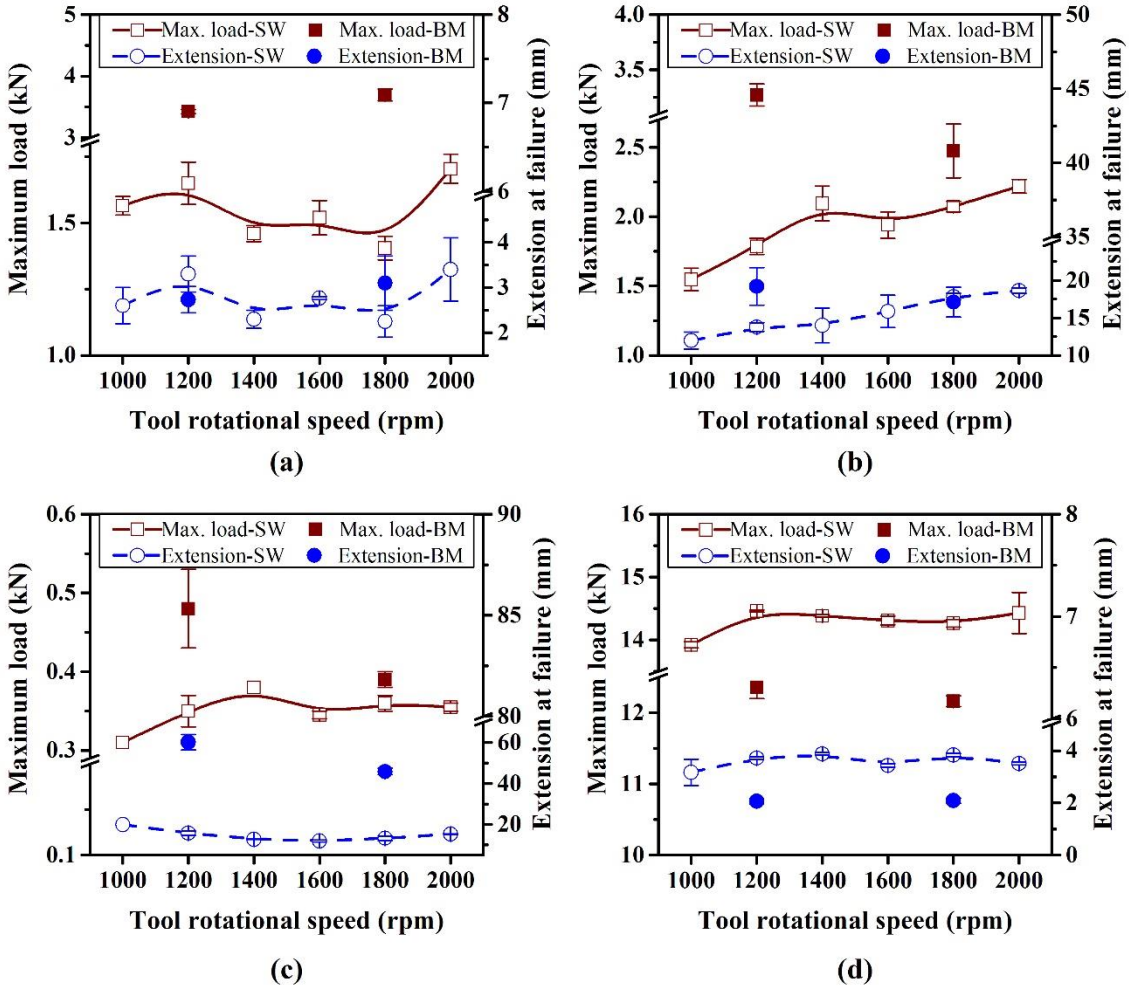

Fig. 2.15 Maximum load and extension at failure for the sandwich and bimetallic sheets: (a) lap shear test, (b) cross-tension test, (c) peel test, and (d) uniaxial tensile test

As per the lap shear test results, the bimetallic failure load increases with an increase in rotation speed. However, a reverse trend was observed (decrease in failure load with an increase in

rotational speed) in case of results obtained from cross-tension test, peel test, and uniaxial tensile test. This is because the lap shear strength has a positive correlation with the effective upper sheet thickness (Rao et al., 2014). The hook geometry of the bimetallic sheet suggests that the effective upper sheet thickness is increased at higher tool rotational speed. Therefore, increase in tool rotational speed results in higher failure load in lap shear test of bimetallic sheet.

In cross-tension test and peel test, the load is applied parallel to the axis of symmetry of the joint. So, the load bearing area will be perpendicular to this axis. The critical location will be the location of the lower hook, where the area is minimum. The hook geometry of the bimetallic sheet suggests that the lower bond width is reduced at higher tool rotational speed. Therefore, the failure load decreases at higher tool rotation speed in bimetallic sheet.

In case of uniaxial tensile test, the load bearing area is perpendicular to the loading direction. This area directly depends on the bonded region. Reduction in lower bond width with tool rotational speed results in reduced load bearing area. Moreover, in this particular test, the whole joint actually deforms and the joint hardness reduces at higher rotational speed. Therefore, the failure load decreases at higher tool rotation speed in bimetallic sheet.

However, unlike previous test results, the bimetallic sheets show inferior strength and extension than sandwich sheets in uniaxial tensile test as shown in Fig. 2.15d. The failure load for bimetallic sheet is about 14% lesser than sandwich sheet at 1200 rpm and 1800 rpm. On the other hand, the extension at failure is about 45% lesser than sandwich sheet at 1200 rpm and 1800 rpm. The peak load and extension at failure remains almost unaffected by the rotational speed for bimetallic sheets.

The loading condition in uniaxial tensile test is completely different from any other test. In lap shear, cross-tension and peel test, the load bearing area lies on a plane perpendicular to the axis of symmetry of the joint. This area is larger for the joint with larger bond width. As seen from the macrographs and hook geometry, the bonded width of FSSW joint in bimetallic sheet is significantly higher than that of sandwich sheet at all rotational speed. That is why; the failure load of bimetallic sheets is higher as compared to sandwich sheet at all rotational speed in the three tests mentioned above.

On the other hand, the load bearing area in case of uniaxial tensile test lies on a plane parallel to the joint axis. This area is larger for sandwich sheet in comparison to the bimetallic sheet because, the overall thickness of sandwich sheet is greater. That is why; the failure load of

sandwich sheets is higher as compared to bimetallic sheet in uniaxial tensile test.

It is known that the weld nugget is weaker than the parent metal. So larger the nugget size, a larger portion of the specimen across the width of the specimen would be weaker. Table 2.4 shows that bimetallic joints have a larger bond width than sandwich joints. Larger bond width signifies larger nugget width and hence larger weaker region's contribution in the tensile sample. This could have improved the performance of sandwich sheets as compared to bimetallic sheets.

At higher rotational speeds, better joint strength and extension at failure can be obtained especially in lap shear and cross tension tests. It is suggested that FSSW at higher rotational speeds, above 1800 rpm, can be selected for joining AA5052-H32/HDPE/AA5052-H32 sandwich sheets for automotive applications.

The fractured surface of upper and lower sheets after each test of FSSW sandwich sheets is shown in Fig. 2.16. Partial nugget failure and nugget pull-out are the two failure modes occurred.

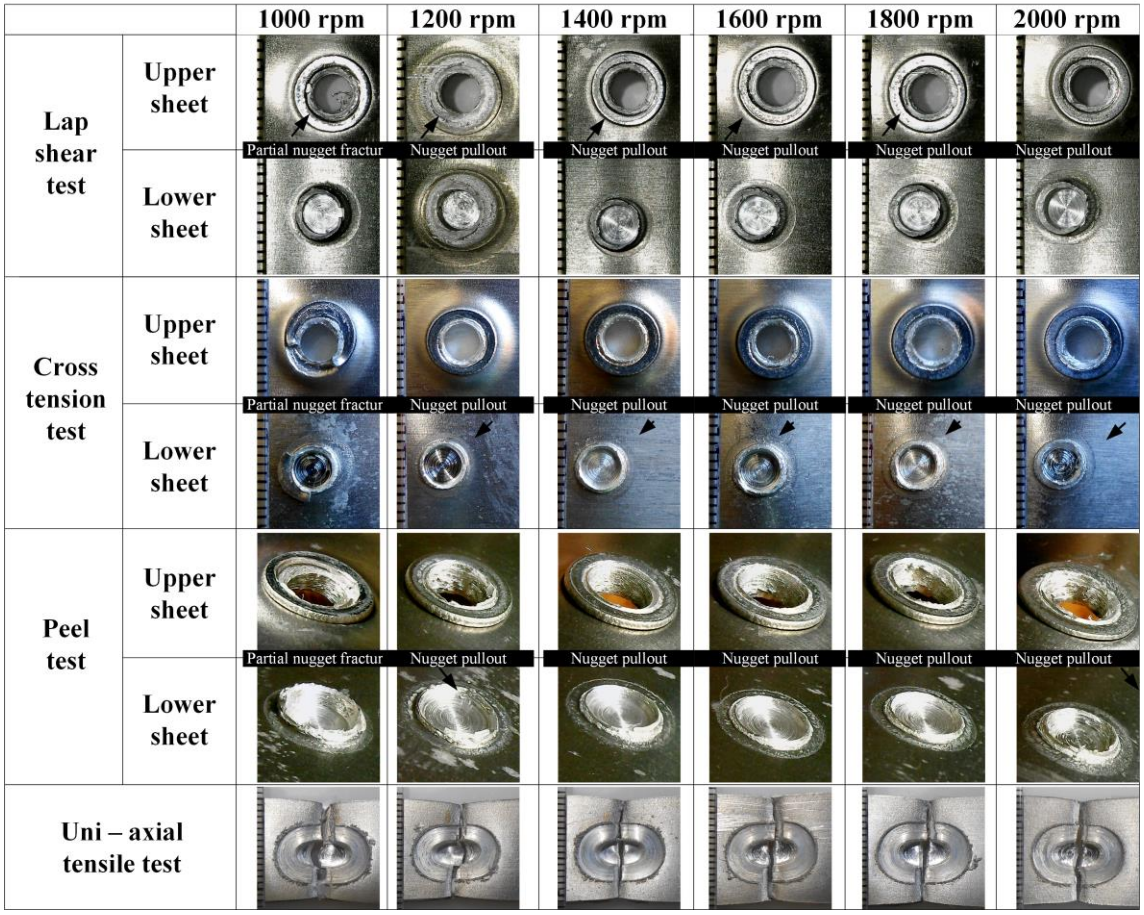

Fig. 2.16 Failure modes of sandwich sheets

Partial nugget fracture occurred at 1000 rpm, while the nugget pull-out mode of fracture in all

the other rotational speeds. 1000 rpm is characterized by a larger lower hook height and smaller lower bond width (Table 2.4Table 4.2). So the larger hook height and lesser bond width of the lower hook are favorable for partial nugget fracture. The joint strength is also least at 1000 rpm in all tests. Hence it can be inferred that partial nugget fracture is always associated with lower joint strength. A summary of failure modes in sandwich sheets welded at different tool rotational speed is tabulated in the Table 2.5.

Table 2.5 Failure modes of sandwich sheets

Rotational speed	Lap shear test	Cross – tension test	Peel test
1000	Partial nugget fracture		
1200	Nugget pull-out		
1400			
1600			
1800			
2000			

The mechanism of nugget pull-out mode is schematically illustrated in Fig. 2.17. During mechanical tests, two cracks initiate at the tip of upper and lower hook which propagate towards keyhole periphery. Weld geometrical measurements shown in Table 2.4 and Fig. 2.8 indicates that the lower bond width is lesser than upper bond width at all rotational speeds. This means that even if both cracks propagate equal, the lower one would reach the keyhole earlier. Now the hardness ahead would decide the rate of crack propagation. The softest section in the lower sheet lies much closer to the keyhole in comparison to the upper sheet. So the lower crack propagates at a faster rate. So, for all rotational speeds, failures would occur by a detachment of nugget from the lower sheet only, which is termed as 'nugget pull-out.'

In general, it can be inferred that the variation in lap shear load at different rotational speeds can be attributed to lower hook geometry rather than nugget size, nugget strength, and failure mode. This is clearly observed in Fig. 2.15a as the failure load and extension varies only in ±0.05 kN and ±7 %. Such variation seems to be not much, though maximum failure load and extension occur at larger rotational speed (>1800 rpm).

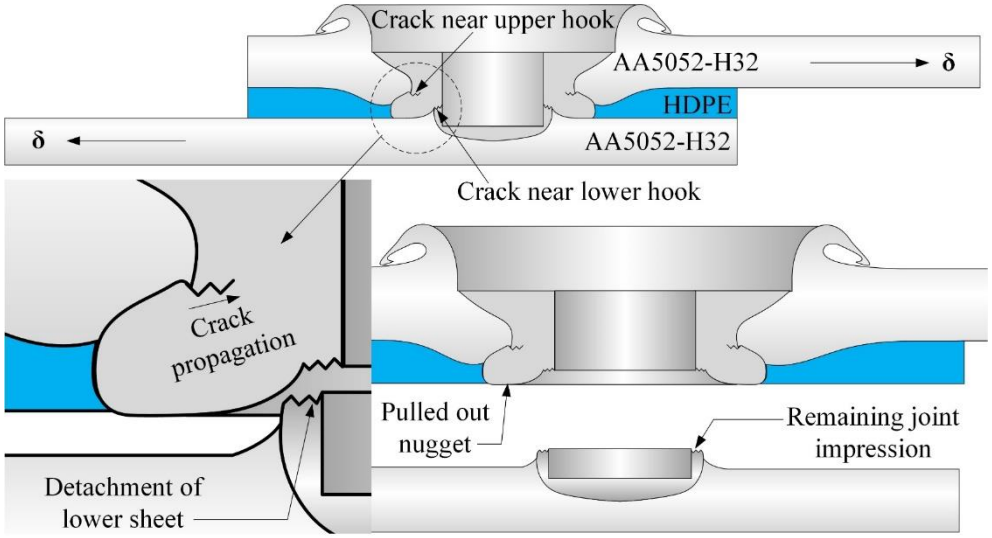

Fig. 2.17 Schematic illustration of mechanism of nugget pull-out failure (explained with lap shear test)

The failure mode is nugget-pullout for sandwich sheets in all tests except uniaxial tensile test and rotational speed except 1000 rpm. This type of failure depends upon the lower hook geometry, as discussed above. The general trend in lower hook is increasing width and decreasing height with increasing rotational speed, as shown in Table 2.4. So, improved mechanical performance of sandwich sheet at higher rotational speed is attributed to higher width and lower height of the lower hook. From Fig. 2.13, the lower hardness value of sandwich sheet at higher rotational speeds evolved after grain growth suggests that the joint performance does not depend upon the joint hardness. Hence, it is inferred that the failure load of FSSW joints in sandwich sheet predominantly depends upon hook geometry rather than the microstructure and hardness of the joint.

In the case of uniaxial tensile test, at 1000 rpm and 1200 rpm, the upper sheet has fractured from the middle of the joint, while the lower sheet fracture has taken place at the keyhole periphery. On the other hand, for rotational speeds above 1200 rpm, both the upper and lower sheets have failed almost at the middle of the keyhole. Table 2.6 shows the failure modes in the case of bimetallic sheets at lower and upper rotational speeds.

Table 2.6 Failure modes of bimetallic sheets

Rotational speed	Lap shear test	Cross – tension test	Peel test
1200	Interfacial separation	Nugget fracture	Interfacial separation
1800	Interfacial separation	Nugget fracture	Upper sheet fracture

2.3 Conclusions

The present work aims to address the influence of rotational speed on the FSSW of AA5052-H32/HDPE/AA5052-H32 sandwich sheets. The following conclusions are drawn from the results.

- The optimum rotational speed is 1800 rpm and above. The sandwich sheets show good mechanical performance.
- Two hooks are fully developed in sandwich sheets, while only one hook in the case of the bimetallic sheet after FSSW. The hook geometries change with rotational speed and eventually affect the joint strength. A larger bond width and smaller hook height are responsible for better mechanical performance at higher tool rotational speeds.
- In comparison to the bimetallic sheet, the lesser peak temperature of sandwich sheets suggests that a part of the heat generated is consumed for the melting of the polymer layer. The reliability of temperature measurement given by thermocouple is more than the IR camera.
- Sandwich sheet exhibits finer grains as compared to the bimetallic sheet due to lesser peak temperature, and grain size increases with an increase in rotation speed due to larger heat generation.
- The presence of polymer has deteriorated the joint performance as observed from lap shear, cross-tension, and peel tests. However, at higher rotational speed (1800 rpm), sandwich sheet performance is closer to bimetallic sheet. In uniaxial tensile test, the superior strength and extension at the failure of sandwich sheet shows its better formability than bimetallic sheet.
- Partial nugget failure and nugget pull-out are the two failure modes occurred in FSSW of sandwich sheets. These are associated with lower and higher joint strength respectively during FSSW of sandwich sheets.

Chapter 3

Influence of tool plunge depth during friction stir spot welding of AA5052-H32/HDPE/AA5052-H32 sandwich sheets

3.1 Experimental procedure

In this section, the FSSW trials, sample preparation, mechanical testing, joint characterization, and temperature measurement procedures are described. The mechanical properties of base materials are already discussed in Chapter 2 in Section 2.1.1.

3.1.1 FSSW and sample preparation

The FSSW is performed at four different tool plunge depths, 3.2 mm, 3.4 mm, 3.6 mm, and 3.8 mm, keeping other process parameters like tool rotational speed, plunge speed, and dwell time constant at 1600 rpm, 8 mm/min, and 15 s, respectively. The selection of tool plunge depth is based on several trials made from 3.1 mm to 3.9 mm in the interval of 0.1 mm. For sandwich sheet at 3.1 mm plunge depth, the joint could not be made due to inadequate plunging, and at 3.9 mm plunge depth resulted in excessive thinning of the upper sheet at the joint region. The value of tool rotational speed, plunge speed, and dwell time are selected based on the available literature on bimetallic FSSW. However, initial FSSW trials for bimetallic sheets show that the joining is possible even at much lower values of welding parameters. So for comparison with sandwich sheets, two extreme ends of plunge depth are selected for bimetallic sheets. The plunge depth is set at 3.2 mm for lower level and 3.8 mm for higher level. All other parameters are kept constant at the same levels (rotational speed: 1600 rpm, plunge speed: 8 mm/min and dwell time: 15 s).

To evaluate the mechanical performance and microscopic analyzes of the FSSW joint, five types of sandwich and bimetallic specimens including samples for lap shear test, cross-tension test, peel test, uniaxial tensile test and macro/micro-structural analyzes are prepared. The geometrical dimensions of each type of specimen are previously shown in Fig. 2.3 of Chapter 2.

3.1.2 FSSW Joint Characterization

The methodology adopted for mechanical testing, microstructural examination, hardness measurement, and temperature measurement is similar to that used in the previous chapter (Chapter 2, Section 2.1.3). FSSW is done for sandwich and bimetallic sheets at two extreme sets of welding parameters, as shown in Table 3.1 for comparison of temperature distribution.

Table 3.1 FSSW parameters for comparing temperature measurement.

Tool plunge depth (mm)	Tool rotational speed (rpm)	Plunge speed (mm/min)	Dwell time (s)
3.2	1100	4	5
3.8	1500	10	20

3.2 Results and discussion

In this section, a detailed examination of FSSW joints of sandwich and bimetallic sheets are done at different tool plunge depths. The FSSW joint characterization is done by evaluating the hook morphologies, flash formation, temperature measurement, microstructural analysis, and hardness measurement. Further, the cumulative effect of all these indexes is described through mechanical performance and failure modes.

3.2.1 Hook formation

The formation of hook-like geometry at the interface of two sheets is an important phenomenon during FSSW. The dimensions and shape of the hook are crucial factors which decide the joint behavior under external loading (Yin et al., 2010a). In the present study, hook formation is observed. The hook always originates from the interface, and it forms because of the upward movement of the trapped oxide layer at the faying surface due to tool plunging (Badarinarayan et al., 2009). It should be noted here that there are two interfaces in the sandwich sheet; the upper interface and the lower interface. The upper interface represents the region between the upper sheet and core, while the lower interface represents the region between the core and lower sheet. On the other hand, the bimetallic sheet has only one interface, which is between the upper and the lower sheet. Therefore, it is believed that the number of hooks formed will be different for sandwich and bimetallic sheets. Interestingly, not only the number of hooks, but also their characteristics are different in sandwich and bimetallic sheets. A comparison between hook formation in FSSW of sandwich and bimetallic sheet is done and shown in Fig. 3.1. Only one hook is prominently seen for bimetallic sheets though two hook formation is initiated at the interface. These are named as primary and secondary hooks. When the pin plunges into the lower sheet, upward movement of

the interface near the joint occur due to backward extrusion of the stirred material beneath pin face. This results in the formation of primary hook. After a while, when the tool shoulder starts plunging the upper sheet, a larger area gets plasticized on the upper sheet. This plasticized material is pushed into the weld by the shoulder. So the upward movement of the material extruded by the pin is restricted by the material coming from the upper sheet. This results in outward flow of stirred material. But this movement is restricted by non-plasticized materials surrounding the weld. So, a boundary between plasticized and non-plasticized materials forms above the interface. This results in the formation of a secondary hook. Usually bimetallic FSSW exhibits formation of only one hook, but there exists a tendency to form secondary hook. Solanki et al. (2012) have found the formation of two distinct hooks in FSSW of magnesium alloy. Rao et al. (2013) have reported that primary and secondary may merge together to appear like a single hook depending upon process parameters.

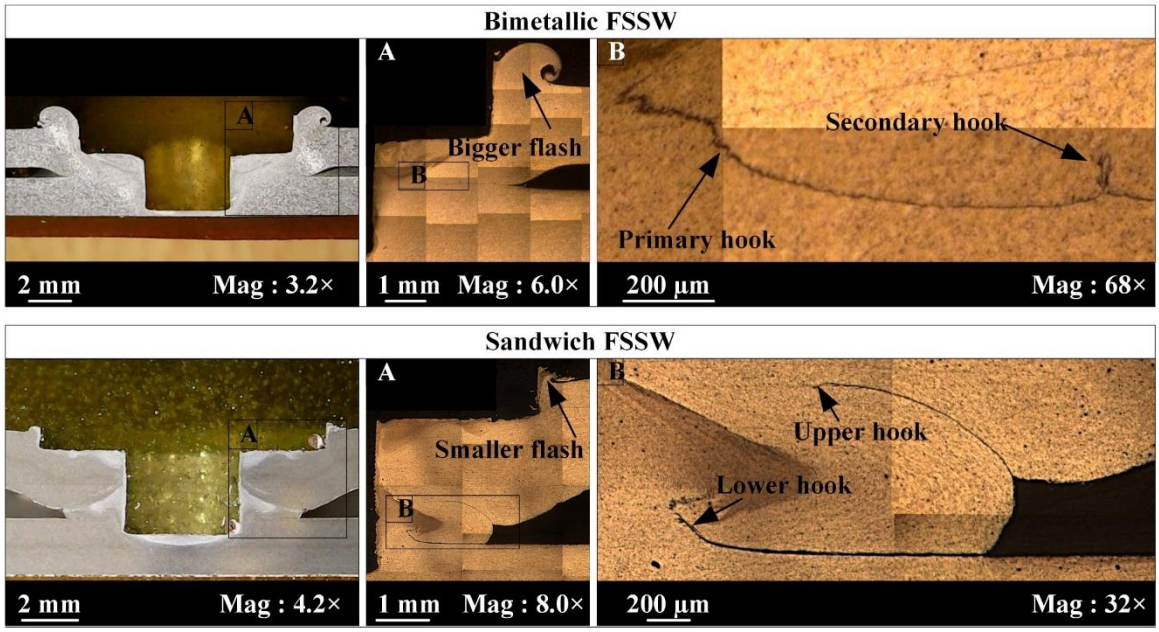

Fig. 3.1 Formation of hook in bimetallic and sandwich sheets during FSSW

In most of the literature of bimetallic FSSW, the formation of a single hook is discussed. Badarinarayan et al. (2009) have done FSSW on aluminum 5754-O sheets, and the micrograph of the weld shows the formation of two hooks, but the secondary hook is so small that effect due to this is insignificant, and finally, a single (primary) hook is analyzed. Sometimes, the secondary hook does not form a hook-like shape. So it is accepted as a small crack. Rao et al. (2015) have found the formation of only one hook in FSSW of dissimilar materials.

For sandwich sheet, in the present work, it is observed that two hooks formed; one at the upper interface and another at the lower interface. For analysis the hook formed at upper and lower interface of the sandwich sheet is named as upper hook and lower hook, respectively. Unlike bimetallic sheet, the material flow pattern is different in sandwich sheet. Due to the presence of polymer in the core, there is an initial gap maintained between upper and lower sheets. When the tool pin starts plunging the lower sheet, the shoulder also starts plunging the upper sheet. So the lower and upper sheets are simultaneously getting plasticized. This creates a downward flow of plasticized material from upper sheet and upward flow from lower sheet. Both materials find an easy passage to flow into the soft polymeric core at the mid-thickness, and a large portion of the stirred material is extruded into the core. The oxide layer present at the lower interface gets fragmented and moves upward, which leads to the formation of lower hook. It should be noted here that the height of the lower hook in sandwich sheet is lesser than in bimetallic sheet. This happens because the upward flow of lower sheet material quickly gets diverted into the core, which ceases upward bending of lower hook. Further, the materials easily flow into the core, so no secondary hook forms at the lower interface, unlike in bimetallic sheet. At the upper interface, it is seen that the hook formation originates from a location much lower than the upper interface because a portion of interface gets suppressed against the polymer core. This happens due to early plasticization of upper sheet material. Similar to lower interface, no sign of secondary hook is observed at upper interface.

The variation in upper and lower hook geometries with respect to four tool plunge depths is observed for sandwich sheets. The macroscopic view of the joint cross-section of sandwich sheets after FSSW is shown in Fig. 3.2. For bimetallic sheets, joint features are studied at two extreme sets of parameters where the tool plunge depth is 3.2 mm and 3.8 mm at lower and upper extreme, respectively. To investigate the effect of tool plunge depth, five geometrical indexes are selected. These are upper bond width, lower bond width, aspect ratio of hook, and effective upper sheet thickness. The upper bond width and lower bond width are the shortest distance between keyhole periphery and the tip of the upper and lower hook. Aspect ratio is the ratio of hook width to hook height. The effective upper sheet thickness is the shortest distance between upper hook and the surface on which the tool shoulder touches. It should be noted here that the nomenclatures associated with the secondary and primary hooks in bimetallic sheet are similar to that with upper and lower hook in sandwich sheets.

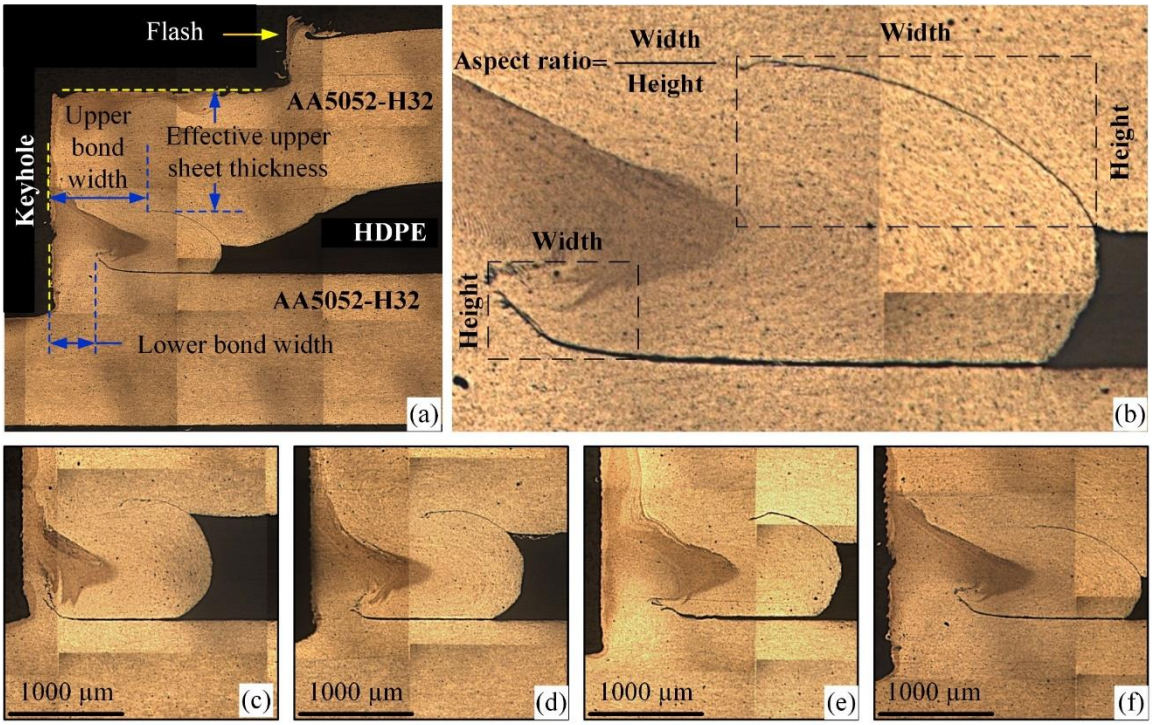

Fig. 3.2 Hook: (a) geometrical nomenclatures, (b) aspect ratio, and formation at tool plunge depth of (c) 3.2 mm, (d) 3.4 mm, (e) 3.6 mm, (f) 3.8 mm

The geometrical measurements of various joint features in sandwich and bimetallic sheets are listed in Table 3.2. It is found that in both the systems, at all plunge depths, the upper bond width is greater than lower bond width. This is attributed to greater heat generation underneath the shoulder surface than at the probe surface due to larger contact area at shoulder surface. Increased heat generation is responsible for higher peak temperatures, which promotes plasticization of material. As the plasticization increases, the outward flow of material also increases resulting in larger bonded width in the vicinity of upper hook. Further, with increasing tool plunge depth, the upper and lower bond width increases for sandwich and bimetallic sheets. When plunge depth increases, more material displacement occurs in the joint region to accommodate the tool. A part of the increased amount of displaced material is contributed by the expelled flash and remaining is trapped within. When plasticized material in the joint region tries to accommodate, it flows away from the keyhole, thereby enlarging bonded width.

Apart from the outward material flow, many other phenomena also affect the bonded width during change of plunge depth. Tutar et al. (2014) have also reported that an increase in plunge depth naturally increases the heat exposure time which in turn widens the weld zones. Further, bimetallic sheets show larger bonded width in comparison to sandwich sheet. This is likely due to larger outward flow of material in bimetallic sheet in absence of polymeric core.

Table 3.2 FSSW weld geometrical measurements of the joint morphologies.

System*	Plunge depth (mm)	Upper bond width (mm)	Lower bond width (mm)	Aspect ratio#		Effective upper sheet thickness (mm)
				UH (or) SH	LH (or) PH	
SW	3.2	0.91	0.18	8.23	0.97	1.93
	3.4	1.01	0.46	5.58	2.67	1.84
	3.6	1.28	0.56	4.11	3.21	1.79
	3.8	1.29	0.66	2.36	3.41	1.60
BM	3.2	1.72	0.62	0.53	2.20	1.26
	3.8	2.23	1.28	0.09	4.36	0.91

* SW: Sandwich sheets; BM: Bimetallic sheets, # UH: Upper hook; SH: Secondary hook; LH: Lower hook; PH: Primary hook; UH and LH are for sandwich sheets; SH and PH are for bimetallic sheets.

Another feature is the aspect ratio of hook, which is the ratio of hook width to hook height. It is observed that with increasing tool plunge depth, aspect ratio of upper hook in sandwich sheet decreases. A decrease in aspect ratio means decreasing width and increasing height. This is likely due to the lowering of hook origin because of increased downward material flow from the shoulder region. In bimetallic sheet, since there is no easy passage in the middle for increased material flow from upper sheet, the downward flow of material diverted into outward flow restricts the growth of secondary hook. This results in the formation of a steeper hook having larger height and lesser width. The secondary hook aspect ratio in bimetallic sheet is much lesser than upper hook ratio in sandwich sheet. However, completely reverse trend is observed for lower hook and primary hook in sandwich and bimetallic sheet respectively. In sandwich sheet, the lower hook width remains almost constant, but hook height decreases with increasing tool plunge depth because the upward growth of the lower hook is annihilated by increased material flow into the core. This results in increasing lower hook aspect ratio. On the other hand, in bimetallic sheet, the vertical growth of primary hook is promoted at higher plunge depth since a large portion of the probe goes into the lower sheet.

The effective upper sheet thickness decreases with increasing tool plunge depth. This is due to upper sheet thinning with increase in plunge depth. In comparison, the sandwich sheet shows larger effective upper sheet thickness than bimetallic sheet. Literature suggests that larger effective upper sheet thickness gives better joint strength in FSSW (Rao et al., 2014).

Another observation is flash formation. It depends upon the displaced material due to tool plunging. In sandwich FSSW, when tool plunging starts, the shoulder plunges into a part of the upper sheet and the pin plunges into a part of the lower sheet, while the pin is fully penetrated

through the polymer core. So the displaced volume of material is the contribution of upper and lower sheet. A little contribution from the polymer can be ignored due to lower density. In bimetallic FSSW, the contribution is totally from upper and lower sheet. At any tool plunge depth level, the pin plunging into lower sheet is not same for sandwich and bimetallic sheet due to difference in their total thickness, but the shoulder plunge depth will remain same. The pin plunge depth in bimetallic sheet will always be 1 mm greater than that in sandwich sheet as shown in Fig. 3.3. Hence, the amount of material displaced is also different in both systems.

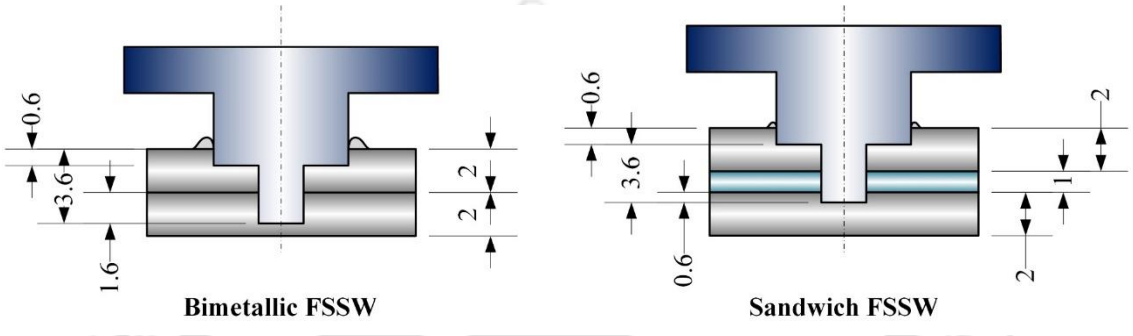

Fig. 3.3 Difference in pin plunge depth in bimetallic and sandwich FSSW

The ideal value of material displaced can be calculated as the volume of the tool inside the system. At different levels of tool plunge depth, the ideal volume displaced is calculated and shown in Table 3.3. It is seen that material displacement in sandwich sheet is always lesser than bimetallic sheet at any particular plunge depth.

Table 3.3 Ideal volume of displaced material during FSSW

System	Tool plunge depth* (mm)	Tool shoulder				Tool pin				Total displaced volume (mm^3)
		Diameter (mm)	Surface area (mm^2)	Plunge depth (mm)	Vol. (mm^3)	Diameter (mm)	Surface area (mm^2)	Height (mm)	Vol. (mm^3)	
SW	3.2	10	78.54	0.2	15.71	4	12.57	3	25.13	40.84
	3.4			0.4	31.42					56.55
	3.6			0.6	47.12					72.26
	3.8			0.8	62.83					87.96
BM	3.2			0.2	15.71				37.70	53.41
	3.8			0.8	62.83					100.53

*tool plunge depth = shoulder plunge depth + pin height

The expelled flash volume is calculated as below. The contour of expelled flash is mapped using AutoCad software. The closed contour is revolved by 360° about a circle of diameter equal to the shoulder diameter of the tool (10 mm). This gives a virtual solid geometry almost equal to flash formed in the actual case. The volume of the virtual flash is calculated in the software.

A comparison is made between sandwich and bimetallic sheets at two extreme sets of parameters. The geometrical measurement of flash is given in Fig. 3.4. In sandwich sheets, a lesser amount of flash is expelled from the system than the bimetallic sheets. For sandwich sheet, the ideal volume of material displaced is also lesser, and a large portion of stirred material gets accommodated in the soft polymeric core. The ideal displaced volume in sandwich sheet at 3.8 mm tool plunge depth is about 88 mm^3, while it is about 100 mm^3 in bimetallic sheet at the same plunge depth (table 5). Hence, in this case, the flash volume of sandwich sheet is much smaller than in bimetallic sheet – 3.46 mm^3 vs. 57.63 mm^3 (Fig. 3.4). It can be concluded that displaced material is accommodated inside the core in sandwich sheet. Flash is a defect, and hence lesser flash formation is always good. Moreover, it does not contribute to load bearing. The flash volume is higher at larger tool plunge depth due to increased material displacement. This has been substantiated by Oladimeji et al. (2016) through expelled flash volume calculations in the FSSW of aluminum alloys.

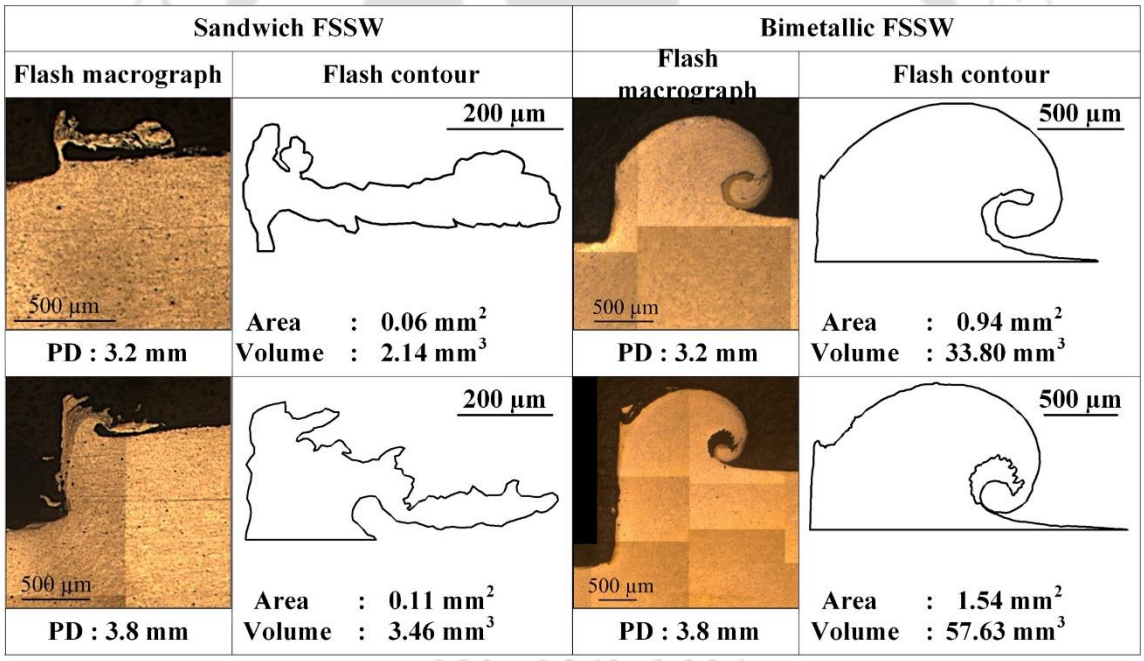

Fig. 3.4 Volume change in flash for the sandwich and bimetallic sheet

3.2.2 Temperature evaluation

The distribution of maximum temperature attained around the joint during FSSW is shown in Fig. 3.5. A higher temperature field is observed in the keyhole vicinity (Fig. 3.5a). The temperature distribution by IR camera and thermocouple is compared in the upper sheet of sandwich, as shown in Fig. 3.5b. For comparison, the temperature reached when the shoulder touches the upper sheet

is considered. Preliminary observation suggest that the temperature recorded by the thermocouple is lesser than the IR camera. This is due to presence of holes at the edges, which reduces the frictional force between tool and sheet. Also, the accurate value of material emissivity is difficult to find. The temperature data obtained by thermocouple is found more reliable, so selected for further analysis. The higher peak temperature is observed at larger plunge depth. This is attributed to increased heat input associated with larger material deformation, larger tool-work-piece interface area, and increased processing time. Further, the influence of plunge depth in sandwich sheet is smaller than bimetallic sheet. This is confirmed by lesser temperature difference in sandwich sheet (ΔT_{SW} = 129°C) than bimetallic sheet (ΔT_{BM} = 218°C) near the keyhole as shown in Fig. 3.5c. Similar observation is found in lower sheet (Fig. 3.5d) also (ΔT_{SW} = 9°C, ΔT_{BM} = 114°C).

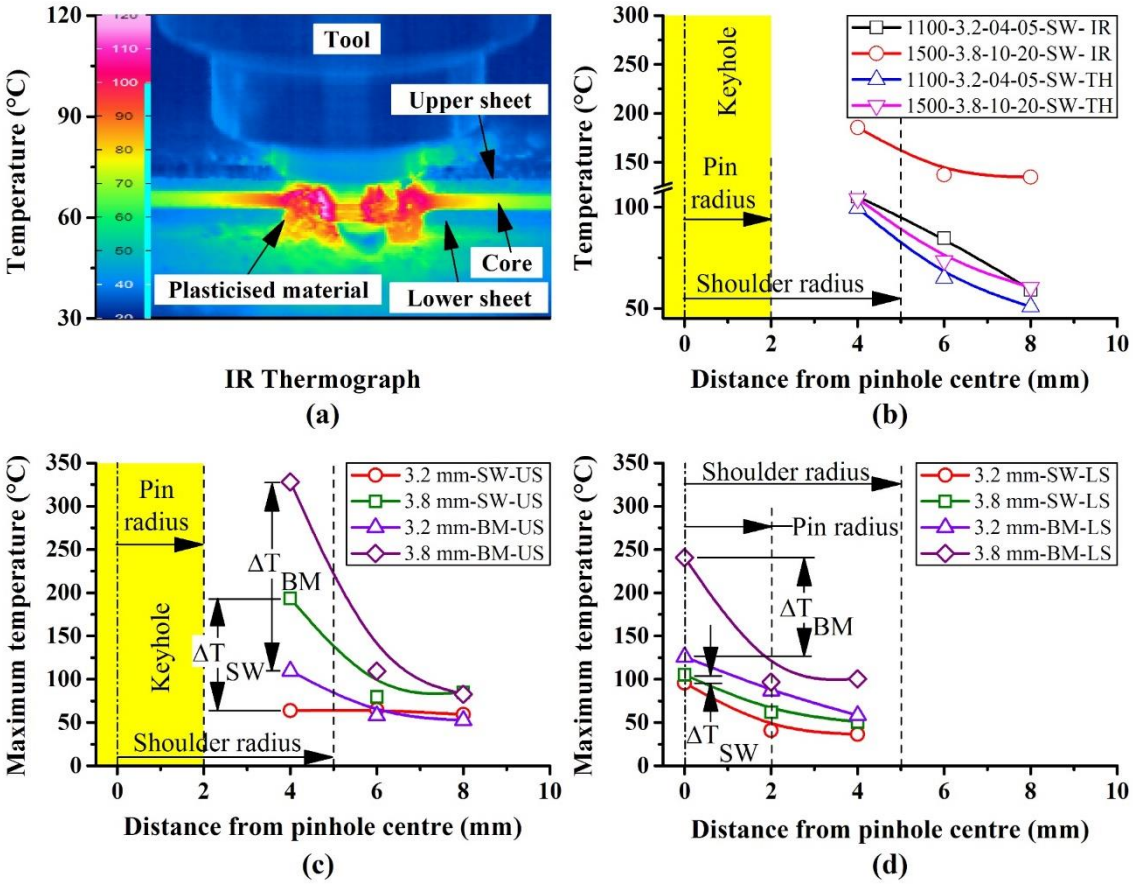

Fig. 3.5 (a) Infrared image of FSSW at the edge, (b) temperature of the upper sheet of SW in both measuring techniques, peak temperature distribution at mid-thickness of (c) the upper sheets of SW and BM measured by thermocouples, and (d) the lower sheets of SW and BM measured by thermocouples [SW: Sandwich sheets; BM: Bimetallic sheets; US: upper sheet; LS: lower sheet]; the sequence in the legend of (b) is tool rotational speed-plunge depth-plunge speed-dwell time-measuring method

In comparison to bimetallic sheet, lesser peak temperature is recorded in sandwich sheet. It likely is due to lesser frictional contact area between tool and the metallic sheet in sandwich. The temperature gradient through thickness is lesser for sandwich sheet, especially at higher plunge depth. The temperature gradient through-thickness is measured by the difference in peak temperature of upper and lower sheet at a distance 4 mm from keyhole center. Further, the temperature gradient with respect to the distance from keyhole in upper sheet of sandwich sheet is lesser than that in bimetallic sheet. In contrast, the temperature of upper sheet is larger than the lower sheet. This confirms the fact that a major part of the heat generated in FSSW comes from friction between tool shoulder and work-piece. Moreover, a part of the heat generated at the lower sheet gets transferred into the base plate. Further, the peak temperature gradient with respect to distance from keyhole in the upper sheet is larger than in lower sheet.

3.2.3 Grain size and hardness distribution

The microstructure of the upper sheet on the joint at 1 mm distance from the keyhole periphery and parent metal are shown in Fig. 3.6a-e. The measured grain size is plotted in Fig. 3.6f. With respect to parent metal microstructure, grain refinement occurred due to dynamic recrystallization at high temperature in all the FSSW joints. However, Fig. 3.6a for sandwich sheet at 3.2 mm plunge depth reveal almost same grain size with respect to parent metal. This is due to the lowest peak temperature (refer Fig. 3.5c) restricting the dynamic recrystallization to occur within the identified zone for grain size evaluation.

With increasing plunge depth, grain size increases in bimetallic sheets (Fig. 3.6c, d, f). This is attributed to grain growth at a higher temperature at higher plunge depth, as seen in Fig. 3.5(c) on temperature distribution. In contrast, at 3.8 mm plunge depth, the sandwich sheet shows finer grains as compared to 3.2 mm plunge depth, though the temperature developed is larger in 3.8 mm plunge depth (Fig. 3.5c). This is probably because, at 3.2 mm plunge depth, the effect is insignificant to change the grain size in case of a sandwich. In this case, the deformation provided and temperature rise is insufficient, and hence grain size remains almost the same as that of the parent sheet. When the plunge depth is increased to 3.8 mm, though there exist deformation and temperature rise, it is insufficient to increase the grain size to the extent seen in 3.2 mm plunge depth (Fig. 3.6a, e, f). There is a significant difference in grain size between the sandwich and bimetallic sheet only at lower plunge depth, but not at higher plunge depth. This is attributed mainly due to an insignificant change in the grain size of the sandwich sheet at 3.2 mm as compared to the parent sheet (Fig. 3.6a, e, f).

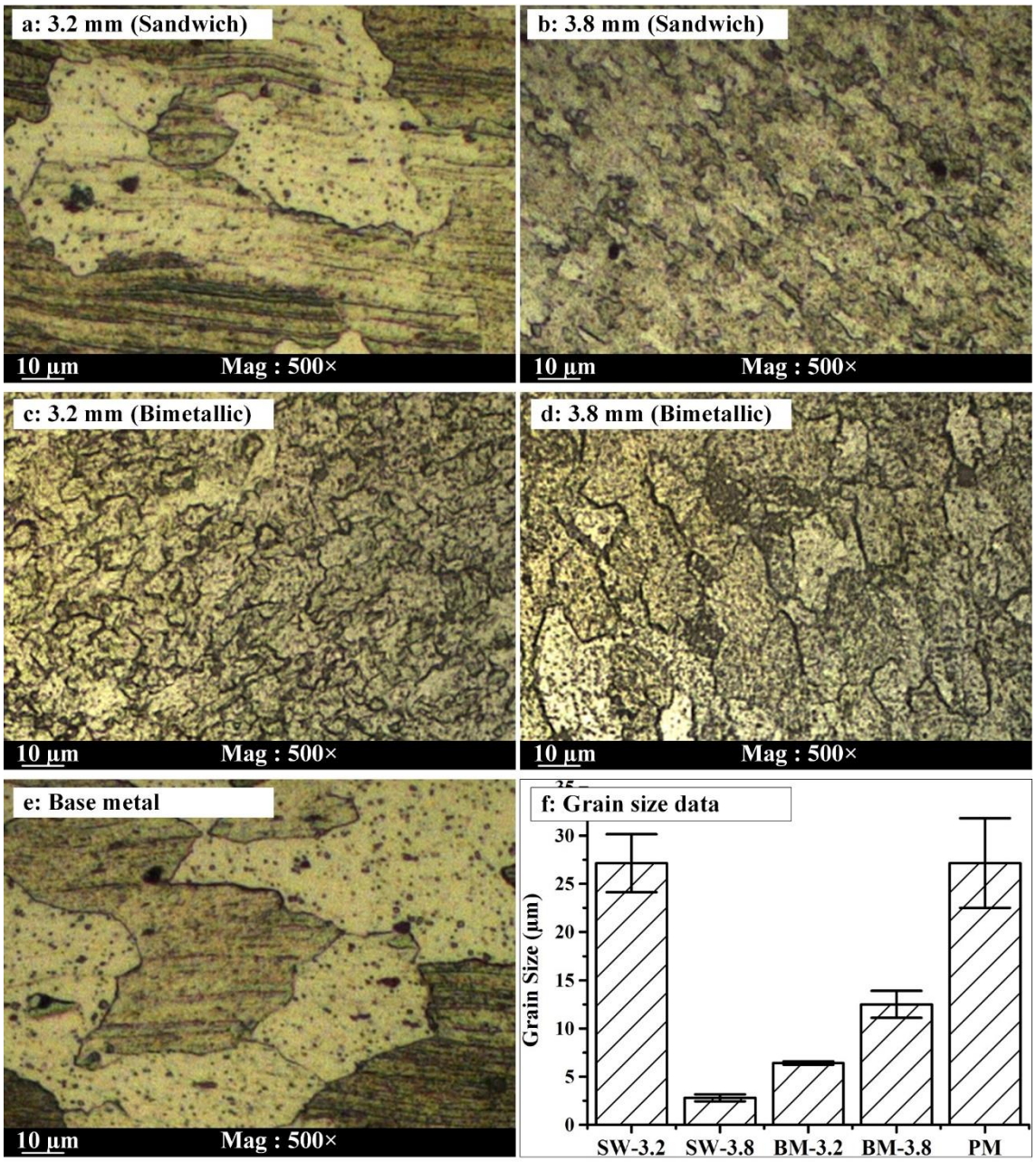

Fig. 3.6 Microstructure of the upper sheet at a distance of 1 mm from keyhole periphery of (a) 3.2 mm-Sandwich, (b) 3.8 mm-Sandwich (c) 3.2 mm-Bimetallic, (d) 3.8 mm-Bimetallic, (e) base metal microstructure, and (f) grain size measurement [SW: Sandwich sheets; BM: Bimetallic sheets]

The variation in hardness across the joint cross-section is evaluated and shown in Fig. 3.7. It is observed that the hardness is symmetrical about the keyhole axis, and maximum hardness is attained in the region closer to the tool or keyhole. The reason behind this is that the degree of dynamic recrystallization is more in the vicinity of the tool because of larger heat generation. With increasing tool plunge depth, the hardness increases in the sandwich sheet due to grain refinement. In the bimetallic sheet, the hardness increases with increasing plunge depth though grain size

increases. It is reported by Huskins et al. (2010) that strengthening mechanisms of AA5XXX alloys are not straightway controlled by grain size, rather it is mainly governed by dislocation density. Sato et al. (2001) have reported that the distribution of second phase particles also plays a major role in controlling the hardness of AA5XXX alloys. It is believed that at higher plunge depth, intense stirring due to higher temperatures would result in fragmentation of second phase particles. This could have possibly improved the hardness of the bimetallic sheet at higher plunge depth. The bimetallic sheets are slightly harder than the sandwich sheets (Fig. 3.7). This is mainly due to increased stirring. The bimetallic sheet exhibits a larger temperature evolution than sandwich sheets in most of the cases (Fig. 3.5), which resulted in increased intensity of stirring.

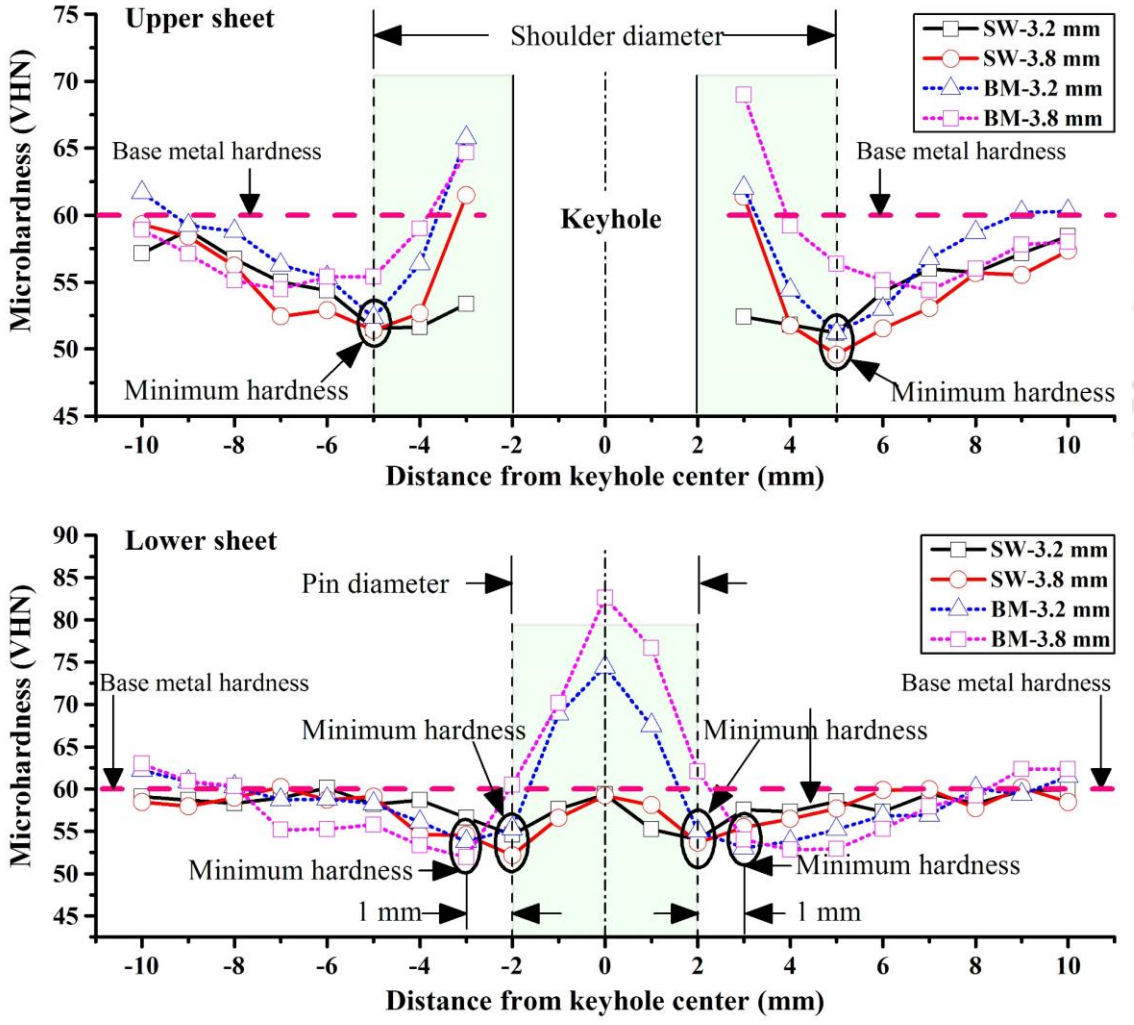

Fig. 3.7 Hardness distribution at mid-thickness of the upper and lower sheet. Error variation: ± 1.5 VHN [SW: Sandwich sheets; BM: Bimetallic sheets]

In the upper sheet, hardness varies prominently within shoulder diameter, while it is pin diameter in the lower sheet. The lowest hardness location in the upper sheet exists farther from

keyhole than in the lower sheet. The location of minimum hardness in the upper sheet of the sandwich system coincides with that in the bimetallic sheet and lies just below the shoulder edge. However, in the lower sheet, the minimum hardness location lies below the probe edge for sandwich sheet, but it is 1 mm away from the probe edge for bimetallic sheet. It is known that in FSSW of AA5XXX alloys, metallurgical recovery causes localised softening (Kesharwani et al., 2014). The location of this zone lies where dynamic recrystallization ceases and material undergoes only thermal cycle, typically known as heat-affected zone (HAZ). The farther existence of minimum hardness location in lower sheet of bimetallic system is due to higher temperature which shifts the HAZ away from keyhole.

3.2.4 Mechanical performance and failure modes

The effect of tool plunge depth on the joint strength and extension at the failure of sandwich and bimetallic sheets during various loading conditions is shown in Fig. 3.8. Due to the complex geometry of FSSW joint and typical shapes of specimens, the joint strength is characterized by maximum load attained during the test, and ductility is related with extension up to maximum load.

With increasing tool plunge depth, joint strength and ductility considerably improved in sandwich sheets. In lap shear test (Fig. 3.8a), the joint strength of the sandwich sheet consistently increases up to 3.8 mm plunge depth. The uniform elongation increases up to 3.4 mm plunge depth, then remains the same. In cross-tension test and peel tests, a consistent improvement in joint strength and ductility is observed with increasing tool plunge depth. It should be noted here that the extension recorded in cross-tension and peel test is the combined effect of the sheet bending and elongation in the joint. In the uniaxial tensile test, the influence of tool plunge depth is not much in the sandwich sheet. Better joint performance of the sandwich sheet at higher plunge depth is associated with larger bond width and larger joint hardness. During mechanical testing, crack forms at the weakest section in the joint. It is evident from Fig. 3.7 that the joint region near the lower sheet is weaker than the upper sheet. Further, the hooks are the favorable site for crack initiation. So, the failure of the joint begins at the lower hook tip, and the crack propagates towards the keyhole. The lower bond width represents the length of the crack propagation path and decides the failure load. Since the lower bond width increases with tool plunge depth, the failure load will also increase. A larger value of upper bond width and joint hardness at higher plunge depth in the upper sheet further adds some strength to the joint. However, the effect of other joint features such as hook aspect ratio and effective upper sheet thickness is insignificant, although they are affected

by process parameters. The effect of tool plunge depth on the joint behavior of the bimetallic sheet is found to be significant. In lap shear test and peel test, the joint performance is improved, while it is deteriorated in the cross-tension test and uniaxial tensile test.

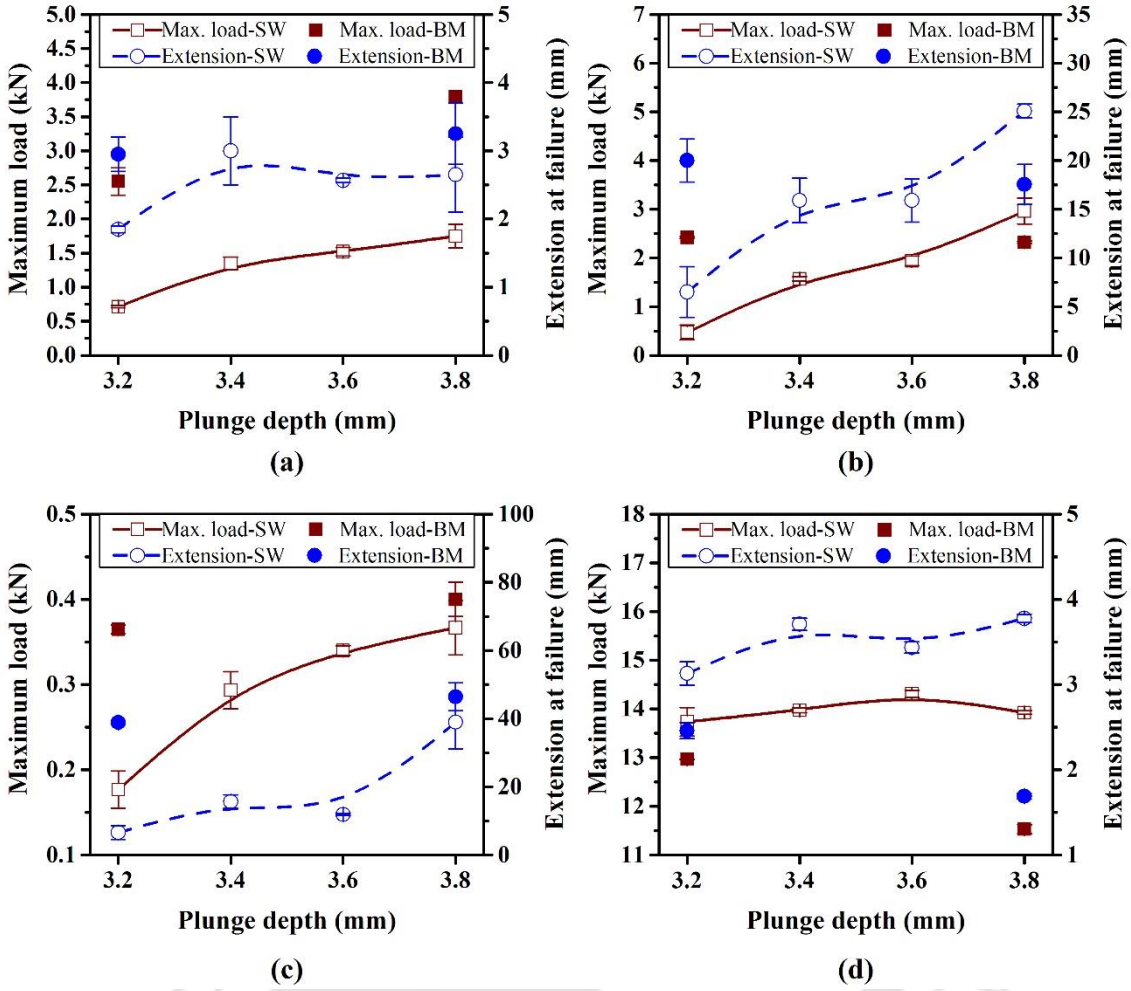

Fig. 3.8 Maximum load and extension at failure for the sandwich and bimetallic sheets: (a) lap-shear test, (b) cross-tension test, (c) peel test, and (d) uniaxial tensile test

A comparative analysis of the failure loads of sandwich and bimetallic system for each test at two plunge depths, 3.2 mm and 3.8 mm, is performed in Table 3.4. The improvement in the joint strength of sandwich sheet in all loading conditions is much greater than the bimetallic sheet. The maximum influence of tool plunge depth for sandwich system is seen in the cross-tension test, while it is lap shear test for bimetallic system. This particular analysis suggests that the sandwich FSSW can be greatly employed in situation when the sandwich is subjected to loading along the geometrical axis of the joint.

The ratio in failure load of bimetallic sheet and that of sandwich sheet is calculated at 3.2 mm

and 3.8 mm (Table 3.4) plunge depths individually for each test. The bimetallic system produces superior joint at lower plunge depth than at higher plunge depth. Further, at 3.2 mm plunge depth, the best joint performance of bimetallic sheet compared to sandwich sheet is observed in the cross-tension test, while a better joint performance of sandwich sheet is observed in uniaxial tensile test. Moreover, better joint performance shown by sandwich sheet in uniaxial tensile test at 3.2 mm plunge depth. At 3.8 mm plunge depth, difference in failure loads of both systems is minimised. In addition, the joint performance of the sandwich sheet is superior in cross-tension and uniaxial tensile test. From the comparison shown in Fig. 3.8 and Table 3.4, it is concluded that the sandwich sheet gives optimum joint property at tool plunge depth of 3.6 mm and beyond.

Table 3.4 Comparative assessment of joint strength with respect to plunge depth

System / PD (mm)		Lap shear test		Cross-tension test		Peel test		Uniaxial tensile test	
		F_L (kN)	ΔF_L ratio*	F_C (kN)	ΔF_C ratio*	F_P (kN)	ΔF_P ratio*	F_U (kN)	ΔF_U ratio*
SW	3.2	0.67	2.16	0.47	6.30	0.18	2.06	13.74	1.01
	3.8	1.45		2.96		0.37		13.93	
BM	3.2	2.55	1.49	2.42	0.96	0.37	1.08	12.97	0.89
	3.8	3.79		2.33		0.40		11.53	
3.2	SW	0.67	3.81	0.47	5.15	0.18	2.06	13.74	0.94
	BM	2.55		2.42		0.37		12.97	
3.8	SW	1.45	2.61	2.96	0.79	0.37	1.08	13.93	0.83
	BM	3.79		2.33		0.40		11.53	

* ΔF *ratio* = $\Delta F_{3.8}$ / $\Delta F_{3.2}$ or ΔF_{BM} / ΔF_{SW}

The physical appearance of the fracture surfaces of the tested sandwich sheet is shown in Fig. 3.9. It is observed that the mode of fracture is 'nugget pullout' for all specimens at any plunge depth in lap shear, cross-tension, and peel test. The nugget pullout mode of failure is attributed to the smaller value of lower bond width when compared to upper bond width. This is observed in Fig. 3.2 and Table 3.2. The size of upper and lower bond width depends upon the position of upper and lower hook, respectively. These hooks are the geometrical defect in FSSW, which always reduces joint integrity and is a favorable site for crack propagation. During loading, the crack propagates through upper and lower hooks. The early reach of crack through lower hook at the keyhole is expected since the lower hook tip is nearer to the keyhole. This phenomenon creates a situation of lower sheet detachment from the bond. So the nugget or weld remains attached to the upper sheet in the 'nugget pullout' fracture. A summary of failure modes in sandwich sheets welded at different tool plunge depth is tabulated in the Table 3.5.

The failure mode is completely different in uniaxial tensile test due to different loading conditions. The crack initiates at the keyhole boundary and starts propagating outward till

complete fracture of upper sheet. Once the upper sheet fractures, entire load is carried by lower sheet, which fails almost like in standard uniaxial tensile tests. The failure modes of bimetallic sheet, namely nugget fracture and interface separation is shown in Table 3.6.

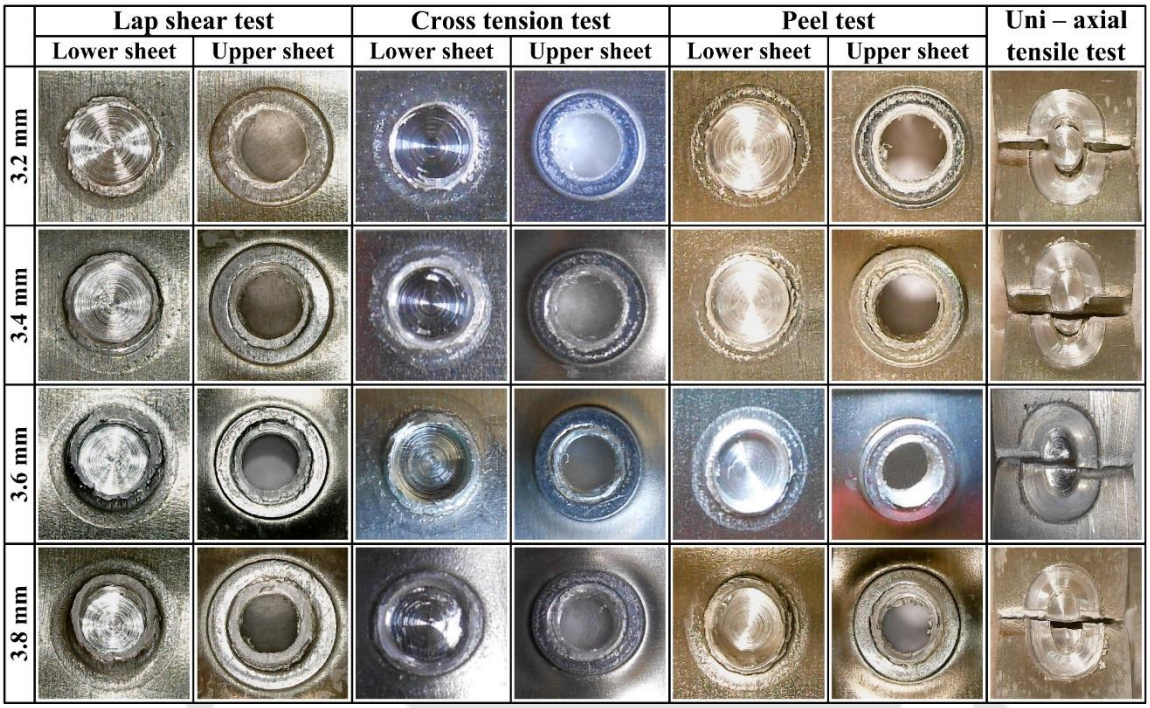

Fig. 3.9 Failure modes of sandwich sheets

Table 3.5 Failure modes of sandwich sheets

Tool plunge depth	Lap shear test	Cross – tension test	Peel test
3.2 mm	Nugget pullout		
3.4 mm			
3.6 mm			
3.8 mm			

Table 3.6 Failure modes of bimetallic sheets

Tool plunge depth	Lap shear test	Cross – tension test	Peel test
3.2 mm	Interfacial shear	Interfacial separation	Interfacial separation
3.8 mm	Interfacial shear	Nugget pullout	Partial sheet fracture

3.3 Conclusions

In the present work, effect of tool plunge depth on the FSSW of three layered AA5052-H32/HDPE/AA5052-H32 is investigated. The following are the important findings:

- FSSW joint of sandwich sheet with acceptable performance is obtained at tool plunge depth of 3.6 mm and greater.
- Two hooks are formed, one at each interface in sandwich sheet. In bimetallic sheet, two hooks

are formed at single interface. But one of the hooks (secondary hook) is much smaller as compared to the other one in bimetallic sheet. However, no direct dependence of joint strength on hook geometry is observed, instead it depends on bond width and joint hardness.

- The expelled flash volume increases with tool plunge depth in sandwich and bimetallic sheets. However, in comparison to bimetallic sheet, lesser flash forms in sandwich sheet due to larger material volume accommodation in polymeric core.
- Temperature measurement data reveals that highest temperature is recorded on the upper sheet of bimetallic system at higher plunge depth. This is obtained because larger frictional contact area between tool and metal
- The micro-structural observation closer to the keyhole of sandwich and bimetallic FSSW reveal finer grains in sandwich sheet due to lesser peak temperature.
- Deterioration of joint performance is observed in sandwich sheets due to presence of polymer. Formation of smaller bond width at lower sheet side is responsible for this. However, at higher plunge depth superior joint performance of sandwich sheet is observed in cross-tension and uniaxial tensile tests. Though this the case, the flash formation is lesser in sandwich sheets as compared to bimetallic. By using sandwich sheets, the flash defect can be minimized.
- In all the tests, nugget-pull-out mode of failure occurred due to smaller value of lower bond width. The failure mode is also found to be independent of the test method. So, it is confirmed that failure mode in the present study depend only on relative size of lower bond width.

Chapter 4

Friction stir spot welding of AA5052-H32/HDPE/AA5052-H32 sandwich sheets at varying plunge speeds

4.1 Experimental procedure

4.1.1 FSSW and specimen preparation

The plunge speed is one of the most important process parameters involved in FSSW. With changing plunge speed, the processing time and deformation rate changes. This affects the net heat input into the weld zone. The heat input governs the temperature of the weld. The temperature, coupled with the processing time, decides the final weld quality. Several aspects of FSSW at changing plunge speed are reported in the existing literature of bimetallic sheets. However, no such information is available for the sandwich sheet. Hence, it is important to investigate the effect of plunge speed on FSSW of sandwich sheet. The plunge speed is varied within a suitable range at equal intervals. The range is selected based on the existing literature of bimetallic FSSW of aluminum sheets having a similar thickness, where the effect of plunge speed is found considerable.

Song et al. (2014) have investigated the effect of tool plunge speed on the FSSW of AA6061-T6 sheets of 2 mm thickness. It is reported that when the shoulder of the tool started plunging, its speed affects the performance of the final joint produced. The selected range of shoulder plunge speed by Song et al. (2014) is 2, 4, 6, 8, and 10 mm/min. It is found that the tensile shear load initially increases up to 6 mm/min. and then remains almost constant. Liu et al. (2013) have attempted FSSW of 2A12-T4 aluminum alloy of 3 mm thickness. The tool plunge speed is changed from 5 mm/min. to 40 mm/min. The bonded area and tensile shear load are decreasing continuously with increasing tool plunge speed, but the significant effect is observed only up to 20 mm/min. Karthikeyan and Balasubramanian (2010) have selected plunge speed of 4, 8, 12, 16, and 20 mm/min. for FSSW of AA2024-T3 of 2.7 mm thickness. The obtained results suggest that lap shear tensile load initially increases and later decreases after 12 mm/min. Yoon et al. (2012) have attempted a higher range of plunge speed between 100-500 mm/min. for FSSW of AA5454-O aluminum alloy plates. No remarkable effect of tool plunge speed is found in the entire range.

Based on the referred articles, six different tool plunge speeds are chosen, ranging from 2 mm/min. to 12 mm/min. in the interval of 2 mm/min for sandwich sheets in the present work. For bimetallic sheets, 4 mm/min. and 10 mm/min. are the two extreme plunge speeds chosen from this range for comparison. Other process parameters are kept at a constant level. The fixed value of tool rotational speed, tool plunge depth, and dwell time is 1600 rpm, 3.6 mm, and 15 s, respectively. Here, the tool plunge depth is the addition of shoulder plunge depth and pin length (3 mm). Though the total thickness of SW is 1 mm larger than that of BM, and the tool plunge depth is kept constant in both the cases to keep consistency in the input. Same technique is used for sample preparation as used in previous chapters.

4.1.2 FSSW joint Characterization

The methodology adopted for mechanical testing, microstructural characterization, hardness measurement, and temperature measurement is similar to that used in previous studies (Chapter 2, and Chapter 3).

4.1.3 Finite Element (FE) simulation to predict failure modes

The main aim here is to predict the failure modes during the mechanical performance tests. To achieve this, a three dimensional model of the overlapped sandwich assembly is simulated using ABAQUS/Explicit (ver. 6.17) FE code. Each part of the 3D model is prepared in AutoCAD separately and imported in the ABAQUS. The size, position, and orientation of the parts are replicated exactly as per the actual test conducted in the laboratory. The joint is prepared by revolving the edge contour obtained from the joint cross-section. The hook geometry and deformed HDPE layer is also considered while mapping the edge contour. The planner symmetry is suitably applied in the model. After assembly, the sliding friction condition is defined in all the surface to surface interaction. The coefficient of friction is assumed as 0.1 (Park et al., 2008). The mechanical properties of the metallic skin and polymeric core are assigned as that of AA5052-H32 and HDPE obtained from the standard tensile test. However, the mechanical properties obtained from the uniaxial tensile test of FSSWed sandwich sheet is selected for the joint. It is assumed that in the particular case, since the total elongation is only 4-5 mm and failure occurs in the joint region, the deformation is concentrated in the joint only. The tensile properties of the weld region is difficult to evaluate because the exact load bearing area is unknown. Therefore, mechanical behaviour (load-extension data) is shown in most of the cases rather than tensile properties. However, estimating load bearing area is difficult only in lap shear, cross-tension, and peel test because of

typical loading condition. In case of uniaxial tensile test, it is possible to estimate a typical value of load bearing area from the joint cross-section. The available macrostructure is used to generate a contour of the bonded region. The hook separates the bonded and un-bonded region. Once, the area is calculated, the load-extension data are converted into the stress-strain data. This way, the tensile properties of the joint is evaluated. The material properties assigned to different sections of the model are listed in Table 4.1. The von Mises yield function is used to model the yielding of base metal. The schematic illustration of assigning properties in different locations of FE model is shown in Fig. 4.1.

Table 4.1 Properties of different sections of the FSSW joint used for FE simulation

	AA5052-H32	**Joint region**	**HDPE**
Density (g/cc)	2.66	2.66*	0.96
Poisson's ratio	0.33 (Baruah et al., 2017)	0.33*	0.46
Young's modulus (GPa)	70.3 (Baruah et al., 2017)	5.22	-
Yield strength (MPa)	155	123	-
Strength coefficient (MPa)	356	401	-
Strain hardening coefficient	0.16	0.30	-

* Assumed same as base metal

The ten-node modified quadratic tetrahedron elements, C3D10M element, is selected. This type of element is successfully used in ABAQUS by Zivojinovic et al. (2013), where the crack growth is analyzed in friction stir welded joints. Variable element sizes are selected in different regions. Since, the failure occurs in the joint region, finer element is selected in the joint and coarser in other parts of the model. The mesh sensitivity analysis is done by varying mesh size of the joint. The element sizes in the joint region are selected as 0.3 mm, 0.6 mm, 0.9 mm, and 1.2 mm. The load-extension behavior is compared at different mesh sizes. The behavior is not changing much. Hence, 1.2 mm element size is selected for rest of the analysis because of least computational time. Appropriate mass scaling is applied to reduce the simulation time. In boundary condition, one side of the assembly is kept fixed and another side is displaced with a velocity of 1 mm/min. Lap shear test, peel test, cross-tension test and uniaxial tension tests are simulated to predict the failure location and modes. The predictions are compared with experimental observation.

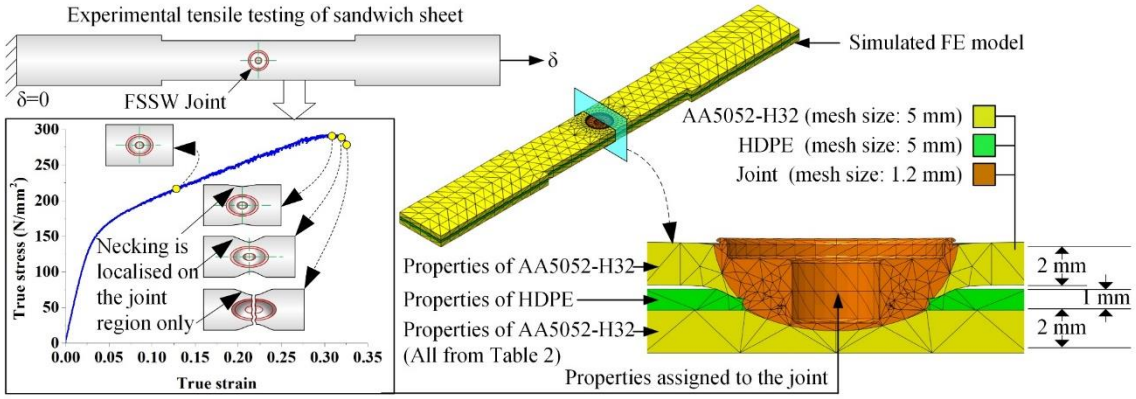

Fig. 4.1 Property assignment in FE model

4.2 Results and discussion

4.2.1 Hook formation

The macrostructure at the weld cross-section revealing the formation of geometrical features at the joint is shown in Fig. 4.2. The magnified macrostructure suggests that there are un-bonded or partially bonded regions in the joint. These are the characteristic features of FSSW joint and referred to as 'hook' due to its curved profile (Badarinarayan et al., 2009). The primary reason for the formation of the hook is the upward movement of the interface caused by penetration of tool pin into lower sheet during plunging. The secondary reason is the presence of oxide layer on the surface of aluminum sheets. The oxide layers are trapped at the faying surface and prevent metallurgical bonding of sheets. During stirring, the oxide film breaks into particles and gets distributed in the stirred material. Depending upon the distribution of the oxide particles, a region of complete metallurgical bonding, partial metallurgical bonding and un-bonded region exist in the joint. The distribution of these oxide particles are significant near the tool pin periphery due to severe stirring and decreases while moving away from the pin surface. The region of complete metallurgical bonding exist near the tool where severe stirring causes random distribution of oxide particles and elimination of the faying surface. Next to this is the region of partial metallurgical bonding where reduced deformation causes the broken oxide particles to be arranged in an array along the curved interface. After this region, the deformation straining is not severe enough to break the oxide layer of the interface and the region remains un-bonded. The curved portion of the interface along the un-bonded region is considered as hook where the oxide layer is not broken. It can be said that hook always originate from the interfaces of the overlapping sheets and it is a geometrical defect in the FSSW joint because it is the un-bonded region in the joint, which acts as a pre-existing crack during external loading.

The hook formation in sandwich and bimetallic sheet is entirely different. This is due to the different original configuration of both the system. There are two interfaces in the sandwich sheet; upper sheet-core and core-lower sheet. On the other hand, the bimetallic sheet has only one interface between upper sheet and lower sheet. In the sandwich sheet, one hook forms at each interface. When the rotating tool plunges into the sandwich sheet, the plasticized region gets stirred. The stirring results in intermixing of upper and lower sheet material. The stirred material forms a symmetric weld nugget around the tool. It is difficult to differentiate the upper sheet and lower sheet in the weld nugget because of disappearance of sheet interface. Further, the plasticized material tends to displace away from the tool axis and find an easy passage to flow into the soft polymeric core. A typical extrusion of the materials occurs here and due to continuous plunging of the tool, the interfaces bend upward and form an upper hook and lower hook (Fig. 4.2b).

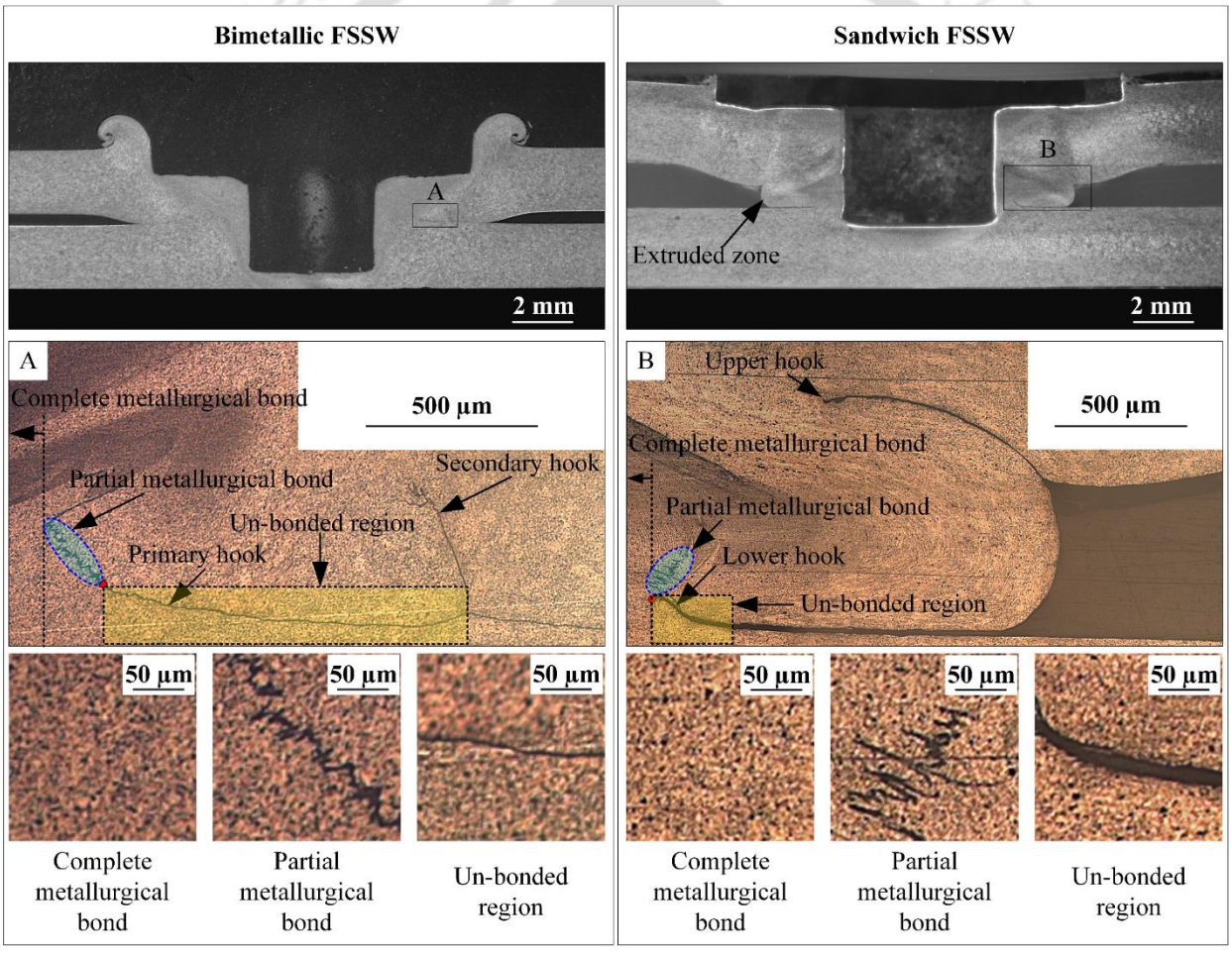

Fig. 4.2 Formation of hook in (a) bimetallic, and (b) sandwich sheets during FSSW

On the other hand, in the bimetallic sheet, two hook forms at one interface (Fig. 4.2a). The hook which is closer to the keyhole is defined as primary hook and another one is the secondary hook.

Two hook formation is also reported by Solanki et al. (2012) in FSSW of AZ31 magnesium alloy. However, it is also possible that the two hooks merge together and exhibit only one single hook as reported by Rao et al. (2013) and Arul et al. (2008). Furthermore, the sandwich sheet forms an annular nugget due to extrusion of plasticized material through the core layer and the lesser material is expelled out as a flash.

The schematic of measuring hook geometry and definition of associated terminologies are illustrated in Fig. 4.3a. The bonded region, hook height and hook width are measured. The bonded region is measured by upper bond width and lower bond width. The upper bond width (*a*) and the lower bond width (*b*) are the horizontal distance of keyhole boundary from upper hook tip and lower hook tip respectively. Lin et al. have reported the importance of bond width as it affects the joint performance (Lin et al., 2012). Hook height and hook width are the vertical and horizontal distance of hook tip from hook originating point. The effective upper sheet thickness (*g*) is also measured which is the shortest distance of hook tip from shoulder touching surface. It is seen from literature that the joint with larger bond width combined with smaller hook height and larger effective upper sheet thickness possesses better joint performance (Yin et al., 2010a).

The effect of plunge speed on the joint macro-structure of the sandwich sheet is shown in Fig. 4.3b. The morphological changes in the hook geometry is observed from the macrographs. Only one side of the joint cross-section is analyzed because of symmetry. In all the cases two hooks are formed and the upper bond width is always larger than the lower bond width.

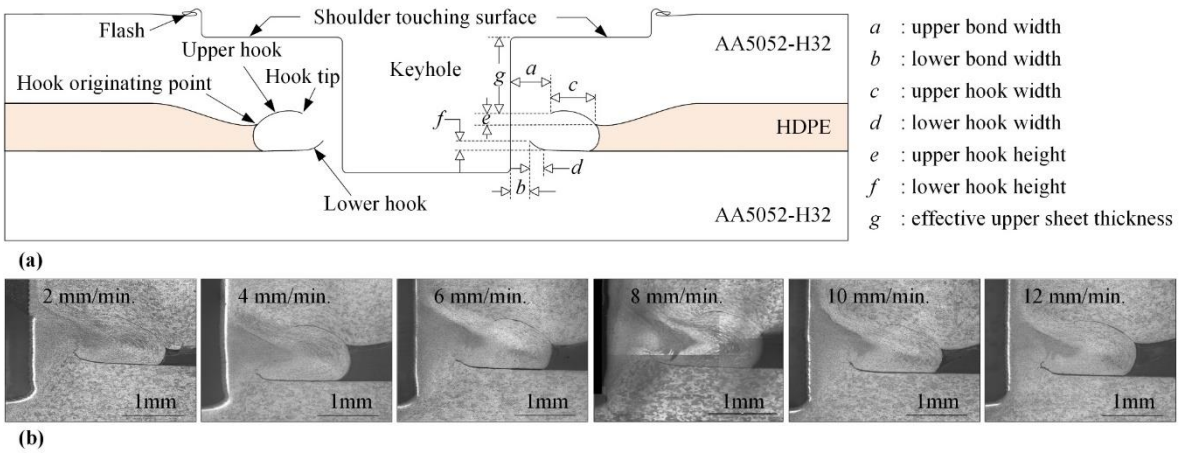

Fig. 4.3 (a) Schematic illustration of terminologies associated with hook geometry, (b) hook geometry of sandwich sheets at different plunge speeds

The material flow in FSSW of sandwich sheet and its influence on the hook geometry are shown in Fig. 4.4. The plasticized material in the vicinity of tool rotates around the pin and shoulder in

circular motion, while material slightly away from the tool flows from bottom of the pin and shoulder into the core as shown in Fig. 4.4a. At the beginning of the process, when the tool pin plunges into the upper sheet, heat generates underneath the pin, which melts the polymer layer locally. The melted polymer displaces radially outward due to tool plunging. This allows the upper sheet to bend slightly in the direction of tool plunge. When the tool shoulder touches the upper sheet, the pin starts plunging into the lower sheet. Thereafter, the material underneath the shoulder plasticizes by heating and flows downward and the upper sheet deform further due to plunge force. At the same time, the material from pin bottom starts flowing upward. This way, the upper and lower sheet material mix to form the joint. A part of mixed material is stirred around the pin and form the stir zone. The remaining part is extruded into the soft polymeric core and form an extruded zone. Fig. 4.4b, c, d explains the relation between material flow and hook geometry. When the material flow is larger, the bond width increases and the hook width decreases as shown in Fig. 4.4b. With increasing plunge speed, the material flow increases because of larger heat generation. The upper hook height depends upon the upward metal flow as shown in Fig. 4.4c. The metal flow in upward direction depends upon the processing time. At higher plunge speed, the processing time is lesser which reduces the upward metal flow, and thereby the upper hook height. Further, as the material flow increases in the extruded zone, the lower hook gets flatten reducing the lower hook height as shown in as shown in Fig. 4.4c.

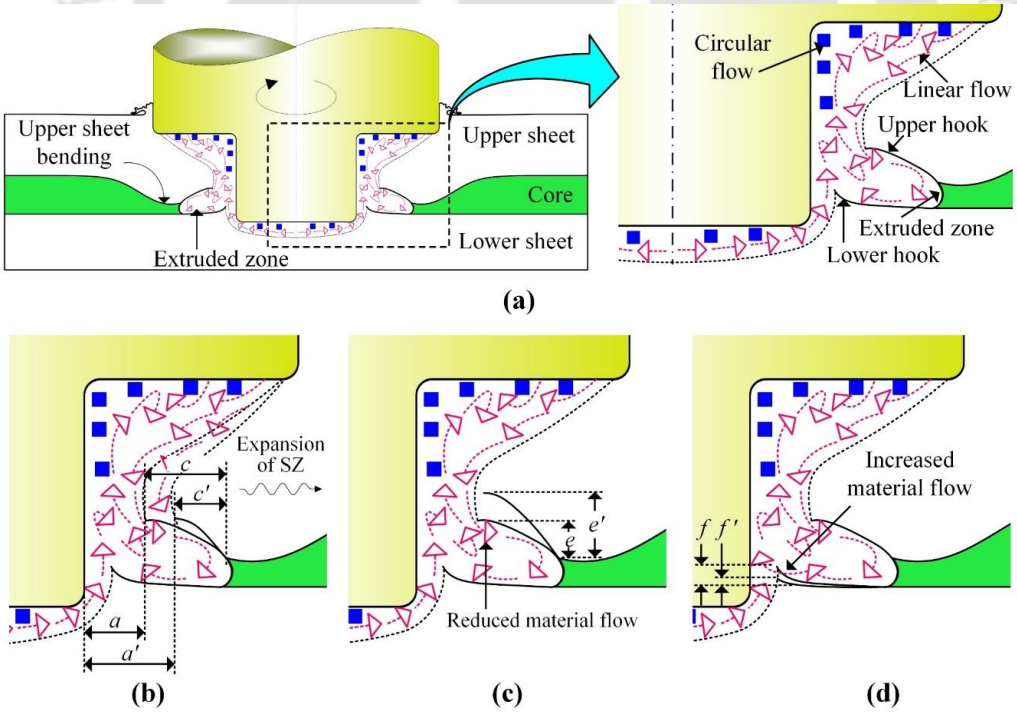

Fig. 4.4 (a) Material flow in FSSW of sandwich sheet, influence of material flow in: (b) bond width and hook width, (c) upper hook height, (d) lower hook height

The quantitative variation in the hook geometry at different plunge speeds is shown in Table 4.2. For sandwich sheet, the upper bond width (*a*) initially increases with increasing plunge speed, attains a maximum value at 8 mm/min., and then decreases. The upper and lower bond widths (*a* and *b*) are associated with the stir zone (SZ) size. Larger the SZ, larger would be the bond width. As the plunge speed increases, the SZ expands as a result of increased plasticization at higher temperature. Higher temperature at higher plunge speed is evident in the next section. Moreover, when the plunge speed crosses its critical value (8 mm/min.), the stirring time of the tool is reduced which restricts the growth of the SZ. This could be a possible reason behind the decrease in upper bond width (*a*) at larger plunge speed. Inverse relationship between tool plunge speed and size of the SZ is also reported (Song et al., 2014). The upper hook width (*c*) initially decreases, then increases with increasing plunge speed. It is noted that the upper bond width (*a*) and the upper hook width (*c*) are inversely related. When the SZ increases, a portion of the hook gets merged into the SZ, thereby hook width decreases and bond width increases. The upper hook height (*e*) also decreases slightly with increasing plunge speed. At higher plunge speed, the processing time is lesser. It is believed that at lesser processing time, plasticization of material would be lesser which reduces the upward movement of the material. This results in smaller hook height. Cao et al. (2016) have also reported that there is a positive correlation between hook height and joining time. There is an inverse correlation between upper hook height (*e*) and the effective upper sheet thickness (*g*). The effective upper sheet thickness (*g*) is highest, and upper hook height (*e*) is lowest at 8 mm/min. plunge speed. However, the effect of plunge speed on the lower bond width (*b*) is not significant. The larger effect on the upper sheet is because the heat generated and the plastic deformation near the tool shoulder is always larger than that near the tool pin (Awang and Mucino, 2010). Larger heat generation promotes stirring. The lower hook width (*d*) is not changed considerably because the lower bond width (*b*) is not changing significantly. The lower hook height (*f*) initially decreases and then increases after attaining the lowest value at 8 mm/min. plunge speed. The initial decrease in lower hook height (*f*) is due to flattening of the lower hook because of increased material flow in the core layer. However, as the plunge speed increases after 8 mm/min., the reduced processing time allows lesser material flow in the core layer. This results in the upward displacement of lower sheet material to be more pronounced, thereby increasing the lower hook height (*f*).

On the other hand, in the bimetallic sheet, all the hook features slightly decrease with increasing plunge speed, except the lower hook height (*f*), and the effective upper sheet thickness (*g*). Song et al. (2014) have also confirmed decrement in bond width at higher plunge speed. The change in

lower hook height (*f*) is not much and the larger value of effective upper sheet thickness (*g*) is due to the inverse relationship with upper hook height. However, with respect to the sandwich sheet, the bimetallic sheet has larger bond widths, i.e., *a* and *b*. In bimetallic sheets, the plasticization and stirring are more intense due to larger temperature generation. This results in the expansion of SZ and hence larger bond widths (*a* and *b*). The effective upper sheet thickness (*g*) depends on the position of the upper hook in the sandwich sheet and secondary hook in the bimetallic sheet.

Table 4.2 FSSW weld geometrical measurements of the joint morphologies.

System	Plunge speed (mm/min.)	*a* (mm)	*b* (mm)	*c* (mm)	*d* (mm)	*e* (mm)	*f* (mm)	*g* (mm)
Sandwich sheets	2	1.01	0.66	1.16	0.44	0.52	0.17	1.58
	4	1.12	0.50	0.92	0.33	0.27	0.13	1.67
	6	1.27	0.65	0.93	0.35	0.35	0.11	1.56
	8	1.31	0.54	0.75	0.26	0.19	0.07	1.78
	10	1.22	0.68	0.94	0.34	0.36	0.11	1.59
	12	1.05	0.59	1.01	0.21	0.28	0.20	1.63
Bimetallic sheets	4	2.18	1.24	0.12	1.06	0.25	0.10	1.17
	10	2.00	1.18	0.06	0.88	0.14	0.15	1.27

The upper hook position again depends on the position of the upper interface in the sandwich sheet. The upper interface gets plunged down into soft polymeric core near the joint in the sandwich sheet. So, the upper hook formation starts at a thickness level much lower than the original position of the upper interface. This results in a larger effective upper sheet thickness (*g*) in the sandwich sheet. On the other hand, during FSSW, the interface position remains almost the same in the bimetallic sheet due to the absence of the polymeric core. So, the secondary hook tip lies nearer to the shoulder touching surface. This results in a shorter effective upper sheet thickness (*g*) in the bimetallic sheet.

The polymer sheet gets degraded by local melting near the keyhole boundary. The degradation is more pronounced at the surface interfaces with the upper sheet. The physical appearance of this surface is compared at two plunge speeds is shown in Fig. 4.5. The polymer surface is degraded more at lower plunge depth because of larger processing time.

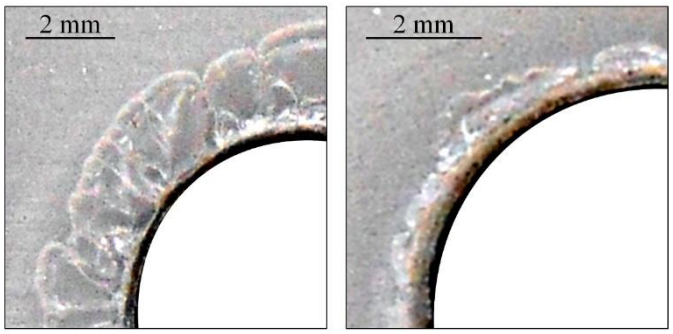

Fig. 4.5 Degradation of polymer surface at (a) 4 mm/min., and (b) 10 mm/min.

4.2.2 Temperature evaluation

The infrared thermograph revealing the temperature distribution at the weld cross-section just before reaching the peak temperature is shown in Fig. 4.6a. The temperature is higher near the keyhole boundary. The peak temperature distribution obtained by the IR camera and thermocouple is compared in Fig. 4.6b. The temperature values are taken at 1 s before reaching the peak temperature near the keyhole boundary. The temperature data recorded by the IR camera continuously fluctuates with time. It is observed that at time 1 s before reaching the peak temperature, the temperature recorded by the thermocouple is consistently lesser than that recorded by the IR camera in all the four cases shown in Fig. 4.6b. The fluctuation in temperature measured by the IR camera occurs due to the continuous expulsion of plasticized material and uncontrolled metal flow at the open edge of the weld. The lesser temperature recorded by the thermocouple is likely due to the presence of holes across the thickness of the sheets for fixing of thermocouples. The holes reduce the plunging force and hence the deformation resulting in lesser temperature.

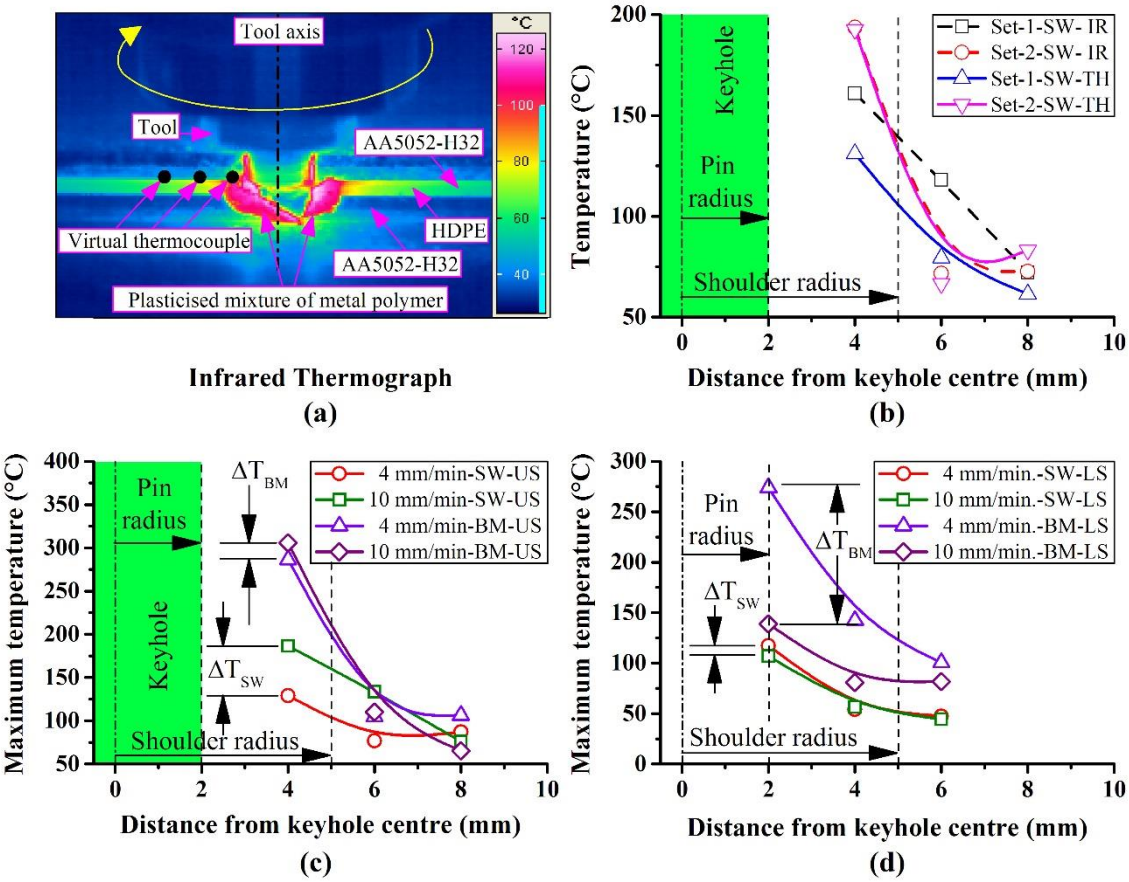

Fig. 4.6 (a) Infrared image of FSSW at the edge, (b) comparison of temperature from IR camera and thermocouple, peak temperature distribution at the (c) mid-thickness of the upper sheet, and (d) mid-thickness of the lower sheet. Error variation in temperature = ± 11 °C [SW: Sandwich sheets; BM: Bimetallic sheets; IR: Infrared; TH: Thermocouple; US: Upper sheet; LS: Lower sheet]

Further, the emissivity values of material are temperature dependent, which affects the temperature output of the IR camera. The emissivity values are kept constant in the present work. When the repeatability of the temperature measurement technique is checked, the thermocouple is found to be reliable. So, the temperature data obtained from the thermocouple is considered for further analysis.

The peak temperature distribution on the upper sheet of the sandwich and bimetallic sheets is shown in Fig. 4.6c. The peak temperature near the keyhole ranges from 129°C to 186°C in the sandwich sheet. In actual FSSW, the temperature would be higher than this. The HDPE melts at 140°C (Capiati and Porter, 1975). So, the polymer sheet melts during welding.

For the sandwich sheet, a larger temperature is observed at higher plunge speed. At higher plunge speed, the tool attains its maximum plunge depth earlier than the lower plunge speed. This also means that the tool shoulder touches the upper sheet at a much earlier stage, which results in

a sudden increase in temperature. Veljic et al. (2013) have also reported a sudden rise in work-piece temperature when the tool shoulder touches the work-piece. The dwell period and tool retracting time is the same in the process, and hence the effect is negligible. Further, the deformation rate at higher plunge speed is large, so the heat generation would also be larger. In the lower sheet, the effect of plunge speed is not significant because of lesser deformation and the frictional contact area between tool pin and work-piece (Fig. 4.6d). Even in bimetallic sheets, the slightly larger peak temperature is recorded on the upper sheet at higher plunge speed. However, in the lower sheet, the temperature at 4 mm/min. plunge speed is larger than at 10 mm/min. This is because in the bimetallic sheet, there is no polymer layer, and hence the heat generated in the upper sheet gets easily transported to the lower sheet. Since at 4 mm/min. plunge speed, the total processing time is larger, heat balancing occurs between the upper and lower sheet, and the temperature becomes almost the same. This is not the case in 10 mm/min. plunge speed due to the lower processing time. The effect of plunge speed is more pronounced in the upper sheet of the sandwich sheet, while it is in the lower sheet of the bimetallic sheet.

In comparison to the bimetallic sheet, the temperature of the sandwich sheet is lesser. A part of the total heat generated is used to melt the polymer core, reducing the temperature attained in the sandwich sheet as compared to bimetallic sheets.

4.2.3 Grain size and hardness distribution

The microstructures of the parent metal and SZ of sandwich and bimetallic sheets FSSWed at 4 mm/min. and 10 mm/min. are shown in Fig. 4.7a–e. The grains in parent metal is non-uniform and non-equiaxed, having an average grain size of 29 µm. In SZ, finer grains are observed. During FSSW, the material in the SZ undergoes severe plastic deformation. This results in grain refinement in the SZ caused by dynamic recrystallization. The dynamic recrystallization occurs when crystalline materials are deformed at elevated temperature, where sub-grains form by the continuous annihilation of dislocations (Sakai and Jonas, 1984). Kwon et al. (2009) have also reported the phenomena of grain refinement by dynamic recrystallization in the SZ during FSW of AA5052. With increasing plunge speed, the SZ grain size increases for both the sandwich and bimetallic sheets, as shown in Fig. 4.7f. This is attributed to static growth during cooling. Since the peak temperature at higher plunge speed is higher (Fig. 4.6c), the grain growth would occur. The SZ grain sizes are 5.2 µm, 11.4 µm for sandwich sheet, and 19.2 µm, 24.6 µm respectively at 4 mm/min. and 10 mm/min. plunge speeds. Larger grains in the bimetallic sheet is observed due to larger static grain growth occurred at higher temperature associated with higher plunge speed.

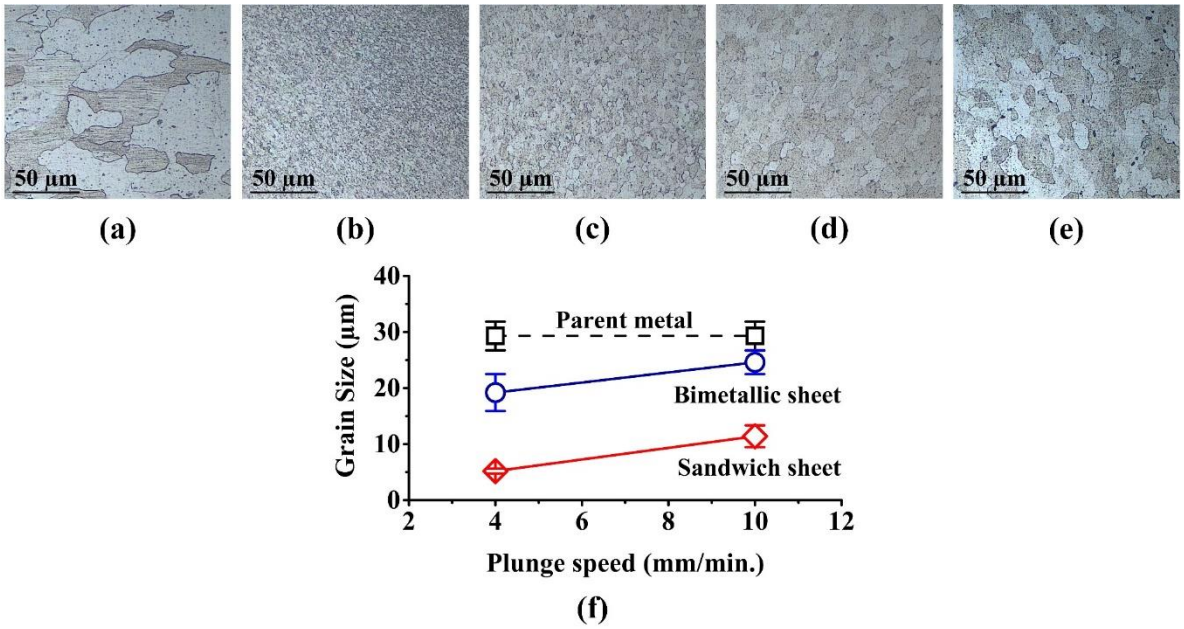

Fig. 4.7 (a) Microstructure of parent metal, SZ microstructure of (b) 4 mm/min.–Sandwich, (c) 10 mm/min.–Sandwich, (d) 4 mm/min.–Bimetallic, (e) 10 mm/min.–Bimetallic, and (f) grain size variation with plunge speed

The hardness distribution across the joint is shown in Fig. 4.8. The region surrounding the joint is found to be harder than the region away from the joint. This is attributed to the formation of finer grains by dynamic recrystallization. The hardness decreases in the outward direction from the keyhole to a certain level, then further increases up to base metal hardness (60-65 VHN). This local softening is caused by the metallurgical recovery in AA5XXX alloy (Kesharwani et al., 2014). The location of the weakest zone lies below the tool shoulder periphery in the upper sheet and below the pin periphery in the lower sheet. The hardness variation with the plunge speed in the upper sheet is insignificant. However, in the lower sheet, it is significant. In the sandwich sheet, higher hardness is observed at higher plunge speed. This is because of the strain hardening of the raw material AA5052-H32 with an increase in plunge speed during FSSW. During deformation, dislocations interact with the dislocations and second phase particles resulting in strain hardening (Huskins et al., 2010); (Sato et al., 2001).

A similar effect is observed in the bimetallic sheet, with an increase in plunge speed. However, in comparison to the bimetallic sheet, the hardness of the sandwich sheet is larger at any particular plunge speed. This is attributed to the deformation at a relatively lower temperature in SW during FSSW (Fig. 4.6c).

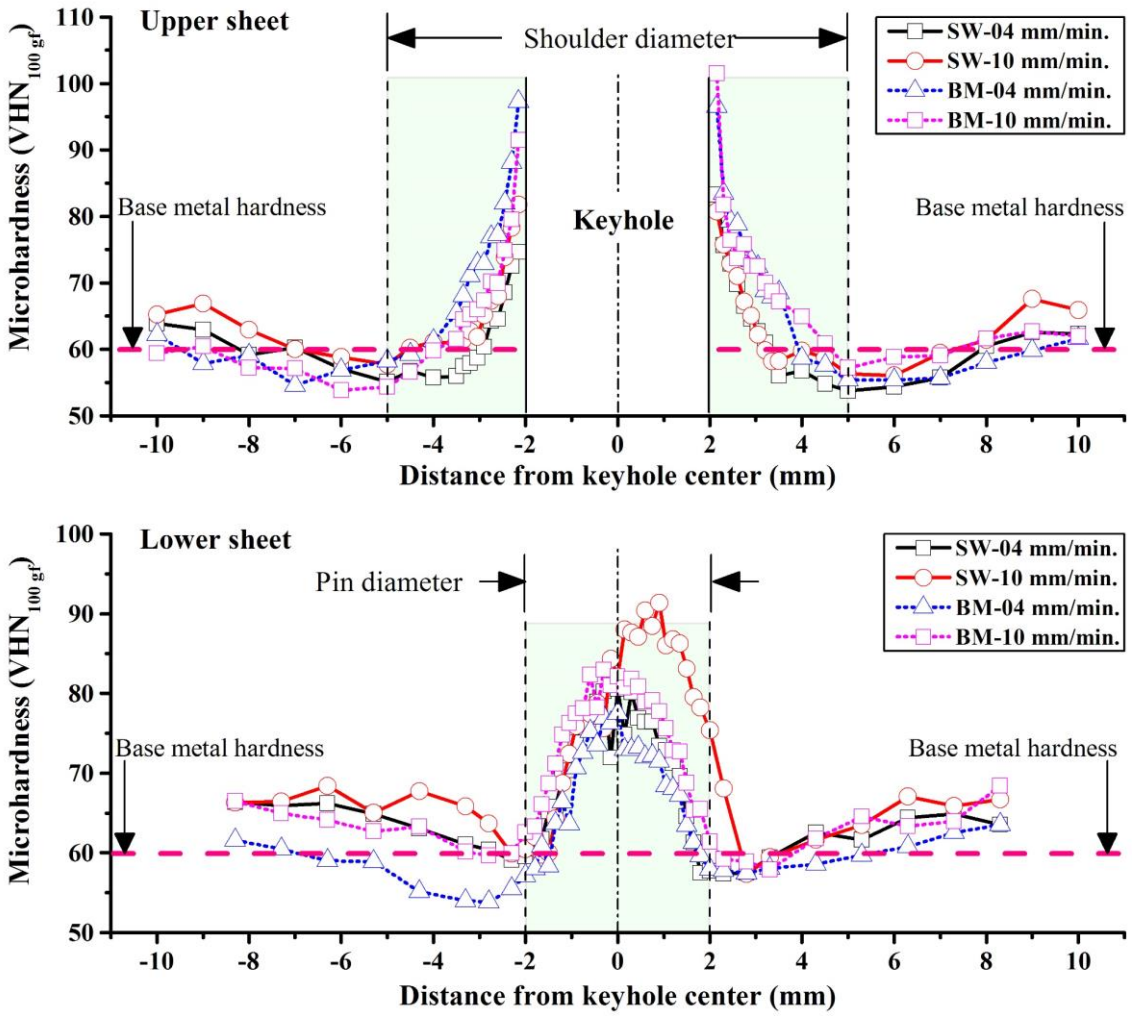

Fig. 4.8 Hardness distribution at (a) mid-thickness of the upper sheet, (b) mid-thickness of the lower sheet. Error variation: ± 2 VHN [SW: Sandwich sheets; BM: Bimetallic sheets]

4.2.4 Mechanical performance and failure modes

The joint performance of sandwich and bimetallic sheets at different plunge speeds is evaluated by measuring joint strength and extension at failure, as shown in Fig. 4.9. The lap shear failure load of the joint initially increases and then decreases after attaining a peak value with increasing plunge speed (Fig. 4.9a). The maximum value is obtained at 8 mm/min. plunge speed. Though hardness of the joint increases with plunge speed, reduction of joint performance after 8 mm/min. plunge speed indicates that other factors apart from hardness also affect joint performance during loading. It is shown earlier in Table 4.2 that the upper bond width (*a*) and effective upper sheet thickness (*g*) are maximum, whereas the upper hook height (*e*) and lower hook height (*f*) are minimum at 8 mm/min. plunge speed. Larger bond width provides a larger resistance for lap shear loading. Lesser hook height reduces the stress concentration. Further, larger effective upper sheet thickness (*g*) makes the joint stronger in the upper region. The combined effect of all these factors

delivers better joint performance in the lap shear test. Yin et al. (2010a) have also reported that larger bond width combined with a smaller hook height and larger effective upper sheet thickness gives better FSSW joint performance in lap shear test. The extension at failure is also considerably larger at 8 mm/min. plunge speed suggesting better ductility of the joint. The proportional relation between lap shear strength of the FSSW joint and its ductility is also confirmed by Mitlin et al. (2006). In the case of a cross-tension test (Fig. 4.9b), the failure load and extension initially increases up to 6 mm/min. plunge speed then decreases and remains almost the same for all succeeding plunge speeds. In this test, it should be noted that the total extension includes sheet bending as well. The actual extension of the joint is only 1-2 mm. The extension at failure is almost proportional to the failure loads. The initial increase in the failure load is attributed to the higher joint hardness at higher plunge speed. Further, in relation with the hook geometry, the effective upper sheet thickness (g) is least in the sandwich sheet at 6 mm/min. plunge speed. The smaller g value results in easy bending of the upper sheet about the upper hook during the cross-tension test. This creates the stress generated by cross-tension to distribute at the upper and lower hook tip. Consequently, the joint performance would be decided by upper and lower bond width (a, and b) together. The summation of the upper sheet has got maximum value at 6 mm/min. plunge speed. This gives largest failure load and extension at 6 mm/min. plunge speed in cross-tension test. The joint performance and ductility in the peel test improves with increasing plunge speed (Fig. 4.9c). It is explained earlier that the joint hardness increases with the plunge speed. It is believed that the joint hardness near the lower sheet is the most dominating factor which decides the failure load. In all the plunge speeds, the joint fails from the lower sheet only. A poor correlation is observed between hook geometry and joint performance in peel test. The uniaxial tensile test result shown in Fig. 4.9d suggests that there is no significant effect of plunge speed on the joint performance.

The bimetallic sheet performance is also affected by the plunge speed. With increasing plunge speed, the failure load and extension at the failure of the bimetallic sheet decrease in lap shear and peel tests, and remain almost constant in the cross-tension test. The reduced performance of the bimetallic sheet at higher plunge speed is due to the lesser upper and lower bond widths (a, and b), as indicated in Table 4.2.

Compared to the bimetallic sheet, when failure load is compared, the sandwich sheet performance is inferior in lap shear test and cross-tension test but superior in the peel test and the uniaxial tensile test. However, in the cross-tension test, the difference in the failure load of the bimetallic and sandwich sheet is less. Hence, it can be concluded that wherever the FSSW joint is

subjected to loading conditions identical to the cross-tension, peel off, or uniaxial tension and the sandwich sheet may perform at par with or better than the bimetallic sheet.

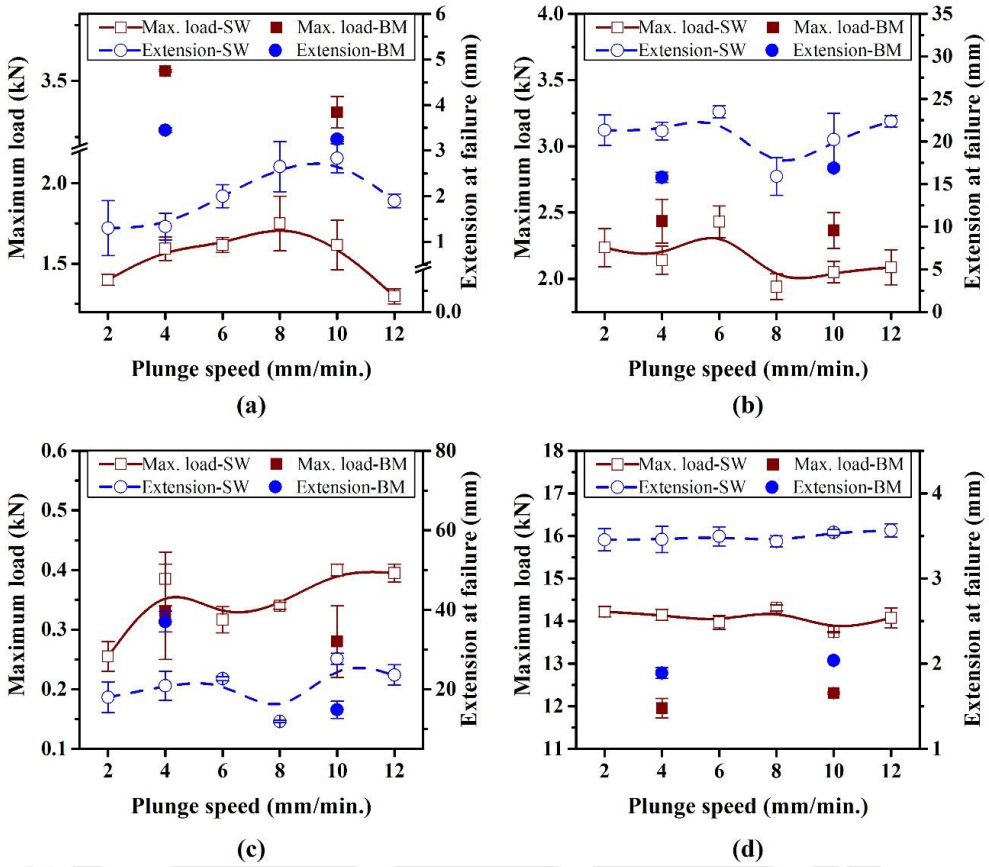

Fig. 4.9 Maximum load and extension at failure for the sandwich and bimetallic sheets: (a) lap shear test, (b) cross-tension test, (c) peel test, and (d) uniaxial tensile test [SW: Sandwich sheets; BM: Bimetallic sheets]

The modes of failure in each test are shown in Fig. 4.10. In lap shear test, partial nugget fracture is observed for the sandwich sheet welded at 2 mm/min. plunge speed. This type of failure mode occurs in the lap shear test when the lower hook height (*f*) is larger, and the region near the lower hook is not stronger. The larger hook height creates excessive stress concentration, and the softer region promotes crack propagation during loading. At lower plunge speed, a larger lower hook height (*f*) is seen (Table 4.2) and Fig. 4.8 shows that the region near the keyhole is relatively softer. In all other plunge speeds, the failure mode is 'nugget pull-out' in lap shear test. In the cross-tension test, and peel test, irrespective of plunge speed, the sandwich sheet failed as 'nugget pull-out' mode. The 'nugget pull-out' mode of failure occurs because of the lesser lower bond width (*b*) as compared to the upper bond width (*a*) (Table 4.2). During loading, the cracks nucleate at the hook tip and propagate towards keyhole. Since the lower hook tip exists closer to the keyhole, the crack originated from the lower hook reach the keyhole boundary earlier than that from the

upper hook. This results in detachment of nugget from the lower sheet, which is called 'nugget pull-out.' The mechanism of nugget pull-out mode of failure in FSSW of the sandwich sheet is explained elsewhere.

The joint of the bimetallic sheet is failed by 'interfacial separation' in lap shear and peel tests at all plunge speeds. In the cross-tension test, the 'nugget pull-out' mode of failure is observed. However, the 'nugget pull-out' mode of failure in the bimetallic sheet is different than that in the sandwich sheet. In the bimetallic sheet, the nugget remains attached to the lower sheet after failure, while in the sandwich sheet it is with the upper sheet. This is mainly due to lesser effective upper sheet thickness (g) of the bimetallic sheet (Table 4.2) as compared to sandwich sheet.

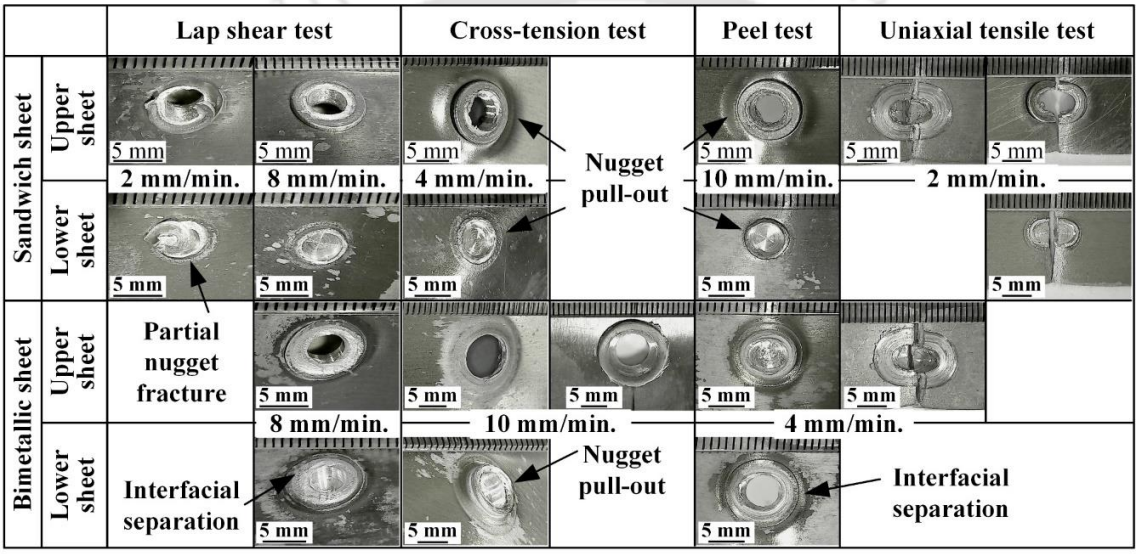

Fig. 4.10 Failure modes of sandwich and bimetallic sheets

In the uniaxial tensile test, fracture occurs in the middle of the joint. This is likely due to the presence of keyhole developing high-stress concentration around the joint. The bimetallic and sandwich sheets at all plunge speeds failed in a similar manner. The fracture surface of bimetallic and sandwich sheets is analyzed by scanning electron microscopy, as shown in Fig. 4.11 for FSSW at 4 mm/min. plunge speed. The presence of dense and large dimples in the sandwich sheet suggests that the ductility of the joint is larger than the bimetallic sheet. Larger ductility of the FSSW joint of the sandwich sheet is confirmed in Fig. 4.9d.

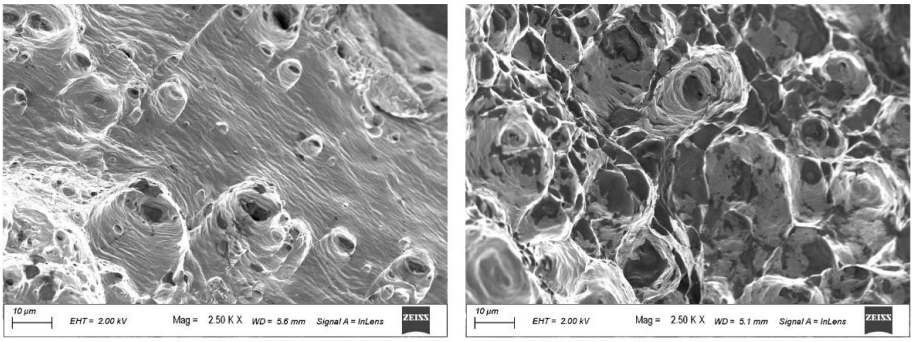

(a) (b)

Fig. 4.11 SEM image of the fractured surface in the stir zone of (a) bimetallic sheet, and (b) sandwich sheet

The von Mises stress distribution in sandwich sheets during mechanical tests predicted by FE analysis is shown in Fig. 4.12. The maximum stress is developed only in the joint region irrespective of the testing method. Further, the maximum stress is concentrated near the lower hook in the joint.

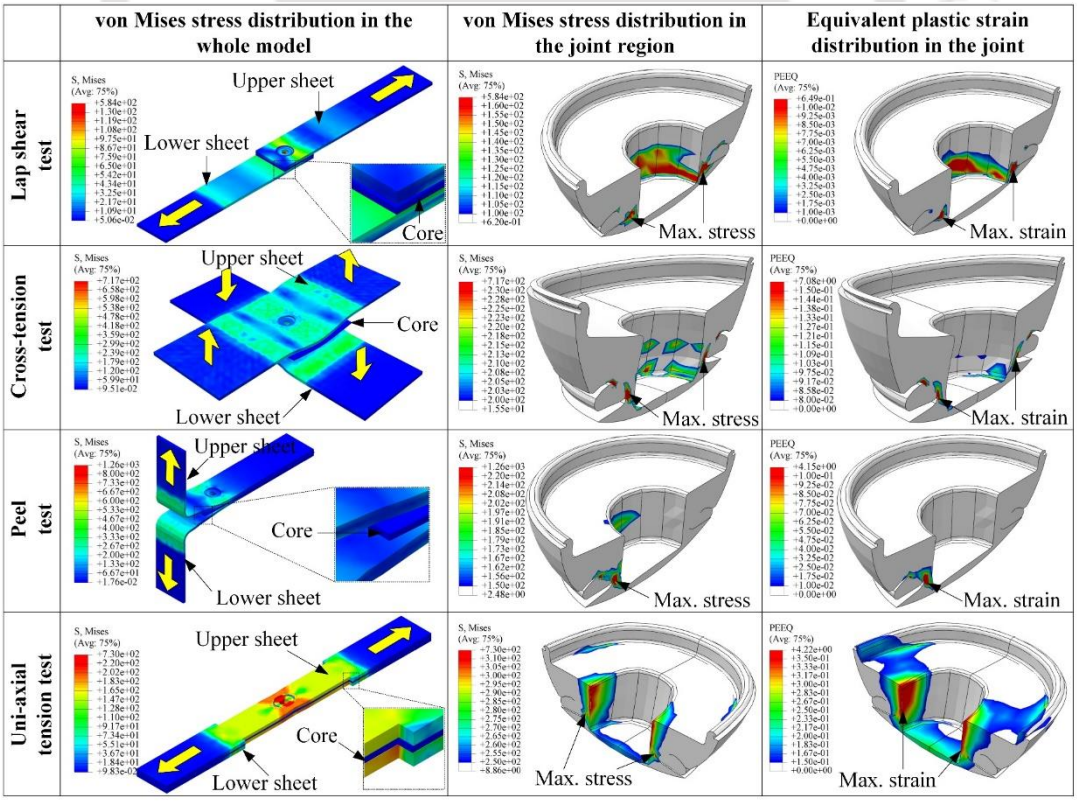

Fig. 4.12 FE simulation of mechanical tests and equivalent stress and equivalent strain distribution in the joint

The equivalent plastic strain is also found to be maximum at the same location. Hence, it is

predicted that failure would occur in this location, and the failure mode would be 'nugget pull-out' as seen in experiments. In the uniaxial tensile test, the maximum stress and maximum equivalent plastic strain location lie along the diameter of the joint. So, the fracture is likely to occur in this location. Similar results are observed in the experimental data. Lacki and Derlatka have also confirmed that the location of the maximum strain location decides the failure location, which exists at the sheet interface and outer edge of the spot (Lacki and Derlatka, 2016).

4.3 Conclusions

The objective of the present work is to investigate the influence of tool plunge speed during FSSW of sandwich sheets of type AA5052-H32/HDPE/AA5052-H32. The performance of sandwich sheets and bimetallic sheets is also compared. The following are the major conclusions obtained from the results.

- The hook geometry changes significantly with plunge speed in the sandwich sheet. With an increase in plunge speed, (a) the upper bond width initially increases and then decreases because of change in SZ size, (b) the upper hook width initially decreases and then increases due to hook merging in SZ, (c) the upper hook height slightly decreases due to reduced material flow in the upward direction, (d) the lower hook geometry does not change much. However, lower hook flattening results in a decrease in lower hook height.
- The best joint performance of the sandwich sheet in the lap shear test and cross-tension test is obtained at a moderate range of 8 mm/min. and 6 mm/min. respectively. In the peel test, the failure load continuously increases with plunge speed. The extension at failure is almost proportional to the failure load. The mechanical performance of the bimetallic sheet is superior to the sandwich sheet in lap shear and cross-tension test, while it is inferior in the peel test and uniaxial tension test. However, extension at the failure of the sandwich sheet is larger in cross-tension test at all the plunge speeds and in peel test at higher plunge speed.
- With increasing plunge speed, higher temperature develops in the upper sheet of the sandwich sheet, which is due to the larger deformation rate. The effect of plunge speed is negligible in the lower sheet, due to lesser deformation and the frictional contact area between tool pin and work-piece. In bimetallic sheets, a slightly larger temperature is recorded at higher plunge speed in the upper sheet. The temperature attained in the sandwich sheet is lesser because a part of the total heat generated is used to melt the polymer core.
- A coarser microstructure is obtained at higher plunge speed due to higher peak temperature.

The higher temperature also produces larger grains in the bimetallic sheets.

- With increasing plunge speed, the hardness of the joint improves due to a higher rate of deformation. The sandwich sheet shows higher hardness than the bimetallic sheet because of deformation at lower temperatures.
- The failure modes observed in the sandwich sheet are 'partial nugget fracture' and 'nugget pull-out.' The 'partial nugget fracture' occurs when the lower hook height is larger, and the hardness is lesser, and the joint is deformed by lap shear. The 'nugget pull-out' mode of failure occurs when the lower bond width is lesser than the upper bond width. The bimetallic sheet fails by 'interfacial separation' in lap shear and peel test, while 'nugget pull-out' in the cross-tension test.
- The FE analysis reveals that the von Mises equivalent stress and equivalent plastic strain distribution is maximum near the lower hook. This allows the lower sheet to detach from the joint at this location. It is confirmed in the experiments by the 'nugget pull-out' mode of failure, which occurs predominantly in the sandwich sheet in all the tests at every plunge speed, except lap shear test at 2 mm/min.
- The fractograph of the specimen suggests that the joint produced in the sandwich sheet are more ductile than the bimetallic sheet when FSSW is done at the same plunge speed.

Chapter 5

Influence of dwell time during friction stir spot welding of AA5052-H32/HDPE/AA5052-H32 sandwich sheets

5.1 Experimental procedure

The description of material and sample preparation technique is already discussed in Chapter 2. Similar procedure is followed in the present chapter also. The process parameters selected for FSSW is mentioned in Table 5.1. The dwell time is varied with fixed values of other parameters.

Table 5.1 FSSW process parameters for joining sandwich and bimetallic sheets

	Sandwich sheet						Bimetallic sheet	
	Set-1	**Set-2**	**Set-3**	**Set-4**	**Set-5**	**Set-6**	**Set-2**	**Set-5**
Dwell time (s)	0	5	10	15	20	25	5	20
Rotational speed (rpm)	1600 (kept constant)							
Plunge depth (mm)	3.6 (kept constant)							
Plunge speed (mm/min.)	8 (kept constant)							

5.1.1 FSSW joint Characterization

The procedure of mechanical tests, microstructural examination, hardness measurement, and temperature measurement are already mentioned in Chapter 2. Temperature measurement is performed at 5 s, and 20 s dwell times only. A comparison of the temperature evolution obtained from these methods is made on the joint made at 1200 rpm rotational speed, 3.6 mm plunge depth, 6 mm/min. plunge speed and 5 s dwell time.

5.1.2 Prediction of flow visualization during FSSW by FE simulation

In the sandwich sheets, the flow of plasticized material during FSSW is different from that of the bimetallic sheet, which is confirmed by difference in joint features. The material flow behavior during FSSW is analyzed by FE simulation. Chu et al. made a similar attempt by FEA of FSSW of AA2198. The results show morphological changes in the joint during the process (Chu et al., 2018). However, FE simulation has never been applied before on FSSW of sandwich sheets. To understand the formation of joint features, in the present work, the FE simulation of FSSW of SWS is performed in ABAQUS/Explicit code. In the FE model, three deformable parts, and a rigid

tool are assembled, as shown in Fig. 5.1. Boundary conditions are applied in such a way that the bottom face of the lower sheet, including side faces of all the sheets are fully constrained. Here, the fixed bottom face of the lower sheet acts as an anvil. The portion of the upper face of the upper sheet outside the 10.2 mm (slightly larger than the shoulder diameter of 10 mm) diameter circle at the center is fixed in all directions to enable upper sheet clamping. To incorporate temperature degree of freedom in the work-pieces, an 8-node thermally coupled brick, trilinear displacement, and temperature with reduced integration element (C3D8RT) is selected for upper and lower sheets. An identical element is used by Aval et al. (2011), in the thermo-mechanical simulation of FSW of AA5086 to study the effect of heat input on the grain structure. The element type for the core layer is selected as 4-node thermally coupled tetrahedron, linear displacement, and temperature (C3D4T). Variable element sizes are selected in different regions, as depicted in Fig. 5.1.

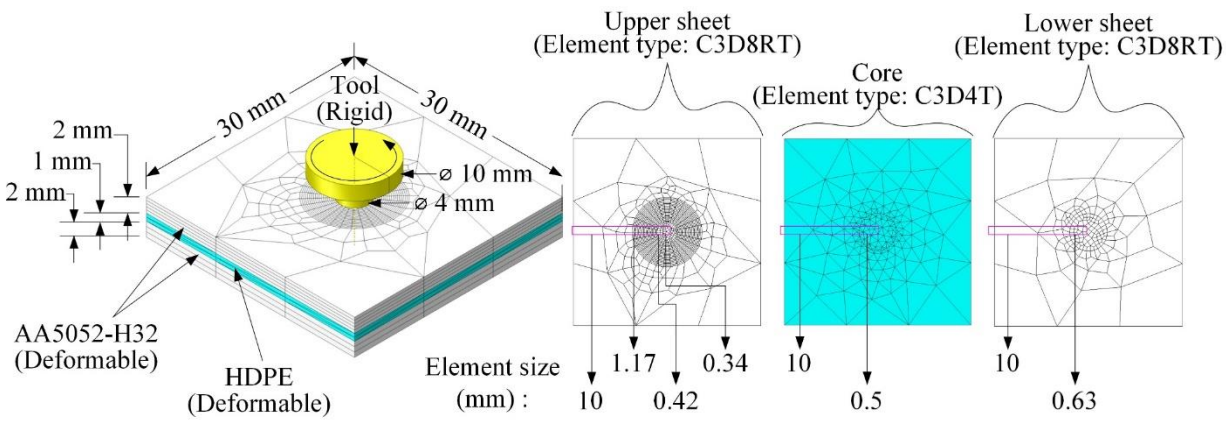

Fig. 5.1 FE model of FSSW of sandwich sheets and element selection

In the work-piece clamping region, which does not deform during FSSW, a larger element size of 10 mm is assigned to reduce computational time. A typical element size variation in the deforming region is shown in Fig. 5.1. The element size decreases towards the center to accommodate finer details of deformation. If elements are bigger than the chosen sizes, simulation aborts due to excessive deformation, while smaller elements increase the computation time. A similar strategy is followed for mesh selection in lower sheet and core layer. The temperature-dependent properties of AA5052-H32 from the existing reference are incorporated during the FE simulation (Fig. 5.2) (Zhu and Chao, 2002).

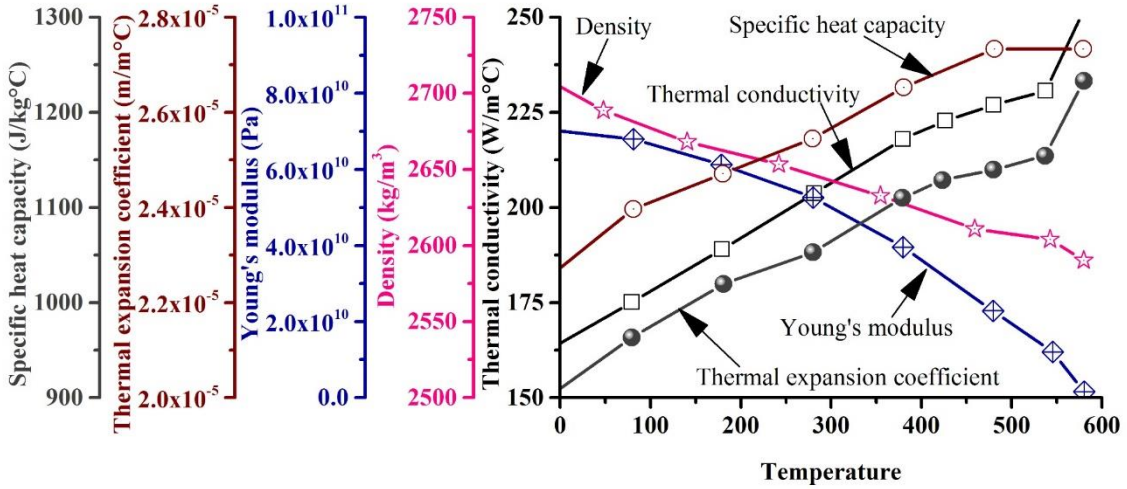

Fig. 5.2 Properties of AA5052-H32 as a function of temperature incorporated during FE simulations

To include the effect of frictional heating in the material behavior, the Johnson-Cook plasticity model is chosen for the skin sheet, which is given by

$$\sigma = \left[A + B\left(\varepsilon_p\right)^n\right].\left[1 + C\ln\left(\frac{\dot{\varepsilon}_p}{\dot{\varepsilon}_0}\right)\right]\left[1 - (T^*)^m\right], \tag{5.1}$$

where σ is the equivalent von Mises stress, and A, B, C, n, m, are quasi-static yield stress, hardening constant, strain-rate sensitivity parameter, hardening exponent, temperature sensitivity parameter respectively. ε_p, $\dot{\varepsilon}_p$, and $\dot{\varepsilon}_0$ are the equivalent plastic strain, equivalent plastic strain-rate, and the reference strain-rate respectively. T^* is the non-dimensional temperature given by

$$T^* = \frac{T - T_0}{T_m - T_0}, \tag{5.2}$$

where T, T_0, and T_m are the current temperature, reference temperature, and the melting temperature, respectively. The Johnson-Cook plasticity parameters used in the present FE simulation are shown in Table 5.2 (Bentouhami, 2018). All the values in Johnson Cook equation are kept as it is to those used in the literature to avoid any unwanted effect on the simulation.

Table 5.2 Johnson-Cook plastic parameters for the skin sheets

A (MPa)	B (MPa)	n	$\dot{\varepsilon}_0$	C	m	T_m (°C)	T_0 (°C)
256	426	0.34	1	0.015	1	550[1]	0

[1] The melting point of AA5052-H32 is considered as 550°C as per the availability. However, the readers may use their own value.

For HDPE, Young's modulus (1.05 GPa) and Poisson's ratios (0.46) of HDPE are taken from Khalajmasoumi et al. (2012) and Zhang and Moore (1997), respectively. The thermal conductivity and density at different temperatures are taken from Santos et al. (2013) and Ramin et al. (2014), respectively, as shown in Fig. 5.3. The plastic stress-strain data for HDPE evaluated from the tensile tests experiment (Fig. 5.3b) are included in the core property in the simulation.

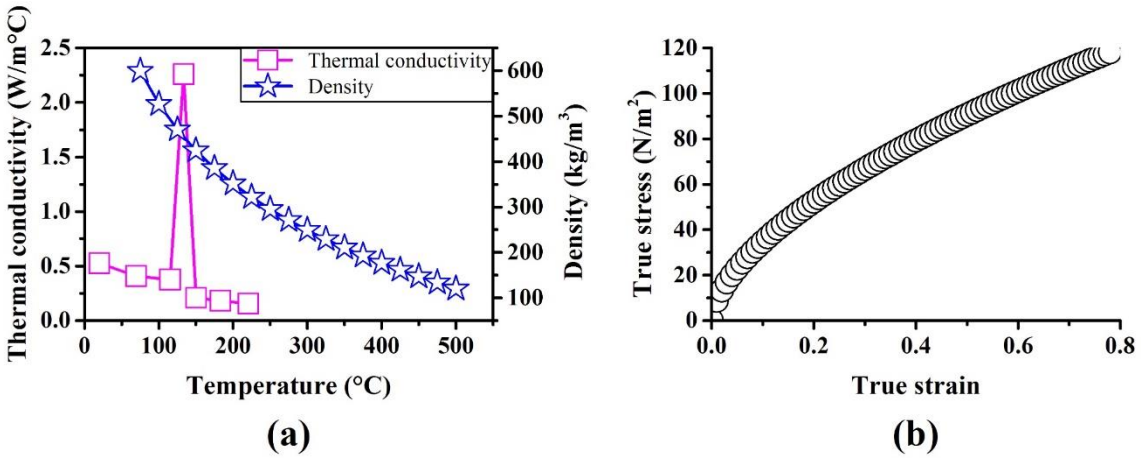

Fig. 5.3 (a) Temperature-dependent properties and (b) True stress – true strain behavior of HDPE incorporated during FE simulations

The core layer completely fails near the joint due to the mixing of upper and lower sheet material. Therefore, in simulation, a damage criterion is required in order to remove elements after failure. The damage criterion includes damage initiation followed by damage evolution. A shear failure criterion is used for damage initiation in elements of the core layer. The shear criterion states that failure starts when the equivalent shear strain $\overline{\varepsilon}^{pl}$ crosses a critical value $\overline{\varepsilon}_S^{pl}$ as described below (Levanger, 2012)

$$\int_0^{\overline{\varepsilon}_S^{pl}} \frac{d\overline{\varepsilon}^{pl}}{\overline{\varepsilon}_S^{pl}\left(\theta_S,\ \dot{\overline{\varepsilon}}^{pl}\right)} = 1, \tag{5.3}$$

where $\overline{\varepsilon}_S^{pl}$ is the equivalent plastic at the onset of damage. $\overline{\varepsilon}_S^{pl}$ depends on shear stress ratio (θ_S) and strain rate ($\dot{\overline{\varepsilon}}^{pl}$), and θ_S is given by

$$\theta_S = \frac{q+k_s P}{\tau_{max}}, \tag{5.4}$$

where q is the von Mises stress, P is the hydrostatic stress, τ_{max} is the maximum shear stress and k_s is a material parameter. The value of k_s for HDPE is chosen as zero. The values of θ_S and

$\dot{\bar{\varepsilon}}^{pl}$ are initially selected as 1 and 1 respectively while the value of $\bar{\varepsilon}_s^{pl}$ is selected as 0.001 based on several iterative trials for the first element to fail. When damage initiates, an effective plastic displacement-based criterion with linear softening and maximum degradation is specified to introduce progressive material damage until the final failure describes the damage evolution. In the damage evolution model, the stress developed in the element is given as

$$\sigma = (1 - D)\bar{\sigma}\,, \tag{5.5}$$

where $\bar{\sigma}$ is the stress due to undamaged response and D is the overall damage variable obtained from

$$\dot{D} = \frac{L\,\dot{\bar{\varepsilon}}^{pl}}{\bar{u}_f^{pl}}\,, \tag{5.6}$$

where L is the characteristic length of the element (0.5 mm) and $\bar{u}_f^{pl}$ is the effective plastic displacement at fracture. $\bar{u}_f^{pl}$ is taken as 0.2 mm by several iterative trials to make complete mesh deletion of the core layer in the pathway of upper sheet metal flow.

The FE model is solved by dynamic coupled thermal-stress analysis using explicit integration. A general contact algorithm is applied with a slip rate and contact pressure-dependent coefficient of friction (Table 5.3).

Table 5.3 Variation in the coefficient of friction with slip rate and contact pressure (Awang, 2007)

Slip rate (m/sec.)	Contact pressure (N/m^2)	Coefficient of friction	Variation
0.002	-	0.295	Linear
0.499	-	0.084	
-	2042950	0.300	Linear
-	1502087730	0.099	

5.1.3 Prediction of failure modes by FE simulation

An attempt is made to predict the failure modes during mechanical testing using FE simulation by ABAQUS FE code. FE simulations are performed on a three-dimensional (3D) model of each test specimen. The 3D models are generated using AutoCAD, in which important geometrical features of the joint such as flash, hook, and extruded zone of the sandwich sheet, are incorporated. These features are obtained from the macro-structural characterization of the joint cross-section. Each specimen consists of three different regions, viz., AA5052-H32, HDPE, and the joint. Individual properties are assigned to different sections. The skin and core properties are obtained

from the tensile tests. The joint properties are taken from the tensile test conducted for the welded specimen, where the deformation is localized near the joint (Fig. 5.4a). The selected element type is C3D10M, which is a ten-node modified quadratic tetrahedron element. Zivojinovic et al. (2013) have used the same element to study the phenomena of crack growth in FSW. Variable element sizes are used at different sections of the model. In the joint region, a finer mesh of 0.5 mm size is used to identify the correct location of the failure. On the other hand, the region away from the joint is assigned with a coarser mesh of 10 mm size to reduce computational time. A typical element size is shown for lap shear specimen (Fig. 5.4b). Further, mass scaling is adapted to reduce computational cost. The deformation speed in the simulation is kept equal to the ram speed in the actual experiment. After completion of the simulation, the failure location in the FE model and the actual specimens are compared and validated.

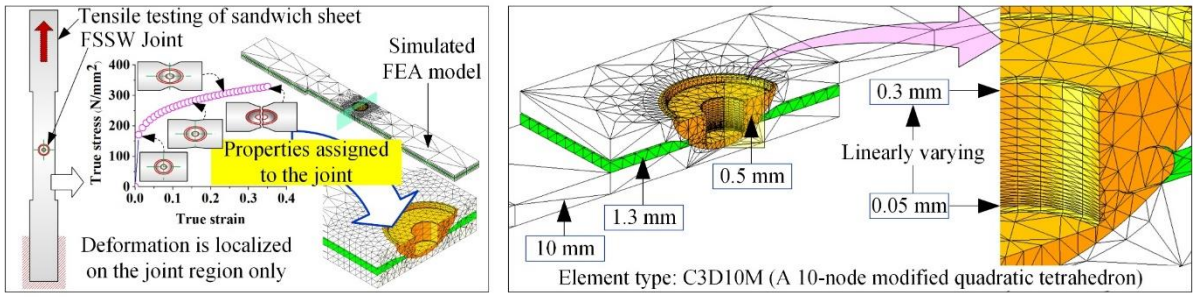

Fig. 5.4 (a) Method of incorporating joint mechanical properties, (b) Element size in the lap-shear specimen in the FE model

5.2 Results and discussion

5.2.1 Hook formation

A hook is a geometric defect and a characteristic feature of FSSW (Badarinarayan et al., 2009). The hook originates at the interface of the overlapped sheet and gets arrested at` the boundary of the stir zone. It is formed due to insufficient metallurgical bonding between two sheets because of the trapped oxide layer at the interface. The oxide layers break into tiny particles by tool rotation and displace upward while tool plunge downwards. The broken oxide particles are properly mixed with the plasticized material in the stir zone and a continuous joint is formed.

However, outside the stir zone, the oxide particles remain unmixed due to reduced stirring. The unmixed oxide particles often follow a curved profile, which appears as a hook-like structure. Typical hook formation is shown in Fig. 5.5. It is observed that two hooks originate from a single

interface in the bimetallic sheet, unlike two separate interfaces in the sandwich sheet.

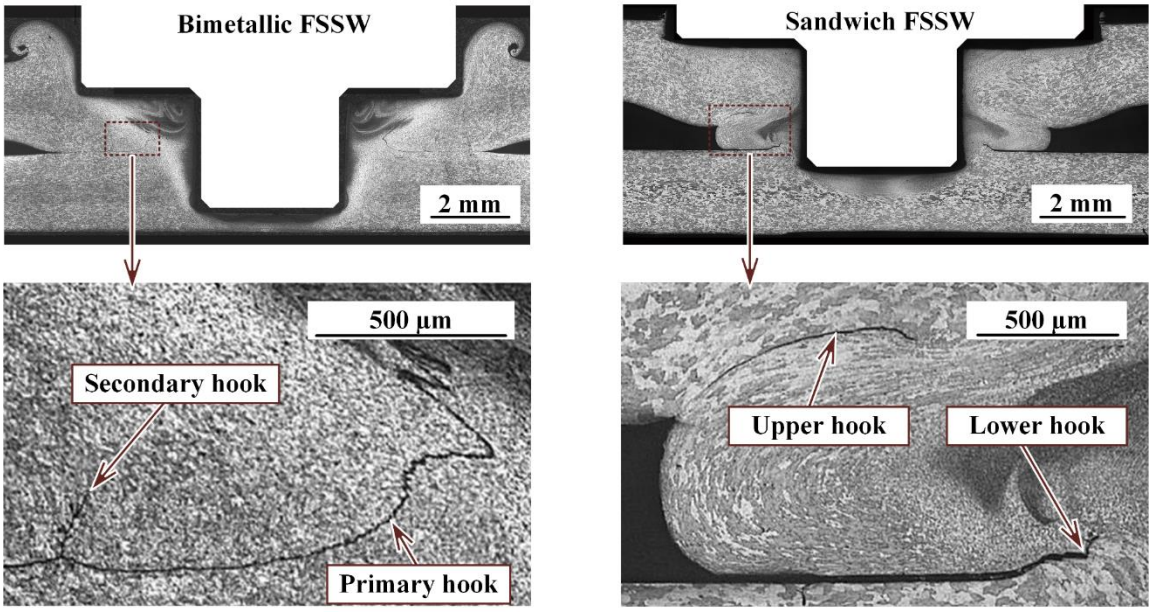

Fig. 5.5 Hook formation in bimetallic and sandwich FSSW joints

The hooks formed at the FSSW joint are characterized by measuring various geometries associated with it. These geometries are schematically described in Fig. 4.3 in Chapter 4. The bond width represents the minimum gap between the hook tip and the keyhole boundary. Lin et al. pointed out that the larger bond width gives better strength to the FSSW joints (Lin et al., 2012). The horizontal and vertical gaps between the hook tip and the hook originating point are the hook width and the hook height, respectively. The minimum distance of shoulder touching surface from the upper hook tip is termed as effective upper sheet thickness. Yin et al. have proposed that the FSSW joint performance improves when bond width increases, hook height decreases, and effective upper sheet thickness increases (Yin et al., 2010a).

Fig. 5.6 demonstrates the hook features formed at different dwell times in sandwich and bimetallic sheets. Typical change in upper and lower hook geometry with dwell time is observed. Furthermore, the material flow in the extruded zone in the sandwich sheet increases with increasing dwell time up to 15 s and then decreases. The initial increase in material flow is attributed to softening caused by larger heat input at a larger dwell period. Moreover, a larger volume of extruded material at prolonged processing time is obvious. However, after 15 s, excessively softened material would exert difficulty in extruding against the polymer layer, which reduces the size of the extruded zone.

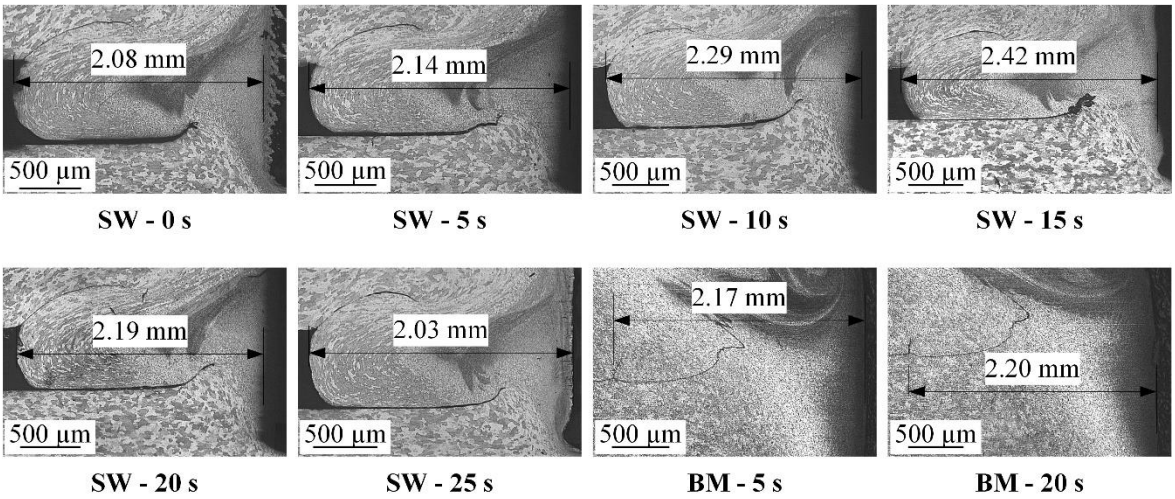

Fig. 5.6 Hook morphologies at varying dwell time

The change in hook geometry with dwell time is shown in Fig. 5.7. The upper bond width initially increases up to a dwell time of 10 s and decreases after that in the sandwich sheet (Fig. 5.7a). With increasing dwell time, the heat input increases, resulting formation of larger bond width. However, after a critical limit, the material softens more, causing slippage between the tool and work-piece, resulting in reduced stirring, which limits the size of the bond width. The upper hook height increases with dwell time up to 20 s and then decreases slightly (Fig. 5.7d).

With increasing dwell time, the upward metal flow increases due to increased plasticization. However, at prolonged dwell time, the metal flow reduces due to reduced stirring. The upper hook width and lower bond width do not change much with dwell time (Fig. 5.7b, c). The lower hook height and width increase with dwell time up to 15 s and then decrease (Fig. 5.7e, f). The lower hook geometry directly depends on the extruded zone characteristics. As shown in Fig. 5.6, maximum extrusion of plasticized metal into the core layer occurred at a dwell time of 15 s. Larger extruded zone signifies greater plasticization. The broken oxide particles from the lower interface displace upward easily due to softer material in the extruded zone. This results in a farther shift of lower hook initiation point from the keyhole boundary, thereby increasing lower hook width. At the same time, the softer extruded zone facilitates the oxide particle to displace upward, which increases the lower hook height. After 15 s, the extruded zone reduces, reducing the height and width of the lower hook. The change in effective upper sheet thickness with dwell time is insignificant.

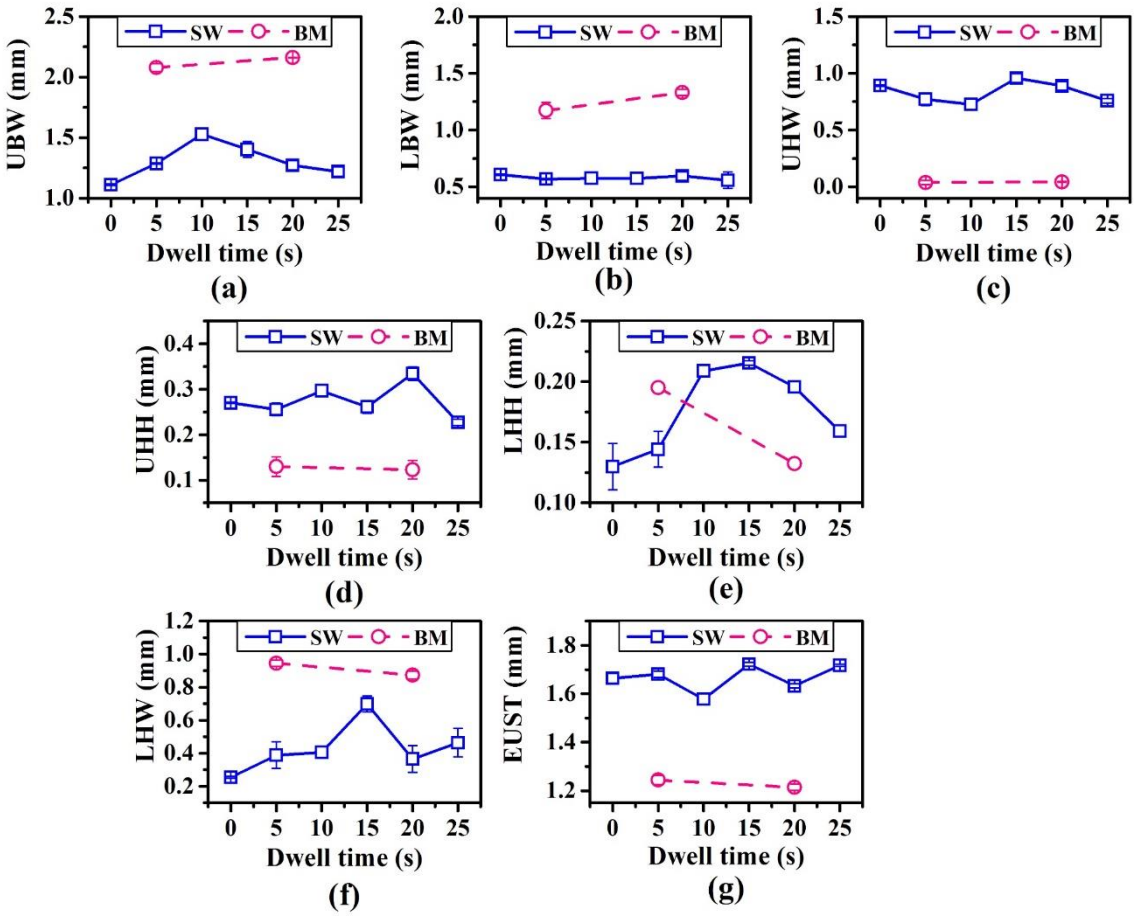

Fig. 5.7 Effect of dwell time on (a) upper bond width, (b) lower bond width, (c) upper hook width, (d) upper hook height, (e) lower hook height, (f) lower hook width, and (g) effective upper sheet thickness

In the bimetallic sheet, the upper and lower bond width increases with dwell time due to the expansion of stirred material with time (Fig. 5.7a, b). Lin et al. (2012) have also reported that the bond width increases at prolonged dwell time due to the extension of the stirred region as a result of greater heat generation. The upper hook and lower hook of the bimetallic sheet mentioned in Fig. 5.7 correspond to secondary and primary hook, respectively. Since the secondary hook in the bimetallic sheet is not fully developed, Fig. 5.7 does not reflect any significant change in the upper hook geometry with dwell time. However, the height and width of the lower hook are decreased at larger dwell time (Fig. 5.7e, f).

In contrast with the bimetallic sheet, the sandwich sheet exhibits smaller bond width (Fig. 5.7a, b) due to formation of smaller (~72 %) stir zone, which is due to the expansion of plasticized material outward, unlike flowing through the core layer in sandwich sheets. Furthermore, the temperature generated in the bimetallic sheet is also higher than in the sandwich sheet, which causes intense stirring and expanding the SZ. The upper hook height and width are lower than

that of the sandwich sheet as these are associated with the secondary hook in the bimetallic sheet, which is partially developed. The smaller bond width results in a lower joint performance of the sandwich sheets. The lower hook height has higher and lower values in contrast with the sandwich sheet, respectively, at lower and higher dwell time. The lower hook geometry becomes important in sandwich sheets because failure is likely to occur from the lower hook. Earlier research shows that when lower hook height increases, the chance of nugget fracture increases during loading, which eventually reduces the joint performance. The lower hook width of the bimetallic sheet is larger due to the farther existence of hook initiation point from the keyhole boundary due to larger stir zone size. The effective upper sheet thickness of the bimetallic sheet is lesser than that of the sandwich sheet (Fig. 5.7g). For the same plunge depth of 3.6 mm, the pin plunging into the lower sheet is higher in the case of bimetallic sheets as compared to sandwich sheets. Consequently, the hook tip is displaced in the upward direction, reducing the effective upper sheet thickness. There is a positive correlation between effective upper sheet thickness and joint performance (Badarinarayan et al., 2009).

During the FSSW of the sandwich sheet, the core layer gets degraded locally at the joint region (Fig. 5.8). The degradation of polymer sheet increases with increasing dwell time, which is due to longer contact time of polymer with nearby stirred metal and large temperature generation at larger dwell time.

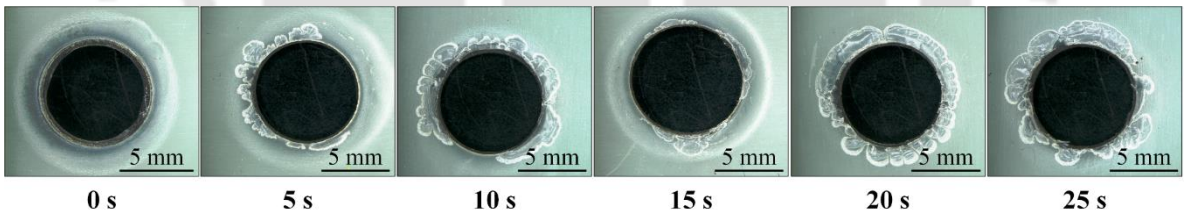

Fig. 5.8 Effect of dwell time on polymer sheet degradation

5.2.2 Material flow visualization during FE simulation

The material flow in the sandwich sheet during FSSW is investigated using FE analysis. The visualization of the joint cross-section and instantaneous displacement vector of each element is shown in Fig. 5.9. The joint clearly shows severe plastic deformation of the material in the joint. The hook formation and extrusion of plasticized material into the core layer are also seen. The same features are observed in experiments (Fig. 5.5, Fig. 5.6). The formation of the lower hook is not seen in the present model since the upper sheet, and the lower sheet are separated by a continuous boundary. However, the tendency to form a lower hook is justified well by the upward

movement of material underneath the tool pin.

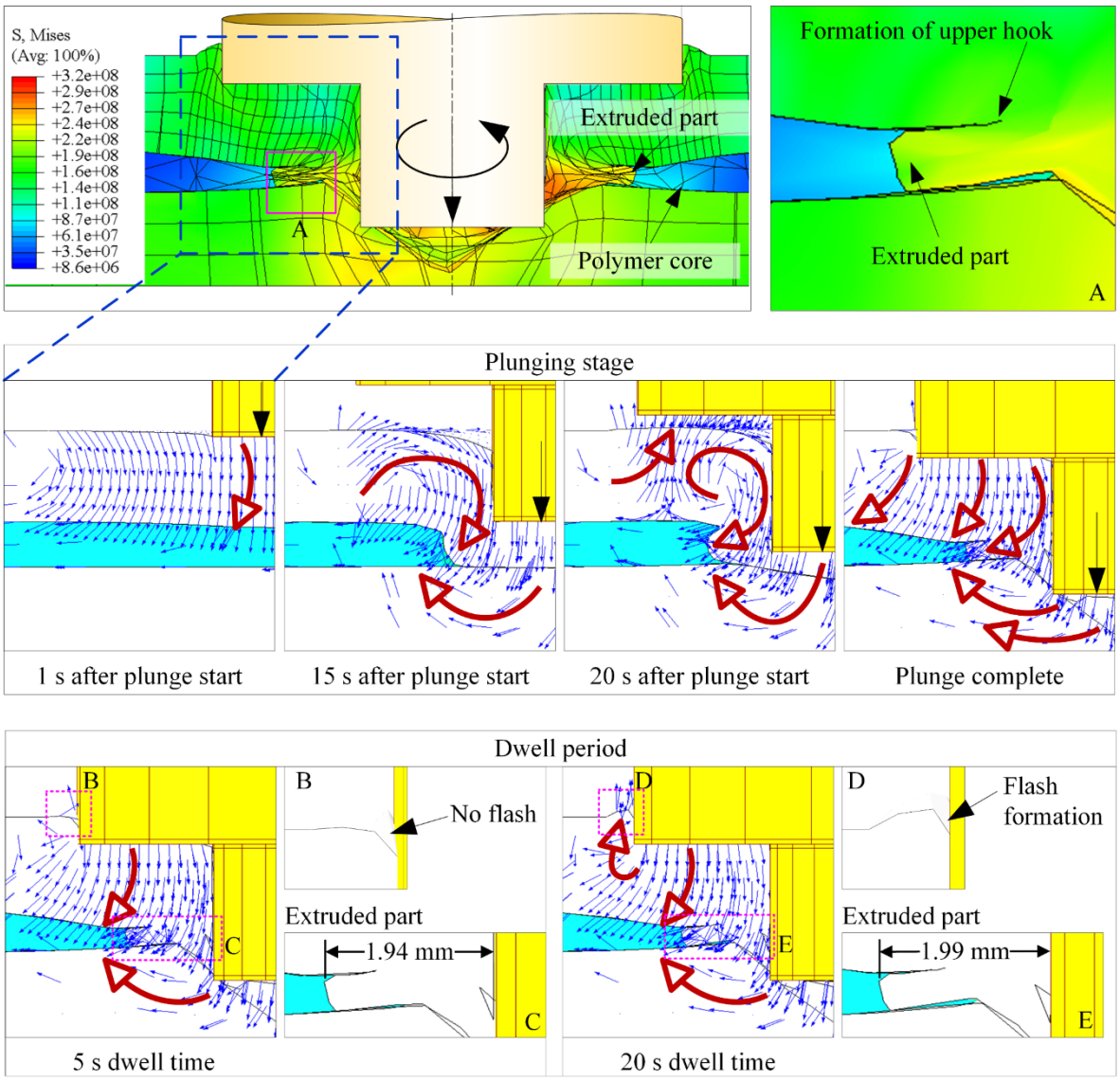

Fig. 5.9 Typical flow pattern of material in FSSW of the sandwich sheet in plunging stage and dwell period from FE simulation

The displacement vectors of elements suggest that at the beginning of the process, say 1 s after plunging start, the upper sheet material under the tool pin displaces vertically downwards. As time passes, material displacement increases. After 15 s, a larger volume of material from the pin surrounding is dragged near the pin surface and displaced in the downward direction. However, the downward movement of material is hindered by the relatively harder lower sheet material. Therefore, the plasticized material easily moves into the polymer core layer. This change in the direction of material flow is confirmed from the displacement vector shown in the frame corresponding to 20 s. With further increase in plunge depth, when pin plunges into the lower

sheet, the upper sheet also gets plunged by the shoulder. Now the local upward movement of upper sheet material is reversed by the tool shoulder. Therefore, a larger volume of material starts flowing downward, as shown by the displacement vectors at the completion of the plunging stage. Here, a larger portion of the upper sheet is being pressed by the shoulder, deforming it significantly. This makes the passage narrower through which the plasticized material flows into the polymer core. This also generates a curved separation boundary between the upper sheet and the extruded portion, which gets extruded significantly into the joint, termed as the upper hook. After the maximum plunge depth, the dwell phase begins.

The material flow is compared at two dwell periods, 5 s and 20 s. The displacement vectors do not show any significant change with change in dwell time. However, plasticization of material is increased at higher dwell time due to larger heat input. The increased plasticization is reflected by the expansion of the extruded portion by 2.58 % and the flash formation. The experimental results also confirm about 2.34 % larger extruded zone for 20 s dwell time in comparison to 5 s (Fig. 5.6).

5.2.3 Temperature measurement

An infrared thermograph captured during the FSSW at the edge of the overlapped sheet is shown in Fig. 5.10a. The thermograph shows a larger temperature field near the weld. A typical temperature profile at the three locations, 4 mm, 6 mm, 8 mm from tool axis, obtained in the sandwich sheet (Fig. 5.10b). Temperature increases from the beginning when the tool touches the work-piece. Point ‘A’ corresponds to the time when the spindle starts rotating, and it attains its maximum rotational speed at point ‘B.’ ‘B-C’ is the time lag for the beginning of the plunge stage. ‘D’ is the point when the pin has completely plunged the upper sheet. This is the first stage of plunging for which the temperature increases continuously. After point ‘D’, the tool starts plunging through the soft polymeric core layer, reducing the plunging force. As a result, the temperature decreases suddenly. When the tool crosses point ‘E,’ the pin descent into the lower sheet, at the same time, the shoulder plunges the upper sheet. Consequently, the temperature increases rapidly. At ‘F,’ the tool attains its maximum plunge depth of 3.6 mm. ‘F-G’ is the dwell time (5 s). After that, the tool retracts, and the joint cools down. At ‘H,’ the process is completed. A comparison between the temperature data obtained from the IR technique and the thermocouple is presented in Fig. 5.10c.

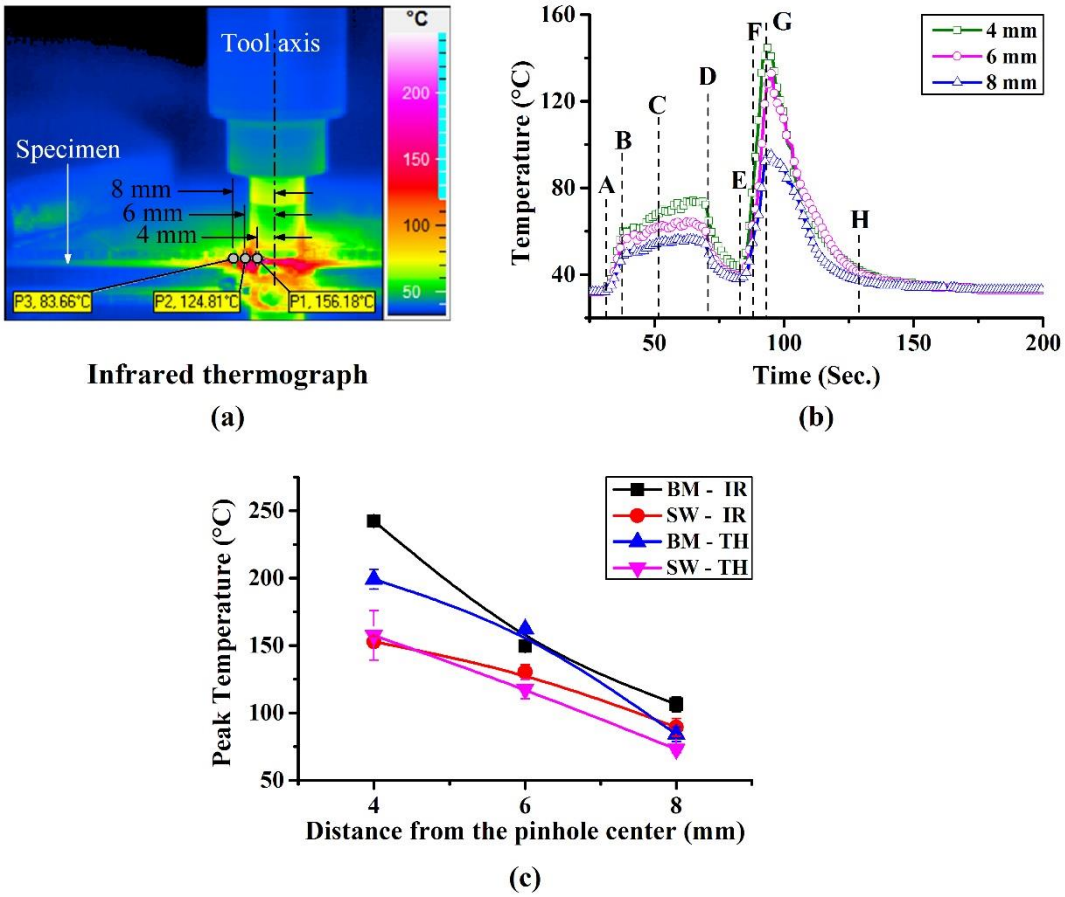

Fig. 5.10 (a) IR thermograph of FSSW, (b) typical temperature profile from IR thermography measured at different distances from the tool axis, (c) comparison of temperature data obtained by two techniques [SW: Sandwich sheets; BM: Bimetallic sheets; IR: Infrared camera; TH: Thermocouple]

The temperature near the keyhole boundary is larger and decreases outward irrespective of the type of material (bimetallic or sandwich) and measuring technique. Thermocouple records lesser temperatures than that measured by the IR technique. This is believed due to a reduction in plunge force due to the presence of holes in the work-piece, which are used to fix the thermocouples. Moreover, the temperature measurement by infrared technique depends on factors such as emissivity of the material, environmental conditions etc. These factors further depend on the working temperature. A constant value of emissivity and environment temperature is used in the present study. Therefore, finding the exact temperature by the IR camera is difficult despite its advantages. Furthermore, when the experiments are repeatedly executed, the thermocouple data are found to be consistent than data from the IR camera. Hence, for the rest of the work, the temperature measurement from thermocouples is considered.

The peak temperature distribution on the sandwich and bimetallic structures is depicted in Fig.

5.11. The temperature in the weld vicinity is larger and gradually reduces while moving away from the tool axis. With increasing dwell time, the heating period increases resulting in higher temperature generation in upper and lower sheets of sandwich sheets. Li et al. (2019) have also reported higher weld temperature at longer dwell time in FSSW of dissimilar metal. Further, a higher temperature is observed on the upper sheet than on the lower sheet due to the larger contact area between the shoulder and upper sheet.

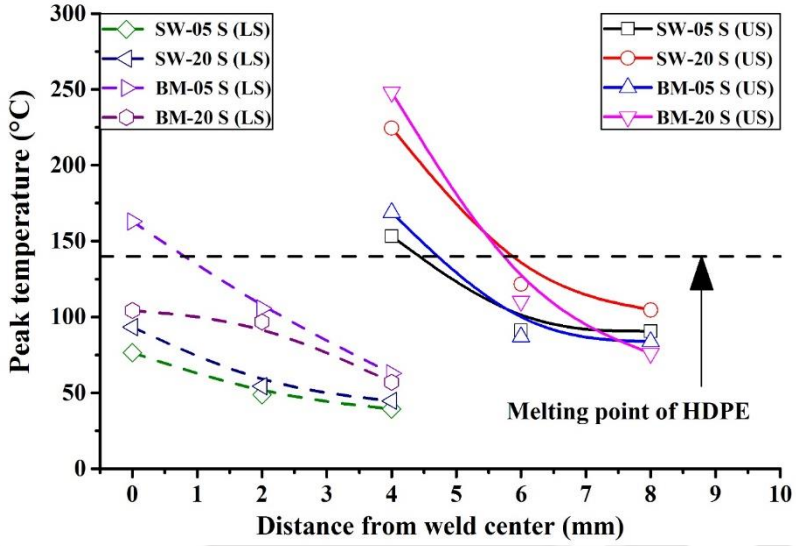

Fig. 5.11 Peak temperature distribution in the sandwich and bimetallic structures [US: Upper sheet; LS: Lower sheet]

In the present work, the contact area of the shoulder with the work-piece is about 68% larger than that of the pin. The temperature difference between the upper and lower sheet represents the temperature gradient across the thickness of the joint. The difference is 113°C and 179°C, respectively, for 5 s and 20 s dwell times at 4 mm from the weld center. Hence, with an increase in dwell time, the thermal gradient across the thickness also increases. This is in accordance with Bakavos and Prangnell (2009) work, in which it is reported that a higher thermal gradient is beneficial as it produces shorter heat affected zone and prevents the aging of grains, which in turn gives improved weld strength. It is evident from Fig. 5.11 that the temperature around the keyhole is sufficient enough to melt a portion of the polymer core in the joint as it has a melting point of 140ºC (Capiati and Porter, 1975).

In bimetallic sheets, the temperature of the upper sheet is higher at a larger dwell time. However, in the lower sheet, the lesser peak temperature is attained for a larger dwell time. As the dwell time increases, heat loss through backing plate increases resulting in lesser temperature in

the lower sheet at the end of the process. Like the sandwich sheet, the thermal gradient exists across the thickness of the bimetallic sheet too. The upper sheet temperature is 106°C higher than the lower sheet at 5 s dwell time, and it is 191°C at 20 s dwell time measured at 4 mm from the weld center. In contrast with bimetallic sheets, peak temperature in the sandwich sheet is lesser, which is because some heat is utilized for polymer melting.

5.2.4 Microstructure evolution and hardness distribution

The joint microstructure in sandwich sheets is depicted in Fig. 5.12a–c. Based on the grain morphology, the weld is divided into three distinct zones, namely, stir zone (SZ), transition zone (TZ), and thermo-mechanically affected zone (TMAZ).

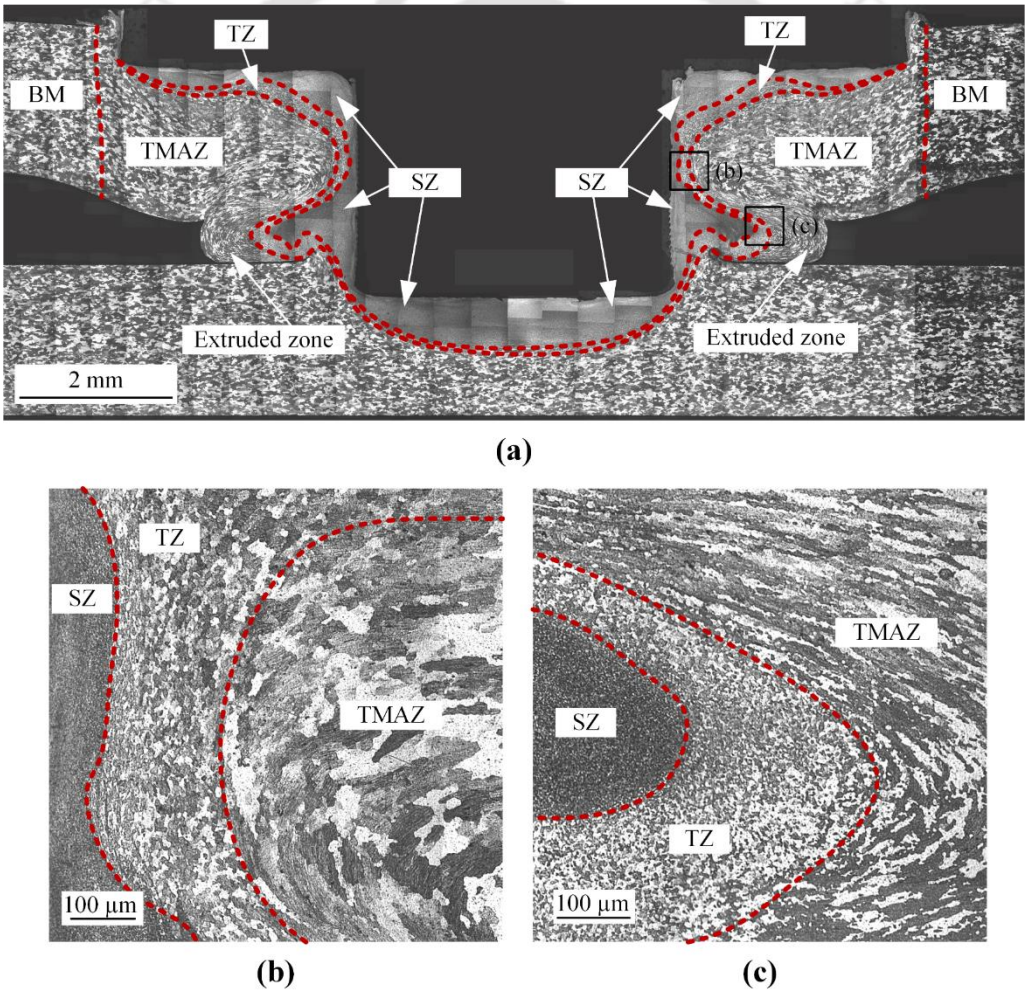

Fig. 5.12 (a) Typical microstructure in sandwich sheet, microstructures in (b) upper sheet [region b in (a)], (c) extruded zone [region c in (a)] [SZ: Stir zone; TZ: Transition zone; TMAZ: Thermo-mechanically affected zone; BM: Base metal]

The heat-affected zone (HAZ) is not visible clearly. The mechanism for microstructure

evolution is different in all the zones. In SZ, the grains are very fine as a result of intense dynamic recrystallization (DRX). DRX is a process of formation of sub-grains in large grains of crystalline materials subjected to deformation at elevated temperatures (Sakai and Jonas, 1984). Y. Lin et al. (2012) proposed that larger plastic strain near the tool yields more nuclei formation during DRX, resulting in finer grains. TMAZ is characterized by highly elongated grains subjected to plastic deformation metal at high temperatures. Tutar et al. (2014) have identical findings in the TMAZ of FSSWed AA3003-H12 alloys. The material in TMAZ is predominately deformed by hot forging by tool penetration, unlike stirring in SZ (Fig. 5.12b, c). The degree of deformation varies across the TMAZ, developing different grain morphologies at different locations. The material beneath the tool shoulder in the upper sheet deforms downward along the direction of tool plunging. However, in the extruded zone, plasticized material flows easily through the soft polymeric core layer in radially outward direction. Therefore grains in the extruded zone are largely elongated (Fig. 5.12c) as compared to the portion below tool shoulder (Fig. 5.12b). TZ is a narrow band that separates the SZ and TMAZ. The grains in this zone are subjected to partial stirring, frictional heating, and shear deformation because of different material flow in SZ and TMAZ. Combination of all these actions produce slightly coarser grains in TZ than SZ, but finer than TMAZ. All three zones are clearly seen in the sandwich and bimetallic sheets for weld produced at each dwell time. However, the heat-affected zone (HAZ) is not visible clearly.

The microstructures of base metal, sandwich, and bimetallic sheets at different dwell times are shown in Fig. 5.13. The grain sizes in a particular zone are not uniform. Moreover, the effect of dwell time on the size of the zone is prominent than the grain size in that zone.

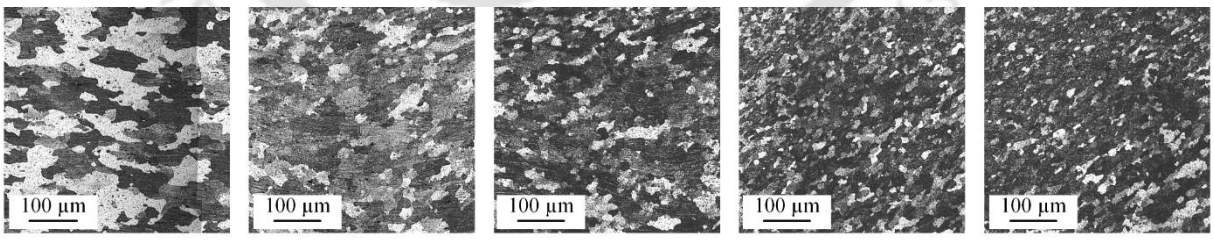

Fig. 5.13 Microstructure of (a) base metal, (b) sandwich sheet (5 s), (c) sandwich sheet (20 s), (d) bimetallic sheet (5 s), and (e) bimetallic sheet (20 s)

A similar effect is observed in the sandwich and bimetallic sheets. Hence, to correctly understand the effect of dwell time on the grain size, the microstructures are selected from the same location in sandwich and bimetallic sheets. The common location is typically found at a distance of 0.6 mm below shoulder touching surface and 4 mm away from the keyhole extremity,

where a notable change in grain size is observed. This location is in TMAZ in the sandwich sheet and TZ in the bimetallic sheet.

The average grain size of the base metal is 34 µm, whereas it is 23 µm and 28 µm in the sandwich sheet at 5 s and 20 s dwell time, respectively. The grains are slightly coarsened with increasing dwell time due to higher heat input. The higher heat input at larger dwell time is verified by higher temperatures, as depicted in Fig. 5.11. The bimetallic sheet also shows larger grains at larger dwell time. In the bimetallic sheet, the average grain size is 17 µm, and 20 µm at 5 s and 20 s dwell time, respectively. Farmanbar et al. (2019) have also reported larger grain size at higher dwell time. However, in comparison to the sandwich sheet, the finer microstructure is revealed in the bimetallic sheet at the same location. This is because the selected location belongs to TZ in the bimetallic sheet, unlike TMAZ, in the sandwich sheet, as mentioned earlier. In the bimetallic sheet, TZ shifts farther from the keyhole due to the expansion of SZ. A comparative graph showing variation in SZ width with dwell time is shown in Fig. 5.14. Since the width of SZ is not uniform across the thickness of the weld, it is measured at 0.6 mm below the shoulder touching surface. With increasing dwell time, SZ expands significantly due to larger heat input. With the expansion of SZ, the TZ and TMAZ shift outward from the keyhole.

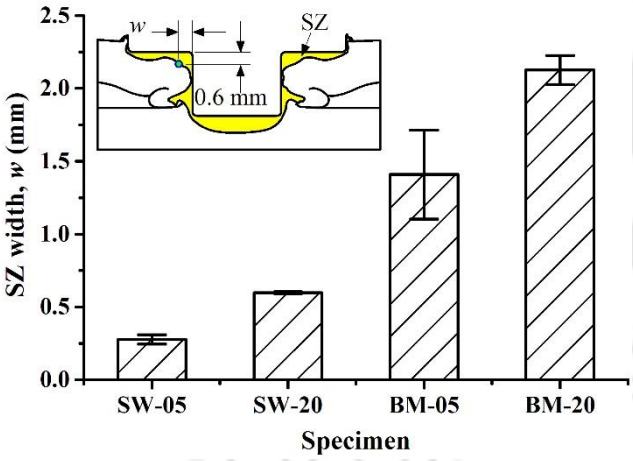

Fig. 5.14 Variation in SZ width with dwell time

The micro-hardness variation across the joint is represented in Fig. 5.15. The hardness near the keyhole is maximum in all the conditions in both the material combinations and decreases from the keyhole boundary. An identical trend in hardness distribution is observed in FSSW of AA5052-H32 alloy by Kumar et al. (2019). The lowest hardness region in the upper and lower sheet exist close to the shoulder and pin diameter, respectively. This indicates that the size of the hardened region is controlled by shoulder and pin dimensions in upper and lower sheets

respectively. In the sandwich sheet, slightly lower hardness at larger dwell time is observed on the upper sheet. However, the hardness difference is prominently seen after 1 mm from the keyhole boundary which is the TMAZ in the upper sheet. The microstructure is shown in Fig. 5.13(b, c) reveal grain growth at larger dwell time. This could be a primary reason for the lower hardness. Zhang et al. have also confirmed local softening in FSSW of AA5052 (Zhang et al., 2011). The hardness variation in the lower sheet is insignificant because the metallurgical changes in the weld are limited only in a small region below the tool pin.

The bimetallic sheet shows slightly larger hardness than sandwich. This is due to larger SZ width in the upper sheet. The SZ is always harder due to small equiaxed grains. With an increase in dwell time, the hardness varies insignificantly because of small variations in grain size. The lower sheet also exhibits almost the same hardness for weld produced at both the dwell times.

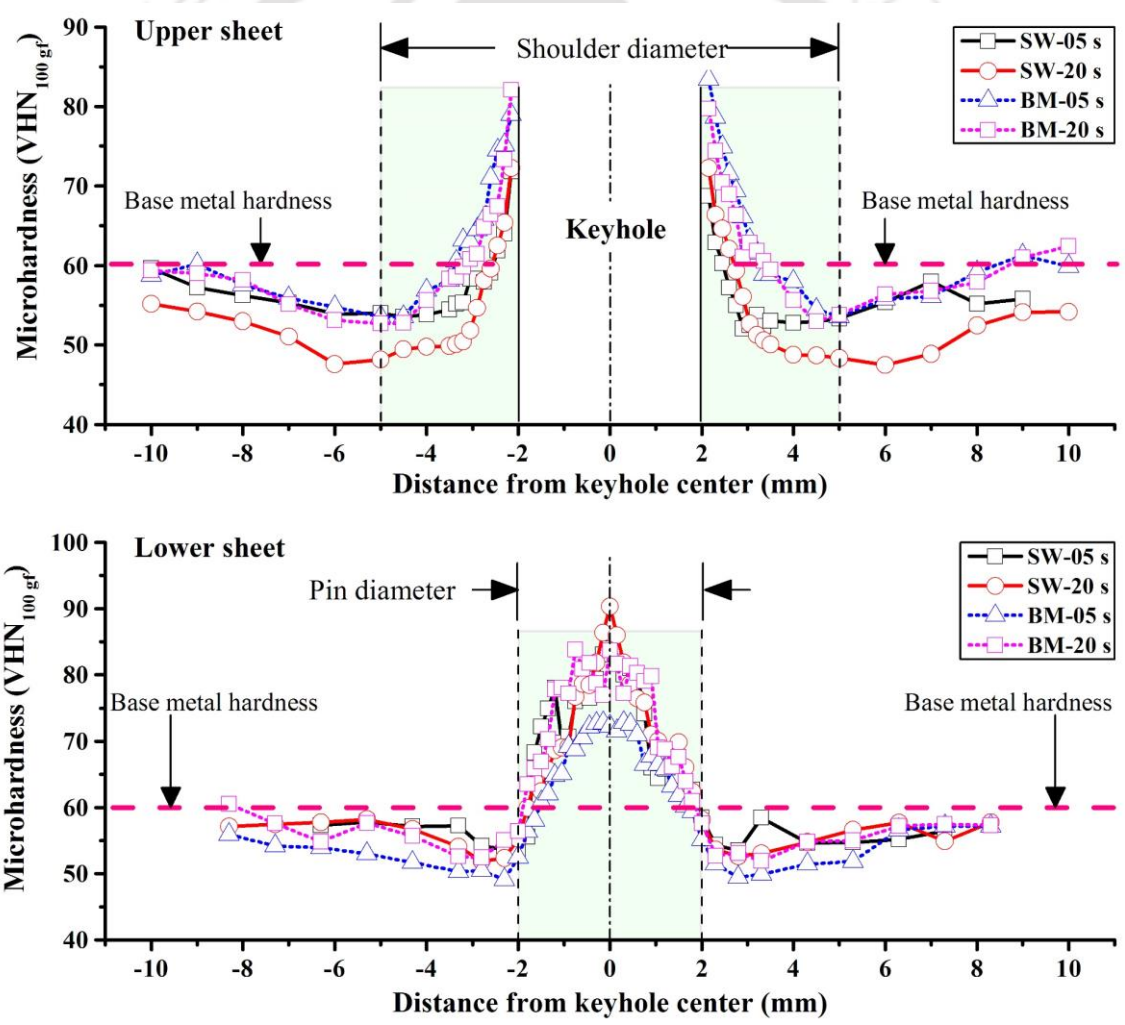

Fig. 5.15 Hardness distribution on (a) upper sheet, and (b) lower sheet. Error variation: ± 2.30 VHN

5.2.5 Mechanical performance and failure modes

This section aims to discuss the load-extension behavior, failure load, and ductility evaluated from different mechanical tests at varying dwell times. Finally, the failure modes are correlated with joint strength and ductility.

5.2.5.1 Lap shear test

Typical load-extension behavior of sandwich and bimetallic sheets in lap shear test is shown in Fig. 5.16a. The bimetallic sheet shows a higher failure load and ductility. In the sandwich sheet, the failure load and ductility increase up to 5 s dwell time, remain almost the same up to 20 s, and then decrease (Fig. 5.16b). The initial improvement in the failure load is due to the expansion of the stir zone with dwell time.

However, excessive dwell time yielded poor joint strength due to the evolution of the coarser microstructure. The bimetallic sheet shows a larger failure load and extension with dwell time. A similar trend is reported by Garg and Bhattacharya during dwell time study in FSSWed AA6061 alloy (Garg and Bhattacharya, 2017). In comparison, the bimetallic sheet shows superior performance than the sandwich sheet because of the larger bond width (Fig. 5.7), providing a greater resisting area during lap shear loading.

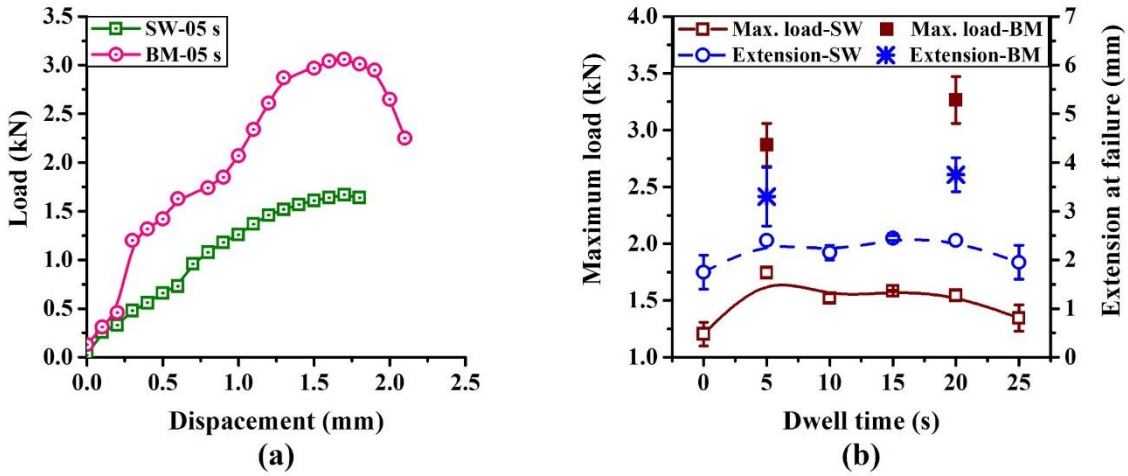

Fig. 5.16 Lap shear test; (a) typical load–extension behavior, (b) failure load, and ductility vs. dwell time

5.2.5.2 Cross-tension test

The FSSW joint of sandwich and bimetallic sheets behave identically during the cross-tension test (Fig. 5.17a). Here the total extension shown is the sum of extension caused by sheet bending

and extension in the joint. The failure load and ductility of joints are lesser in the sandwich sheet as compared to the bimetallic sheet. The cross-tension failure load and ductility of the sandwich sheet are not significantly affected by changing the dwell time (Fig. 5.17b). During the cross-tension test, the sandwich sheets failed by nugget pull out mode, in which fracture occurred from the lower hook tip. Hence, it is believed that the failure of the joint is controlled by lower bond width. The lower bond width is almost the same at all dwell times (Fig. 5.7) and hence the failure load. The bimetallic sheet also shows an insignificant effect of dwell time. Like lap shear test, the cross-tension test shows lesser failure loads at all dwell times for the sandwich sheet in contrast with bimetallic sheets. However, the ductility of the sandwich sheet is almost the same as that of the bimetallic sheet. This suggests that though joint strength is reduced in sandwich sheets, the ductility of the joint is maintained at par with a bimetallic sheet. The cross-tension failure loads are lesser than the lap shear failure loads. A similar observation is reported by Tran and Pan (Tran and Pan, 2010).

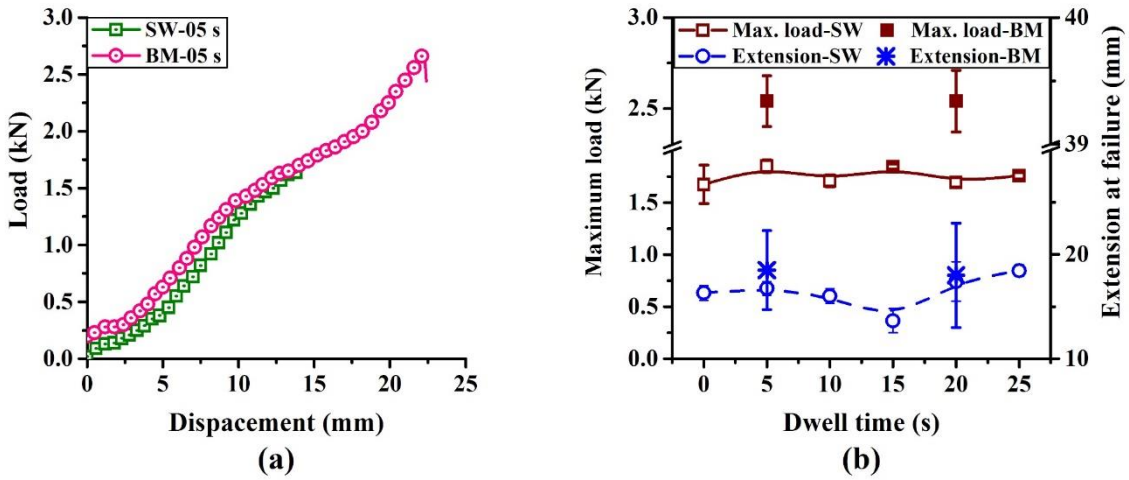

Fig. 5.17 Cross-tension test; (a) typical load–extension behavior, (b) maximum load and ductility vs. dwell time

5.2.5.3 Peel test

The superior performance of the joint is achieved for sandwich sheets (Fig. 5.18a). The failure load of the sandwich sheet initially decreases up to 10 s dwell time, then increases (Fig. 5.18b).

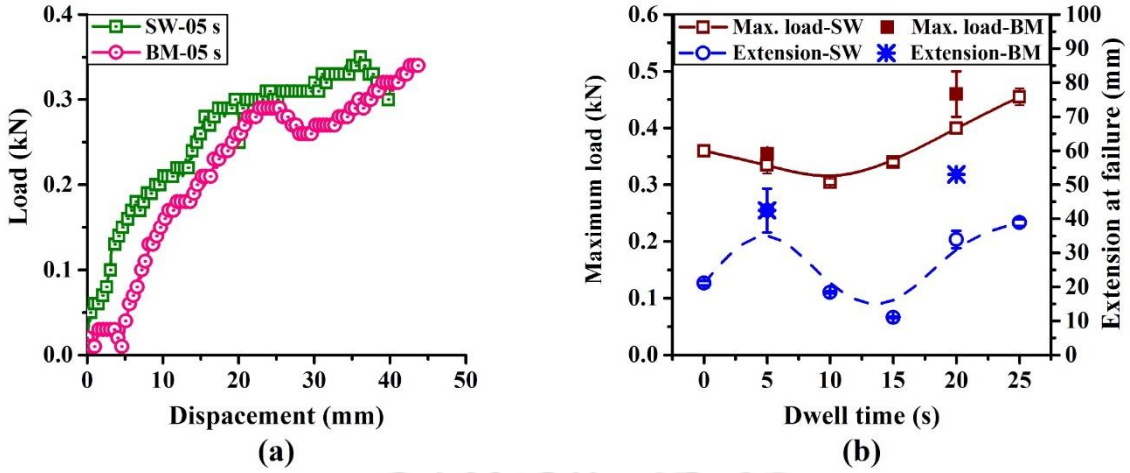

Fig. 5.18 Peel test; (a) typical load–extension behavior, (b) maximum load and ductility vs. dwell time

It is seen earlier that the hardness of the joint decreases with increasing dwell time. This would reduce the joint strength slightly. However, apart from the joint strength, the mechanical performance of the FSSW joints also depend on the hook geometry. The upper bond width is larger at 10 s dwell time (Fig. 5.7a). Larger upper bond width requires larger failure energy, and hence the critical region shifts to lower hook during peel test. In the sandwich sheet, the upper bond width and peel test failure load are inversely related. In the bimetallic sheet, the peel strength and ductility of the joint increases with increasing dwell time. In comparison, the sandwich sheet shows a slightly lower failure load than the bimetallic sheet. However, larger failure load of the sandwich sheet after 10 s dwell time suggests that at higher dwell time, the sandwich sheet would perform better than the bimetallic sheet FSSWed at lower dwell time.

5.2.5.4 Uniaxial tensile test

The stress-strain behavior of the sandwich sheet, bimetallic sheet, skin sheet, and core sheet is shown in Fig. 5.19a. The result shows that the mechanical behaviour of welded sandwich and bimetallic sheet is identical to that of the parent metal. In comparison to the bimetallic sheet, the sandwich sheet shows improved ductility without any expense of strength. The effect of dwell time on the failure load and ductility is insignificant (Fig. 5.19b). This suggests that the FSSW can be applied on the sandwich sheet without scarifying any forming characteristics. The joint made in the bimetallic sheet shows a slight decrease in failure load and extension at higher dwell time. However, the sandwich sheet performance is found to be superior to the bimetallic sheet at any dwell time due to the larger load bearing area at the joint cross-section. Sandwich sheets form a bigger nugget because of extrusion in the core layer. Therefore, the FSSWed sandwich sheet is encouraged whenever a similar forming operation is involved.

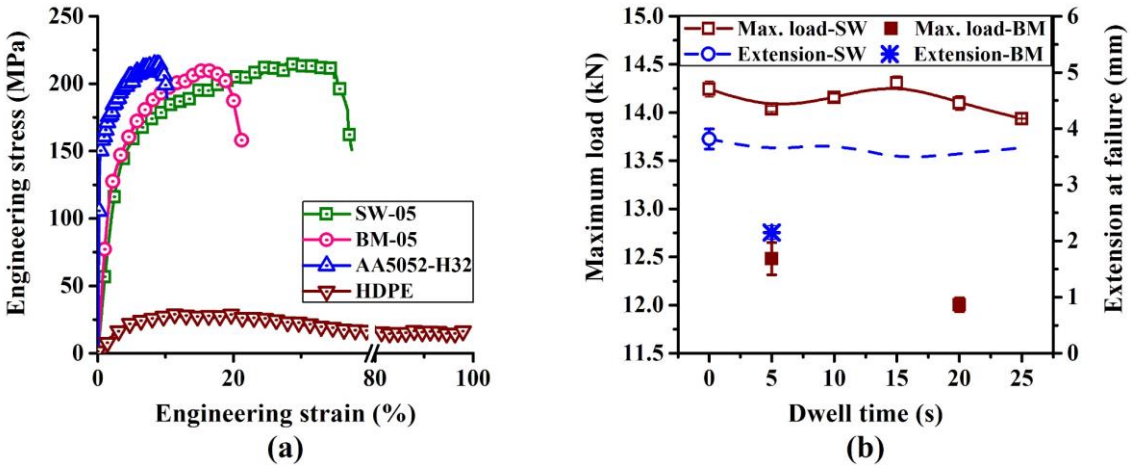

Fig. 5.19 Uniaxial tension test; (a) typical load–extension behavior, (b) maximum load and ductility vs. dwell time

The fracture surfaces of the joints in different tests are shown in Fig. 5.20. In lap shear, cross-tension, and peel tests, the sandwich sheets predominantly failed by nugget pull-out mode at all dwell times. The only exception is observed in the peel test of specimens welded at a dwell time of 15 s. The joints with lesser lower bond width and larger upper bond width are likely to fail by nugget pull-out mode. Lesser lower bond width is evident in Fig. 5.7, which is true for sandwich sheets welded at any dwell time. However, if the joint is pulled along its axis, the portion of nugget material which remains bonded with the lower sheet increases with an increase in lower hook height. When a significant portion of the nugget remains bonded with one sheet after failure, while the remaining portion of the nugget remains bonded with another sheet, it is referred to as the partial nugget fracture. It is seen earlier (Fig. 5.7) that the lower hook height in the sandwich sheet is maximum at 15 s, which is why partial nugget fracture is observed in the peel test in this particular case.

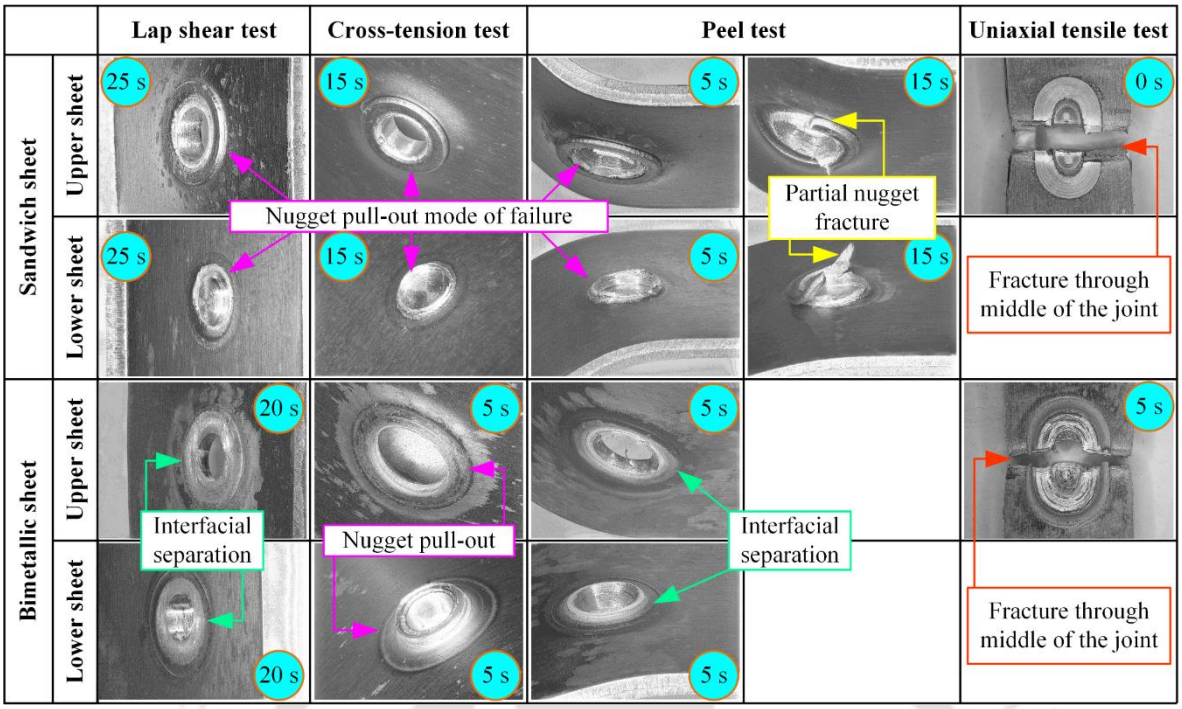

Fig. 5.20 Modes of failure in various mechanical testing procedures

In bimetallic sheets, two modes of failure, interfacial separation, and nugget pull-out, are observed. In interfacial separation, the joint separated into two halves from the sheet interface. It occurs due to existence of primary hook closer to the interface resulting in crack propagation along the interface. This failure mode is seen in lap shear as well as in cross-tension tests at all dwell times. Tran et al. (2009) have also reported interfacial fracture in lap shear test. In cross-tension tests, the nugget pull-out mode of failure is observed at all dwell times. However, the characteristics of nugget pull-out mode are different in bimetallic and sandwich sheets. In the bimetallic sheet, the nugget is separated from the upper sheet and remains attached to the lower sheet, unlike in sandwich sheet, where the nugget is separated from the lower sheet and remains attached to the upper sheet. Similar fracture mode is observed by Tozaki et al. (2007) in FSSW joints under cross-tension test. The sandwich and bimetallic sheets failed along the transverse direction of the joint in the uniaxial tensile tests due to presence of keyhole and geometrical irregularities such as a hook. Therefore, the joint failed from the middle of the joint. In uniaxial test, the failure mode is independent of dwell time.

The FE models of mechanical tests and stress distribution highlighting the critical region and failure location in sandwich sheets are shown in Fig. 5.21.

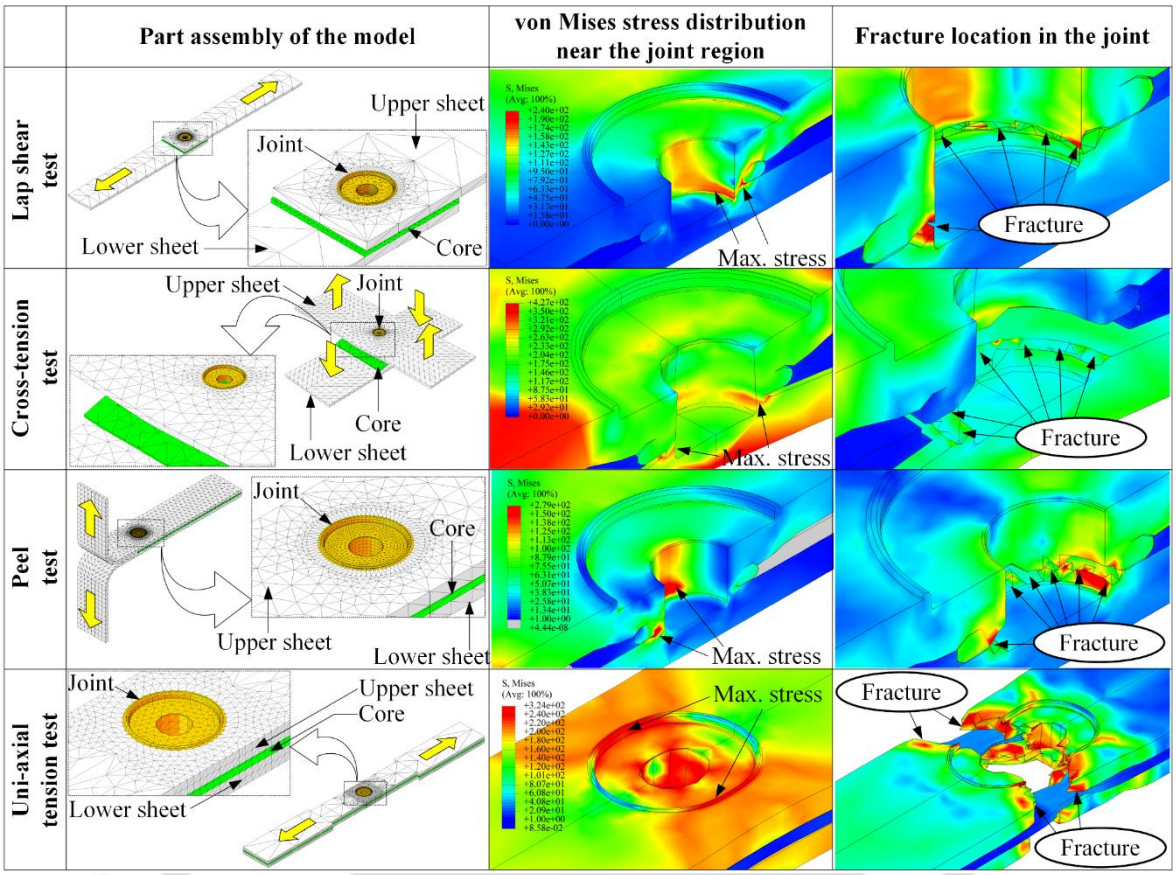

Fig. 5.21 FEA results of mechanical test depicting failure modes in sandwich sheets

The von Mises stress distribution in the joints indicates that maximum stress develops in the portion between the lower hook and the keyhole periphery. Therefore, it is expected that the failure of the joint would occur from this location during testing. The same is confirmed when the joined specimen is extended further. It should be noted here that the 'nugget pull-out' is the mode of failure in the sandwich sheet when the failure occurs from the lower hook. In the actual experiment, the 'nugget pull-out' is seen most often, except in the peel test specimen fabricated at 15 s dwell period. Therefore, the FE simulation and experimental results on failure location match well.

5.3 Conclusions

The consequences of varying dwell time on the FSSW of three-layered polymer core sandwich systems are addressed in the present work. The important findings are summarised as follows.

- The significant effect of dwell time is observed only in lap shear and the peel test. In the lap shear test, the sandwich sheet performs best when the joint is made with the dwell time in the range of 5 s to 20 s. This is likely due to the combined advantage of larger bond width and the

finer microstructure of the joint. In the peel test, a critical dwell time (10 s) is found where the worst performance sandwich sheet is seen. It is believed that the longest upper hook width at this condition favorably shifts the failure location to the lower hook.

- The bimetallic sheet performance is better at higher dwell time in lap shear as well as in peel test due to larger bond width. The bimetallic sheet performs better than sandwich sheet in lap shear, cross-tension, and peel test while worse in uniaxial tensile test.

- With increasing dwell time, significant temperature rise is seen on the upper sheet. Larger dwell time produced higher peak temperature due to heat generation for a prolonged period of time. Moreover, the upper sheet is subjected to higher temperatures due to larger contact area between tool and work-piece. In sandwich sheet, some heat is being utilized in melting the HDPE sheet in the core, therefore, peak temperature attained is lesser than the bimetallic sheet.

- The macro and micro features of the joint also changes with varying dwell time. Higher heat input at larger dwell time results in grain coarsening and expansion of SZ. The width of the SZ in bimetallic sheet is larger than the sandwich sheet due to larger heat input.

- Slightly higher hardness of upper portion of the sandwich joint is observed at larger dwell time due to finer microstructure. However, influence of dwell time on the joint hardness of lower sheet and bimetallic sheet is not significant.

- The FE simulation for flow visualization reveals that increasing dwell time increase material flow in to the extruded zone as a result of increased plasticization. The same is reflected in experiment also. The material flow controls the hook geometry and therefore the joint performance.

- The predominant failure mode in the sandwich sheet is ‘nugget pull-out’ because of the smaller lower bond width and larger upper bond width. However, ‘partial nugget fracture’ occurs in a particular peel test due to a very high lower hook height. On the other hand, ‘interfacial separation’ is observed in the bimetallic sheets in lap shear test and peel test while ‘nugget pull-out’ mode in the cross-tension test.

- The von Mises stress is maximum at the lower hook region, as seen in FE model, which is responsible for the failure of the sandwich sheet by ‘nugget pull-out’ mode. The fracture location also confirms the same.

Chapter 6

Numerical and experimental response of FSSW of AA5052-H32/ Epoxy/AA5052-H32 sandwich sheets with varying core properties

6.1 Experimental procedure

6.1.1 Materials

Two metallic skin sheets are joined in lap configuration by a layer of adhesive in between to fabricate sandwich sheets. The skin is made of AA5052-H32 material of 2 mm thickness. The intermediate core layer is made up of 1 mm thick epoxy resin with resin and hardener in appropriate proportion. Epoxy resin is frequently used in the fabrication of sandwich sheets. Recently, Logesh et al. (2018) have successfully made an AA5052-H32 skin sandwich sheet with a glass fiber core joined together by an epoxy resin binder. Russig et al. (2014) have used an epoxy binder to fabricate Glass-fiber reinforced aluminum (GLARE) sandwich sheet. The total thickness of the sandwich sheet is 5 mm. In order to vary the properties of the core layer, four different h/r ratios are selected. The selection of epoxy quality and its composition are important as they affect the performance of sandwich sheets, such as mechanical strength and cohesive strength. Satheeshkumar & Narayanan (2015) have reported that increasing hardener content in the adhesive improves the formability of adhesive bonded blanks. The mechanical properties of the skin sheet are evaluated by the standard tensile test as per ASTM B557 M-15 standard. Plastic strain ratios along three rolling directions are evaluated as per the ASTM E517-00 standard. To obtain the mechanical properties of epoxy, ASTM D 638–14 standard is followed. Four tensile specimens are prepared by altering the hardener to resin (h/r) ratio at room temperature. The tensile tests are carried out in a universal testing machine (Make: INSTRON, Model: 8801) at 5 mm/min. ram speed. The typical stress-strain behavior of skin sheet and core layers are shown in Fig. 6.1. The strength of epoxy is lesser than AA5052-H32 skin, and ductility increases with the h/r ratio. The increase in ductility with h/r ratio is also reported by Satheeshkumar and Narayanan, (2014). The reported reason behind this is the inediquate cross-linking between hardener and resin molecules at higher h/r ratio.

The mechanical properties of skin and core materials are shown in Table 6.1.

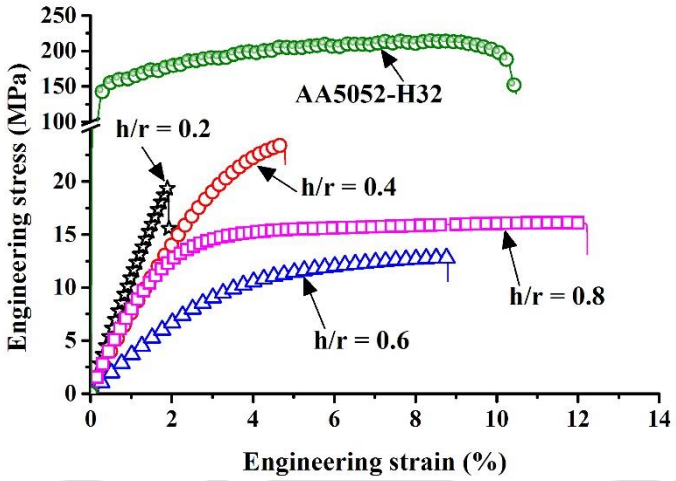

Fig. 6.1 Typical stress-strain behavior of skin and core layers

Table 6.1 Mechanical properties of AA5052-H32 and Epoxy at different h/r ratio

Material	h/r ratio	Rolling direction	Yield strength (MPa)	Ultimate tensile strength (MPa)	Uniform elongation (%)	Total elongation (%)	Strain hardening coefficient	Strength coefficient (MPa)	Plastic strain ratio
AA5052-H32	-	0°	155±1	215±1	7±1	9±1	0.16	356±3	0.62
	-	45°	147±2	206±2	9±1	12±2	0.15	327±4	0.68
	-	90°	148±1	209±1	8±1	13±0	0.16	333±1	0.85
Epoxy	0.2	-	-	20.09±0.62	2.05±0.18	2.06±0.19	-	-	-
	0.4	-	-	23.66±0.23	4.41±0.52	4.49±0.42	-	-	-
	0.6	-	-	12.73±0.11	8.05±0.83	8.20±0.84	-	-	-
	0.8	-	-	16.36±0.34	13.14±1.58	13.61±1.96	-	-	-

6.1.2 Specimen preparation and FSSW

Test specimens with FSSW joint are prepared for lap shear test, peel test, and micrographic examination. Lap shear tests and peel tests are conducted to evaluate the joint performance under shear and peel loading conditions that are observed under the industry environment. For each type of specimen, four different types of cores are fabricated that vary in h/r ratio from 0.2 to 0.8 at 0.2 intervals. This range is chosen based on available literature. Satheeshkumar and Narayanan (2014) have shown that increasing the h/r ratio of epoxy improves the formability of adhesive bonded blanks. They have varied h/r ratio from 0.6 to 1, where larger ductility of adhesive is observed at

higher h/r ratio. However, the variation in the tensile strength of the adhesive is only a little with the h/r ratio. Therefore, the range of h/r ratio in the present work is selected in such a way that both strength and ductility change significantly with h/r ratio, and hence FSSW expecting observable behavior. The epoxy resin in the sandwich sheets is allowed to cure in a furnace at room temperature for 24 hours. The geometrical details of the specimens are kept the same as the previous studies.

FSSW is conducted at 1200 rpm tool rational speed, 0.6 mm plunge depth, 6 mm/min., plunge speed, and 5 s dwell time. The process parameters are chosen suitably based on the results of previous chapters. A straight cylindrical pin with a flat shoulder tool used for FSSW is made of tool steel having a 10 mm shoulder diameter, 4 mm pin diameter, and 3 mm pin length. FSSW is performed at the geometric center of the overlapped region in the sandwich sheets.

6.1.3 FSSW joint Characterization

The metallurgical examination is done to observe the effect of varying core properties on the grain morphology, hook geometry, and micro-hardness of the joint. In order to achieve these, the FSSW joints are sectioned to expose the inner surface. The sectioned joint is cold mounted and polished by waterproof emery papers and Silvo polish on a velvet cloth. A perfectly polished surface is chemically etched by modified Keller's reagent to reveal macro-and microstructure. The etchant is prepared by mixing 2 ml hydrofluoric acid, 3 ml hydrochloric acid, 5 ml nitric, and 10 ml distilled water. First, the microstructure is obtained by etching the sample for about 20 s. Once images are captured, the etched layer is removed by cloth polishing followed by dipping into the same solution for about 60 s resulting in over-etching of stir zone. This reveals the macro-structure (hook geometry and distinct stir zone) of the FSSW joint. The images are taken by the Nikon SMZ25 stereo microscope at lower magnification, which reveals the hook formation in the joint.

After this, the etched layer is removed from the surface by little polishing in order to measure the micro-hardness. The micro-hardness is measured across the thickness at the locations 1 mm below the shoulder touching surface on the upper sheet and 0.4 mm below the keyhole on the lower sheet. The load and dwell time selected for micro-hardness measurement are kept at 100 gf and 15 s, respectively. The mechanical performance of the FSSW joints are evaluated through lap shear test and peel test on a digitally controlled closed-loop servo hydraulic 100 kN dynamic testing machine (make: INSTRON, model: 8801) at room temperature with a cross-head speed of 1 mm/min, and test environment is maintained at room temperature. Typical test setup for peel

test and test stages are shown in Fig. 6.2.

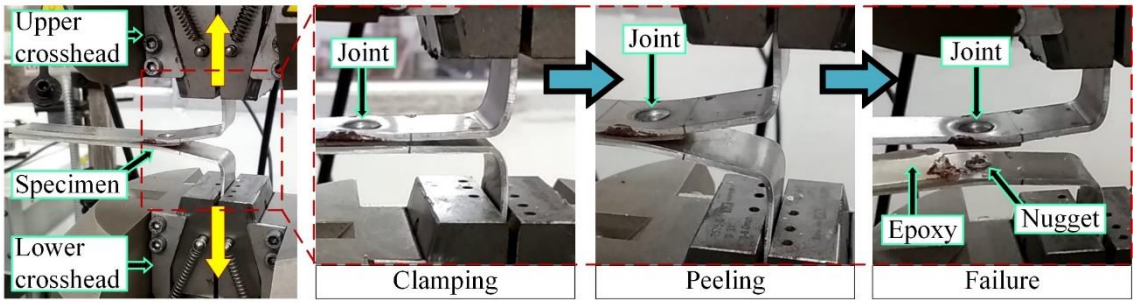

Fig. 6.2 Typical setup for peel test and deformation stages

6.1.4 FE simulation of FSSW of sandwich sheet

6.1.4.1 Cohesive zone modeling (CZM) and evaluation of cohesive zone (CZ) parameters

In order to understand the material flow during FSSW of a sandwich sheet, the FE simulation is carried out in Abaqus. During FE modeling, to model the interface adhesion, cohesive zone modeling is performed. CZM is a useful technique to predict delamination in composite panels. Jang et al. (2017) have conducted a numerical analysis of delamination in a steel-polymer composite sheet. Here, CZM is used to define the interface between steel and polymer, and the peel test validates numerical results. Liu et al. (2012) used CZM to study the formability of a sandwich sheet comprising AA5052 skin and polyethylene core, where CZM is used to specify the interfacial adhesion. Other than adhesion, they have modeled two more interface conditions, separation, and stick. Out of three, the adhesion with CZM has shown good agreement with the experimental results. Stigh et al. (2010) have highlighted the usefulness of CZM in simulation. CZM holds a full signature of interface conditions with fewer variables. No separate geometry is required to create for crack propagation study. Instead, the interfacial failure separates two adjoining surfaces and acts as a crack (Stigh et al., 2010).

In CZM, failure occurs in the cohesive layer, where a crack generates and grows in the course of deformation. Here, the delamination is battled by cohesive traction. The interface condition can be modeled by defining: cohesive surface and cohesive element. In the former one, no separate part is required to be created. Instead, a separation criterion is included in the contact property. On the other hand, in the cohesive element technique, a separate element is defined as a cohesive type, and the separate material property is assigned to it. The cohesive surface method is simple and quick but does not deliver failure details. However, the cohesive element technique reveals the intricate details related to the failure of adhesive at the interface at the expense of computational

cost. Salomonsson and Stigh (2009) have conducted a numerical analysis of adhesive failure using both techniques in elastically deforming a double cantilever beam and found that the load-extension behavior is the same in both cases. In the present work, the cohesive element technique is used, where the failure is associated with the fracture energy, G_c, which is given by the area under the traction-separation curve (Fig. 6.3).

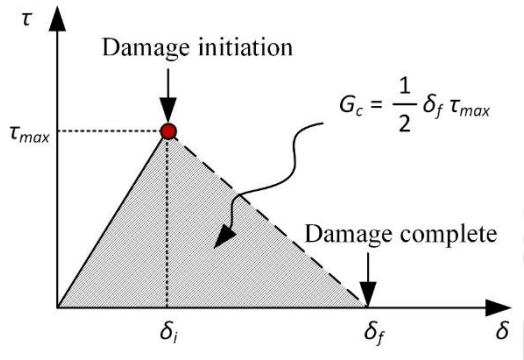

Fig. 6.3 Traction-separation curve for adhesive

Fig. 6.3 defines an irreversible, bilinear softening behavior of adhesive given by (Camanho et al., 2003); (Davila et al., 2001); (Kukreja and Narayanan, 2019)

$$\tau = \begin{Bmatrix} K\delta & ; \delta^* \in [0, \delta_i] \\ (1-D)K\delta & ; \delta^* \in (\delta_i, \delta_f) \\ 0 & ; \delta^* \in [\delta_f, \infty) \end{Bmatrix} \tag{6.1}$$

where K is the penalty stiffness, and D is the scalar damage variable, given by (Camanho et al., 2003); (Davila et al., 2001); (Kukreja and Narayanan, 2019)

$$D = \frac{\delta_f(\delta^* - \delta_i)}{\delta^*(\delta_f - \delta_i)} \tag{6.2}$$

where δ_i is the separation at the onset of damage, δ_f is the separation at complete damage, and δ^* is the maximum separation.

The quadratic nominal stress criterion is used as a damage initiation criteria in Abaqus, which is given by (Camanho et al., 2003); (Davila et al., 2001); (Kukreja and Narayanan, 2019)

$$\left(\frac{\sigma_n}{\sigma_n^c}\right)^2 + \left(\frac{\sigma_s}{\sigma_s^c}\right)^2 + \left(\frac{\sigma_t}{\sigma_t^c}\right)^2 = 1 \tag{6.3}$$

where σ_n, σ_s, and σ_t are the stresses in normal, first shear, and secondary shear directions, and, σ_n^c, σ_s^c, and σ_t^c are the critical values of the corresponding stresses.

The damage evolution is modeled using fracture energy-based power law given by (Camanho et al., 2003); (Davila et al., 2001); (Kukreja and Narayanan, 2019)

$$\left(\frac{G_1}{G_1^c}\right)^{\alpha} + \left(\frac{G_2}{G_2^c}\right)^{\alpha} + \left(\frac{G_3}{G_3^c}\right)^{\alpha} = 1 \tag{6.4}$$

where G_1, G_2, and G_3 are the fracture energies in normal, first shear, and secondary shear directions respectively, and, G_1^c, G_2^c,and G_3^c are the critical values of the corresponding fracture energies. α is the degree of the power-law and is assumed unity (Gustafson and Waas, 2009); (Kukreja and Narayanan, 2019); (Liu et al., 2013).

The damage initiation and evolution criteria are widely used in damage modeling of adhesive bonded and sandwich sheets with adhesive between interlayers. Liu et al. used this damage criterion in CZM of lap shear test and peel test of adhesive bonded polyethylene core aluminum skin sandwich sheet (Liu et al., 2013). Azevedo et al. (2015) estimated cohesive law in adhesive bond using the quadratic nominal stress criterion given by Eq. (6.6). André et al. (2012) analyzed the failure of an adhesive joint between metal and polymer laminates using damage initiation criterion shown above. This damage criterion is based on mix mode delamination, which is likely to occur in most of the composite structures, where deformation is caused by normal as well as shear load (Davila et al., 2001). Other than the power law, other damage evolution laws are available in Abaqus, such as tabular law and Benzeggagh and Kenane (B-K) law. Dai and Mishnaevsky (2013) have compared many damage evolution laws in damage of nano-clay-reinforced polymers and concluded that the power-law gives a more realistic failure pattern than the B-K law. Chen et al. (2009) have also reported better failure prediction of linear power law than the B-K law.

Lap shear test and peel test are simulated to evaluate the values of σ_n^c, σ_s^c, σ_t^c, G_1^c, G_2^c,and G_3^c. At first, some initial values are given to the FE model, and simulation is done. The initial values are decided from the experimental data. The peak stress is obtained from the experimental load-

extension data by dividing the peak load with the load-bearing area. The load-bearing area is the surface area upon which the adhesive is applied. The initial values of σ_n^c, σ_s^c, and σ_t^c are kept as the peak stress, which is believed to cause the onset of delamination. The initial values of fracture energies,G_1^c, G_2^c, and G_3^c, are decided by the area under the load-displacement curve obtained experimentally, which signifies complete delamination. The load-extension behavior is obtained and compared with the experimental load-extension curve. The values are modified iteratively until acceptable error is achieved. Once the error is minimized to the acceptable limit, the values are finalized. Fig. 6.4 describes the optimization procedure, which is usually adopted for CZM by other others as well (Kukreja and Narayanan, 2019); (Jianguang Liu et al., 2013).

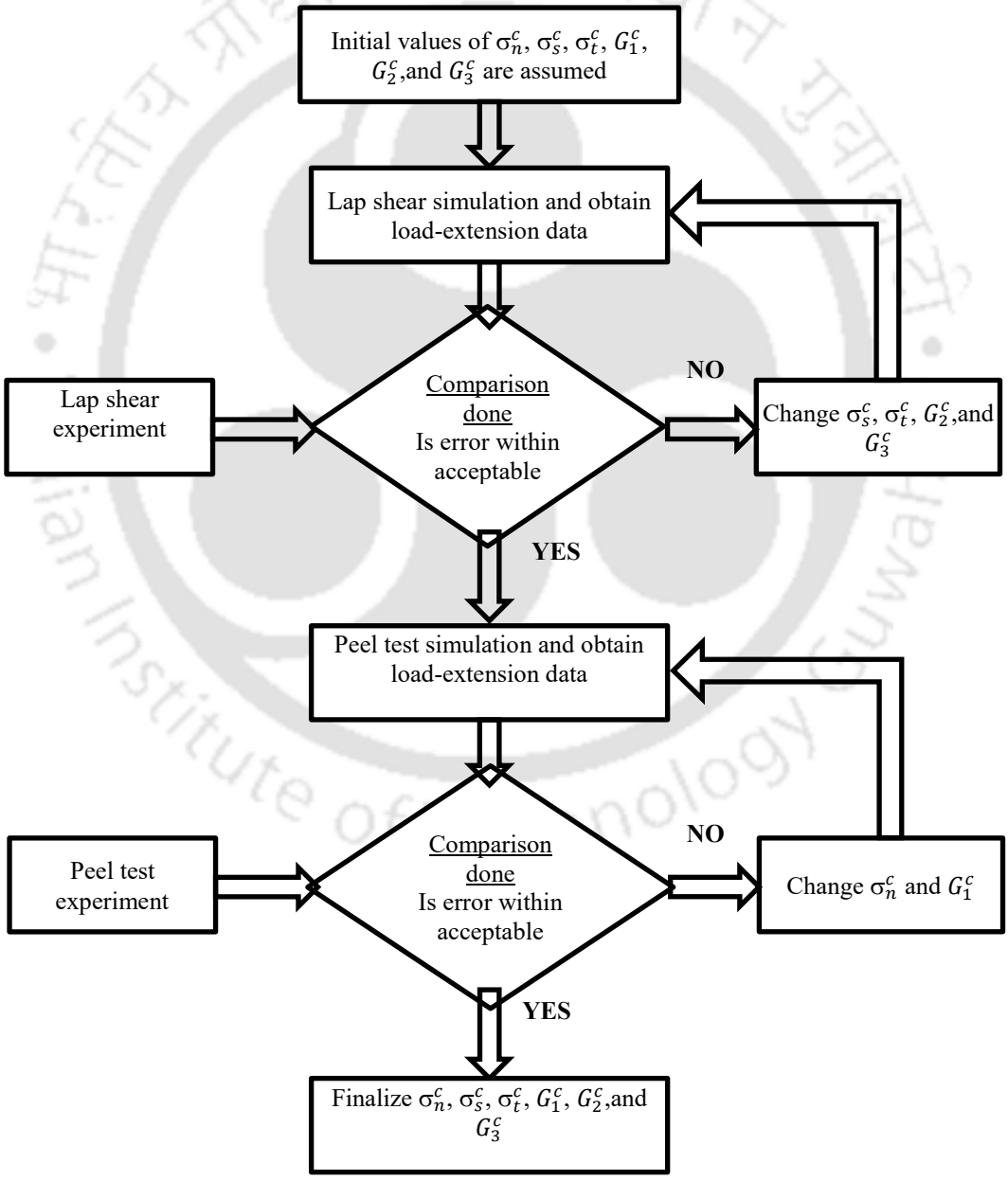

Fig. 6.4 Flow chart for optimizing CZ parameters

In order to select the right element size in the model, trial simulations are done by varying element sizes of the core layer only as the deformation in the skin sheets is insignificant. Three different element sizes, 1 mm, 5 mm, and 10 mm, are assigned to the core layer. The load-extension behavior during the lap shear test and peel test is separately compared at changing element size, as shown in Fig. 6.5. It is observed that there is no effect of changing element size in the lap shear test. However, in the peel test, the load-extension behavior changes slightly for element size 1 mm, but no effect is seen when element size changes from 5 mm to 10 mm. Therefore, to reduce the computational cost, a 10 mm element size is assigned to the core layer during the lap shear test and peel test simulations.

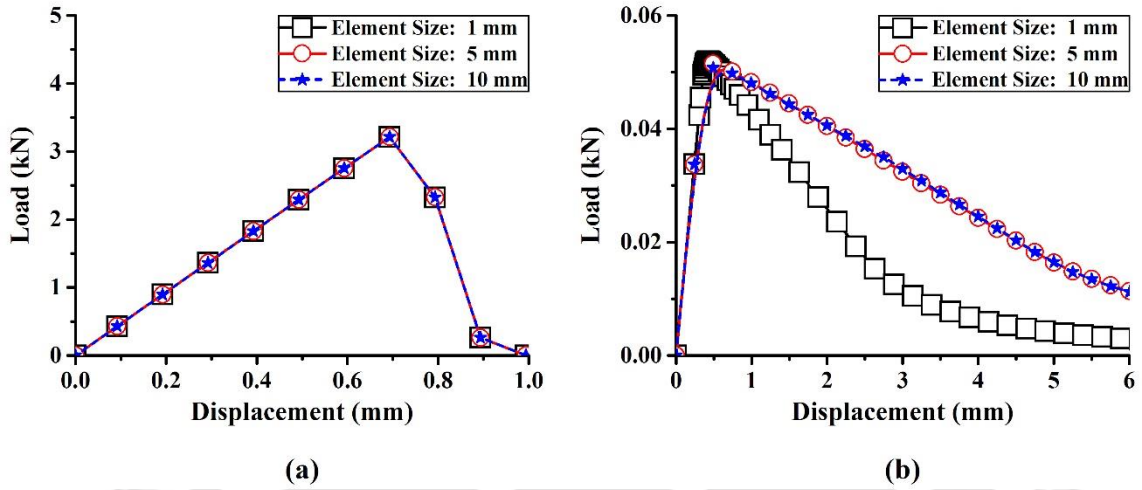

Fig. 6.5 Mesh sensitivity analysis in (a) lap shear test, (b) peel test

6.1.4.2 Prediction of hook formation and delamination by FEA

Failure of the cohesive interface in the sandwich sheet has been investigated to predict the delamination of epoxy core from the skin sheets during FSSW. The FE tool allows visualization of material flow during welding, which helps locate critical zones in the weld, causing delamination. To achieve this, the CZM is integrated with the FSSW in the FE code. Later, simulation results are analyzed, and two quantifiable indexes, namely hook geometry and damage, are compared at different h/r ratios. The simulated model of the sandwich sheet is sectioned about the plane passing through the diameter of the joint. The inner surface of the joint is exposed, where the hook geometry is measured. Molnár and Gravouil (2017) explain the concept of damage and its significance in analyzing fracture of solids. They reported that it is a scalar variable, which affects the stiffness and stress-induced in an element. When damage in an element reaches a value of 1, the stiffness of the element becomes zero. In other words, there is no stress in the element. Imran et al. (2020) have related damage variables with the deformation to explain damage

initiation and evolution in cohesive elements. In an earlier attempt, FEA is performed for FSSW of a bimetallic sheet by Chu et al. (2018). However, the FSSW, coupled with CZM, is not reported elsewhere. In the present investigation, FEA is carried out in ABAQUS. In modeling, three-dimensional geometries are created and assembled, as shown in Fig. 6.6.

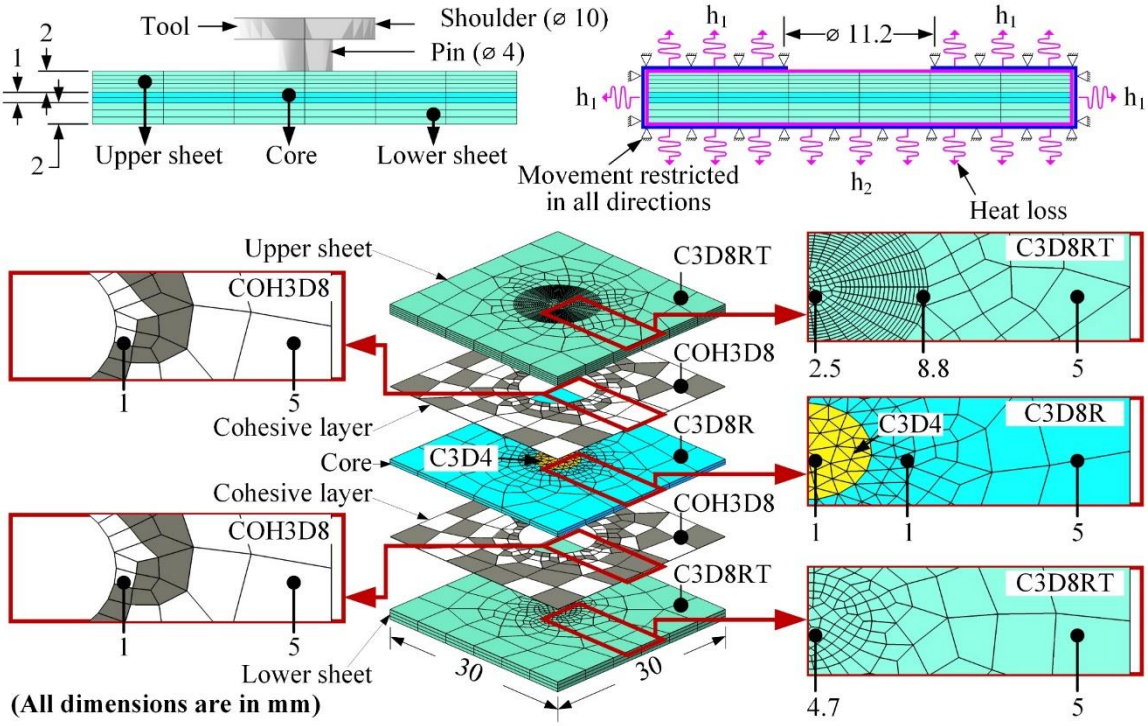

Fig. 6.6 Elements used in numerical modeling of FSSW using CZM

The lower surface of the lower sheet in the assembly is fixed in all directions such that it acts as a backing plate. The four sides of the assembly are completely restrained to ensure perfect clamping. Four different types of elements are used in the parts. The upper and lower sheet is assigned with the C3D8RT element, which is brick-shaped with 8 nodes and having a temperature degree of freedom. The core layer is assigned with two types of elements. In the core region, the C3D4 element is used, which is a 4-node linear tetrahedron type. This central region of the core is allowed to fail during welding. The remaining part of the core layer is assigned with a C3D8R element, which is an 8-node linear brick with reduced integration. Additionally, two layers of zero thickness are created above and below the core layer having cohesive elements. This creates a virtual adhesive bond between core and skin sheets. An 8-noded three-dimensional cohesive element (COH3D8) is chosen for this. The element sizes are shown in Fig. 6.6. It should be noted here that the cohesive elements are not defined throughout the interface. A circular region of 5 mm radius about the weld axis is assumed free from cohesive elements. It is believed that severe

plastic deformation of skin sheets in this region would fail the cohesive element in a very short time. The deformation behavior of skin sheets depends on its physical and mechanical properties that are dependent on temperature. The temperature-dependent properties of the skin sheet used are the same as those in the previous study (Fig. 5.2). All these properties are incorporated during the FE simulation as tabulated values. The core dependent property differences are ignored.

The heat loss to the surrounding from the top surface of the upper sheet and side faces of the upper and lower sheet is modeled by assuming convective heat transfer coefficient (h1) as 30 W/m2-°C (Kim et al., 2010). This value is taken as 2000 W/m2-°C (h2) for the bottom surface of the lower sheet (Kim et al., 2010). Many researchers, believing greater heat loss through the backing plate, consider the higher value of the convective heat transfer coefficient for the bottom surface (Kim et al., 2010). A gap conductance of 100000 is W/m2-°C is defined between upper and lower sheet interface to allow conductive heat interaction between them (Awang and Mucino, 2010). The heat transfer at the interface between tool and work-piece by conduction is ignored as the heat transfer occurs for a very short period of time (Kim et al., 2010). The Johnson-Cook material model incorporating thermal softening of the material is selected to describe the flow stress evolution of the skin AA5052-H32 sheet as described in the previous chapter.

The true stress-strain behavior of the epoxy layer with (different h/r ratios) obtained from the tensile test conducted in the present work (Fig. 6.1) is incorporated in the core layer. It is assumed that the effect of temperature is negligible on the epoxy layer, and the cohesive layer properties totally govern the failure during FSSW (Table 6.2). von Mises yield criterion is used to model the skin and core sheets. Though the skin sheet is anisotropic, as observed from Table 6.1, using anisotropic yield function is kept for future work. Coulomb's friction model is used to define the contact between all the mating parts. The coefficient of friction varies with slip rate and pressure.

In actual FSSW process, the upper and lower skin sheets are joined together by making a solid symmetric annular nugget about the weld axis. In the joint cross-section, this nugget appears as an extruded zone. This makes the pre-existed epoxy to be swept away from the nugget zone. In the FE modeling, this local swiping of epoxy is achieved by incorporating a shear failure criteria. An element is likely to fail when the equivalent shear strain exceeds the predefined limit in the criterion. Mathematically, it is given as (Levanger, 2012)

$$\int_0^{\bar{\varepsilon}_S^{pl}} \frac{d\bar{\varepsilon}^{pl}}{\bar{\varepsilon}_S^{pl}\left(\theta_S,\ \dot{\bar{\varepsilon}}^{pl}\right)} = 1 \tag{6.5}$$

where $\bar{\varepsilon}_S^{pl}$ is limiting value of equivalent shear strain, $\dot{\bar{\varepsilon}}^{pl}$ is the strain rate, and θ_S is the shear stress ratio, which is calculated as (Levanger, 2012)

$$\theta_S = \frac{q + k_s P}{\tau_{max}} \tag{6.6}$$

where q, P, τ_{max}, and k_s are respectively the von Mises stress, hydrostatic stress, maximum shear stress, and the material parameter. The numerical values of θ_S, $\dot{\bar{\varepsilon}}^{pl}$, and $\bar{\varepsilon}_s^{pl}$ are suitably fixed after many iterative trials required for damage initiation. The values of θ_S, $\dot{\bar{\varepsilon}}^{pl}$, and $\bar{\varepsilon}_s^{pl}$ are 1×10^{-8}, 1, 0.0001, in the central region respectively, whereas 1×10^{-5}, 1, 1 in the surrounding region of the core. The values are suitably fixed after several iterations required for damage initiation. The damage evolution is defined by a linear softening model, where the stiffness of an element degrades with an increasing effective plastic displacement of its nodes. Mathematically, it is expressed as (*Abaqus Documentation*)

$$\sigma = (1 - D)\bar{\sigma} \tag{6.7}$$

where σ and $\bar{\sigma}$ are the stress developed in the element and stress due to undamaged responses respectively. D is known as the overall damage variable calculated from (*Abaqus Documentation)*

$$\dot{D} = \frac{L\,\dot{\bar{\varepsilon}}^{pl}}{\bar{u}_f^{pl}} \tag{6.8}$$

where L and $\bar{u}_f^{pl}$ are the characteristic length of the element and the effective plastic displacement at fracture, respectively.

6.1.4.3 Comparison of FSSW simulation with and without CZM

The effect of CZM on FE simulation of sandwich FSSW is well understood when results are compared with that of without CZM. The procedure for FSSW with CZM is already explained in the previous section. A similar procedure is used while FE simulation without CZM, with the only difference, is the absence of any cohesive elements or layer. Instead, Coulomb's friction law is

applicable at the interface between core and skin sheets (same as Table 5.3). The hook geometry at the joint cross-section is measured and compared for with and without CZM. Further, the plastic deformation that occurred in the core layer is predicted by total plastic energy dissipated in both cases, which helps in describing the delamination behavior.

6.2 Results and discussion

6.2.1 Macrostructure

The macrostructure of the joint cross-section of the sandwich sheet is shown in Fig. 6.7. The geometrical features in the joint are similar to that of the sandwich sheet without adhesive bonding having a different polymeric core, as seen in previous chapters.

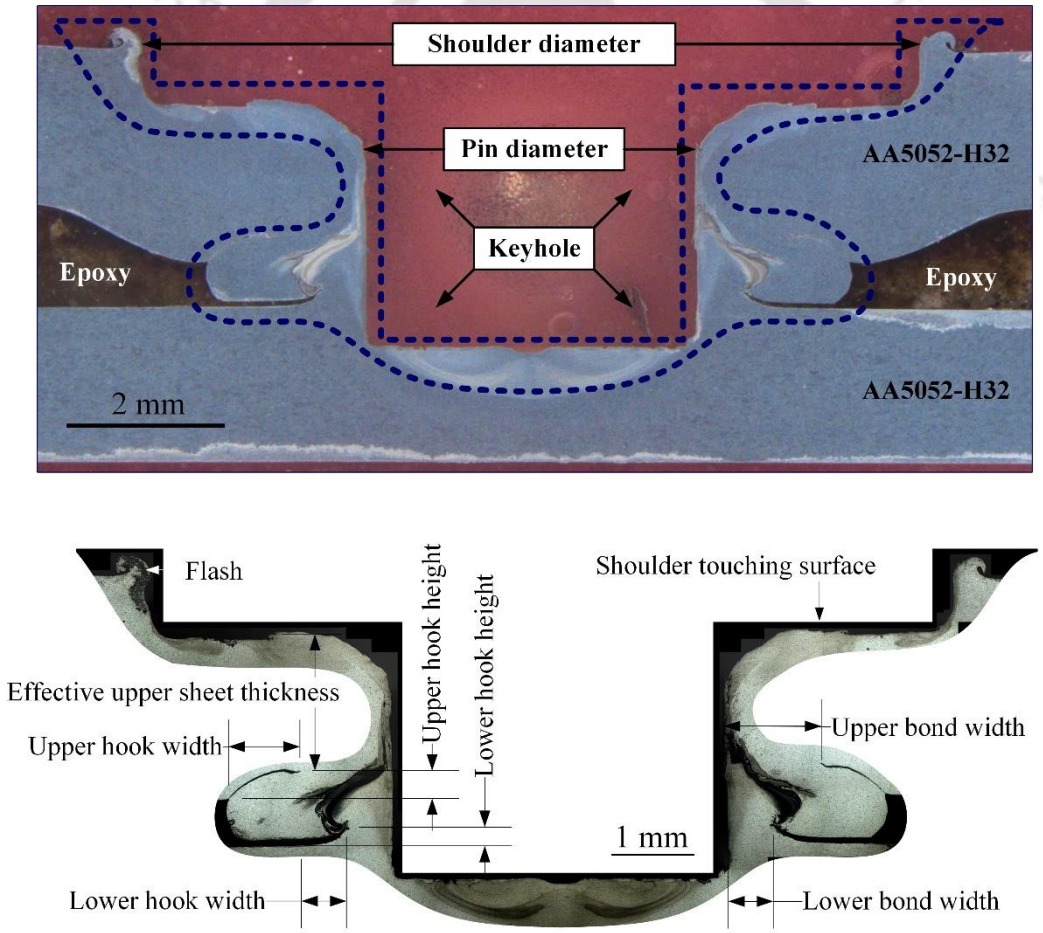

Fig. 6.7 Macrostructure of the joint cross-section of the sandwich sheet with adhesive core

Fig. 6.8 shows the response of change in the h/r ratio on the hook geometries. The upper bond width decreases up to 0.4 h/r ratio and increases after that. There is a positive correlation between the bond width and the volume of stirred plasticized material extruded through the core layer. The

volume of extruded material again depends on the ease of material movement against the core material, which is decided by the quality of core, i.e., h/r ratio. As shown earlier, the epoxy with a 0.4 h/r ratio has larger strength (Fig. 6.1), which means it would exert more resistance to the extrusion of plasticized material through it. That is why the upper bond width is lower at 0.4 h/r ratio.

Similarly, other hook geometries change with the h/r ratio. The lower bond width initially decreases up to 0.6 h/r ratio and then increases. The upper hook width initially increases up to 0.4 h/r ratio and then decreases. The upper bond width initially decreases up to 0.4 h/r ratio, then increases. The upper hook height initially decreases up to 0.6 h/r ratio, then increases. The lower hook height is larger at the higher h/r range (0.6-0.8). The lower hook width initially increases up to 0.6 h/r ratio, then decreases. Variation in the effective upper sheet thickness is insignificant with the h/r ratio.

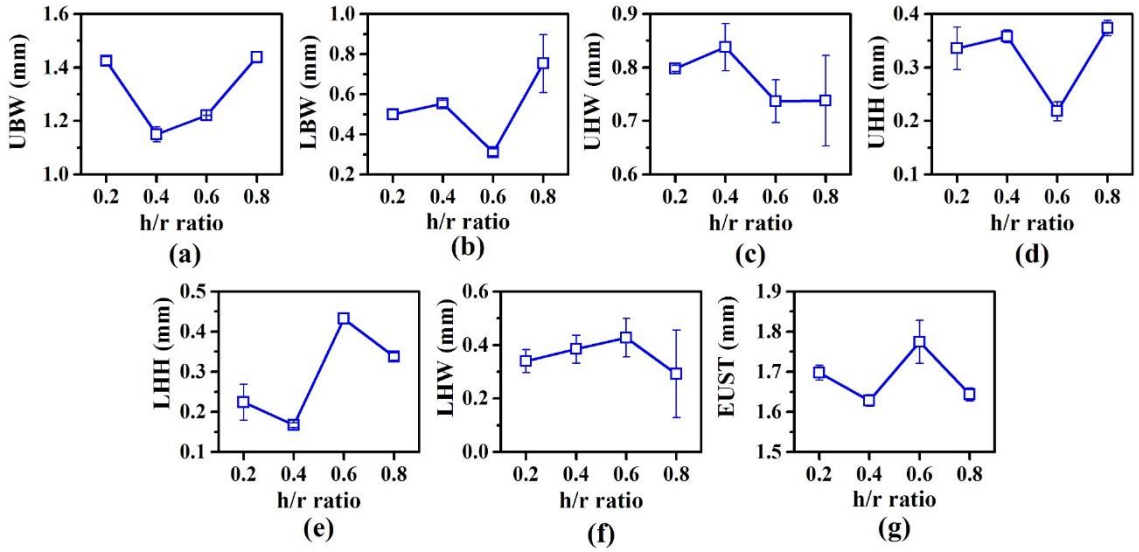

Fig. 6.8 Effect of h/r ratio on (a) upper bond width, (b) lower bond width, (c) upper hook width, (d) upper hook height, (e) lower hook height, (f) lower hook width, and (g) effective upper sheet thickness

6.2.2 Microstructure

The microstructure of the joint region of the sandwich sheet is shown in Fig. 6.9. The microstructural variation with respect to the h/r ratio is observed at 1 mm below the shoulder contact surface. The micrograph reveals fine-grain near the keyhole and coarse grains away from the keyhole for all the h/r ratios. The fine grains near the keyhole is due to dynamic recrystallization. Similar microstructures are obtained in a sandwich sheet having different core qualities. The grain size is measured in regions away from the keyhole for different core properties.

With an increasing h/r ratio, the grain size first increases and decreases when measured at a distance of 0.5 mm from the keyhole boundary. At a slightly farther distance, 1.5 mm away from the keyhole boundary, the average grain size decreases with increasing h/r ratio. However, at 2.5 mm from the keyhole boundary, variation in the grain size is insignificant.

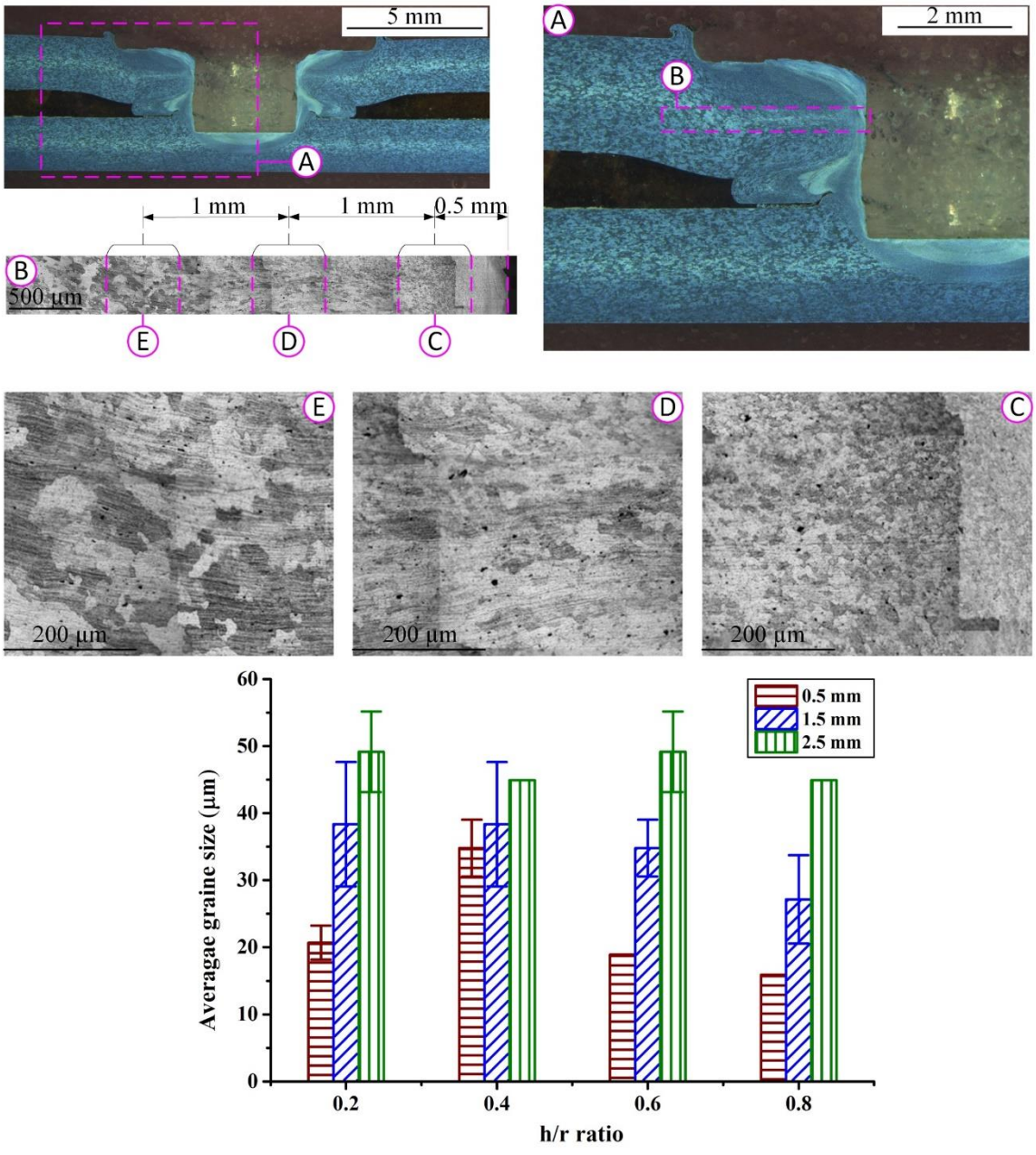

Fig. 6.9 Effect of h/r ratio on the grain size distribution of the sandwich sheet

The microstructure of the FSSW joint is mainly controlled by the degree of deformation and heating, and the extent depends on the alteration of welding parameters, material, tool dimension, work-piece thickness, surface conditions etc. In the present experiment, the welding parameter is fixed, and the only variation is kept in the core property—the core property changes with the h/r

ratio, which controls the plunging force. Therefore, frictional heating and deformation also change. Moreover, the status of the core layer in the joint itself changes when subjected to heating and mechanical pressure. It is believed that the ductile nature of the core layer at a higher h/r ratio allows stirring to a larger volume resulting in expansion of the stirred zone. This could have resulted in the grain refinement at a larger h/r ratio.

6.2.3 Hardness distribution

The hardness distribution on the joint cross-section at different h/r ratios is shown in Fig. 6.10. It is observed that the hardness near the keyhole boundary is higher than in other locations because of the fine grain structure. Moreover, the effect of the h/r ratio on the hardness is insignificant on the upper sheet, whereas in the lower sheet, it is considerable. In the lower sheet, the hardness increases with increasing h/r ratio, specifically in the vicinity of the keyhole (Fig. 6.10b).

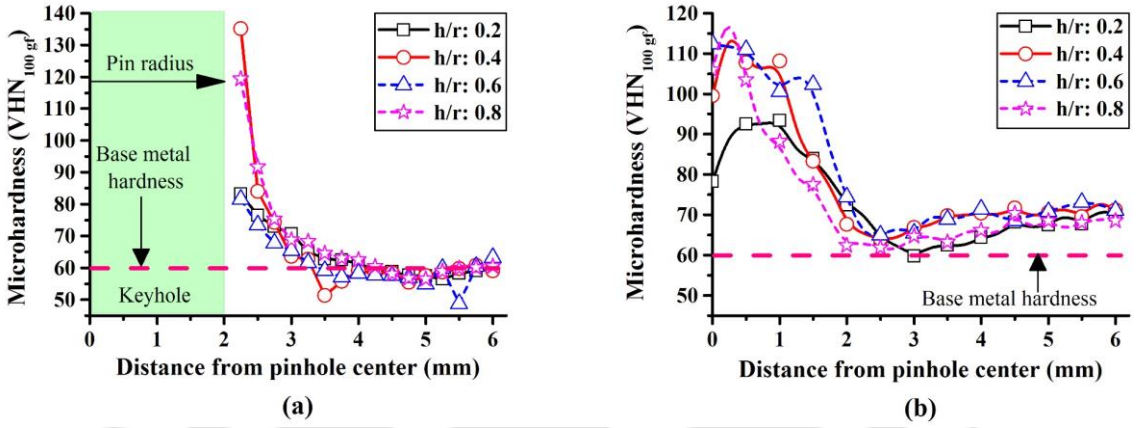

Fig. 6.10 Effect of h/r ratio on the hardness distribution on (a) upper sheet, and (b) lower sheet

It is believed that the lower skin material is deformed to a greater extent at a higher h/r ratio resulting in significant strain hardening. The significant plastic deformation in the lower sheet is evident in Fig. 6.8e, where a sharp jump in lower hook height is observed at a higher h/r ratio.

6.2.4 Mechanical performance

The load-extension behavior, maximum load, and extension at failure evaluated from the lap shear test and peel test at varying h/r ratios are discussed in this section. Further, the modes of failure of the joints are analyzed, and a logical connection is established with the mechanical performance outputs, macrostructure, microstructure, and hardness of the joint.

6.2.4.1 Lap shear test

Typical load-extension behavior of sandwich sheet with adhesive bonding and friction stir spot weld and without weld (only adhesive bonding) in lap shear test is shown in Fig. 6.11a. The load-extension behavior in both cases is similar, while considerable variations in strength and ductility. The maximum load and extension at failure at changing h/r ratio are shown in Fig. 6.11b.

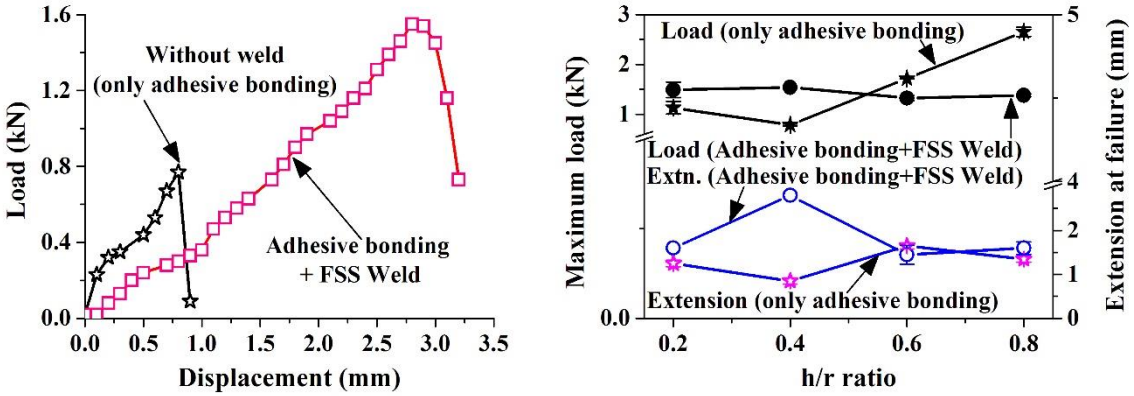

Fig. 6.11 Lap shear test (a) typical load–extension behavior, (b) failure load, and ductility vs. h/r ratio

It is evident that the failure load of the FSSWed sandwich sheet (adhesive bonding + FSS weld) is almost independent of the h/r ratio. However, the failure load of the un-welded sandwich sheet (only adhesive bonding) initially decreases up to 0.4 h/r ratios and then increases considerably. With respect to the un-welded sandwich sheet (only adhesive bonding), the sandwich sheets (FSSW + adhesive bonding) show higher failure load and ductility at a lower h/r ratio but lower at a higher h/r ratio.

The mechanical behavior of an un-welded sandwich sheet (only adhesive bonding) is controlled by the adhesion between core and skin layers, while it is majorly the hook geometry in the case of the FSSWed sandwich sheet (FSSW + adhesive bonding). In some cases, the combined effect of adhesion and hook geometry decides the overall performance of the FSSWed sandwich sheet. At lower h/r ratio, the lower hook height is lesser, which is beneficial in lap-shear performance. At a higher h/r ratio, the lower hook height is larger. Hence, it is expected that the sandwich sheet would fail at a lesser load. However, here the improved adhesion plays a favorable role in the improvement of lap shear failure load. Therefore, the reduction in failure load is compensated thereafter. Nevertheless, FSSW is promising against delamination in a sandwich sheet having a core with a lesser h/r ratio.

6.2.4.2 Peel test

The load-extension behavior during the peel test is shown in Fig. 6.12a. The failure load and ductility of the welded sandwich sheet (FSSW + adhesive bonding) are significantly larger as compared to that of un-welded sheets (only adhesive bonding). The maximum load and extension at failure at changing h/r ratio are shown in Fig. 6.12b.

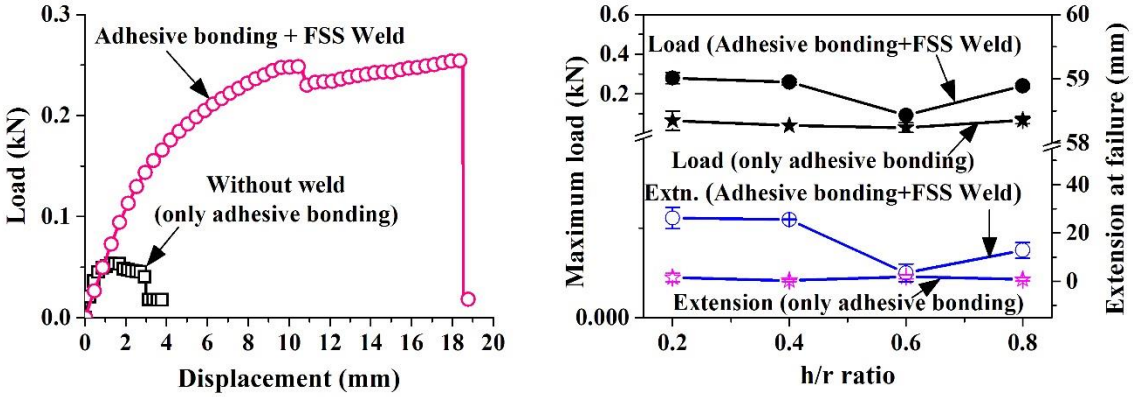

Fig. 6.12 Peel test (a) typical load–extension behavior, (b) failure load, and ductility vs. h/r ratio

Unlike the lap shear test, the peel test performance of the FSSWed sandwich sheet (FSSW + adhesive bonding) is significantly affected by the h/r ratio. It is observed that the failure load of the FSSWed sandwich sheet (adhesive bonding + FSS Weld)decreases initially up to 0.6 h/r ratio, then increases. Hence, a 0.6 h/r ratio represents a critical one in the peel test. It is shown earlier that the lower bond width is minimum at 0.6 h/r ratio (Fig. 6.8b), which could be a possible reason for it to be a critical ratio. Furthermore, the failure load and extension at the failure of FSSWed sandwich sheet (FSSW + adhesive bonding) is higher than that of the un-welded sandwich sheet (only adhesive bonding) irrespective of h/r ratio, which suggests that FSSW is beneficial in adhesive bonded sandwich sheet to avoid delamination.

6.2.4.3 Failure modes

The physical appearance of the fractured surface after mechanical tests are shown in Fig. 6.13. Nugget pullout failure mode is seen irrespective of the loading condition and quality of the core layer. This is due to the lesser lower bond width than the upper bond width in all the joints, as shown in Fig. 6.8. Interestingly, the core layer is significantly affected when the core quality changes. At lower h/r ratio, severe burning and large cracks are observed on the adhesive layer near the joint, which is probably due to the hard and brittle nature of the adhesive.

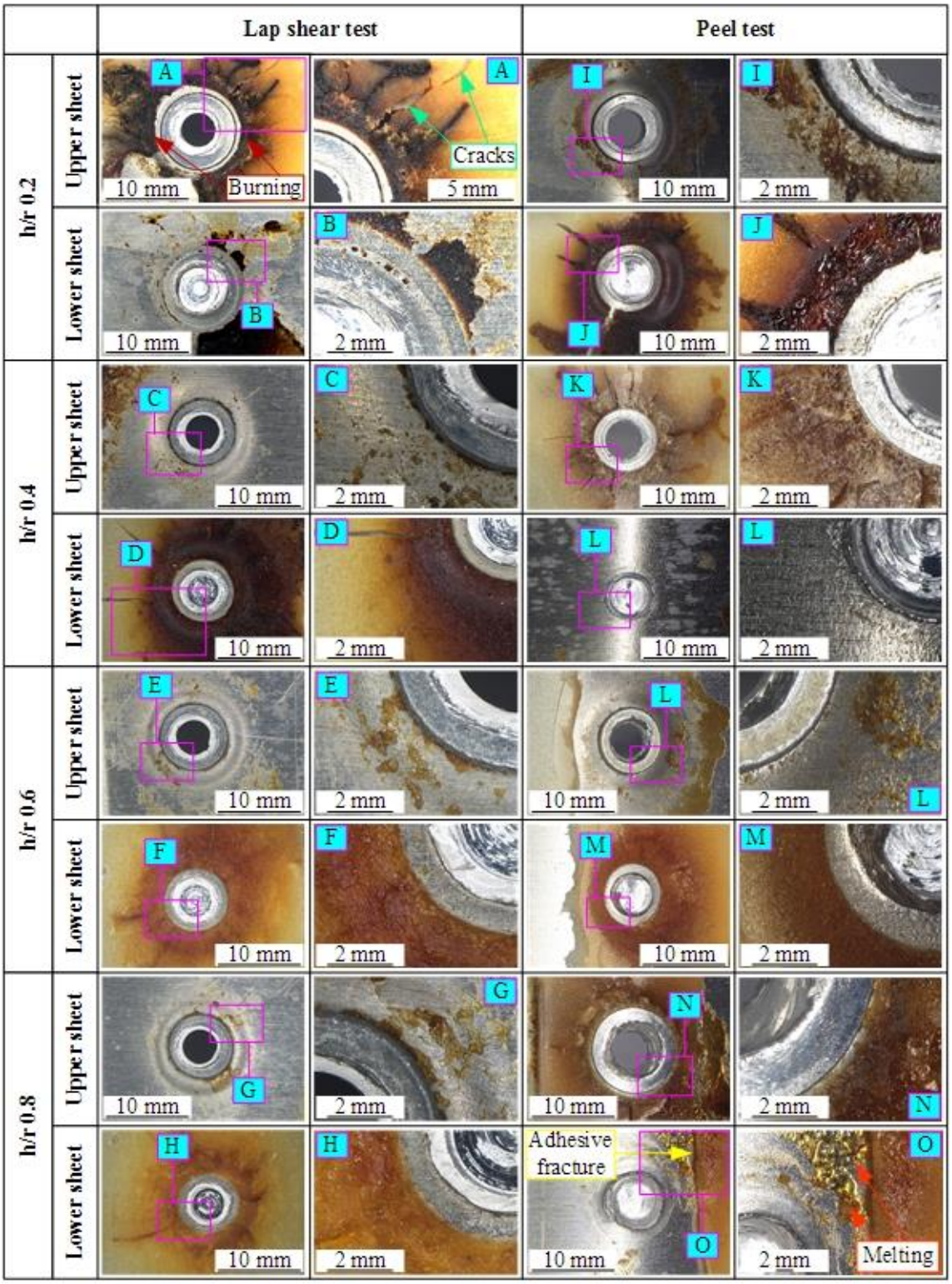

Fig. 6.13 Failure modes of sandwich sheets with different h/r ratio in lap shear and peel test

With increasing h/r ratio, crack formation on the adhesive reduces, and the effect of heat generation is limited only to melting. In other words, epoxy core degradation is less likely to occur in FSSW when h/r ratio is higher. It is believed that at a higher h/r ratio, the plunging force reduces due to softer core adhesive. Reduction in plunge force reduces the frictional heat generation

resulting in lesser degradation of the core layer. It should be noted that the degradation discussed here is attributed to the thick cured epoxy core layer only and not the cohesive interface between core and skin sheets.

6.2.5 Finite element analysis results

6.2.5.1 Selection of CZ parameters

von Mises stress distribution and comparison of load-extension behavior from FE simulation and experiment for lap shear and peel test are shown in Fig. 6.14a-d for optimized CZ parameters. It is evident that the peak loads in the lap shear test and peel test from FE simulation are almost the same as obtained in experiments. Several iterations lead to the correlation. The data fit is shown only for the 0.8 h/r ratio.

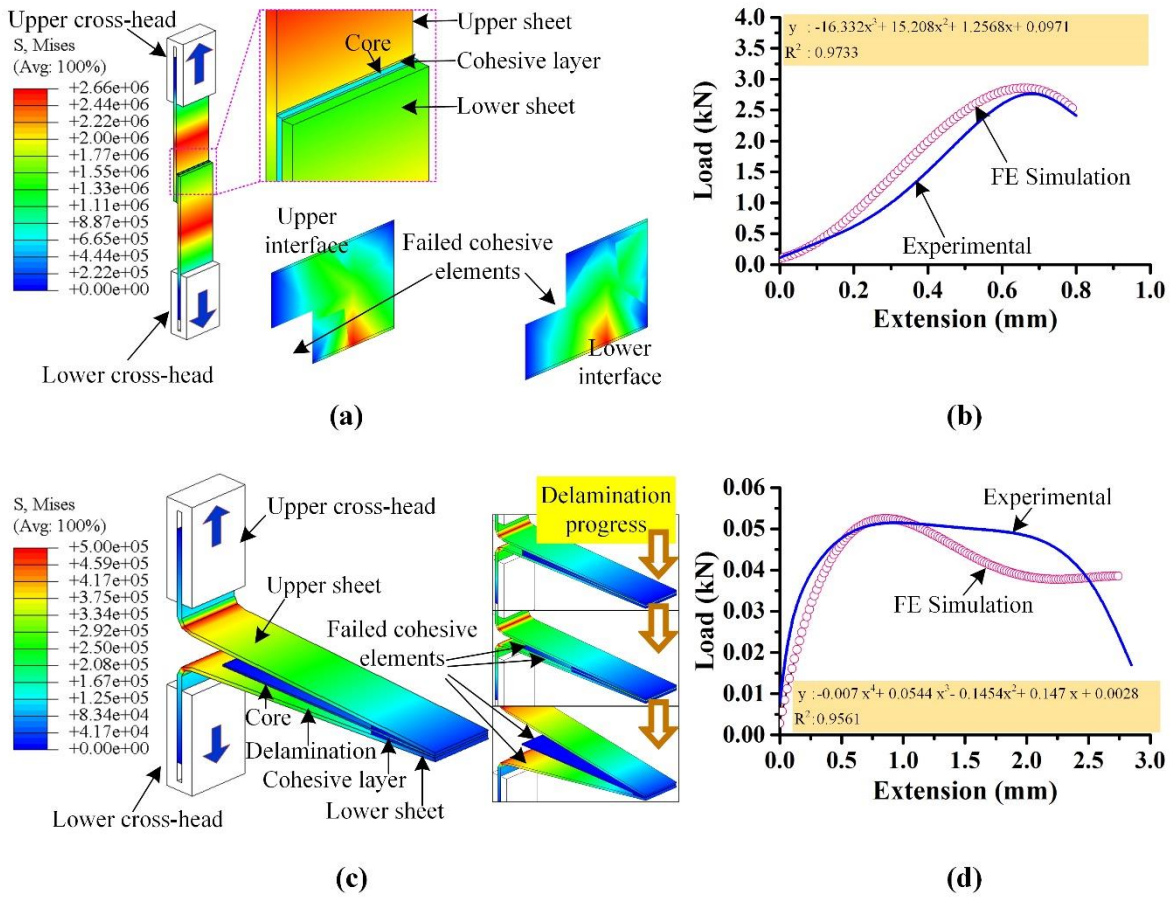

Fig. 6.14 (a) von Mises stress distribution in lap shear test, (b) FE simulation vs. experiment load-extension behavior in lap shear test, (c) von Mises stress distribution in peel test, and (d) FE simulation vs. experiment load-extension behavior in the peel test

A similar analysis is done for all other h/r ratios to finalize the optimized CZ parameters listed in Table 6.2. These values are incorporated in the numerical model of FSSW of the sandwich sheet to study the effect of the h/r ratio. A comparison between damage occurred in the upper and lower

interfaces of the sandwich sheet is shown in Fig. 6.15a. As explained earlier in Section 6.1.4.2, an increase in damage means the stiffness of the element is degraded.

Table 6.2 Optimized CZM parameters used for FE simulation

h/r ratio	E^*	Critical stress (Pa)			Critical fracture energy (J/m^2)			R^2 value
		σ_n^c	σ_s^c	σ_t^c	G_1^c	G_2^c	G_3^c	
0.2	2.60	65000	2050000	2050000	30	850	850	0.9025
0.4	3.50	40000	1320000	1320000	130	280	280	0.9467
0.6	3.00	43000	3000000	3000000	500	1700	1700	0.9488
0.8	18.5	50000	5500000	5500000	50	1200	1200	0.9647

* E is the stiffness of cohesive elements and is assumed equal in normal (E/E_{nn}) and two shear directions (G_1/E_{ss} and G_2/E_{tt})

The result indicates that the damage does not initiate immediately (case of $D = 0$). It starts after some deformation in the element. Once damage initiates, it gradually approaches towards complete fracture (case of $D = 1$). However, the curve shows incomplete damage (case of $D<1$). This is because the damage shown here is the average of damages that occurred in all cohesive elements. Only a few elements are wholly damaged, and some are entirely un-damaged. Therefore, whole cohesive elements are selected to specify damage to maintain consistency. The failure of the adhesive bonding at lower interfaces occurs prior to the upper interface and is valid for any core quality (or h/r ratio). It is believed that the cohesive layer at the upper interface is subjected to the compressive load applied by the upper sheet due to the tool plunge. This keeps the upper sheet and core layer intact. On the other hand, the lower sheet has a tendency to deform in the direction of the tool plunge, creating a favorable situation for detachment of the core layer from the lower sheet slightly. This could be a possible reason behind the early failure of the lower interface.

The effect of changing core quality (h/r ratio) on interfacial degradation is shown in Fig. 6.15b. It should be noted here that the damage behavior of cohesive elements changes with the h/r ratio, but the variation is not linear. Therefore, the failure of cohesive elements does not only depend only on the cohesive strength of the epoxy core. It also depends on the h/r ratio, which changes the adhesion severity. Failure of the core layer element is governed by the shear failure criterion (Eq. (6.5)), while the cohesive elements fail by traction-separation law (Eq. (6.1)). Failure of core layer elements automatically eliminates the corresponding cohesive element, but vice-versa is not true. Hence, delamination may occur either by cohesive element failure or by core element failure. In FSSW, multiple factors are involved simultaneously, which control such a failure. There is relative deformation between core and skin sheets during FSSW, which develops critical traction

on the cohesive element, causing failure. Again, the core layer gets extruded when the plasticized material flows against it, resulting in core layer element failure by shear.

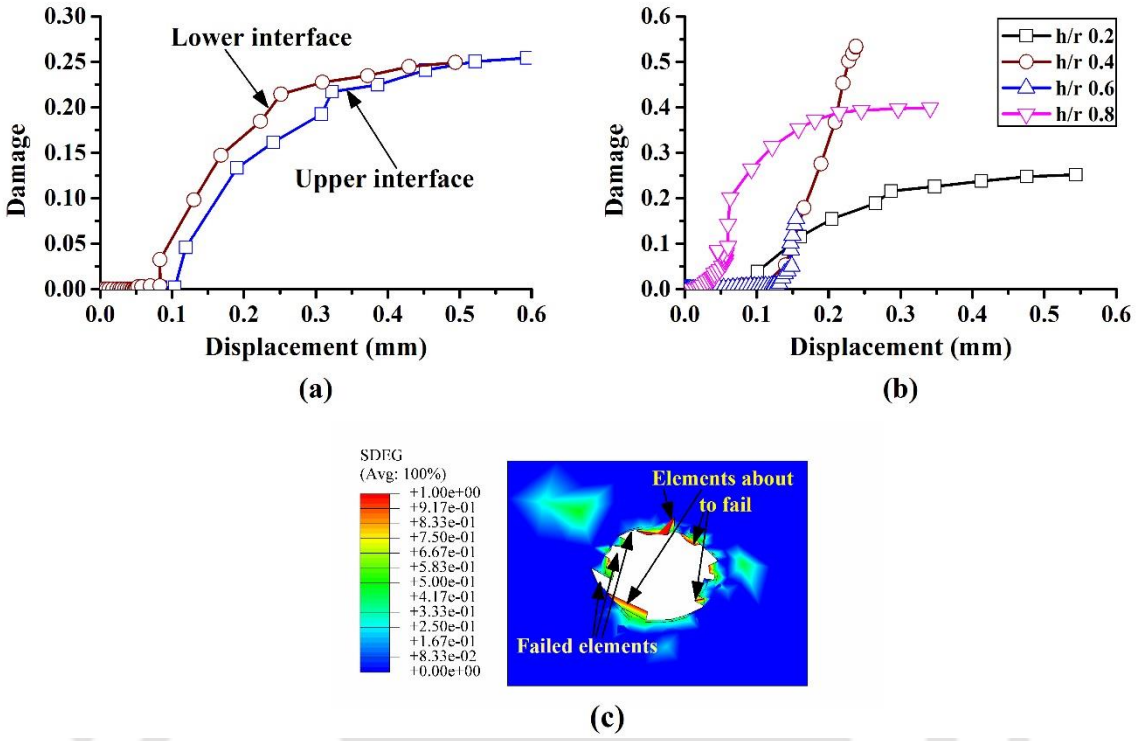

Fig. 6.15 (a) Damage evolution in upper and lower interfaces, (b) effect of core quality (h/r ratio) on the interface damage, and (c) stiffness degradation contour of cohesive elements

In Fig. 6.15b, the initial slope of the curves signify how quickly the interface failure occurs. It is observed that damage initiation occurs at the start of the displacement as the h/r ratio of the core layer increases. It is shown earlier in Fig. 6.1 that ductility of epoxy adhesive increases with h/r ratio. It is believed that higher ductility facilitates the cohesive element to reach the separation required for damage initiation ($\delta^* = \delta_i$ in Eq. (6.2)). Furthermore, it is also observed that the maximum and minimum damage occurred in 0.4 and 0.6 h/r ratios, respectively. The base adhesive with a 0.4 h/r ratio shows maximum tensile strength, and that of 0.6 h/r ratio is minimum (Table 6.1). From this, a direct correlation can be established that stronger the core layer, interface damage would be more considerable, indicating chances of significant delamination. In particular, adhesive with 0.4 h/r ratio is brittle when compared to 0.6 h/r ratio. Therefore, the brittleness of the core layer has to be reduced in order to prevent delamination. Hence, it is concluded that FSSW is best suited in a sandwich sheet with the ductile core as delamination starts early, but the core layer degradation is little. Stiffness degradation contour of cohesive elements shown in Fig. 6.15c depicts that the elements closer to the weld are excessively degraded and are most likely to fail during joining.

The cross-section views of the joint in the FE simulation of sandwich sheets after FSSW are shown in Fig. 6.16. The formation of the hook and the extruded zone is seen similar to that of the experiment. However, lower hook formation is not visible in FE simulation because the plasticized material always deforms above the upper surface of the lower sheet.

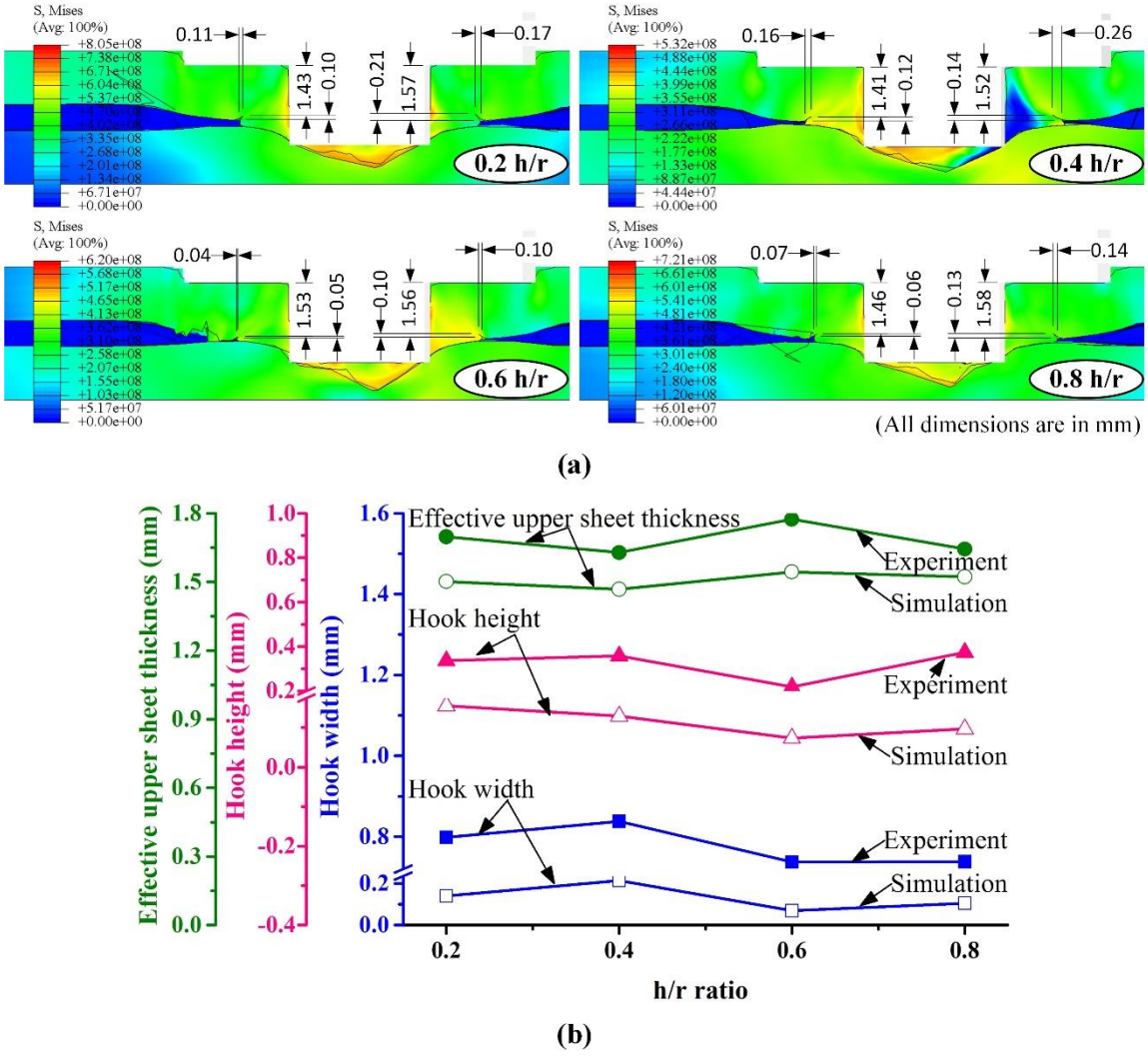

Fig. 6.16 Hook geometries from FE simulation with changing core quality (a) at joint cross-section and (b) simulation vs. experiment

In order to form the lower hook in FE simulation, a continuous connection between the upper and lower sheet is required. This way, a portion of the lower interface (interface between the core and lower sheet) ceases to exist in the continuous joint region, and the lower hook would have formed. But, the softer plasticized material can not penetrate the harder lower sheet to make a continuous connection as the same failure criteria are assumed for both the sheets. Further, material intermixing is extremely difficult to model in FSSW as the excessive deformation of elements creates convergence problems in Abaqus. Since only upper hook formation occurs in

numerical simulation, three important indexes, namely upper hook width, upper hook height, and effective upper sheet thickness, are compared. The upper hook width initially increases up to 0.4 h/r ratios, then decreases. The hook height decreases with increasing h/r ratio. However, it increases slightly after the 0.6 h/r ratios. The effective upper sheet thickness is inversely related to the hook height. The hook geometry obtained from the FE simulation is compared with that from the experiment, as shown in Fig. 6.16b. Some difference exists between the numerical and experimental values. This difference is obvious because the material intermixing between upper and lower sheets does not take place in simulation, unlike in experiments. Only the plastic deformation of the skin sheets takes place under the action of thermomechanical action of the tool. The material intermixing in simulation is prohibited by the excessive elemental deformation, which causes the simulation to stop. However, the characteristic variation with the h/r ratio is similar. The difference in hook geometry is due to the absence in modeling lower hook formation during FE simulation.

6.2.5.2 Influence of integrating CZM in FE simulation

An investigation is performed to understand the effect of CZM on FE simulation results. For this, separate FE simulations are carried out with changing core quality (h/r ratio) without incorporating any interfacial bonding between core and skin sheets.

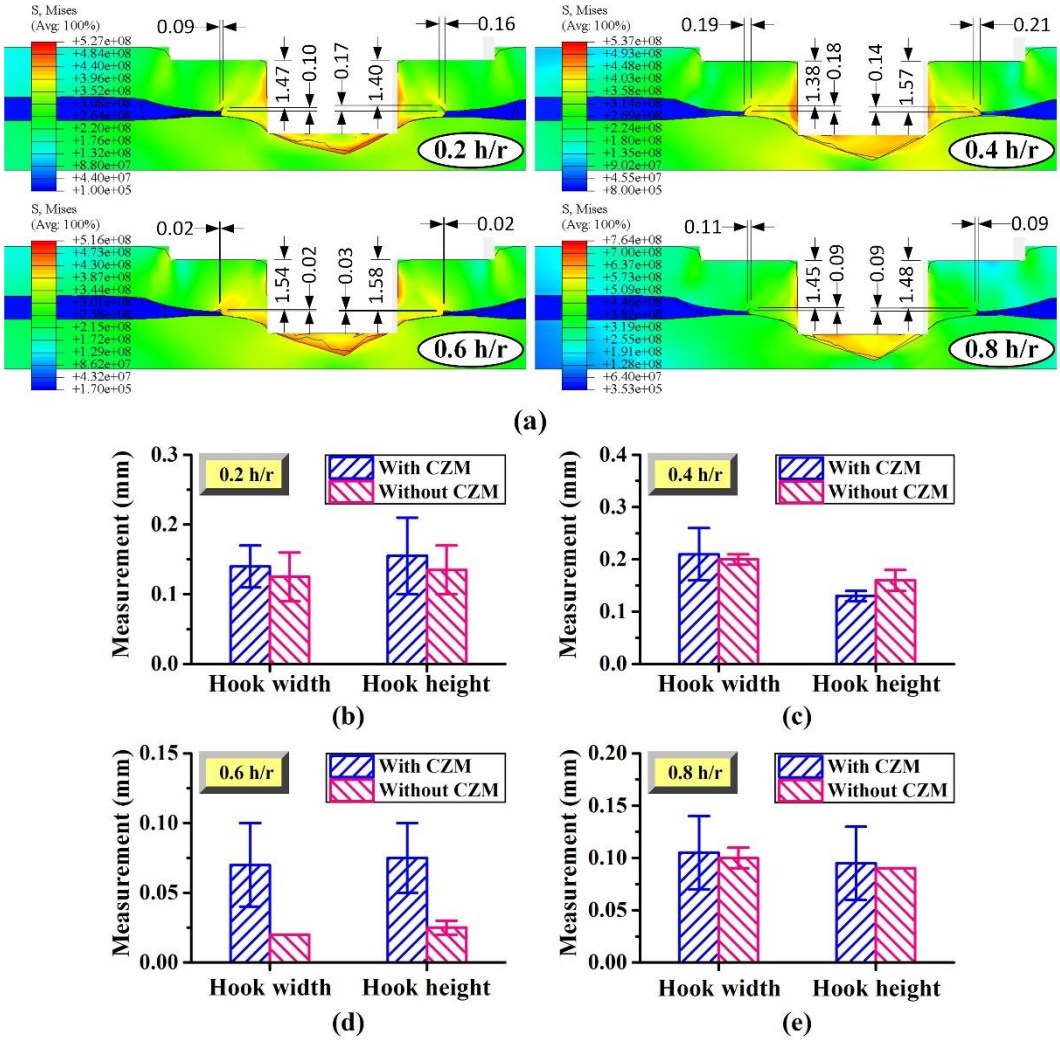

Fig. 6.17 Hook geometries with changing core quality (a) from FE simulation without CZM, comparison of hook geometry from FE simulation with and without CZM for (b) 0.2 h/r, (c) 0.4 h/r, (d) 0.6 h/r, and (e) 0.8 h/r

It is assumed that all three layers are stacked one above another before joining. All other conditions followed during CZM are kept the same. The internal features of the joint are predicted and compared with that of prediction with CZM. Hook geometries from FE simulation without CZM and its comparison with that with CZM is shown in Fig. 6.17.

Though the hook geometries are influenced by the h/r ratio, they vary little if compared with that of from simulation with CZM. The hook width and height are slightly lesser in joint without CZM than that in with CZM at all h/r ratios with the only exception of hook height at 0.4 h/r ratio (Fig. 6.17c). Moreover, in the 0.6 h/r ratio, the measured values of hook geometry suggest that the hook is not fully developed (Fig. 6.17d). It is fully developed when modeled with CZM. This suggests that adopting CZM in FE simulation of FSSW of the sandwich sheet results in a situation closer to that in experiments (Fig. 6.16a).

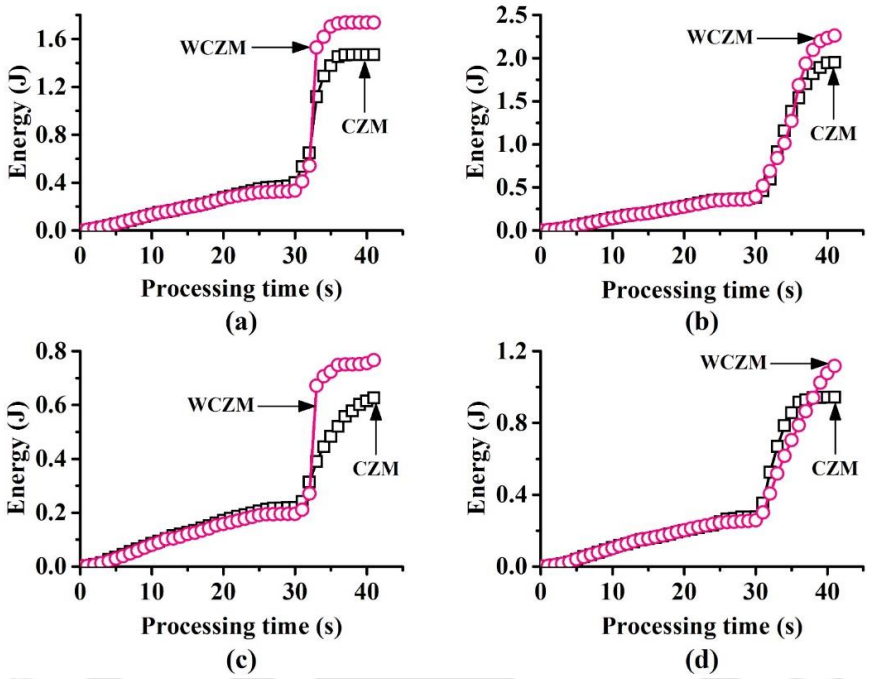

Fig. 6.18 Plastic energy dissipated into the core layer with (a) 0.2, (b) 0.4, (c) 0.6, and (d) 0.8 h/r ratios; CZM: cohesive zone modeling, WCZM: without cohesive zone modeling

Further, the total plastic energy dissipated in the core layer obtained from FE simulations with and without CZM is compared (Fig. 6.18). The energy dissipated is more significant in the case without CZM than in the case with CZM, irrespective of core quality (h/r ratio), which illustrates that plastic deformation is significant in the core layer when there is no adhesive bonding at the interface. In actual composite panels, core and skin layers are usually bonded by adhesive. Therefore, in the present work, incorporating CZM during the FE simulation yields a more realistic model. Moreover, CZM has shown its prominence in predicting the delamination behavior in sandwich sheets.

6.3 Conclusions

The effect of changing core properties on the FSSW of epoxy-based three-layered sandwich systems is addressed in the present work through experiments and numerical simulations. Cohesive Zone Modeling is used to model the core-skin interface to predict the formation of hook and delamination. The numerical technique adopted in the present research work resulted in a better understanding of two key features of FSSW of sandwich sheet: delamination of adjoining layers, and hook geometry. It is found that the overall delamination is promoted when the core polymer is brittle in nature. The location of onset of delamination is also predicted. The core delaminates from the lower skin prior to the upper skin. Further, incorporating cohesive zone modelling improves the development of hook geometries. The critical findings are summarised as

follows.

- The hook geometry is significantly affected by the h/r ratio. The upper bond width increases with the h/r ratio but after 0.4. A good correlation is achieved between hook geometry and h/r ratio. The joints formed at 0.4 h/r ratio are characterized by smaller upper bond width, greater upper hook width, and shorter lower hook height, whereas, that formed at 0.6 h/r ratio have smaller lower bond width, smaller upper hook height, greater lower hook height, and greater lower hook width.
- A significant variation in the grain size is seen closer to the keyhole when the h/r ratio is changed. The grain size decreases with the h/r ratio, but after 0.4. This is due to increased ductility of the core layer results in grater stirring leads to finer grains.
- The hardness of the joint is significantly affected by the h/r ratio at the lower sheet in the vicinity of the keyhole, where it increases with the h/r ratio because of greater plastic deformation.
- The lap shear failure load of an un-welded sandwich sheet (only adhesive bonding) initially decreases up to 0.4 h/r ratio, then increases. Conversely, for the FSSWed sandwich sheet (adhesive bonding + FSS weld), the effect of changing the h/r ratio is insignificant. Moreover, joint performance in the lap shear test improved after FSSW at a lower h/r ratio while it deteriorated at a higher h/r ratio. It is inferred that smaller lower hook height and improved adhesion are advantageous for lower and higher h/r ratios, respectively.
- On the contrary, the performance of the FSSWed sandwich sheet is significantly affected by the h/r ratio in the peel test, while the unwelded sandwich sheet performance is almost unaffected. Moreover, a 0.6 h/r ratio is crucial in the peel test, where minimum failure load and extension at failure is obtained. This is attributed to the smaller lower bond width. Further, FSSW has improved the peel test joint performance at all h/r ratio.
- Nugget pullout failure is observed in the peel test and lap shear test. The h/r ratio does not affect the failure mode.
- FE simulation results suggest that overall delamination at the skin core interface reduces with increasing h/r ratio. Moreover, delamination near the joint is larger than the region away from it. Further, delamination occurs at the lower interface prior to that in the upper interface. It is suggested that the FSSW is suitable for a sandwich sheet with the ductile core.
- The characteristic variation in the hook geometry with the h/r ratio in FE simulation and

experiment is alike. With increasing h/r ratio, the upper hook width initially increases up to 0.4, then decreases, while the hook height decreases up to 0.6, then increases. Contrarily, the effective upper sheet thickness increases up to 0.6, then decreases.

- Incorporation of CZM during FE simulation results in better development of hook geometry. Substantial plastic deformation in the core layer occurs when FE simulation is carried out without CZM. Furthermore, the CZM facilitates a better explanation of delamination.

Chapter 7

Conclusions and scope of future work

7.1 Conclusions

In this research work, a detailed analysis is carried out to propose an alternative way of joining polymer core sandwich panels. Many joining difficulties associated with the multi-material composite sheet are resolved. The achieved findings are encouraging for automobile industries towards adopting lightweight sandwich sheets. Major conclusions drawn from the present work are as follows

- The sandwich sheet FSSW essentially contains an extruded zone, where a portion of the plasticized material is accommodated and forms the nugget of the joint. The accommodation of plasticized material is facilitated by the soft polymeric core layer, which melts near the joint during FSSW and displaces outward by the stirred material.
- In all FSSW conditions, the sandwich sheet forms two distinct hooks, unlike one hook in the bimetallic sheet. The hook geometries change with process parameters and eventually affect the joint strength. The failure mode is strongly related to the hook geometry.
- The mechanical performance of the FSSWed sandwich sheet not only depends on the process parameter but also on the loading condition. Though this the case, the acceptable range of FSSW parameters for the sandwich sheet is rotational speed 1800 rpm and above, plunge depth of 3.6 mm and higher, plunge speed between 8 mm/min. and 6 mm/min, and dwell time between 5 s to 20 s. The sandwich sheets show excellent mechanical performance when welded within these ranges.
- In comparison to the bimetallic sheet, the lesser peak temperature of sandwich sheets suggest that a part of the heat generated is consumed for the melting of the polymer layer. Another reason for lesser peak temperature of sandwich sheets is smaller contact area between tool and work piece. The reliability of temperature measurement given by thermocouple is more than the IR camera.
- Sandwich sheet exhibits finer grains in the joint as compared to the bimetallic sheet due to lesser peak temperature, and grain size increases with an increase in rotation speed due to more

heat generation.

- Deterioration of joint performance is observed in sandwich sheets due to the presence of polymer. The formation of smaller bond width at the lower sheet side is responsible for this. However, it is possible to make a stronger joint in the sandwich sheet by suitably adjusting the welding parameters. Though this the case, the flash formation is lesser in sandwich sheets as compared to bimetallic. By using sandwich sheets, the flash defect can be minimized.
- The sandwich sheet joints perform better than the bimetallic sheet in uniaxial tensile tests irrespective of the welding condition, which signifies its better formability.
- The predominant failure mode in the sandwich sheet is 'nugget pull-out' because of the smaller lower bond width and larger upper bond width. However, 'partial nugget fracture' occurs when the lower hook height is larger. Moreover, the 'nugget pull-out' and 'partial nugget fracture' are associated with lower and higher joint strength, respectively.
- The FE analysis reveals that the von Mises equivalent stress and equivalent plastic strain distribution is maximum near the lower hook. This allows the lower sheet to detach from the joint at this location, resulting in a 'nugget pull-out' mode of failure.
- Changing the quality of the core layer in the sandwich sheet significantly affects the hook geometry, microstructure, and hardness of the joint. All these together decide the joint performance. A sandwich sheet with a ductile core is suitable for FSSW, where the overall delamination is less. Therefore, less degradation occurs in the damping characteristics of the sandwich sheet.
- The FE simulation is very useful in understanding the material flow and predicting delamination during FSSW of the sandwich sheet. Furthermore, it is also possible to predict the failure mode of FSSWed joints in different loading conditions.

7.2 Scope of future work

Although the effect of important process variables is investigated in detail, further study may be carried out to explore the influence of other factors. Moreover, optimizing the FSSW of the sandwich sheet to meet a specific requirement in the automobile industry can be attempted. The following future works are recommended for further exploration of this field

- The FSSW of sandwich sheets is affected by the quality of the core layer and it is expected that the thickness of the core layer will also affect the process. So, the FSSW of sandwich sheet at varying core thickness can be studied by experimental and numerical techniques. Furthermore,

the FSSW is successfully applied on polymer core sandwich sheet and adhesive core sandwich sheet separately. Therefore, the FSSW can be applied on a sandwich sheet having the polymer core layer bonded by adhesive to establish optimum joining condition on actual sandwich sheets.

- FSSW is a successful joining technique for sandwich sheet with HDPE or epoxy core. So, FSSW can be analyzed on the sandwich sheet with variety of core and skin materials to justify the process capability. Joining of a sandwich to the sandwich sheet can also be attempted.
- The process parameters can be varied beyond the selected range in this work for the improvement of joint performance.
- The mechanical behavior of FSSWed sandwich sheet shows better formability than FSSWed bimetallic sheet. Therefore, the formability of the FSSWed sandwich sheet can be studied in detail by conducting deep drawing and stretching operations.
- The FE simulation integrated with CZM shows delamination of sandwich sheet during FSSW. Similar numerical technique can be used to predict delamination in post welding forming operations.

References

Abaqus Documentation. (2014). Simulia, Abaqus 6.14, Dassault Systèmes, Abaqus Analysis User's Manual, 24.2.3.

Abibe, A. B., Sônego, M., dos Santos, J. F., Canto, L. B., and Amancio-Filho, S. T. (2016). On the feasibility of a friction-based staking joining method for polymer-metal hybrid structures. *Materials and Design*, 92 , 632–642.

Akour, S. N., and Maaitah, H. Z. (2010). Effect of core material stiffness on sandwich panel behavior beyond the yield limit. *WCE 2010 - World Congress on Engineering 2010*.

Amancio, S. (2007). Friction Riveting: development and analysis of a new joining technique for polymer-metal multi-materials structures.

André, A., Haghani, R., and Biel, A. (2012). Application of fracture mechanics to predict the failure load of adhesive joints used to bond CFRP laminates to steel members. *Construction and Building Materials*, 27 (1), 331–340.

Arici, A., and Mert, S. (2008). Friction Stir Spot Welding of Polypropylene. *Journal of Reinforced Plastics and Composites*, 27 (18), 2001–2004.

Arul, S. G., Miller, S. F., Kruger, G. H., Pan, T.-Y., Mallick, P. K., and Shih, A. J. (2008). Experimental study of joint performance in spot friction welding of 6111-T4 aluminium alloy. *Science and Technology of Welding and Joining*, 13 (7), 629–637.

ASM International. (1990). ASM Handbook Volume 2 Properties and selection: Nonferrous alloys and special-purpose materials. In *ASM International Handbook*.

Aval, H. J., Serajzadeh, S., and Kokabi, A. H. (2011). Theoretical and experimental investigation into friction stir welding of AA 5086. *The International Journal of Advanced Manufacturing Technology*, 52 (5–8), 531–544.

Awang, M. (2007). Simulation of Friction Stir Spot Welding (FSSW) Process: Study of Friction Phenomena [College of Engineering and Mineral Resources at West Virginia University]. https://www.researchgate.net/profile/Victor_Mucino2/publication/266577752_Simulation_of_Friction_Stir_Spot_Welding_FSSW_Process_Study_of_Friction_Phenomena/links/56f16f5308ae1cb29a3d0f2b.pdf

Awang, M., and Mucino, V. H. (2010). Energy Generation during Friction Stir Spot Welding (FSSW) of Al 6061-T6 Plates. *Materials and Manufacturing Processes*, 25 (1–3), 167–174.

Azevedo, J. C. S., Campilho, R. D. S. G., da Silva, F. J. G., Faneco, T. M. S., and Lopes, R. M. (2015). Cohesive law estimation of adhesive joints in mode II condition. *Theoretical and Applied Fracture Mechanics*, 80 , 143–154.

Badarinarayan, H., Shi, Y., Li, X., and Okamoto, K. (2009). Effect of tool geometry on hook formation and static strength of friction stir spot welded aluminum 5754-O sheets. *International Journal of Machine Tools and Manufacture*, 49 (11), 814–823.

Baek, S. W., Choi, D. H., Lee, C. Y., Ahn, B. W., Yeon, Y. M., Song, K., and Jung, S. B. (2010). Microstructure and mechanical properties of friction stir spot welded galvanized steel. *Materials Transactions*.

Bagheri, B., Abbasi, M., and Hamzeloo, R. (2020). The investigation into vibration effect on microstructure and mechanical characteristics of friction stir spot vibration welded

aluminum: Simulation and experiment. *Proceedings of the Institution of Mechanical Engineers, Part C: Journal of Mechanical Engineering Science*, 234 (9), 1809–1822.

Bakavos, D., and Prangnell, P. B. (2009). Effect of reduced or zero pin length and anvil insulation on friction stir spot welding thin gauge 6111 automotive sheet. *Science and Technology of Welding and Joining*, 14 (5), 443–456.

Balle, F., Wagner, G., and Eifler, D. (2007). Ultrasonic spot welding of aluminum sheet/carbon fiber reinforced polymer – joints. *Materialwissenschaft Und Werkstofftechnik*, 38 (11), 934–938.

Barnes, T. ., and Pashby, I. . (2000). Joining techniques for aluminium spaceframes used in automobiles. *Journal of Materials Processing Technology*, 99 (1–3), 62–71.

Baruah, A., Pandivelan, C., and Jeevanantham, A. K. (2017). Optimization of AA5052 in incremental sheet forming using grey relational analysis. *Measurement: Journal of the International Measurement Confederation*, 106 , 95–100.

Baskoro, A. S., Hadisiswojo, S., Kiswanto, G., Winarto, Amat, M. A., and Chen, Z. W. (2020). Influence of welding parameters on macrostructural and thermomechanical properties in micro friction stir spot welded under high-speed tool rotation. *The International Journal of Advanced Manufacturing Technology*, 106 (1–2), 163–175.

Bentouhami, A. (2018). Experimental and numerical analysis of behavior of honeycomb sandwiches panels subjected to impact [Ferhat Abbas University, Algeria]. http://dspace.univ-setif.dz:8888/jspui/handle/123456789/1493

Bilici, M. K., and Yukler, A. I. (2012). Effects of welding parameters on friction stir spot welding of high density polyethylene sheets. *Materials & Design*, 33 , 545–550.

Bilici, M. K., and Yükler, A. I. (2012). Influence of tool geometry and process parameters on macrostructure and static strength in friction stir spot welded polyethylene sheets. *Materials and Design*, 33 (1), 145–152.

Bilici, M. K., Yükler, A. İ., and Kurtulmuş, M. (2011). The optimization of welding parameters for friction stir spot welding of high density polyethylene sheets. *Materials & Design*, 32 (7), 4074–4079.

Bozkurt, Y. (2012). The optimization of friction stir welding process parameters to achieve maximum tensile strength in polyethylene sheets. *Materials & Design*, 35 , 440–445.

Bozzi, S., Helbert-Etter, A. L., Baudin, T., Klosek, V., Kerbiguet, J. G., and Criqui, B. (2010). Influence of FSSW parameters on fracture mechanisms of 5182 aluminium welds. *Journal of Materials Processing Technology*, 210 (11), 1429–1435.

Burchitz, I., Boesenkool, R., van der Zwaag, S., and Tassoul, M. (2005). Highlights of designing with Hylite - A new material concept. *Materials and Design*, 26 (4), 271–279.

Camanho, P. P., Davila, C. G., and de Moura, M. F. (2003). Numerical Simulation of Mixed-Mode Progressive Delamination in Composite Materials. *Journal of Composite Materials*, 37 (16), 1415–1438.

Cao, J. Y., Wang, M., Kong, L., and Guo, L. J. (2016). Hook formation and mechanical properties of friction spot welding in alloy 6061-T6. *Journal of Materials Processing Technology*, 230 , 254–262.

Capiati, N. J., and Porter, R. S. (1975). The concept of one polymer composites modelled with high density polyethylene. *Journal of Materials Science*, 10 (10), 1671–1677.

Carradò, A., Faerber, J., Niemeyer, S., Ziegmann, G., and Palkowski, H. (2011). Metal/polymer/metal hybrid systems: Towards potential formability applications. *Composite Structures*, 93 (2), 715–721.

Cavaliere, P., De Santis, A., Panella, F., and Squillace, A. (2009). Effect of welding parameters on mechanical and microstructural properties of dissimilar AA6082–AA2024 joints produced by friction stir welding. *Materials & Design*, 30 (3), 609–616.

Cavaliere, P., Squillace, A., and Panella, F. (2008). Effect of welding parameters on mechanical and microstructural properties of AA6082 joints produced by friction stir welding. *Journal of Materials Processing Technology*, 200 (1–3), 364–372.

Chao, C. K., Liu, C. H., and Wu, H. J. (1994). A study of the stretching process of steel-polymer-steel laminate. *Journal of Materials Processing Technology*, 40 (1–2), 155–172.

Chen, C. M., and Kovacevic, R. (2003). Finite element modeling of friction stir welding - Thermal and thermomechanical analysis. *International Journal of Machine Tools and Manufacture*.

Chen, J., Ravey, E., Hallett, S., Wisnom, M., and Grassi, M. (2009). Prediction of delamination in braided composite T-piece specimens. *Composites Science and Technology*, 69 (14), 2363–2367.

Chen, Y. C., Liu, S. F., Bakavos, D., and Prangnell, P. B. (2013). The effect of a paint bake treatment on joint performance in friction stir spot welding AA6111-T4 sheet using a pinless tool. *Materials Chemistry and Physics*, 141 (2–3), 768–775.

Choi, D.-H., Ahn, B.-W., Lee, C.-Y., Yeon, Y.-M., Song, K., and Jung, S.-B. (2011). Formation of intermetallic compounds in Al and Mg alloy interface during friction stir spot welding. *Intermetallics*, 19 (2), 125–130.

Chowdhury, S. H., Chen, D. L., Bhole, S. D., Cao, X., and Wanjara, P. (2013). Materials Science & Engineering A Lap shear strength and fatigue behavior of friction stir spot welded dissimilar magnesium-to-aluminum joints with adhesive. *Materials Science & Engineering A*, 562 , 53–60.

Chu, Q., Yang, X. W., Li, W. Y., Vairis, A., and Wang, W. B. (2018). Numerical analysis of material flow in the probeless friction stir spot welding based on Coupled Eulerian-Lagrangian approach. *Journal of Manufacturing Processes*, 36 , 181–187.

Commin, L., Dumont, M., Masse, J.-E., and Barrallier, L. (2009). Friction stir welding of AZ31 magnesium alloy rolled sheets: Influence of processing parameters. *Acta Materialia*, 57 (2), 326–334.

Cui, L., Fujii, H., Tsuji, N., and Nogi, K. (2007). Friction stir welding of a high carbon steel. *Scripta Materialia*.

Dai, G., and Mishnaevsky, L. (2013). Damage evolution in nanoclay-reinforced polymers: A three-dimensional computational study. *Composites Science and Technology*, 74 , 67–77.

Dashatan, S. H., Azdast, T., Ahmadi, S. R., and Bagheri, A. (2013). Friction stir spot welding of dissimilar polymethyl methacrylate and acrylonitrile butadiene styrene sheets. *Materials & Design*, 45 , 135–141.

Davila, C., Camanho, P., and de Moura, M. (2001, June 11). Mixed-mode decohesion elements for analyses of progressive delamination. *19th AIAA Applied Aerodynamics Conference*.

Dawood, H. I., Mohammed, K. S., Rahmat, A., and M.B., U. (2015). The influence of the surface roughness on the microstructures and mechanical properties of 6061 aluminium alloy using friction stir welding. *Surface and Coatings Technology*, 270 , 272–283.

De Matteis, G., and Landolfo, R. (1999). Mechanical fasteners for cladding sandwich panels: *Thin-Walled Structures*, 35 (1), 61–79.

Dehghani, M., Amadeh, A., and Akbari Mousavi, S. A. A. (2013). Investigations on the effects of friction stir welding parameters on intermetallic and defect formation in joining aluminum alloy to mild steel. *Materials & Design*, 49 , 433–441.

dos Santos, W. N., de Sousa, J. A., and Gregorio, R. (2013). Thermal conductivity behaviour of polymers around glass transition and crystalline melting temperatures. *Polymer Testing*, 32 (5), 987–994.

Elangovan, K., and Balasubramanian, V. (2008). Influences of tool pin profile and welding speed on the formation of friction stir processing zone in AA2219 aluminium alloy. *Journal of Materials Processing Technology*, 200 (1–3), 163–175.

Esteves, J. V., Goushegir, S. M., dos Santos, J. F., Canto, L. B., Hage, E., and Amancio-Filho, S. T. (2015). Friction spot joining of aluminum AA6181-T4 and carbon fiber-reinforced poly(phenylene sulfide): Effects of process parameters on the microstructure and mechanical strength. *Materials and Design*, 66 (PB), 437–445.

Fanelli, P., Vivio, F., and Vullo, V. (2012). Experimental and numerical characterization of Friction Stir Spot Welded joints. *Engineering Fracture Mechanics*, 81 , 17–25.

Farmanbar, N., Mousavizade, S. M., and Ezatpour, H. R. (2019). Achieving special mechanical properties with considering dwell time of AA5052 sheets welded by a simple novel friction stir spot welding. *Marine Structures*, 65 , 197–214.

Ferreira, A. C., Campanelli, L. C., Suhuddin, U. F. H., de Alcântara, N. G., and dos Santos, J. F. (2020). Investigation of internal defects and premature fracture of dissimilar refill friction stir spot welds of AA5754 and AA6061. *The International Journal of Advanced Manufacturing Technology*.

Filho, S. T. A., and Santos, J. F. dos. (2009). Joining of Polymers and Polymer–Metal Hybrid Structures: Recent Developments and Trends. *Polymer Engineering & Science*, 49 , 1461–1476.

Garg, A., and Bhattacharya, A. (2017). On lap shear strength of friction stir spot welded AA6061 alloy. *Journal of Manufacturing Processes*, 26 , 203–215.

Genna, S., Leone, C., and Tagliaferri, V. (2017). Characterization of laser beam transmission through a High Density Polyethylene (HDPE) plate. *Optics and Laser Technology*, 88 , 61–67.

Gerlich, A., Su, P., and North, T. H. (2005). Tool penetration during friction stir spot welding of Al and Mg alloys. *Journal of Materials Science*, 40 (24), 6473–6481.

Gibson, L. J., and Ashby, M. F. (1997). Cellular Solids: Structure and Properties (Second, p. 345). Cambridge University Press.

Gower, H. L., Pieters, R. R. G. M., and Richardson, I. M. (2006). Pulsed laser welding of metal-polymer sandwich materials using pulse shaping. *Journal of Laser Applications*, 18 (1), 35–41.

Guo, J. F., Chen, H. C., Sun, C. N., Bi, G., Sun, Z., and Wei, J. (2014). Friction stir welding of dissimilar materials between AA6061 and AA7075 Al alloys effects of process parameters. *Materials & Design (1980-2015)*, 56 , 185–192.

Gustafson, P. A., and Waas, A. M. (2009). The influence of adhesive constitutive parameters in cohesive zone finite element models of adhesively bonded joints. *International Journal of*

Solids and Structures, 46 (10), 2201–2215.

Hao, M., Osman, K. A., Boomer, D. R., and Newton, C. J. (1996). Developments in Characterization of Resistance Spot Welding of Aluminum. *Welding Journal*, 1s-8s.

Harhash, M., Sokolova, O., Carradó, A., and Palkowski, H. (2014). Mechanical properties and forming behaviour of laminated steel/polymer sandwich systems with local inlays - Part 1. *Composite Structures*.

Hirasawa, S., Badarinarayan, H., Okamoto, K., Tomimura, T., and Kawanami, T. (2010). Analysis of effect of tool geometry on plastic flow during friction stir spot welding using particle method. *Journal of Materials Processing Technology*.

Hirata, T., Oguri, T., Hagino, H., Tanaka, T., Chung, S. W., Takigawa, Y., and Higashi, K. (2007). Influence of friction stir welding parameters on grain size and formability in 5083 aluminum alloy. *Materials Science and Engineering: A*, 456 (1–2), 344–349.

Huskins, E. L., Cao, B., and Ramesh, K. T. (2010). Strengthening mechanisms in an Al-Mg alloy. *Materials Science and Engineering A*, 527 (6), 1292–1298.

Ikuta, A., Yin, Y. H., and North, T. H. (2012). Influence of tool thread on mechanical properties of dissimilar Al alloy friction stir spot welds. *Science and Technology of Welding and Joining*, 17 (8), 622–629.

Imran, M., Szyndler, J., Afzal, M. J., and Bambach, M. (2020). Dynamic recrystallization-dependent damage modeling during hot forming. *International Journal of Damage Mechanics*, 29 (2), 335–363.

Jang, J., Sung, M., Han, S., and Yu, W.-R. (2017). Prediction of delamination of steel-polymer composites using cohesive zone model and peeling tests. *Composite Structures*, 160 , 118–127.

Jedrasiak, P., and Shercliff, H. R. (2019). Small strain finite element modelling of friction stir spot welding of Al and Mg alloys. *Journal of Materials Processing Technology*, 263 , 207–222.

Kalaiselvan, K., and Murugan, N. (2013). Role of friction stir welding parameters on tensile strength of AA6061-B4C composite joints. *Transactions of Nonferrous Metals Society of China (English Edition)*.

Karthikeyan, R., and Balasubramanian, V. (2010). Predictions of the optimized friction stir spot welding process parameters for joining AA2024 aluminum alloy using RSM. *International Journal of Advanced Manufacturing Technology*, 51 (1–4), 173–183.

Katayama, S., and Kawahito, Y. (2008). Laser direct joining of metal and plastic. *Scripta Materialia*, 59 (12), 1247–1250.

Kesharwani, R. K., Panda, S. K., and Pal, S. K. (2014). Experimental Investigations on Formability of Aluminum Tailor Friction Stir Welded Blanks in Deep Drawing Process. *Journal of Materials Engineering and Performance*, 24 (2), 1038–1049.

Khalajmasoumi, M., Koloor, S. S. R., Arefnia, A., Ibrahim, I. S., and Yatim, J. M. (2012). Hyperelastic Analysis of High Density Polyethylene under Monotonic Compressive Load. *Applied Mechanics and Materials*, 229–231 , 309–313.

Khodabakhshi, F., Haghshenas, M., Sahraeinejad, S., Chen, J., Shalchi, B., Li, J., and Gerlich, A. P. (2014). Microstructure-property characterization of a friction-stir welded joint between AA5059 aluminum alloy and high density polyethylene. *Materials Characterization*, 98 , 73–82.

Kim, D., Badarinarayan, H., Kim, J. H., Kim, C., Okamoto, K., Wagoner, R. H., and Chung, K. (2010). Numerical simulation of friction stir butt welding process for AA5083-H18 sheets. *European Journal of Mechanics - A/Solids*, 29 (2), 204–215.

Kim, D., Badarinarayan, H., Ryu, I., Kim, J. H., Kim, C., Okamoto, K., Wagoner, R. H., and Chung, K. (2010). Numerical simulation of friction stir spot welding process for aluminum alloys. *Metals and Materials International*, 16 (2), 323–332.

Kim, J.-K., and Yu, T.-X. (1997). Forming and failure behaviour of coated, laminated and sandwiched sheet metals: a review. *Journal of Materials Processing Technology*, 63 (1–3), 33–42.

Kim, K. J., Kim, D., Choi, S. H., Chung, K., Shin, K. S., Barlat, F., Oh, K. H., and Youn, J. R. (2003). Formability of AA5182/polypropylene/AA5182 sandwich sheets. *Journal of Materials Processing Technology*, 139 (1-3 SPEC), 1–7.

Kim, Kee Joo, Rhee, M. H., Choi, B.-I., Kim, C.-W., Sung, C.-W., Han, C.-P., Kang, K.-W., and Won, S.-T. (2009). Development of application technique of aluminum sandwich sheets for automotive hood. *International Journal of Precision Engineering and Manufacturing*, 10 (4), 71–75.

Kukreja, G., and Narayanan, R. G. (2019). Forming of Adhesive-Bonded Sandwich Sheets with a Rubber Pad. *Metallurgical and Materials Transactions A*.

Kumar, A., Arora, K. S., Gupta, R. K., and Harmain, G. A. (2019). Investigation on interface morphology and joint configuration of dissimilar sheet thickness FSSW of marine grade Al alloy. *Journal of the Brazilian Society of Mechanical Sciences and Engineering*, 41 (9), 381.

Kumar, K., and Kailas, S. V. (2008). On the role of axial load and the effect of interface position on the tensile strength of a friction stir welded aluminium alloy. *Materials & Design*, 29 (4), 791–797.

Kundu, S., Roy, D., Bhola, R., Bhattacharjee, D., Mishra, B., and Chatterjee, S. (2013). Microstructure and tensile strength of friction stir welded joints between interstitial free steel and commercially pure aluminium. *Materials & Design*, 50 , 370–375.

Kwon, Y. J., Shim, S. B., and Park, D. H. (2009). Friction stir welding of 5052 aluminum alloy plates. *Transactions of Nonferrous Metals Society of China (English Edition)*, 19 (SUPPL. 1), 2–6.

Lacki, P., and Derlatka, A. (2016). Experimental and numerical investigation of aluminium lap joints made by RFSSW. *Meccanica*, 51 (2), 455–462.

Lacki, P., and Derlatka, A. (2017). Strength evaluation of beam made of the aluminum 6061-T6 and titanium grade 5 alloys sheets joined by RFSSW and RSW. *Composite Structures*, 159 , 491–497.

Lambiase, F. (2015). Mechanical behaviour of polymer-metal hybrid joints produced by clinching using different tools. *Materials and Design*, 87 , 606–618.

Lee, C.-Y., Choi, D.-H., Yeon, Y.-M., and Jung, S.-B. (2009). Dissimilar friction stir spot welding of low carbon steel and Al–Mg alloy by formation of IMCs. *Science and Technology of Welding and Joining*, 14 (3), 216–220.

Lee, W.-B., Kim, J.-W., Yeon, Y.-M., and Jung, S.-B. (2003). The Joint Characteristics of Friction Stir Welded AZ91D Magnesium Alloy. *Materials Transactions*, 44 (5), 917–923.

Lee, W. B., Yeon, Y. M., and Jung, S. B. (2003). The improvement of mechanical properties of friction-stir-welded A356 Al alloy. *Materials Science and Engineering: A*, 355 (1–2), 154–

159.

Levanger, H. (2012). Simulating Ductile Fracture in Steel using the Finite Element Method: Comparison of Two Models for Describing Local Instability due to Ductile Fracture (Issue May). University of Oslo Norway.

Li, G., Zhou, L., Zhou, W., Song, X., and Huang, Y. (2019). Influence of dwell time on microstructure evolution and mechanical properties of dissimilar friction stir spot welded aluminum–copper metals. *Journal of Materials Research and Technology*, 8 (3), 2613–2624.

Li, W., Li, J., Zhang, Z., Gao, D., Wang, W., and Dong, C. (2014). Improving mechanical properties of pinless friction stir spot welded joints by eliminating hook defect. *Materials & Design (1980-2015)*, 62 , 247–254.

Lin, P., Pan, J., and Pan, T. (2008). Failure modes and fatigue life estimations of spot friction welds in lap-shear specimens of aluminum 6111-T4 sheets. Part 2: Welds made by a flat tool. *International Journal of Fatigue*, 30 (1), 90–105.

Lin, Y.-C., Liu, J., Lin, B.-Y., Lin, C., and Tsai, H. (2012). Effects of process parameters on strength of Mg alloy AZ61 friction stir spot welds. *Materials & Design*, 35 , 350–357.

Liu, H., Zhao, Y., Su, X., Yu, L., and Hou, J. (2013). Microstructural Characteristics and Mechanical Properties of Friction Stir Spot Welded 2A12-T4 Aluminum Alloy. *Advances in Material Science Nd Engineering*, 2013 , 1–11.

Liu, Jian-guang, Liu, W., and Wang, J. (2012). Influence of interfacial adhesion strength on formability of AA5052/polyethylene/AA5052 sandwich sheet. *Transactions of Nonferrous Metals Society of China*, 22 , s395–s401.

Liu, Jian-guang, and Xue, W. (2013). Formability of AA5052/polyethylene/AA5052 sandwich sheets. *Transactions of Nonferrous Metals Society of China*, 23 (4), 964–969.

Liu, Jianguang, Liu, W., and Xue, W. (2013). Forming limit diagram prediction of AA5052/polyethylene/AA5052 sandwich sheets. *Materials & Design*, 46 , 112–120.

Logesh, K., Bupesh Raja, V. ., and Krishnaraj, C. (2018). Stretch Formability Behaviour of Glass Fibre Reinforced Nanoclay on Fiber Metal Laminated Composites. *International Journal of Vehicle Structures and Systems*, 10 (2), 115–121.

Mazda. (2003). *Mazda develops world's first aluminum joining technology using friction heat*. MAZDA: Backnumber. https://www2.mazda.com/en/publicity/release/archive/2003/200302/0227e.html

Merzoug, M., Mazari, M., Berrahal, L., and Imad, A. (2010). Parametric studies of the process of friction spot stir welding of aluminium 6060-T5 alloys. *Materials and Design*, 31 (6), 3023–3028.

Messler, R. W. (2004). Joining of Materials and Structures. In *Joining of Materials and Structures: From Pragmatic Process to Enabling Technology*. Elsevier.

Mishra, R. S., and Ma, Z. Y. (2005). Friction stir welding and processing. *Materials Science and Engineering: R: Reports*, 50 (1–2), 1–78.

Mitlin, D., Radmilovic, V., Pan, T., Chen, J., Feng, Z., and Santella, M. L. (2006). Structure-properties relations in spot friction welded (also known as friction stir spot welded) 6111 aluminum. *Materials Science and Engineering A*, 441 (1–2), 79–96.

Molnár, G., and Gravouil, A. (2017). 2D and 3D Abaqus implementation of a robust staggered phase-field solution for modeling brittle fracture. *Finite Elements in Analysis and Design*,

130 , 27–38.

Mortimer, J. (2005). Jaguar “Roadmap” rethinks self□piercing technology. *Industrial Robot: An International Journal*, 32 (3), 209–213.

Moshwan, R., Rahmat, S. M., Yusof, F., Hassan, M. A., Hamdi, M., and Fadzil, M. (2015). Dissimilar friction stir welding between polycarbonate and AA 7075 aluminum alloy. *International Journal of Materials Research*, 106 (3), 258–266.

Mousa, S., and Kim, G.-Y. (2015). Experimental study on warm roll bonding of metal/polymer/metal multilayer composites. *Journal of Materials Processing Technology*, 222 , 84–90.

Muraoka, Y., and Miyaoka, H. (1993). Development of an all-aluminum automotive body. *Journal of Materials Processing Technology*, 38 (4), 655–674.

Nguyen, N.-T., Kim, D.-Y., and Kim, H. Y. (2011). Assessment of the failure load for an AA6061-T6 friction stir spot welding joint. *Proceedings of the Institution of Mechanical Engineers, Part B: Journal of Engineering Manufacture*, 225 (10), 1746–1756.

Oladimeji, O. O., Taban, E., and Kaluc, E. (2016). Understanding the role of welding parameters and tool profile on the morphology and properties of expelled flash of spot welds. *Materials and Design*, 108 , 518–528.

Oliveira, P. H. F., Amancio-Filho, S. T., Dos Santos, J. F., and Hage, E. (2010). Preliminary study on the feasibility of friction spot welding in PMMA. *Materials Letters*, 64 (19), 2098–2101.

Ozlati, A., Movahedi, M., Tamizi, M., Tartifzadeh, Z., and Alipour, S. (2019). An alternative additive manufacturing-based joining method to make Metal/Polymer hybrid structures. *Journal of Manufacturing Processes*, 45 , 217–226.

Paidar, M., Sadeghi, F., Najafi, H., and Khodabandeh, A. R. (2015). Effect of pin and shoulder geometry on stir zone and mechanical properties of friction stir spot-welded aluminum alloy 2024-T3 sheets. *Journal of Engineering Materials and Technology, Transactions of the ASME*, 137 (3), 3–9.

Palkowski, H., and Carradò, A. (2014). Three-layered sandwich material for lightweight applications. *Emerging Materials Research*, 3 (3), 130–135.

Park, H., Kim, S.-J., Lee, J., Kim, J. H., and Kim, D. (2020). Delamination behavior analysis of steel/polymer/steel high-strength laminated sheets in a V-die bending test. *International Journal of Mechanical Sciences*, 173 , 105430.

Park, S. K., Hong, S. T., Park, J. H., Park, K. Y., Kwon, Y. J., and Son, H. J. (2010). Effect of material locations on properties of friction stir welding joints of dissimilar aluminium alloys. *Science and Technology of Welding and Joining*.

Park, S., Lee, C. G., Han, H. N., Kim, S., and Chung, K. (2008). Improvement of the Drawability Based on the Surface Friction Stir Process of AA5052-H32 Automotive Sheets. *METALS AND MATERIALS International*, 14 (1), 47–57.

Parsa, M. H., Ettehad, M., and Al Ahkami, S. N. (2009). FLD determination of AL 3105/Polypropylene/AL 3105 sandwich sheet using numerical calculation and experimental investigations. *International Journal of Material Forming*, 2 (S1), 407–410.

Parsa, M. H., Ettehad, M., Matin, P. H., and Al Ahkami, S. N. (2010). Experimental and Numerical Determination of Limiting Drawing Ratio of Al3105-Polypropylene-Al3105 Sandwich Sheets. *Journal of Engineering Materials and Technology*, 132 (3), 0310041–03100411.

Pathak, N., Bandyopadhyay, K., Sarangi, M., and Panda, S. K. (2013). Microstructure and Mechanical Performance of Friction Stir Spot-Welded Aluminum-5754 Sheets. *Journal of Materials Engineering and Performance*, 22 (1), 131–144.

Pickin, C. G., Young, K., and Tuersley, I. (2007). Joining of lightweight sandwich sheets to aluminium using self-pierce riveting. *Materials & Design*, 28 (8), 2361–2365.

Raikoty, H., Ahmed, I., and Talia, G. E. (2005). High speed friction stir welding: A computational and experimental study. *Proceedings of the ASME Summer Heat Transfer Conference*, 3 , 431–436.

Rajakumar, S., Razalrose, A., and Balasubramanian, V. (2013). Friction stir welding of AZ61A magnesium alloy: A parametric study. *International Journal of Advanced Manufacturing Technology*.

Rajamanickam, N., Balusamy, V., Madhusudhanna Reddy, G., and Natarajan, K. (2009). Effect of process parameters on thermal history and mechanical properties of friction stir welds. *Materials and Design*.

Ramachandran, K. K., Murugan, N., and Shashi Kumar, S. (2015). Effect of tool axis offset and geometry of tool pin profile on the characteristics of friction stir welded dissimilar joints of aluminum alloy AA5052 and HSLA steel. *Materials Science and Engineering: A*, 639 , 219–233.

Ramin, L., Assadi, M. H. N., and Sahajwalla, V. (2014). High-density polyethylene degradation into low molecular weight gases at 1823K: An atomistic simulation. *Journal of Analytical and Applied Pyrolysis*, 110 , 318–321.

Rao, H. M., Jordon, J. B., Barkey, M. E., Guo, Y. B., Su, X., and Badarinarayan, H. (2013). Influence of structural integrity on fatigue behavior of friction stir spot welded AZ31 Mg alloy. *Materials Science and Engineering A*, 564 , 369–380.

Rao, H. M., Rodriguez, R. I., Jordon, J. B., Barkey, M. E., Guo, Y. B., Badarinarayan, H., and Yuan, W. (2014). Friction stir spot welding of rare-earth containing ZEK100 magnesium alloy sheets. *Materials & Design (1980-2015)*, 56 , 750–754.

Rao, H. M., Yuan, W., and Badarinarayan, H. (2015). Effect of process parameters on mechanical properties of friction stir spot welded magnesium to aluminum alloys. *Materials & Design (1980-2015)*, 66 , 235–245.

Rao, M. D. (2003). Recent applications of viscoelastic damping for noise control in automobiles and commercial airplanes. *Journal of Sound and Vibration*, 262 (3), 457–474.

Ratanathavorn, W., and Melander, A. (2015). Dissimilar joining between aluminium alloy (AA 6111) and thermoplastics using friction stir welding. *Science and Technology of Welding and Joining*, 20 (3), 222–228.

Russig, C., Bambach, M., Hirt, G., and Holtmann, N. (2014). Shot peen forming of fiber metal laminates on the example of GLARE®. *International Journal of Material Forming*, 7 (4), 425–438.

Sakai, T., and Jonas, J. J. (1984). Overview no. 35 Dynamic recrystallization: Mechanical and microstructural considerations. *Acta Metallurgica*, 32 (2), 189–209.

Sakthivel, T., Sengar, G. S., and Mukhopadhyay, J. (2009). Effect of welding speed on microstructure and mechanical properties of friction-stir-welded aluminum. *The International Journal of Advanced Manufacturing Technology*, 43 (5–6), 468–473.

Sakurai, T. (2008). The latest trends in aluminium alloy sheets for automotive body panels.

Kobelco Technology Review, 28 , 22–28. https://www.kobelco.co.jp/english/ktr/pdf/ktr_28/022-028.pdf

Salomonsson, K., and Stigh, U. (2009). Influence of root curvature on the fracture energy of adhesive layers. *Engineering Fracture Mechanics*, 76 (13), 2025–2038.

Salonitis, K., Drougas, D., and Chryssolouris, G. (2010). Finite element modeling of penetration laser welding of sandwich materials. *Physics Procedia*, 5 , 327–335.

Salonitis, K., Stavropoulos, P., Fysikopoulos, A., and Chryssolouris, G. (2013). CO2 laser butt-welding of steel sandwich sheet composites. *International Journal of Advanced Manufacturing Technology*, 69 (1–4), 245–256.

Satheeshkumar, V., and Narayanan, R. G. (2014). Investigation on the influence of adhesive properties on the formability of adhesive-bonded steel sheets. *Proceedings of the Institution of Mechanical Engineers, Part C: Journal of Mechanical Engineering Science*, 228 (3), 405–425.

Satheeshkumar, V., and Narayanan, R. G. (2015). In-plane plane strain formability of adhesive-bonded steel sheets: influence of adhesive properties. *The International Journal of Advanced Manufacturing Technology*, 76 (5–8), 993–1009.

Sato, Y. S., Park, S. H. C., and Kokawa, H. (2001). Microstructural factors governing hardness in friction-stir welds of solid-solution-hardened Al alloys. *Metallurgical and Materials Transactions A*, 32 (12), 3033–3042.

Scialpi, A., De Filippis, L. A. C., and Cavaliere, P. (2007). Influence of shoulder geometry on microstructure and mechanical properties of friction stir welded 6082 aluminium alloy. *Materials & Design*, 28 (4), 1124–1129.

Shen, Z., Yang, X., Zhang, Z., Cui, L., and Yin, Y. (2013). Mechanical properties and failure mechanisms of friction stir spot welds of AA 6061-T4 sheets. *Materials and Design*, 49 , 181–191.

Shin, K. S., Kim, K. J., Choi, S.-W., and Rhee, M. H. (1999). Mechanical properties of aluminum/polypropylene/aluminum sandwich sheets. *Metals and Materials*, 5 (6), 613–618.

Simoncini, M., and Forcellese, A. (2012). Effect of the welding parameters and tool configuration on micro- and macro-mechanical properties of similar and dissimilar FSWed joints in AA5754 and AZ31 thin sheets. *Materials & Design*, 41 , 50–60.

Sokolova, O. A., Kühn, M., and Palkowski, H. (2012). Deep drawing properties of lightweight steel/polymer/steel sandwich composites. *Archives of Civil and Mechanical Engineering*, 12 (2), 105–112.

Solanki, K. N., Jordon, J. B., Whittington, W., Rao, H., and Hubbard, C. R. (2012). Structure-property relationships and residual stress quantification of a friction stir spot welded magnesium alloy. *Scripta Materialia*, 66 (10), 797–800.

Song, X., Ke, L., Xing, L., Liu, F., and Huang, C. (2014). Effect of plunge speeds on hook geometries and mechanical properties in friction stir spot welding of A6061-T6 sheets. *The International Journal of Advanced Manufacturing Technology*, 71 (9–12), 2003–2010.

Stigh, U., Alfredsson, K. S., Andersson, T., Biel, A., Carlberger, T., and Salomonsson, K. (2010). Some aspects of cohesive models and modelling with special application to strength of adhesive layers. *International Journal of Fracture*, 165 (2), 149–162.

Tanco, J. S., Nielsen, C. V., Chergui, A., Zhang, W., and Bay, N. (2015). Weld nugget formation in resistance spot welding of new lightweight sandwich material. *The International Journal*

of Advanced Manufacturing Technology, 80 (5–8), 1137–1147.

Thomas, W. M., Nicholas, E. D., Needham, J. C., Murch, M. G., Temple-Smith, P., and Dawes, C. J. (1994). Improvements relating to friction welding. In *European Patent Application No. 94120385.3*.

Threadgill, P. L. (2007). Terminology in friction stir welding. *Science and Technology of Welding and Joining*, 12 (4), 357–360.

Tozaki, Y., Uematsu, Y., and Tokaji, K. (2007). Effect of tool geometry on microstructure and static strength in friction stir spot welded aluminium alloys. *International Journal of Machine Tools and Manufacture*, 47 (15), 2230–2236.

Tran, V.-X., and Pan, J. (2010). Failure modes of friction stir spot welds in cross-tension specimens of dissimilar aluminium sheets. *Science and Technology of Welding and Joining*, 15 (4), 286–292.

Tran, V.-X., Pan, J., and Pan, T. (2009). Effects of processing time on strengths and failure modes of dissimilar spot friction welds between aluminum 5754-O and 7075-T6 sheets. *Journal of Materials Processing Technology*, 209 (8), 3724–3739.

Trimble, D., O'Donnell, G. E., and Monaghan, J. (2015). Characterisation of tool shape and rotational speed for increased speed during friction stir welding of AA2024-T3. *Journal of Manufacturing Processes*, 17 , 141–150.

Tutar, M., Aydin, H., Yuce, C., Yavuz, N., and Bayram, A. (2014). The optimisation of process parameters for friction stir spot-welded AA3003-H12 aluminium alloy using a Taguchi orthogonal array. *Materials & Design*, 63 , 789–797.

Uematsu, Y., and Tokaji, K. (2009). Comparison of fatigue behaviour between resistance spot and friction stir spot welded aluminium alloy sheets. *Science and Technology of Welding and Joining*, 14 (1), 62–71.

Ulysse, P. (2002). Three-dimensional modeling of the friction stir-welding process. *International Journal of Machine Tools and Manufacture*, 42 (14), 1549–1557.

Veljic, D., Rakin, M., Perovic, M., Medjo, B., Radakovic, Z., Todorovic, P., and Pavisic, M. (2013). Heat generation during plunge stage in friction stir welding. *Thermal Science*, 17 (2), 489–496.

Vural, M. (2014). Welding Processes and Technologies. In *Comprehensive Materials Processing* (pp. 3–48). Elsevier.

Wang, J., and Yang, C.-K. (2013). Failure analysis of hydroforming of sandwich panels. *Journal of Manufacturing Processes*, 15 (2), 256–262.

Watanabe, T., Takayama, H., and Yanagisawa, A. (2006). Joining of aluminum alloy to steel by friction stir welding. *Journal of Materials Processing Technology*, 178 (1–3), 342–349.

Weiss, M, Dingle, M. E., Rolfe, B. F., and Hodgson, P. D. (2007). The influence of temperature on the forming behavior of metal/polymer laminates in sheet metal forming. *Journal of Engineering Materials and Technology*, 129 (4), 530–537.

Weiss, Matthias, Rolfe, B. F., Dingle, M. E., and Hodgson, P. (2004). The influence of interlayer thickness and properties on spring-back of SPS-(steel/polymer/steel) laminates. *Steel Grips*, 2 (Supplement), 445–449.

Xu, W., Liu, J., Zhu, H., and Fu, L. (2013). Influence of welding parameters and tool pin profile on microstructure and mechanical properties along the thickness in a friction stir welded

aluminum alloy. *Materials & Design*, 47 , 599–606.

Yan, Y., Shen, Y., Lei, H., and Zhuang, J. (2019). Influence of welding parameters and tool geometry on the morphology and mechanical performance of ABS friction stir spot welds. *The International Journal of Advanced Manufacturing Technology*, 103 (5–8), 2319–2330.

Yang, X. W., Fu, T., and Li, W. Y. (2014). Friction Stir Spot Welding: A Review on Joint Macro- and Microstructure, Property, and Process Modelling. *Advances in Materials Science and Engineering*, 2014 , 1–11.

Yin, Y. H., Sun, N., North, T. H., and Hu, S. S. (2010a). Influence of tool design on mechanical properties of AZ31 friction stir spot welds. *Science and Technology of Welding and Joining*, 15 (1), 81–86.

Yin, Y. H., Sun, N., North, T. H., and Hu, S. S. (2010b). Microstructures and mechanical properties in dissimilar AZ91/AZ31 spot welds. *Materials Characterization*, 61 (10), 1018–1028.

Yin, Y. H., Sun, N., North, T. H., and Hu, S. S. (2010c). Hook formation and mechanical properties in AZ31 friction stir spot welds. *Journal of Materials Processing Technology*, 210 (14), 2062–2070.

Yoon, S., Kang, M., Kwon, Y., Hong, S., Park, D., Lee, K., Lim, C., and Seo, J. (2012). Influences of tool plunge speed and tool plunge depth on friction spot joining of AA5454-O aluminum alloy plates with different thicknesses. *Transactions of Nonferrous Metals Society of China*, 22 , s629–s633.

Yuan, W., Mishra, R. S., Carlson, B., Verma, R., and Mishra, R. K. (2012). Material flow and microstructural evolution during friction stir spot welding of AZ31 magnesium alloy. *Materials Science and Engineering: A*, 543 , 200–209.

Yusof, F., Miyashita, Y., Seo, N., Mutoh, Y., and Moshwan, R. (2012). Utilising friction spot joining for dissimilar joint between aluminium alloy (A5052) and polyethylene terephthalate. *Science and Technology of Welding and Joining*, 17 (7), 544–549.

Zhang, C., and Moore, I. D. (1997). Nonlinear mechanical response of high density polyethylene. Part I: Experimental investigation and model evaluation. *Polymer Engineering & Science*, 37 (2), 404–413.

Zhang, F., Su, X., Chen, Z., and Nie, Z. (2015). Effect of welding parameters on microstructure and mechanical properties of friction stir welded joints of a super high strength Al–Zn–Mg–Cu aluminum alloy. *Materials & Design*, 67 , 483–491.

Zhang, Z., Yang, X., Zhang, J., Zhou, G., Xu, X., and Zou, B. (2011). Effect of welding parameters on microstructure and mechanical properties of friction stir spot welded 5052 aluminum alloy. *Materials & Design*, 32 (8–9), 4461–4470.

Zhu, X. K., and Chao, Y. J. (2002). Effects of temperature-dependent material properties on welding simulation. *Computers & Structures*, 80 (11), 967–976.

Zivojinovic Danijela, Aleksandar, S., and Aleksandar, G. (2013). Crack growth analysis in friction stir welded joint zones using extended finite element method. *Structural Integrity and Life*, 13 (3), 179–188.

Publications from the present work

Refereed Journals

[1] **Rana, P.K.**, Narayanan, R.G., 2020. Numerical and experimental response of FSSW of AA5052-H32/epoxy/AA5052-H32 sandwich sheets with varying core properties. International Journal of Material Forming. DOI: https://doi.org/10.1007/s12289-020-01596-3

[2] **Rana, P.K.**, Narayanan, R.G., Kailas, S. V., 2019. Friction stir spot welding of AA5052-H32/HDPE/AA5052-H32 sandwich sheets at varying plunge speeds. Thin-walled structures. 138, pp. 415–429. DOI: https://doi.org/10.1016/j.tws.2019.02.016

[3] **Rana, P.K.**, Narayanan, R.G., Kailas, S. V., 2018. Effect of rotational speed on friction stir spot welding of AA5052-H32/HDPE/AA5052-H32 sandwich sheets. Journal of Materials Processing Technology. 252, pp. 511–523. DOI: https://doi.org/10.1016/j.jmatprotec.2017.10.016

Book Chapters

[1] **Rana, P.K.**, Narayanan, R.G., Kailas, S. V., 2019. Influence of Tool Plunge Depth During Friction Stir Spot Welding of AA5052-H32/HDPE/AA5052-H32 Sandwich Sheets, Strengthening and Joining by Plastic Deformation. Lecture Notes on Multidisciplinary Industrial Engineering. Springer, Singapore, pp. 95–121. DOI: https://doi.org/10.1007/978-981-13-0378-4_5

Refereed Conferences

[1] **Rana, P.K.**, Narayanan, R.G., Kailas, S. V., 2018. Thermal and Mechanical Response in FSSW of Sandwich Sheets at Different Dwell Periods, Proceedings of National Conference on Advanced Materials, Manufacturing and Metrology (NCAMMM – 2018). Durgapur, pp. 235–240.

[2] **Rana, P.K.**, Narayanan, R.G., Kailas, S. V., Influence of Rotational Speed on the Friction Stir Spot Welding of Polymer Core Sandwich Sheets; Proceedings of 6th International & 27th All India Manufacturing Technology, Design and Research Conference (AIMTDR-2016), College of Engineering, Pune, Maharashtra, INDIA, December 16-18, 2016, pp. 926-930